IAEA TECDOC SERIES

IAEA-TECDOC-1916

IAEA-TECDOC-1916

Landscape Salinity and Water Management for Improving Agricultural Productivity

Joint FAO/IAEA Programme
Nuclear Techniques in Food and Agriculture

IAEA
International Atomic Energy Agency

LANDSCAPE SALINITY AND WATER MANAGEMENT FOR IMPROVING AGRICULTURAL PRODUCTIVITY

The Agency's Statute was approved on 23 October 1956 by the Conference on the Statute of the IAEA held at United Nations Headquarters, New York; it entered into force on 29 July 1957. The Headquarters of the Agency are situated in Vienna. Its principal objective is "to accelerate and enlarge the contribution of atomic energy to peace, health and prosperity throughout the world''.

IAEA-TECDOC-1916

LANDSCAPE SALINITY AND WATER MANAGEMENT FOR IMPROVING AGRICULTURAL PRODUCTIVITY

PREPARED BY THE
JOINT FAO/IAEA DIVISION OF NUCLEAR TECHNIQUES IN FOOD AND AGRICULTURE

INTERNATIONAL ATOMIC ENERGY AGENCY
VIENNA, 2020

For further information on this publication, please contact:

Soil and Water Management and Crop Nutrition Section
International Atomic Energy Agency
Vienna International Centre
PO Box 100
1400 Vienna, Austria
Email: Official.Mail@iaea.org

Printed by the IAEA in Austria
June 2020

IAEA Library Cataloguing in Publication Data

Names: International Atomic Energy Agency.
Title: Landscape salinity and water management for improving agricultural productivity / International Atomic Energy Agency.
Description: Vienna : International Atomic Energy Agency, 2020. | Series: IAEA TECDOC series, ISSN 1011–4289 ; no. 1916 | Includes bibliographical references.
Identifiers: IAEAL 20-01328 | ISBN 978–92–0–110520–2 (paperback : alk. paper) |
ISBN 978–92–0–110620–9 (pdf)
Subjects: LCSH: Salinity. | Water quality management. | Crops and water.

FOREWORD

Addressing soil and water salinity in agricultural landscapes involves either reducing salinity (mitigation) or making agriculture resilient to it (adaptation) by using innovative soil and water management technologies and practices in salt-affected soils and saline water. Efficient investment in salinity mitigation requires an understanding of how different landscapes respond to alternative land and water use options at the field and landscape scale. This involves identifying ways to reduce existing soil salinity and the risk of further salinization in agricultural landscapes. Integrated soil and water management practices have been used in agricultural production systems to adapt to existing soil and water salinity and to mitigate the potential development of salinity. These practices include accurate irrigation scheduling based on soil water monitoring using sensor based technologies to improve crop irrigation efficiency, soil water storage, water infiltration and leaching of excess salt from the crop rooting zone; permanent raised bed technology to improve crop productivity, reduce irrigation water requirement and lower the risk of groundwater recharge; and conservation soil management practices including reduced tillage, incorporation of crop residues, gypsum and manure application, crop rotation and growing cover crops to increase soil organic matter and hence soil water holding capacity and infiltration. Nevertheless, there is still a need to better understand the complex interactions between soil, water, plants and applied nutrient inputs, and the influence of these interactions under different farm management practices to improve water use efficiency and crop yield/quality, without increasing soil and water salinity.

A coordinated research project (CRP) on Landscape Salinity and Water Management for Improving Agricultural Water Productivity was developed to address salinization problems in agricultural landscapes and protect the soil and water resources needed to sustain food production; to identify ways to improve crop productivity and sustainability through water and salinity management; and to define approaches and technologies to assess and monitor soil water content and salinity at field and area-wide scales, to reduce the impacts on food production of climate change and variability, and the widespread increase in landscape water and soil salinity.

Several methodologies were developed in the CRP, including the use of the oxygen-18 isotopic technique to assess the contribution of seawater intrusion, relative to poor irrigation management, in salt-affected water where rice production has been affected by salinity. Project participants tested irrigation scheduling using soil moisture neutron probes and improved salt management and the use of salt-tolerant crops such as barley, rice and wheat. The AquaCrop model of the Food and Agriculture Organization of the United Nations was used for simulation modelling to extrapolate the results from field to landscape scale. Finally, a new landscape soil moisture measuring tool, the cosmic ray neutron probe, for area-wide soil water measurements was also tested.

This CRP was implemented between 2013 and 2018 following the recommendations of a consultants meeting of international experts. The research network included participants from Bangladesh, China, the Islamic Republic of Iran, the Republic of Korea, Pakistan, Viet Nam and the United States of America. It was supported by research and development on the use of the cosmic ray neutron sensor for landscape soil water measurement at the IAEA Environment Laboratories. The IAEA is grateful to all the CRP participants for their valuable contributions. The IAEA officer responsible for this publication was L.K. Heng of the Joint FAO/IAEA Division of Nuclear Techniques in Food and Agriculture.

CONTENTS

1. INTRODUCTION

The rationale for the Co-ordinated Research Project (CRP) "Landscape Salinity and Water Management for Improving Agricultural Productivity (D1.20.13)" was the urgent need to address the problem of advancing salinity in irrigated soils of arid and semi-arid regions, and in river deltas subject to intrusions of sea-water. In many developing countries, the reclamation of salt-affected soil is not a viable option due to the lack of sufficient rainfall or available freshwater to leach salt from the soil profile, together with the need to install expensive drainage systems to dispose of the leached saline water. Therefore, alternative strategies are needed. One approach is to use salt tolerant crops, but when irrigation is required due to drought, often the only available water is brackish ground- or surface-water. Therefore, depending on the salinity (electrical conductivity) of the water available, the challenge becomes how to manage the amount and frequency of irrigation to limit yield reduction while attempting to avoid secondary salinity. This CRP endeavours to address these management issues. Studies from seven countries including Bangladesh, China (China Academy of Agricultural Sciences (CAAS) & China Agricultural University (CAU)), Islamic Republic of Iran, Republic of Korea, Pakistan, United States of America and Viet Nam (Ninh Co River from the North and Mekong Delta from the South) are reported in this publication (Table 1).

1.1. OBJECTIVES

(i) To identify ways to improve crop productivity and sustainability through water and salinity management.

(ii) To define approaches and technologies to assess and monitor soil water content and salinity at field and area-wide scales.

(iii) To reduce the impacts of climate change and variability on the widespread increase in landscape salinity.

1.2. CRP ACHIEVEMENTS AND CONCLUSIONS

1.2.1. Bangladesh

During the dry season, soil and water salinity increased with time and reached maximum values in April-May. Soil water content was reduced during the months of November-May, causing difficulties in growing cereal crops without irrigation water supply. Irrigation at 35% depletion of soil water content was found to be the most suitable strategy. Application of 100 kg gypsum per hectare along with the recommended dose of nitrogen, phosphorus and potassium (NPK), plus an additional amount of K (90 kg ha^{-1}) and N in 3 splits gave the highest yield, yield components and N fertilizer use efficiency. The tested wheat cultivars can be irrigated at 55% soil moisture depletion with irrigation water salinity of 3.0-6.0 dS m^{-1}. The AquaCrop model simulation study clearly showed a decreasing yield trend for wheat under increased salinity as well as with decreasing irrigation frequency. Good agreement was found between simulated and measured wheat yields.

1.2.2. China (CAAS)

Five treatments consisting of various combinations of fresh and saline water applied at three wheat growth stages (seedling, turning green-jointing, flowering-filling) were evaluated. Irrigating winter wheat with saline water at non-sensitive growth stages and freshwater at sensitive stages alleviated the salt stress on biomass accumulation and grain yield and acquired the higher biomass and grain yield among the five treatments. The best irrigation model for alternately irrigating winter wheat with fresh and saline water was irrigated with freshwater at the turning green-jointing stage and saline water at the flowering-filling stage, due to higher water use efficiency (WUE) and moderate yields of winter wheat in the North China Plain. There was a highly significant negative correlation between WUE and carbon isotope discrimination ($\delta^{13}C$, ‰) in leaf material. However, after saline water irrigation for a long-term (e.g. 30 years), flood irrigation with a large volume of water (100~150 mm) at intervals of 5~6 years is recommended in order to move salt in the root zone to deep soil layers to decrease the effects of soil salinization on crop growth and harvestable yield. AquaCrop model is a robust tool to predict crop productivity and salt accumulation of a wheat field irrigated alternately with saline and freshwater at different growth stages and is also used to assess the long-term effects on crop productivity and soil salinization.

1.2.3. China (CAU)

Water shortage and soil salinization increasingly become the main factors constraining sustainable agriculture in southern Xinjiang, China. Mulched drip irrigation, a water-saving irrigation method, has been widely applied in southern Xinjiang for cotton production. In order to evaluate the feasibility of two-dimensional model for simulating soil water and salt dynamics under mulched drip irrigation, numerical simulations employing planar 2-D and 3-D models were conducted and compared with field observations at Aksu, southern Xinjiang province. No significant difference was found between the planar 2-D and 3-D simulations for soil water flow, except for the early stage of an irrigation event. The planar 2-D model had a poorer performance in predicting the salt distribution in wide strip during the entire irrigation event. The soil water and salt contents simulated by the planar 2-D model, however, were close to the mean values between two adjacent emitters simulated by the 3-D model, and also coincided with the measurements with corresponding RMSE less than 0.040 $cm^3\ cm^{-3}$ and 2.27 $g\ kg^{-1}$, indicating that the planar 2-D model was reliable for field irrigation management. Subsequently, hypothetical numerical experiments were further performed considering different irrigation durations and emitter spacings. The results revealed that the planar 2-D model performed better at smaller emitter spacing for delineating soil water and salt transport processes under mulched drip irrigation, and the upper limit value of the emitter spacing suitable for the planar 2-D simulation increased with the prolonged irrigation duration. However, if the effect of solute reaction on retarding solute transport was obvious, the emitter spacing suitable for the planar 2-D simulation should relatively decrease.

1.2.4. Islamic Republic of Iran

The objectives of this study were to investigate the effect of different scenarios of irrigation (crop growth stages) on wheat yield, to separate evaporation (E) and transpiration (T) using isotopic techniques. Different soil moisture depletion levels had significant ($P < 0.001$) effects on wheat grain yield. The maximum harvest index occurred at 55% soil moisture depletion and the lowest HI% was observed at 75% soil moisture depletion. AquaCrop model successfully simulated grain yield and biomass in saline-sodic conditions with high accuracy. The highest yield loss was simulated in scenarios where saline water for irrigation was used at sowing, tilling and booting stages. Salinity stress at these stages is likely to affect leaf growth, tiller generation, canopy development and other crop traits which resulted in decreasing biomass production and final grain yield. The error of the model in simulating soil salinity is greater than that in simulating soil water content. The proportion of evaporation to total evapotranspiration was smaller when wheat was sown in early November. Adjusting planting date by AquaCrop model indicated that higher biomass and grain yield are likely to be obtained when winter wheat is sown in early November than in October possibly due to better crop canopy cover.

1.2.5. Republic of Korea

The 12-year continuous monitoring in a multi-species afforestation site established on degraded, highly salinized cropland shows that water availability does not preclude the afforestation due to effective utilization of shallow saline groundwater by trees. However, soil salinity increased significantly as the tree plantations matured under non-irrigated conditions, requiring occasional salt leaching at the plantation sites which therefore are not entirely independent of irrigation. Monitoring of foliar $\delta^{13}C$ appears promising for interpreting the relative salt tolerance among the tree species, given the consistent $\delta^{13}C$ variations for tree species and the responsiveness of $\delta^{13}C$ values to salt leaching. The efficient N_2-fixation by actinorhizal *Elaeagnus angustifolia* greatly contributed to self-sufficiency in nitrogen nutrition of the afforestation system under non-fertilized conditions. Including *E. angustifolia* as a nursing plant in tree plantations may assist in restoration of *Populus euphratica* dominated native riparian forests and in revegetation of degraded croplands. The ^{15}N natural abundance method allows quantification of biological nitrogen fixation in trees but the results need to be carefully interpreted considering the sampling material used (foliar or whole-plant), plant age, and reference species due to the confounding of ^{15}N signals during the successional changes in tree stands over time.

1.2.6. Pakistan

FAO's AquaCrop model was calibrated and evaluated to simulate the effect of irrigation water quality / strategies on barley yield and water use efficiency grown on saline soil in the semi-arid environment of Pakka Anna, Pakistan. The model was calibrated using two years (2016-17 and 2017-18) datasets measured from different combinations of soil and irrigation water salinity. The data of soil moisture (measured using soil moisture neutron probe), in-season biomass and canopy cover, biomass, grain yield at harvest and water use efficiency based on biomass and grain yield was used to calibrate the model. The calibrated model was then evaluated using three years (214-15, 2105-16 and 2016-17) independent datasets measured from the experiments involving saline soil and different irrigation regimes. Evaluation with the measured data showed that performance of the model was realistic as indicated by four independent parameters between measured and simulated values of soil moisture, biomass and grain yield at harvest. However, the performance was less satisfactory for high soil moisture stress applied to the crop grown under higher soil and irrigation water salinity.

1.2.7. United States of America

Several new technologies suitable for evaluation of field soil water contents including (i) time domain reflectometry (TDR) probes with pulse generation directly coupled to the electrodes (ii) prototypes of profiling soil water sensors based on directly-coupled TDR and

(iii) a cosmic ray neutron probe (CRNP) that senses background fast neutrons generated by cosmic rays as well as background thermal neutrons. Laboratory investigations of the directly-coupled TDR probes demonstrated that they can estimate soil water contents with accuracies of ≤ 0.03 m^3 m^{-3} at bulk electrical conductivities up to 2.5 to 3.0 dS m^{-1} in fine textured soils (clay ≤ 400 g kg^{-1}) with a soil specific calibration. In coarser textured soils, accurate estimation of soil water content using these sensors is feasible up to a bulk electrical conductivity of ~5 dS m^{-1}. The corresponding electrical conductivity of the pore water at saturation would range from 5 to 10 dS m^{-1}. Several prototypes of the profiling soil water sensor were designed, evaluated, and found to be satisfactory. However, the principal difficulty was achieving a structural design that could withstand the forces of installation while keeping manufacturing costs reasonable. The CRNP was evaluated during two seasons and found to respond positively to elevated near-surface atmospheric humidity and be sensitive only to water within a shallow soil depth (< 0.3 m). Consequently, the CRNP data would have little relevance for irrigation management for the field crops commonly grown in the Southern Great Plains. Field evaluations of arrays of EM sensors deployed at multiple depths demonstrated that sensed changes in stored profile water could resolve daily changes in evapotranspiration (ET) and correlated strongly with changes in storage determined with the neutron probe. This indicates the possibility that properly deployed EM sensors of the types used here could provide change in storage data accurate enough to determine ET from the soil water balance.

1.2.8. Viet Nam (Ninh Co River, North)

The stable isotopic signatures in water within the root zone of rice revealed that it originated from the Ninh Co River that irrigated the field, whereas the coastal tide did not affect the groundwater table beyond the root zone. Seawater did not intrude into the shallow aquifer in the study region. Under the traditional farming practice, the pattern of the variation of $\delta^{18}O$ in soil pore-water during the meteoric year was similar to those in the local rain water, but in between the two rice seasons the $\delta^{18}O$ soil in pore-water became more enriched compared to this signature during the cropping period. At the same time, the chloride concentration in water within the root zone did not change much within a wide range of the $\delta^{18}O$ variation, indicating the intensive evaporation of irrigation water under the traditional cultivation practice. An alternative irrigation practice including keeping the irrigation water in the field without burning straw after rice harvesting was investigated. The salinity in water within the root zone could diffuse downwards throughout the year by gravity, thus reducing the concentration of salinity in water in the cultivated soil layer. The new farming practice resulted in an increase in rice yield in the experimental field by up to 5%.

1.2.9. Viet Nam (Mekong Delta, South)

Soil salinization from sea water intrusion is a big threat for sustainable rice production in the coastal Mekong Delta of Vietnam. Two on-farm studies quantified the effectiveness of flushing salinity from paddy soil and identified strategies for rice production under salinity intrusion, by applying the $\delta^{18}O$ technique combined with hydro-geological and bio-economical methods. Soil desalinization using rainwater and evaporation strongly influenced salinity in the root zone of rice. Rainwater was the important source while irrigation canal water was not reliable for soil desalinization. Only about 40% of saltwater in the root zone was flushed out in the rainy season. Potassium and organic fertilizer application to rice highly facilitated flushing sodium from the root zone and improving rice yields.

TABLE 1.1. EXPERIMENTAL VARIABLES

Country	Location	Crops & years	Treatment variables	Models	Nuclear techniques
Bangladesh	Vatkhali, 22.33 ºN, 89.10 ºE	Wheat, 4 crops, 2013-17	Levels of N, split applications, irrigation and nutrient management, levels of salinity	AquaCrop[2]	^{15}N enriched urea
China (CAAS)	Hengshui, 37.54 ºN, 115.4 2ºE	Wheat, 2 crops. 2014-16	Water quality (saline/ non-saline/crop growth stage), deficit irrigation	AquaCrop	SMNP, $\delta^{13}C$ CID
China (CAU)	Aksu, 40°37′N, 80°45′E	Cotton, 2 crops, 2015, 2016	Drip irrigation level (3), wide and narrow spaced mulching,	COMSOL[3]	CRNP
Iran	Roudasht, 32º 29' N, 52º 10' E	5 wheat cultivars	3 levels of soil moisture depletion	AquaCrop	SMNP, $\delta^{18}O$
Korea	Khorezm, Uzbekistan; 41°65′ N, 60°62′ E	Afforestation species (3); 2003-14	Winter deciduous tree species including one actinorhizal	None	$\delta^{15}N$ BNF; $\delta^{13}C$ CID;
Pakistan	Pakka Anna, 73º05'E, 31º24'N	Barley, 4 crops, 2014-18	Soil moisture and combinations of soil and water salinity	AquaCrop	SMNP
USA	Bushland, TX; 35°1'N, 102°06'W; Albacete, Spain	Maize 2013; soybean 2017; garlic	Irrigation water management; soil water sensors	None	CRNP
Viet Nam (North)	Hai Thinh, Red River delta	Rice, 2 crops, 2015-17	Source of saline water (surface or sea-water)	None	$\delta^{18}O$, $\delta^{2}H$
Viet Nam (South)	3 sites, Mekong River delta	Rice, rotation with shrimp farming	Source of saline water, nutrient management	None	$\delta^{18}O$

[a] SMNP, soil moisture neutron probe; CID, carbon isotope discrimination; CRNP, cosmic ray neutron probe; BNF, biological nitrogen fixation

[2] http://www.fao.org/aquacrop/en/

[3] https://www.comsol.com/

2. LANDSCAPE SALINITY AND WATER MANAGEMENT IN COASTAL REGION OF BANGLADESH FOR IMPROVING AGRICULTURAL PRODUCTIVITY

M.E. UL HAQUE, M.H. ALI, M.S. MONDAL
Bangladesh Institute of Nuclear Agriculture
Mymensingh, Bangladesh

D. SAHA
Bangladesh University of Engineering and Technology
Dhaka, Bangladesh

S. PERVEEN
Bangladesh Agricultural University,
Mymensingh, Bangladesh

L.K. HENG
International Atomic Energy Agency
Vienna, Austria

Abstract

Field studies were carried out in the salinity affected area of Vatkhali in the Sathkhira district of Bangladesh for four years from 2013-14 to 2016-2017. In addition, a pot study was conducted at Mymensingh. Several irrigation and fertilizer management strategies were evaluated using wheat varieties as test crops. ^{15}N-labeled fertilizer studies were performed with different N rates and methods of applications. Soil amendments of gypsum and additional potassium (K) fertilizer were evaluated as conditioners for saline soil. Climate data were recorded in the field. Water and soil samples from several depth intervals were collected periodically and analyzed for salinity (electrical conductivity). Wheat grain and straw samples were harvested for dry matter; N concentration was measured to determine N yield, and ^{15}N enrichment determined to estimate N fertilizer recovery. Yield components were measured, and yields were simulated using the AquaCrop model.

During the dry season soil and water salinity increased with time and reaches maximum values in April-May. Soil water content was reduced during the months of November-May, causing difficulties in growing cereal crops without irrigation water supply. Irrigation at 35% depletion of soil water content was found to be the most suitable strategy. Application of 100 kg gypsum per hectare along with the recommended dose of NPK, plus an additional amount of K (90 kg ha^{-1}) and N in 3 splits gave the highest yield, yield components and N fertilizer use efficiency. The tested wheat cultivars can be irrigated at 55% soil moisture depletion with irrigation water salinity of 3.0-6.0 dS m^{-1}.

The AquaCrop model simulation study clearly showed a decreasing yield trend for wheat under increased salinity as well as with decreasing irrigation frequency. Good agreement was found between simulated and measured wheat yields.

2.1. INTRODUCTION

Bangladesh is a deltaic country with a coastal region of 29 000 km^2 (about 20% of the land area of the country), which covers more than 30% of the cultivable land. Of the 1.689 Mha of coastal lands, about 1.056 Mha are adversely affected by varying degrees of soil salinity [1], and due to climate change the area is increasing at an alarming rate, which was estimated as 2.83 Mha of saline land during 2011. Hence, soil salinity is a major, and the most persistent, threat to irrigated agriculture in many deltas, such as in coastal Bangladesh [2]. To bring the vast salt affected land of Bangladesh under year-round cultivation for increasing crop production, proper landscape planning for salinity management along with water management practices is the prime need in Bangladesh agriculture. Therefore, a landscape salinity plan along with water management strategies are needed with a detailed multidimensional and simultaneous study on monitoring the salinity status (both from soil and water), soil water content, availability of quality irrigation water, and a feasibility study of freshwater from different sources and landscape planning to synchronize the best fit management practices with salt tolerant crop varieties, especially wheat.

Wheat is an important cereal crop in most dry regions of the world, and it is characterized as being moderately tolerant to salinity [3]. Careful fertilizer and water management are also essential on such soils to get sustainable yields. The major constraints under saline agriculture are the availability of essential nutrients and water to the plant, which are adversely affected by excessive salts in the soil solution. Among the essential plant nutrients, N plays a key role in plant growth and productivity. To take up N from the soil solution, plants compete with a range of N removal processes/losses including immobilization, leaching, and gaseous emissions of N as ammonia (NH_3), nitrous oxide (N_2O), nitric oxide (NO) and molecular nitrogen (N_2) into the atmosphere. Because of these N losses, the N use efficiency (kg of dry matter produced per kg of N applied) or the useful use of N by the plant is invariably less than 50% of the applied N [4–6]. The extent to which N is removed from soils or made unavailable to plants by the above biogeochemical processes is of both economic and environmental importance. Quantifying N use efficiency and the sources of N losses enables researchers to develop 'technology packages' which can enhance N uptake and minimize N losses, thus allowing for sustainable crop productivity under saline conditions.

The AquaCrop model is widely used for simulating crop yield under different field and climatic conditions and has been parameterized and tested on a number of cereal and non-cereal crops worldwide [7–17]. The results from the model worldwide showed that AquaCrop can be a vital tool to improve water productivity and crop yields under arid and semi-arid climatic conditions by promoting sustainable management options. Using the salinity module of this model, the yields of wheat obtained from the experimental data of the above mentioned project were simulated to determine the consistency of yields with the experiments and to assess the performance of the AquaCrop model in simulating yield response of wheat in different field conditions.

The present study was undertaken i) to assess and monitor the soil water content and salinity level on yield at an area-wide scale, ii) to identify the way of improving crop productivity through water, nitrogen and salinity management and iii) to evaluate the performance of the AquaCrop model in simulating dry season wheat yields with saline irrigation water.

2.2. MATERIALS AND METHODS

2.2.1. Impact of nitrogen level and split applications on wheat production using ^{15}N tracer (2013-14)

^{15}N isotope-aided field experiments were conducted on the effect of different levels of N with different split applications on wheat during the winter season of 2013-14. The experiments were conducted in the farmers field at Vatkhali (22.33ºN, 89.10ºE), Satkhira district, in the southern part of Bangladesh, and the test variety of wheat was Barigom 25. Three treatments were assigned in a RCBD with 3 replications i) N_1 = Application of 50 kg N ha^{-1}; ii) N_2 = Application of 100 kg N ha^{-1} and iii) N_3 = Application of 150 kg N ha^{-1}. For the isotopic study, ^{15}N labelled urea was applied in the micro-plot. Each plot was divided into two parts, a) Yield plot (3 m × 4 m) and b) sampling plot (3 m × 4 m). Each sampling plot consist of two isotope micro plots, a) one micro-plot (1 m × 1 m) was used for ^{15}N application in two splits and b) the 2nd micro-plot (1 m × 1 m) was used for ^{15}N application in three splits. Each micro-plot was surrounded by an iron sheet (inserted into the soil up to 15 cm depth) for prevention of N loss by horizontal seepage. The ^{15}N urea was applied into two ways, for micro-plot A, two splits: i) ⅓ N as a basal dose after final land preparation, ii) ⅔ N as top-dressing during the crown root initiation stage (CRI) and for micro-plot B, three splits: i) ⅓ N as a basal dose after final land preparation, ii) ⅓ N as a top-dressing during the crown root initiation stage (CRI) and iii) ⅓ N as a top-dressing during the flowering / anthesis stage. Normal N fertilizer was applied (same amount and same time of ^{15}N) into the yield plot and the rest of the sampling plot. Wheat seeds were sown on the 15th December 2013 and the harvest was completed on 8th April 2014. During harvest, the data for yield and yield components were recorded and analyzed statistically.

2.2.2. Effect of irrigation and nutrient management strategies on wheat production in saline soil (2014-15)

A field experiment was conducted to evaluate the effect of irrigation and nutrient management strategies on wheat production in the saline area at Vatkhali (22.33ºN, 89.10ºE), Satkhira district, in the southern part of Bangladesh, during the winter season of 2014-15. Wheat seeds were sown on the 25th November 2014 and harvest was completed on 16th March 2015. The treatments were assigned in a RCBD split-plot design which included four irrigation strategies as the main plot treatments i) I_1: Irrigate the plot at 35% soil moisture depletion from PAW; ii) I_2: Irrigate the plot at 55% soil moisture depletion from PAW; iii) I_3: Irrigate the plot at 75% soil moisture depletion from PAW and iv) I_4: Irrigate the plot as farmer practice (2 flood irrigations). Two nutrient management practices were tested as subplot treatments i) T_1: application of fertilizer (N, P, K, S, Zn etc.) according to STB (Soil Test Basis) and ii) T_2: T_1 + addition of gypsum @ 190 kg ha^{-1}. Soil salinity status of the experimental plots was determined at different dates up to wheat harvest. During harvest, the data for yield and yield components were recorded and analyzed statistically.

2.2.3. Effects of irrigation strategies on wheat production under levels of salinity (2015-16)

Two experiments (pot and field study) were conducted with wheat to observe the effect of different irrigation strategies under different salinity levels during the year 2015-16. The field experiment was carried out in the farmers field at Vatkhali in the Satkhira district. The test variety was BARIghom-25. Ten irrigation treatments were assigned following the RCBD design, with 3 replications, such as - T_1 = Farmers practice with 3 dS m^{-1} saline water (2 irrigations at 30 and 50 DAS); T_2 = Irrigation at 35% depletion of PAW with 3 dS m^{-1} saline water; T_3 = Irrigation at 35% depletion of PAW with 6 dS m^{-1} saline water; T_4 = Irrigation at 35% depletion of PAW with 9 dS m^{-1} saline water; T_5 = Irrigation at 55% depletion of PAW with 3 dS m^{-1} saline water; T_6 = Irrigation at 55% depletion of PAW with 6 dS m^{-1} saline water; T_7 = Irrigation at 55% depletion of PAW with 9 dS m^{-1} saline water; T_8 = Irrigation at 75% depletion of PAW with 3 dS m^{-1} saline water; T_9 = Irrigation at 75% depletion of PAW with 6 dS m^{-1} saline water and T_{10} = Irrigation at 75% depletion of PAW with 9 dS m^{-1} saline water. The wheat seeds were sown on December 7, 2015 and harvested on March 20, 2016. All cultural practices (e.g. weeding, thinning, insecticide spray) were done when needed. Soil moisture and salinity data were monitored at 10-day intervals. The irrigation treatments were imposed according to the schedule. Yield and yield parameters were recorded at harvest time.

Similarly, a pot experiment was conducted at BINA Head-quarter, Mymensingh, following a RCBD with split-plots and two replications. The main plot consisted of ten irrigation strategies as in the field study with two wheat varieties, L-880-43 and BARIghom-25. The seeds were sown on November 26, 2015 and harvested on March 9, 2016. All cultural practices (e.g. weeding, thinning, insecticide spray) were done when needed. Soil moisture and salinity data were monitored at 10-day intervals. The irrigation treatments were imposed according to the schedule. Yield and yield parameters were recorded at harvest time.

2.2.4. Effect of soil amendments and N fertilizer application on the growth and yield of wheat in saline soil (2016-17)

Field experiments were conducted to evaluate the effect of soil amendments and N fertilizer application on the growth and yield of wheat in saline soil during the year 2016-2017 at Satkhira, Bangladesh. Seven treatments were assigned : T_1 = recommended dose of N, P and K + application of gypsum @ 150 kg ha^{-1} and N application in 3 splits, T_2 = recommended dose of N, P and K + application of gypsum @ 150 kg ha^{-1} and N application in 2 splits, T_3 = recommended dose of N, P and K + additional application of K @ 120 kg ha^{-1} and N application in 3 splits, T_4 = recommended dose of N, P and K + additional application of K @ 120 kg ha^{-1} and N application in 2 splits, T_5 = recommended dose of N, P and K + additional application of K @ 90 kg ha^{-1} + application of gypsum @ 100 kg ha^{-1} and N application in 3 splits, T_6 = recommended dose of N, P and K + additional application of K @ 90 kg ha^{-1} + application of gypsum @ 100 kg ha^{-1} and N application in 2 splits and T_7 = only recommended dose of N, P and K (following Fertilizer Guide) and N application in a single dose. The treatments were arranged in a RCBD with 3 replications. For all treatments P and K fertilizers were applied @ 20 and 50 kg ha^{-1}, respectively. In the case of N fertilizer, urea was applied in splits according to the treatment descriptions. Regarding the isotopic study, a similar amount of ^{15}N-labelled urea (5.15 atom % ^{15}N excess) was applied in micro plots (1 m × 1 m). The other soil amendments such as gypsum and K were applied following the treatment descriptions.

2.2.5. Simulation of wheat yield in saline soil using the AquaCrop Model (2015-16 and 2016-17)

Field experiments were conducted with wheat variety Barigom-25 at BINA farm in Mymensingh and also in the Satkhira district of the south-west coastal region of Bangladesh during the dry season of 2015-2016 and 2016-2017. The experiments were conducted with three levels of irrigation water salinity and three irrigation water application strategies which were assembled in ten treatments. The first treatment (T_1) was farmers irrigation practice with a water salinity of 3 dS m^{-1} throughout the growth season. The second, third and fourth treatments (T_2, T_3 and T_4) were with irrigation water salinity of 3, 6 and 9 dS m^{-1}, respectively with irrigation at 35% depletion of PAW. The T_5, T_6 and T_7 treatments were with same salinity but irrigated at 55% depletion of PAW. The rest of the treatments, T_8, T_9 and T_{10} were also with same salinity and 75% depletion of PAW.

2.2.5.1. Data incorporation in the model

In the climate component of the AquaCrop model, climate data were incorporated for calculation of the evaporative demand of the atmosphere, i.e., reference crop evapotranspiration (ETo), in the 'ETo Calculator' software [3]. Using the ETo values, rainfall and temperature data, a climate file was created in the AquaCrop model.Then other crop, soil and management data were incorporated in the components of the model. Most of the required data were collected from the field investigations during the growth period of wheat. Measured data in the field that were incorporated in the model included initial and maximum canopy covers, maximum rooting depths, days to maximum canopy, senescence, maturity and harvesting, days to build up harvest index, duration of flowering, irrigation events and irrigation water salinity for each treatment and field condition, groundwater depth and salinity, initial soil salinity etc. Relevant conservative data for the model were obtained from the crop library of AquaCrop and its Reference Manual [18].

2.2.5.2. Model calibration and validation

After collection of necessary primary and secondary data, these were incorporated in different components of the AquaCrop model for calibration and validation. The model was first calibrated with treatment T_2 and then validated with the other nine treatments.

2.3. RESULTS AND DISCUSSION

2.3.1. Impact of nitrogen level and split applications on wheat production using ^{15}N tracer (2013-14)

2.3.2. N levels

Different levels of nitrogen fertilizer significantly affected the grain yield of wheat grown at Satkhira (Fig. 2.1). The highest grain yield was observed in the N_3 treatment (3.65 t ha^{-1}), where 150 kg N ha^{-1} was applied and was not significantly different from treatment N_2 (3.50 t ha^{-1}). The minimum grain yield was recorded in N_1 (2.46 t ha^{-1}), where only 50 kg N ha^{-1} was applied. In the case of wheat straw, there was no significant difference among the different N levels.

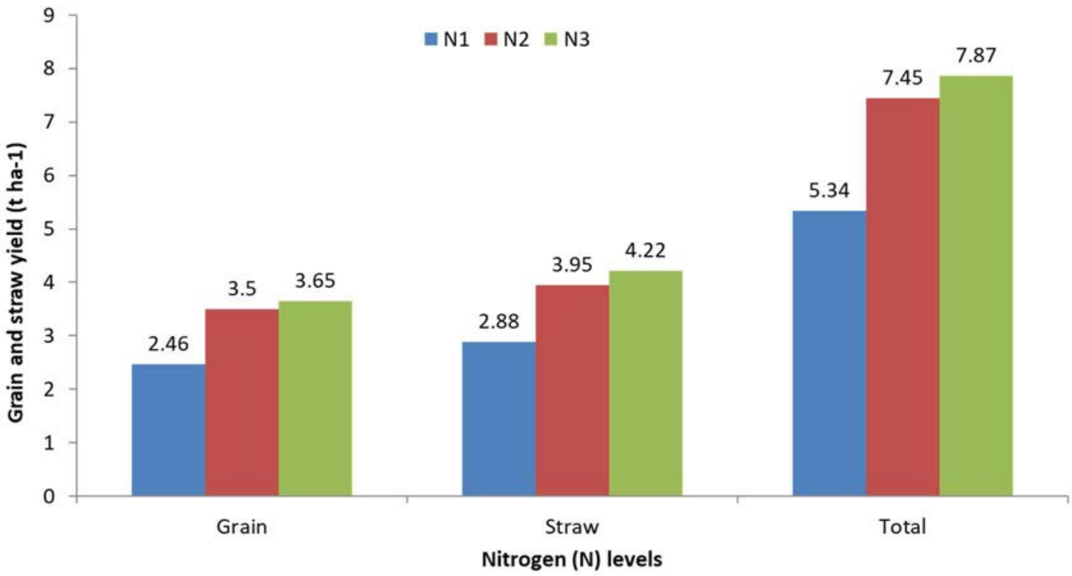

FIG.2.1. Effect of different nitrogen levels on the grain and straw yield (t ha^{-1}) of wheat during 2013-14. N_1, N_2, N_3 = 50, 100 and 150 kg N ha^{-1}, respectively.

2.3.3. ^{15}N enrichment and % N derived from fertilizer and soil

Nitrogen derived from fertilizer (Ndff), nitrogen derived from soil (Ndfs), nitrogen yield and fertilizer N recovery are shown in Table 2.1. Among the different N levels and their spilt applications, the average maximum amount of Ndff was observed as 16.3 kg ha^{-1} in wheat grain in the N_3 treatment. Due to split applications of N fertilizer, the amount of Ndff varied even for same dose, i.e. 12.8 and 20.5 kg ha^{-1} in the treatment N_3A and N_3B, respectively (Table 2.2). Under the treatment N_3B, the N fertilizer was applied in three splits and the Ndff value (20.5 kg ha^{-1}) was comparatively 63% higher than the value of 12.8 kg ha^{-1} for the treatment N_3A, where N was applied in two splits. In the case of wheat straw, similar trends were observed (Table 2.3).

TABLE 2.1. EFFECT OF RATE AND METHOD OF N APPLICATION ON ^{15}N ENRICHMENT AND N DERIVED FROM FERTILIZER IN WHEAT GRAIN AND STRAW DURING 2013-14

Treatment	^{15}N enrichment (atom % excess)		N derived from fertilizer (%) in	
	Grain	Straw	Grain	Straw
N_1A	1.758	1.354	16.8	13.0
N_1B	2.145	2.214	20.5	21.2
N_2A	1.957	1.906	18.7	18.2
N_2B	2.579	2.487	24.7	23.8
N_3A	1.805	1.754	17.3	16.8
N_3B	2.674	2.684	25.6	25.7

[a] N_1A, 50 kg N ha^{-1} in 2 splits; N_1B, 50 kg N ha^{-1} in 3 splits; N_2A, 100 kg N ha^{-1} in 2 splits; N_2b, 100 kg N ha^{-1} in 3 splits; N_3A, 150 kg N ha^{-1} in 2 splits; N_2B, 150 kg N ha^{-1} in 3 splits

TABLE 2.2. EFFECT OF RATE AND METHOD OF N APPLICATION ON N CONCENTRATION, N YIELD, N DERIVED FROM FERTILIZER AND FROM SOIL IN WHEAT GRAIN DURING 2013-14

Treatment	N concentration ($g\ kg^{-1}$)	N yield ($kg\ ha^{-1}$)	N ($kg\ ha^{-1}$) derived from	
			Fertilizer	Soil
N_1A	17.8	43.8	7.4	36.4
N_1B	20.2	49.7	10.2	39.5
N_2A	19.2	67.1	12.6	54.5
N_2B	21.8	76.2	18.8	57.4
N_3A	19.3	70.5	12.2	58.3
N_3B	21.9	80.0	20.5	59.6

[a] N_1A, 50 kg N ha^{-1} in 2 splits; N_1B, 50 kg N ha^{-1} in 3 splits; N_2A, 100 kg N ha^{-1} in 2 splits; N_2b, 100 kg N ha^{-1} in 3 splits; N_3A, 150 kg N ha^{-1} in 2 splits; N_2B, 150 kg N ha^{-1} in 3 splits

TABLE 2.3. EFFECT OF RATE AND METHOD OF N APPLICATION ON N CONCENTRATION, N YIELD, N DERIVED FROM FERTILIZER AND FROM SOIL IN WHEAT STRAW DURING 2013-14

Treatment	N concentration ($g\ kg^{-1}$)	N yield ($kg\ ha^{-1}$)	N ($kg\ ha^{-1}$) derived from	
			Fertilizer	Soil
N_1A	2.4	6.9	0.9	6.0
N_1B	3.1	8.9	1.9	7.0
N_2A	2.7	10.7	2.0	8.7
N_2B	4.5	17.8	4.2	13.6
N_3A	3.2	13.5	2.3	11.2
N_3B	4.7	19.8	5.1	14.7

[a] N_1A, 50 kg N ha^{-1} in 2 splits; N_1B, 50 kg N ha^{-1} in 3 splits; N_2A, 100 kg N ha^{-1} in 2 splits; N_2b, 100 kg N ha^{-1} in 3 splits; N_3A, 150 kg N ha^{-1} in 2 splits; N_2B, 150 kg N ha^{-1} in 3 splits

Considering total values (grain plus straw), total N uptake, Ndff and Ndfs were highly influenced by the different levels of N with their split applications (Fig. 2.2). When N was applied in 3 splits, the total N uptake by wheat was comparatively higher than the N uptake in 2 splits. Due to the different treatment and split application system, the maximum total nitrogen uptake (mean value) by wheat was observed as 99.8 kg ha^{-1} under the N_3B treatment, where 150 kg N ha^{-1} was applied in 3 equal splits. The minimum total N uptake was found as 50.7 kg ha^{-1} in the N_1A treatment, where N was applied as 50 kg ha^{-1} in 2 splits. The maximum amount of TNdff was observed in the N_3B treatment (25.6 kg ha^{-1}). It was observed that, due to 3 split application of N fertilizer, the N uptake by wheat from the fertilizer sources increased in all treatments. Similarly, the highest and lowest value of TNdfs were observed as 74.3 and 42.4 kg ha^{-1} under the treatments N_3B and N_1A, respectively (Fig. 2.2). Fertilizer N recovery (%) in wheat (kg ha^{-1}) affected by different nitrogen level × split application at Satkhira are summarized in Fig. 2.3.

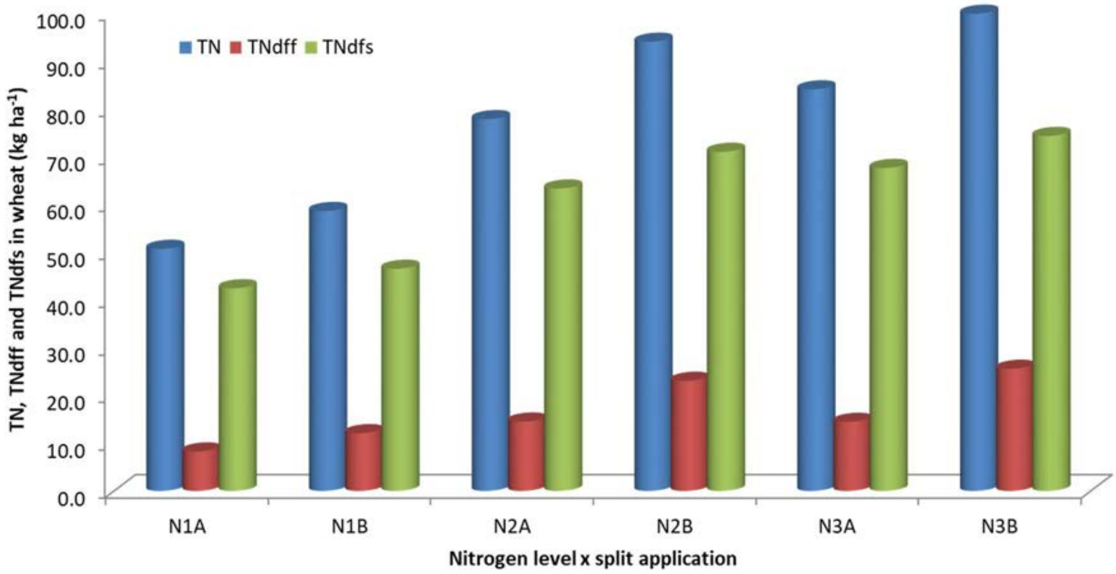

FIG. 2.2. TN, TNdff and TNdfs in wheat (kg ha^{-1}) affected by different nitrogen level x split application in 2013-14. N_1A = 50 kg N ha^{-1} applied in two splits; N_1B = 50 kg N ha^{-1} applied in three splits; N_2A = 100 kg N ha^{-1} applied in two splits; N_2B = 100 kg N ha^{-1} applied in three splits; N_3A = 150 kg N ha^{-1} applied in two splits; N_3B = 150 kg N ha^{-1} applied in three splits; TN = total N; TNdff = total N derived from fertilizer; TNdfs = total N derived from soil.

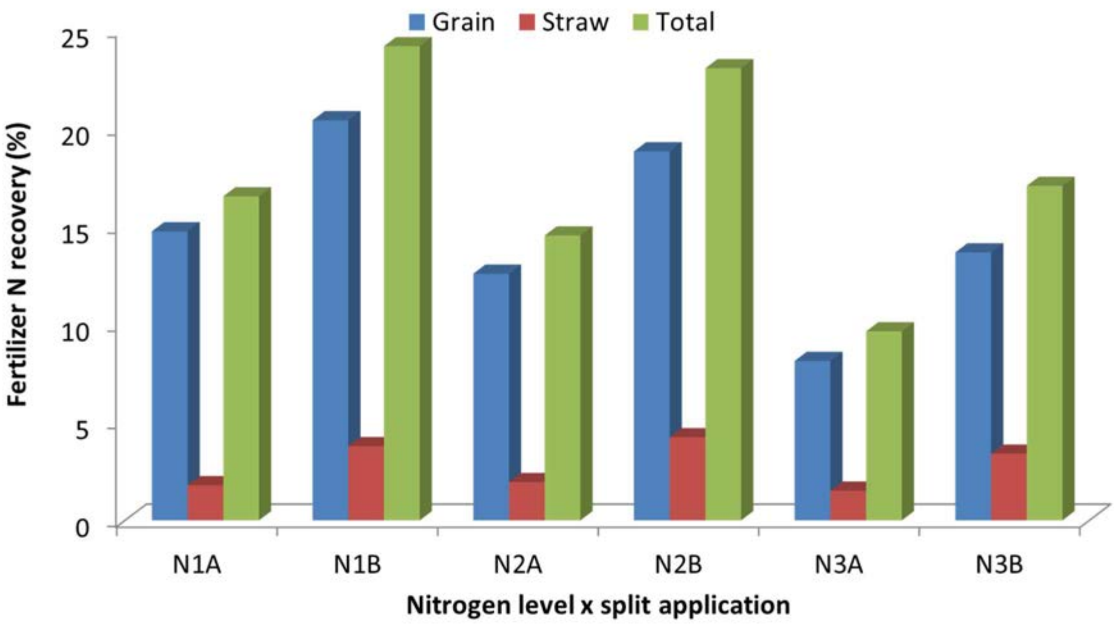

FIG. 2.3. Fertilizer N recovery (%) in wheat (kg ha^{-1}) affected by different nitrogen level x split application in 2014-15. N_1A = 50 kg N ha^{-1} applied in two splits; N_1B = 50 kg N ha^{-1} applied in three splits; N_2A = 100 kg N ha^{-1} applied in two splits; N_2B = 100 kg N ha^{-1} applied in three splits; N_3A = 150 kg N ha^{-1} applied in two splits; N_3B = 150 kg N ha^{-1} applied in three splits.

2.3.4. Effect of irrigation and nutrient management strategies on wheat production under soil salinity (2014-15)

2.3.4.1. Weather data

During the experimental period (November 2014 to March 2015) different weather parameters such as – maximum, minimum and average daily temperature (°C), daily rainfall (mm), bright sunshine hours and relative humidity (%) etc. were collected from the nearby weather sub-station at Satkhira, which are given in Fig. 2.4.

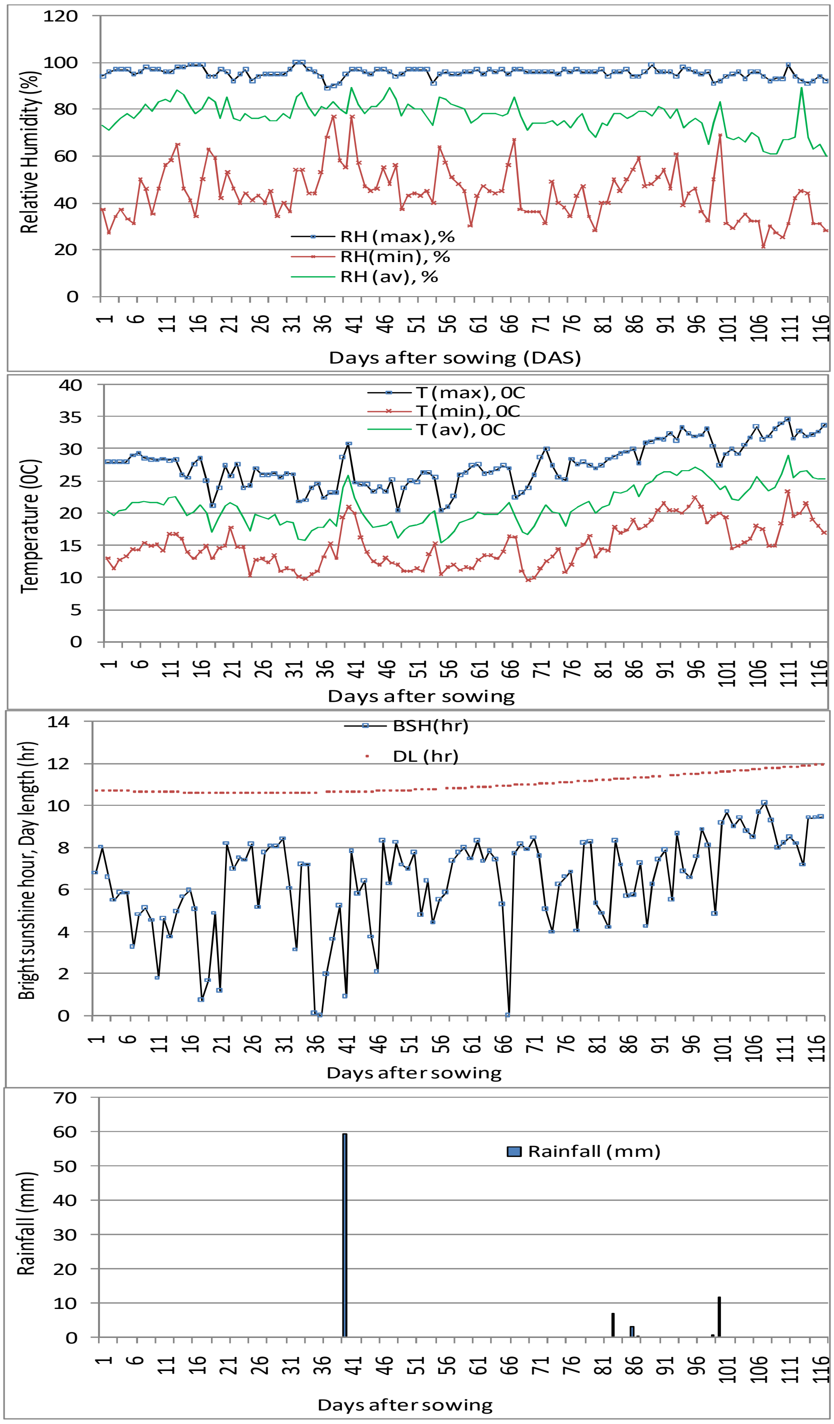

FIG. 2.4. Weather (daily basis) of the experimental area during the wheat growing period. T = temperature (°C); RH = relative humidity (%); BSH = bright sunshine hours; DL = day length.

The average relative humidity ranged from 60 to 89%, average temperature ranged from 15.5 to 29 ºC, and the bright sunshine duration mostly ranged from 7 to 9 hour against day-length of 10.6 to 12 hour. There was a substantial amount of rainfall at day 39 after sowing (59 mm).

2.3.4.2. Soil salinity status

Soil samples collected from the experimental plots at different dates from wheat sowing up to harvest were analyzed for soil salinity (dS m^{-1}). Soil salinity status affected by irrigation strategies at different soil depth intervals at different dates are presented in Table 2.4. Initially (during November at wheat sowing) the salinity level was lower (ranged from 1.1 to 2.1 dS m^{-1}) and gradually increased up to 8.1 dS m^{-1} at harvest.

TABLE 2.4 EFFECT OF IRRIGATION STRATEGY ON THE TIME COURSE OF SOIL SALINITY (DS M^{-1}) AT THREE DEPTH INTERVALS DURING 2014-15

Irrigation[a]	Depth (cm)	25/11/14	14/12/14	27/12/14	25/01/15	6/02/15	26/02/15	16/03/15
I_1	0-15	1.5	1.7	3.6	4.4	6.7	6.9	7.8
	15-30	1.8	2.5	3.8	4.0	5.3	6.1	6.7
	30-45	1.7	2.5	3.4	3.9	5.5	6.1	6.0
I_2	0-15	1.8	3.5	4.0	4.7	6.7	6.9	8.1
	15-30	1.4	3.2	4.1	4.3	6.1	6.0	7.2
	30-45	2.1	1.3	3.3	3.8	5.1	6.5	6.6
I_3	0-15	1.6	3.7	4.6	5.3	7.1	7.1	8.0
	15-30	1.1	2.8	3.9	4.1	6.4	6.2	7.3
	30-45	1.7	3.4	4.1	3.8	6.1	6.0	7.3
I_4	0-15	1.6	3.2	4.3	6.7	7.3	6.6	8.1
	15-30	2.1	3.1	3.8	4.4	5.6	6.7	7.3
	30-45	1.1	3.1	3.6	4.6	6.1	6.7	6.8

[a] I_1, 35% soil moisture depletion from field capacity (SMD); I_2, 55% SMD, I_3, 75% SMD; I_4, farmer flooding practice

2.3.4.3. Irrigation strategies

The mean effect of different irrigation strategies significantly influenced the yield and yield components of wheat with some exceptions (Table 2.5 and Fig. 2.5). The maximum value of plant height was observed under the irrigation treatment I_1 (89.9 cm), where irrigation was maintained at 35% moisture depletion from the field capacity moisture content. This result was statistically identical (87.9 cm) with the irrigation treatment I_4, which was practiced by farmers.

The number of tillers per plant, spike length and number of grains per spike were not significantly different among treatments. Considering the grain and straw yield of wheat, the highest results were found under I_1 treatment as 3.74 and 4.58 t ha^{-1} and the lowest yield of 3.21 and 3.57 t ha^{-1} were found under the I_2 treatment.

TABLE 2.5 EFFECT OF IRRIGATION STRATEGY ON THE YIELD COMPONENTS OF WHEAT DURING 2014-15

Treatment[a]	Dimension (cm)		Number		1000 grain weight (g)
	Plant height	Spike length	Tillers $plant^{-1}$	Grains $spike^{-1}$	
I_1	89.9	9.3	7.1	45.3	42.9
I_2	83.7	8.8	6.5	43.4	45.1
I_3	81.7	7.8	5.7	44.0	44.4
I_4	87.9	9.2	6.4	45.1	43.7
CV (%)	3.8	10.9	5.3	4.2	9.5
Significance[b]	*	ns	ns	ns	*

[a] I_1, 35% soil moisture depletion from field capacity (SMD); I_2, 55% SMD, I_3, 75% SMD; I_4, farmer flooding practice[b] *, $P < 0.05$; ns, not significant

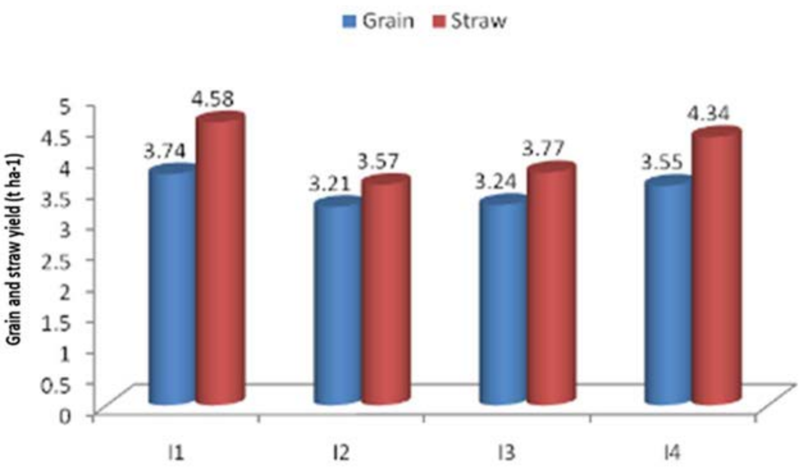

FIG. 2.5. Mean effect of different irrigation approaches on the grain and straw yield (t ha^{-1}) of wheat during 2014-15. I_1 = Irrigation at 35% soil moisture depletion from FC; I_2 = Irrigation at 55% soil moisture depletion from FC; I_3 = Irrigation at 75% soil moisture depletion from FC; I_4 = Irrigation as farmer practices (4 flooding irrigations).

2.3.5. Nutrient management

The mean effect of nutrient management on the growth and yield of wheat at Satkhira during 2014-15 is shown in Table 2.6. Comparatively, the higher values of plant height, number of tillers per plant and spike length, were observed as 87.1 cm, 7.0 tillers per plant and 9.1 cm under the treatment T_2, where additional gypsum (190 kg ha^{-1}) was added with the recommended dose of fertilizer based on STB. The maximum grain and straw yields of wheat were also recorded under the same treatment T_2, and here the yields were 3.72 and 4.44 t ha^{-1} for grain and straw, respectively.

TABLE 2.6 EFFECT OF FERTILIZER MANAGEMENT STRATEGY ON THE YIELD AND YIELD COMPONENTS OF WHEAT DURING 2014-15

Treatment[a]	Dimension (cm)		Number		1000 grain weight (g)	Yield (t ha^{-1})	
	Plant height	Spike length	Tillers $plant^{-1}$	Grains $spike^{-1}$		Grain	Straw
T_1	84.5 b	8.5 b	5.8 b	44.7	43.4 b	3.2 b	3.7 b
T_2	87.1 a	9.1 a	7.0 a	44.2	44.7 a	3.7 a	4.4 a
CV (%)	3.8	5.3	10.9	4.2	9.3	7.5	6.9
Significance[b]	*	*	*	ns	*	*	*

[a] T_1, application of N, P and K fertilizer according to STB; T_2, T_1 + addition of gypsum @ 190 kg ha^{-1}
[b] *, $P < 0.05$; ns, not significant; Data within a column followed by different lower-case letters are significantly different

2.3.5.1. Interaction of irrigation and nutrient management strategies

The interaction of irrigation and nutrient management strategies significantly influenced the yield and yield components of wheat (Table 2.7). The tallest wheat plant was found under the treatment combination of $I_1 \times T_2$ (90.9 cm), which was statistically similar with the treatments $I_4 \times T_2$ (89.2 cm), $I_1 \times T_1$ (89.0 cm), $I_4 \times T_1$ (86.9 cm) and $I_2 \times T_2$ (85.5 cm). Similarly, the maximum tiller number per plant and spike length were recorded under the same treatment combination as 7.6 and 9.7 cm, respectively. In the case of grain and straw yield, similar trends were observed and the highest yields of 4.01 and 4.83 t ha^{-1} were from the treatment combination $I_1 \times T_2$, respectively (Fig. 2.6).

TABLE 2.7 INTERACTIONS OF IRRIGATION AND NUTRIENT MANAGEMENT STRATEGIES ON THE YIELD AND YIELD COMPONENTS OF WHEAT DURING 2014-15

Treatment[a]	Dimension (cm)		Number		1000 grain weight (g)
	Plant height	Spike length	Tillers $plant^{-1}$	Grains $spike^{-1}$	
$I_1 \times T_1$	89.0 ab	8.9 a-c	6.5 c	46.3 a	41.4
$I_1 \times T_2$	90.9 a	9.7a	7.6 a	44.3 ab	44.5
$I_2 \times T_1$	82.0 cd	8.6 bc	5.9 d	44.1 ab	44.6
$I_2 \times T_2$	85.5 a-d	9.1 ab	7.1 b	42.8 b	45.7
$I_3 \times T_1$	80.4 d	7.6 d	5.4 e	43.0 ab	44.0
$I_3 \times T_2$	83 b-d	8.0 b-d	5.9 d	45.0 ab	44.8
$I_4 \times T_1$	86.9 a-c	8.7 bc	5.5 e	45.4 ab	43.5
$I_4 \times T_2$	89.2 a	9.7 a	7.4 ab	44.9 ab	43.9
CV (%)	3.8	5.3	10.9	4.2	
Significance[b]	*	*	*	*	ns

[a] I_1, 35% soil moisture depletion from field capacity (SMD); I_2, 55% SMD, I_3, 75% SMD; I_4, farmer flooding practice; T_1, application of N, P and K fertilizer according to STB; T_2, T_1 + addition of gypsum @ 190 kg ha^{-1}
[b] *, $P < 0.05$; ns, not significant; Data within a column followed by different lower-case letters are significantly different

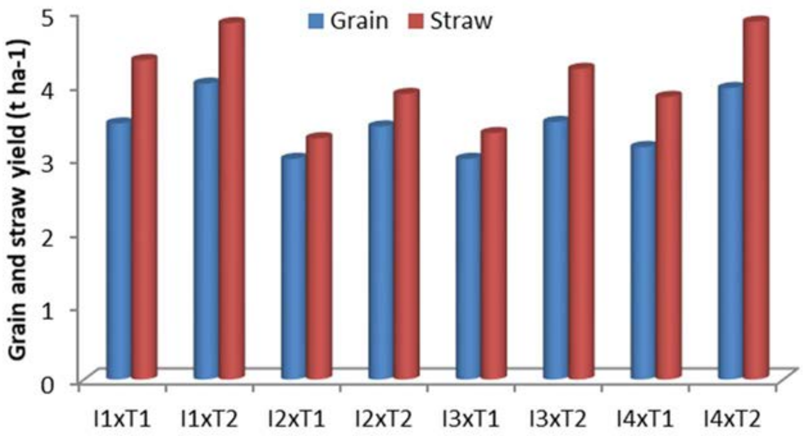

FIG. 2.6. Interaction effect of different irrigation and fertilizer management strategies on the grain and straw yield of wheat during 2014-15. I_1 = Irrigation at 35% soil moisture depletion from FC; I_2 = Irrigation at 55% soil moisture depletion from FC; I_3 = Irrigation at 75% soil moisture depletion from FC; I_4 = Irrigation as Farmer Practices (4 Flooding irrigations); T_1, application of N, P and K fertilizer according to STB; T_2, T_1 + addition of gypsum @ 190 kg ha^{-1}.

2.3.5.2. Soil moisture monitoring, irrigation scheduling, total water used and water productivity

Soil moisture was monitored in the experimental wheat field at different times for proper irrigation scheduling, for determination of the quantity of irrigation water needed for wheat growth and also to calculate the water productivity for wheat production. Soil moisture fluctuations under different irrigation treatments during the wheat growing period are clearly depicted in Fig. 2.7. The irrigation water requirement, total growing season ET, grain yield and irrigation water productivity are summarized in Table 2.8. The traditional farmer's practice produced statistically identical yield with 35% depletion of plant available soil-water (I_1). The treatment I_3, irrigation at 75% depletion of plant available soil-water, showed higher irrigation-water productivity of 873 and 748 kg ha^{-1} cm^{-1}, i.e. here irrigation water was used effectively but with lower yield. The traditional practice or irrigation at 35% depletion can be chosen as a preliminary result, however, this is in need of confirmation.

2.3.6. Effects of irrigation strategies on wheat production under soil salinity (2015-16)

The rainfall distribution during the cropping period is depicted in Fig. 2.8. A significant amount of rainfall occured during 79 to 82 days after sowing. The pattern of soil salinity throughout the growing season under different treatments are depicted in Fig. 2.9-2.10. The mean effects of irrigation treatments on yield parameters and grain yield are presented in Table 2.9. The treatments showed nonsignificant difference in yield parameters except for 1000 grain weight. The grain yield and straw yield also showed nonsignificant difference. At 55% depletion of soil moisture, the yield was reasonable for all tested salinity levels, although decreasing trend with increasing salinity. The frequency of irrigation and amount under different treatments are given in Table 2.10. The crop water use, water productivity, and irrigation water productivity under different treatments are summarized in Table 2.11. The water productivity showed the highest value in the T_5 treatment. The results of yield, irrigation water and salinity level, suggest that the tested cultivar can be irrigated at 55% soil moisture depletion and with irrigation water salinity of 3.0-6.0 dS m^1.

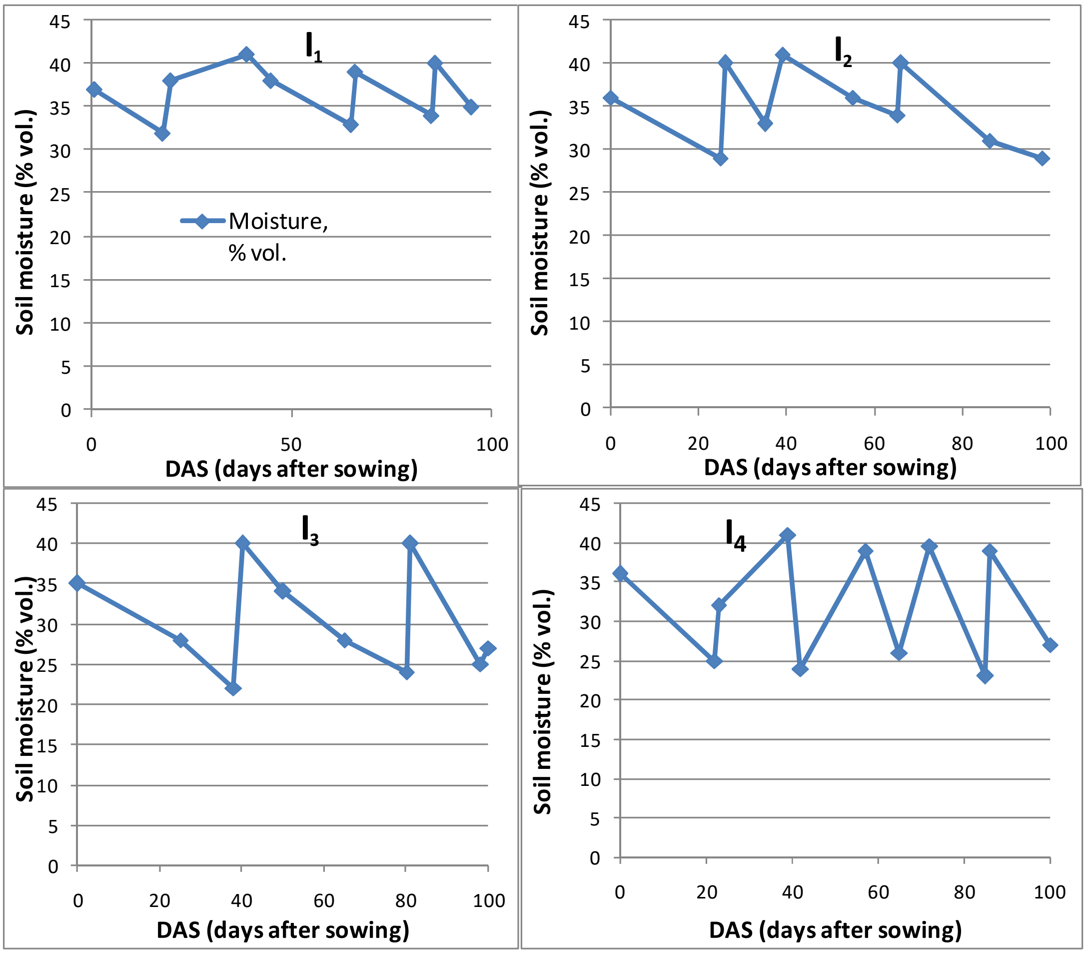

FIG. 2.7. Soil moisture under different treatments during the wheat growing period. I_1 = Irrigation at 35% soil moisture depletion from FC; I_2 = Irrigation at 55% soil moisture depletion from FC; I_3 = Irrigation at 75% soil moisture depletion from FC; I_4 = Irrigation as farmer practices (4 flooding irrigations).

2.3.7. Effect of soil amendments and nitrogen fertilizer application on the growth and yield of wheat in saline soils of Bangladesh (2016-17)

2.3.7.1. Weather data

During the experimental period (30 November 2016 to 26 March 2017) different weather parameters such as maximum and minimum average daily temperature (°C), daily rainfall (mm), bright sunshine hours and relative humidity (%) were collected from the nearby weather sub-station at Satkhira, which are given in Fig. 2.11-2.14. The average relative humidity ranged from 62 to 88% and average temperature ranged from 8 to 33.5 °C.

TABLE 2.8 INTERACTION OF IRRIGATION AND FERTILIZER MANAGEMENT STRATEGIES ON TOTAL WATER USED AND IRRIGATION WATER PRODUCTIVITY OF WHEAT DURING 2014-15

Treatment[a]	Number of irrigations	Water (cm)				Grain yield (t ha^{-1})	Irrigation productivity (kg ha^{-1} cm^{-1})
		Irrigation (IR)	Rainfall (Re)	Depletion (□SM)	Consumption (IR+Re+□SM)		
$I_1 \times T_1$	3	9	7.47	3.64	20.11	3.47 b-d	386
$I_1 \times T_2$						4.01 a	446
$I_2 \times T_1$	2	6		7.95	21.42	2.99 d	498
$I_2 \times T_2$						3.43 cd	572
$I_3 \times T_1$	1	4		8.70	20.17	2.99 d	748
$I_3 \times T_2$						3.49 bc	873
$I_4 \times T_1$	4	12		2.14	21.61	3.15 cd	263
$I_4 \times T_2$						3.95 ab	329

[a] I_1, 35% soil moisture depletion from field capacity (SMD); I_2, 55% SMD, I_3, 75% SMD; I_4, farmer flooding practice; T_1, application of N, P and K fertilizer according to STB; T_2, T_1 + addition of gypsum @ 190 kg ha^{-1}

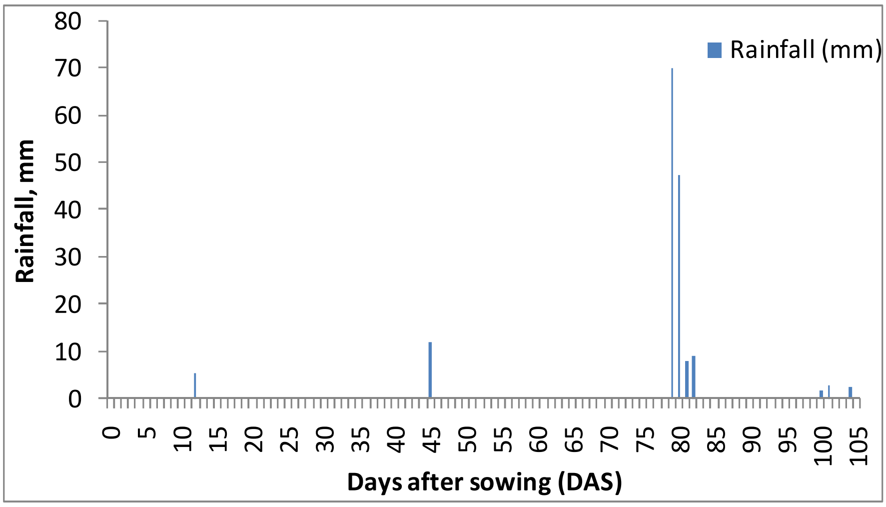

FIG. 2.8. Rainfall amount and distribution during the experimental period in 2015-16.

2.3.7.2. Soil salinity status

Soil samples were collected from the experimental plots at different dates starting from wheat sowing up to harvest and analyzed for soil salinity (dS m^{-1}). Soil salinity values as affected by different irrigation approaches at different soil depth intervals at different dates are presented in Table 2.12. Initially (during November at wheat sowing) the salinity level was lower (ranged from 4.7 to 5.2 dS m^{-1}) and gradually increased up to 8.8 dS m^{-1} at harvest during the month of March.

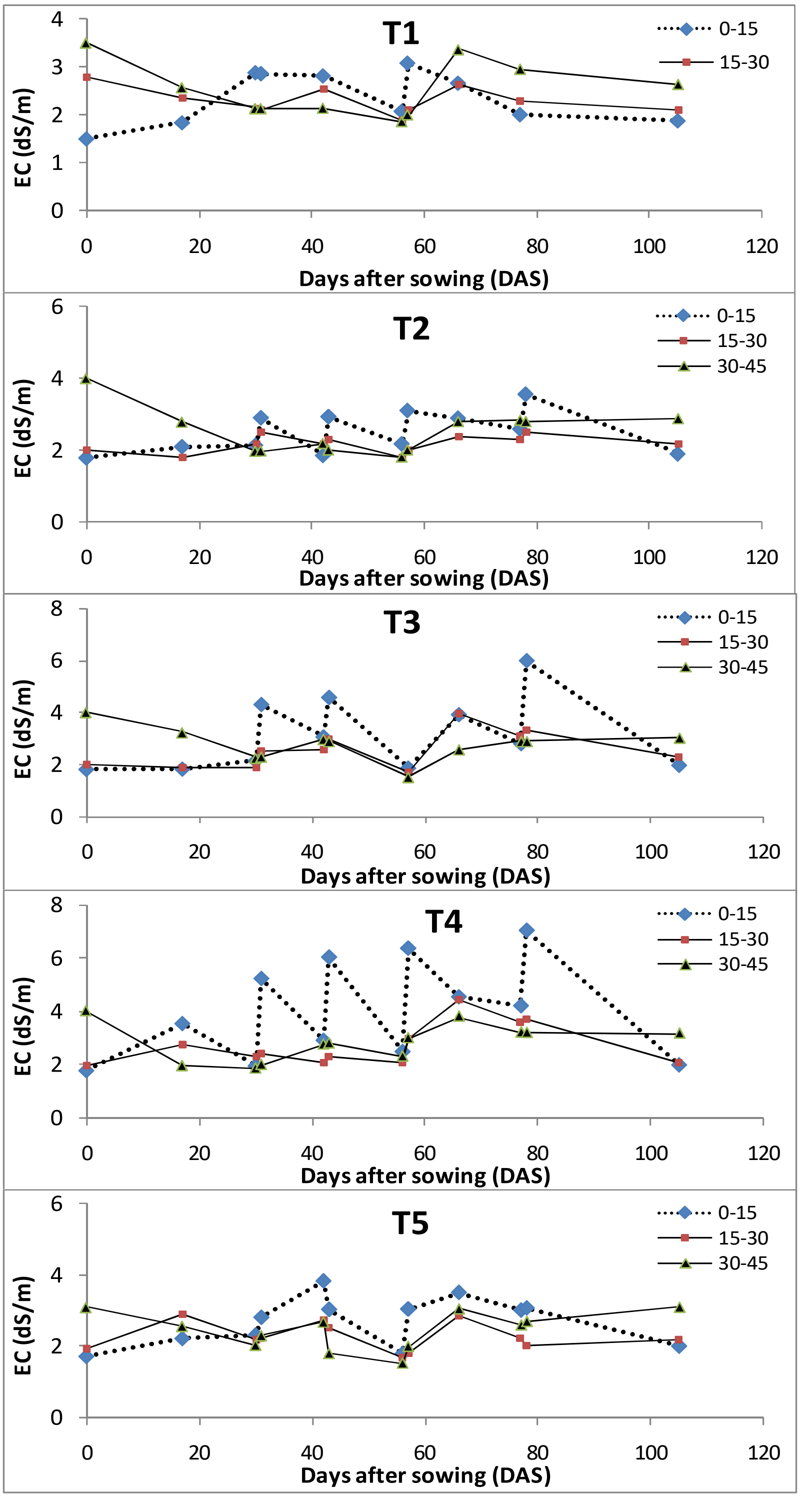

FIG. 2.9. Soil electrical conductivity throughout the growing season during 2015-2016. T_1 = Farmer's practice with 3 dS m^{-1} saline water; T_2 = Irrigation at 35% depletion of PAW with 3 dS m^{-1} saline water; T_3 = Irrigation at 35% depletion of PAW with 6 dS m^{-1} saline water; T_4 = Irrigation at 35% depletion of PAW with 9 dS m^{-1} saline water; T_5 = Irrigation at 55% depletion of PAW with 3 dS m^{-1} saline water.

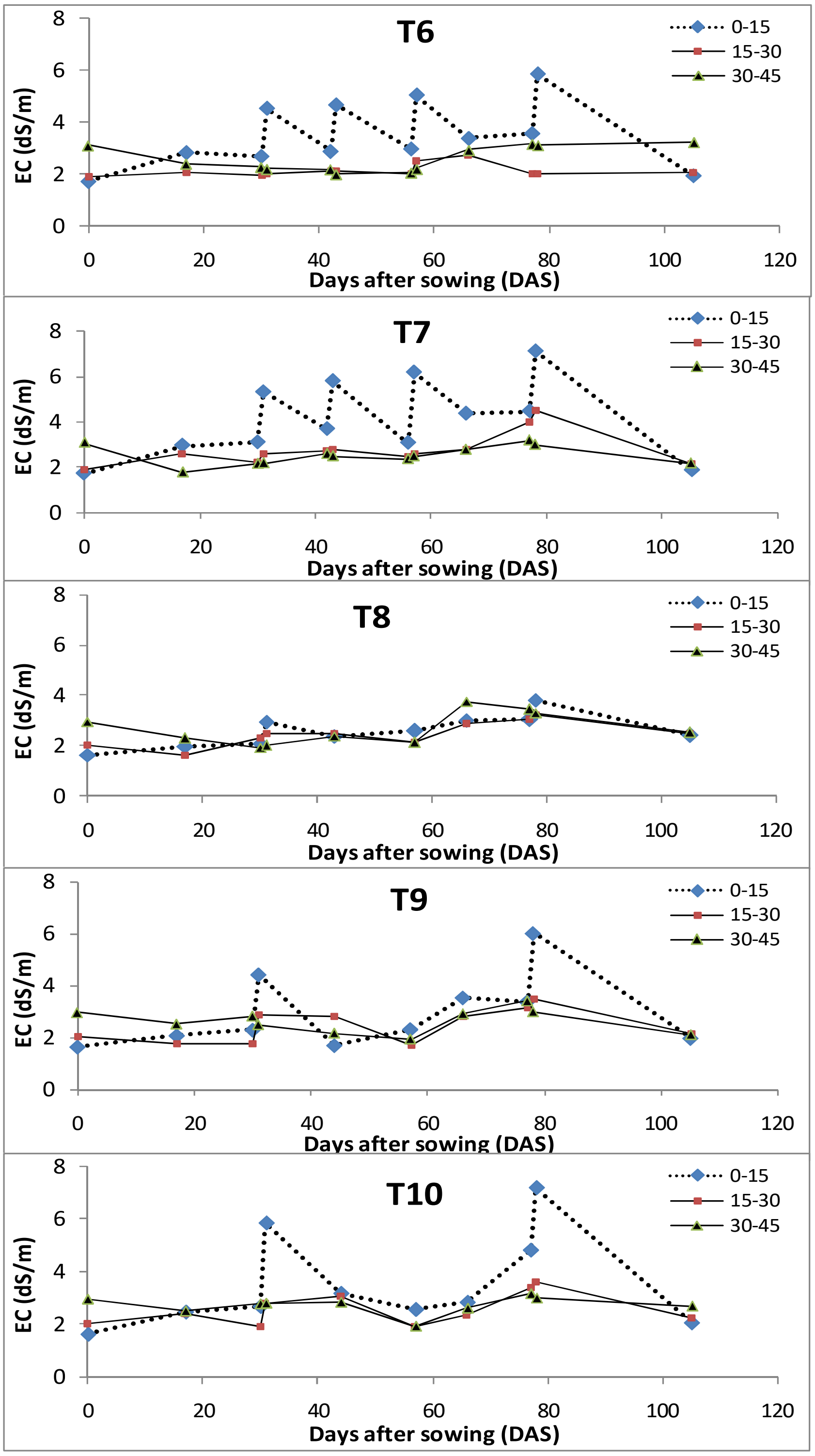

FIG. 2.10. Pattern of soil EC level throughout the growing season of the experimental plot during 2015-2016. T_6 = Irrigation at 55% depletion of PAW with 6 dS m^{-1} saline water; T_7 = Irrigation at 55% depletion of PAW with 9 dS m^{-1} saline water; T_8 = Irrigation at 75% depletion of PAW with 3 dS m^{-1} saline water; T_9 = Irrigation at 75% depletion of PAW with 6 dS m^{-1} saline water; T_{10} = Irrigation at 75% depletion of PAW with 9 dS m^{-1} saline water.

TABLE 2.9 EFFECT OF SALINITY LEVEL ON THE YIELD AND YIELD COMPONENTS OF WHEAT DURING 2015-2016

Treatment[a]	Dimensions (cm)		Number of		1000 grain weight (g)	Yield (t ha^{-1})	
	Plant height	Spike length	Tillers $plant^{-1}$	Seeds $spike^{-1}$		Grain	Straw
T_1	78	9.0	3.9	36	22.2 a	2.22	4.68
T_2	80	9.0	4.0	32	19.6 abc	2.43	5.04
T_3	80	8.8	4.4	32	18.4 bc	2.32	3.76
T_4	76	9.4	4.3	32	17.5 c	2.25	3.49
T_5	79	9.2	4.9	33	19.2 abc	2.55	4.44
T_6	78	9.9	4.9	29	17.7 c	2.12	5.02
T_7	81	8.5	4.4	30	18.9 bc	1.97	4.97
T_8	80	9.4	4.3	35	22.1 a	2.00	4.29
T_9	80	8.8	4.0	34	21.0 ab	1.88	4.58
T_{10}	77	9.0	3.8	29	20.5 abc	1.85	3.63
Tukey[b]	ns	ns	ns	ns	*	ns	ns

[a] T_1 = Farmer's practice with 3 dS m^{-1} saline water; T_2 = Irrigation at 35% depletion of PAW with 3 dS m^{-1} saline water; T_3 = Irrigation at 35% depletion of PAW with 6 dS m^{-1} saline water; T_4 = Irrigation at 35% depletion of PAW with 9 dS m^{-1} saline water; T_5 = Irrigation at 55% depletion of PAW with 3 dS m^{-1} saline water; T_6 = Irrigation at 55% depletion of PAW with 6 dS m^{-1} saline water; T_7 = Irrigation at 55% depletion of PAW with 9 dS m^{-1} saline water; T_8 = Irrigation at 75% depletion of PAW with 3 dS m^{-1} saline water; T_9 = Irrigation at 75% depletion of PAW with 6 dS m^{-1} saline water; T_{10} = Irrigation at 75% depletion of PAW with 9 dS m^{-1} saline water

[b] *, $P < 0.05$; ns, not significant; Data within a column followed by different lower-case letters are significantly different

TABLE 2.10. IRRIGATION FREQUENCY, TIME OF IRRIGATION, AMOUNT OF WATER USED AT EACH IRRIGATION AND IRRIGATION DEPTH FOR WHEAT DURING 2015-16

Treatment[a]	Irrigation frequency	Irrigation applied (DAS)[b]	Water applied (cm) irrigation^{-1}	Total irrigation depth (cm)
T_1	2	30, 50	4.0, 3.2	7.2
T_2	4	25, 42, 56, 77	4.0, 4.0, 2.9, 4.0	14.9
T_3				
T_4				
T_5		30, 42, 56, 77	4.0, 4.0, 2.9, 4.0	14.9
T_6				
T_7				
T_8		30, 77	4.0, 4.0	8.0
T_9				
T_{10}				

[a] T_1 = Farmer's practice with 3 dS m^{-1} saline water; T_2 = Irrigation at 35% depletion of PAW with 3 dS m^{-1} saline water; T_3 = Irrigation at 35% depletion of PAW with 6 dS m^{-1} saline water; T_4 = Irrigation at 35% depletion of PAW with 9 dS m^{-1} saline water; T_5 = Irrigation at 55% depletion of PAW with 3 dS m^{-1} saline water; T_6 = Irrigation at 55% depletion of PAW with 6 dS m^{-1} saline water; T_7 = Irrigation at 55% depletion of PAW with 9 dS m^{-1} saline water; T_8 = Irrigation at 75% depletion of PAW with 3 dS m^{-1} saline water; T_9 = Irrigation at 75% depletion of PAW with 6 dS m^{-1} saline water; T_{10} = Irrigation at 75% depletion of PAW with 9 dS m^{-1} saline water

[b] DAS, days after sowing

TABLE 2.11. EFFECT OF IRRIGATION STRATEGY ON WATER USE AND WATER PRODUCTIVITY OF WHEAT DURING 2015-2016

Treatment[a]	Water (cm)				Yield	Water productivity	
	Irrigation (IR)	Effective rainfall (Re)	Depletion (□SM)	Crop evapo-transpiration	(t ha^{-1})	(kg ha^{-1} cm^{-1})	
						Water	Irrigation
T_1	7.2	10.6	1.3	19.1	2.22	116	308
T_2	14.9		–1.7	23.8	2.25	95	152
T_3			–3.5	22.0	2.32	106	156
T_4			–4.8	20.6	2.43	118	164
T_5	14.9		–5.7	19.7	2.55	129	172
T_6			–5.5	20.0	2.12	106	143
T_7			–4.0	21.5	1.97	92	133
T_8	8.0		2.1	20.7	1.85	89	231
T_9			2.0	20.6	2.00	97	250
T_{10}			1.9	20.5	1.88	92	235

[a] T_1 = Farmer's practice with 3 dS m^{-1} saline water; T_2 = Irrigation at 35% depletion of PAW with 3 dS m^{-1} saline water; T_3 = Irrigation at 35% depletion of PAW with 6 dS m^{-1} saline water; T_4 = Irrigation at 35% depletion of PAW with 9 dS m^{-1} saline water; T_5 = Irrigation at 55% depletion of PAW with 3 dS m^{-1} saline water; T_6 = Irrigation at 55% depletion of PAW with 6 dS m^{-1} saline water; T_7 = Irrigation at 55% depletion of PAW with 9 dS m^{-1} saline water; T_8 = Irrigation at 75% depletion of PAW with 3 dS m^{-1} saline water; T_9 = Irrigation at 75% depletion of PAW with 6 dS m^{-1} saline water; T_{10} = Irrigation at 75% depletion of PAW with 9 dS m^{-1} saline water

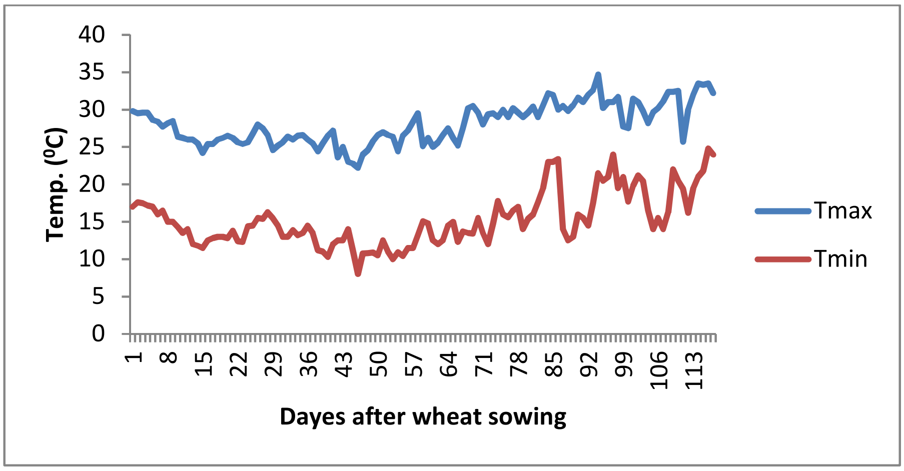

FIG. 2.11. Maximum and minimum temperature of the experimental area during 2016-17.

2.3.8. Depth of ground water table and salinity status

Results of a study conducted adjacent to the wheat experimental field to monitor the ground water table depth and the salinity status of the ground water collected at different dates are presented in Figs. 2.15, 2.16.

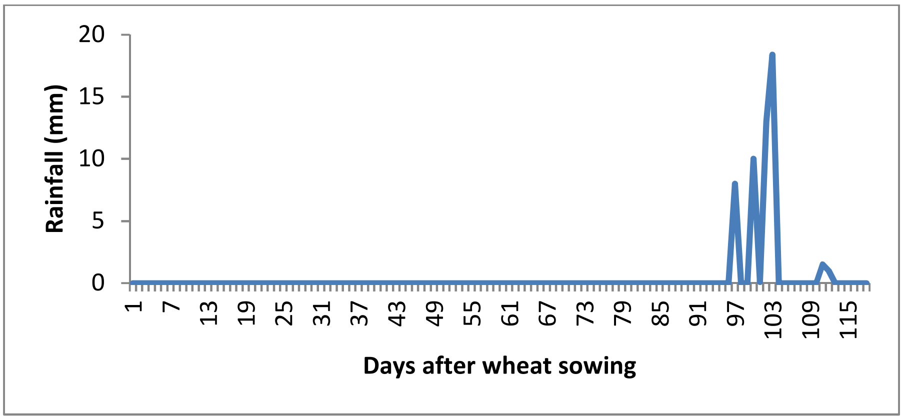

FIG. 2.12. Daily rainfall during the wheat crop from 30 November 2016 to 26 March 2017.

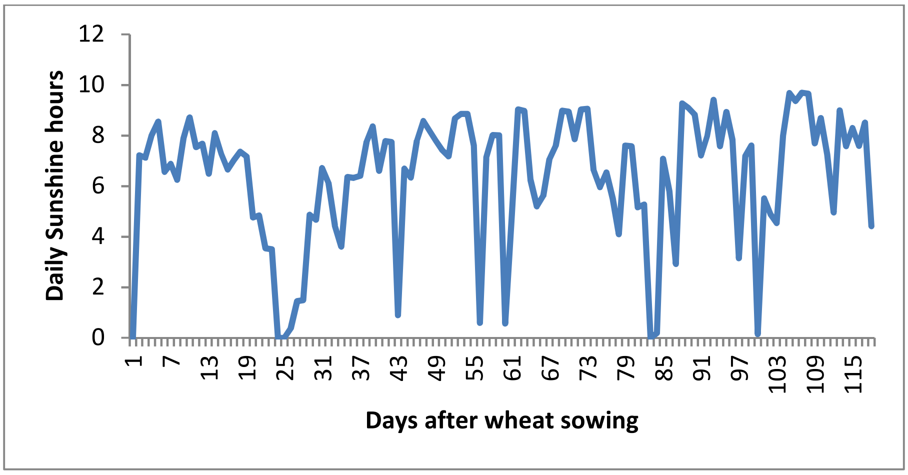

FIG. 2.13. Daily sunshine hours during the wheat crop from 30 November 2016 to 26 March 2017.

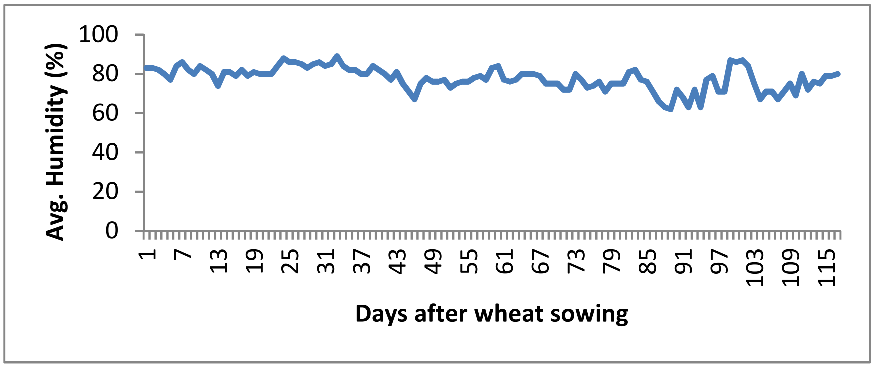

FIG. 2.14. Average humidity (%) during the wheat crop from 30 November 2016 to 26 March 2017.

TABLE 2.12. TIME COURSE OF SOIL SALINITY (DS M^{-1}) AT SOIL DEPTH INTERVALS DURING 2016-17

Depth (cm)	30/11/16	14/12/16	27/12/16	25/01/17	6/02/17	26/02/17	26/03/17
0-15	5.2	5.7	4.6	5.4	6.7	7.9	8.8
15-30	4.8	4.5	3.8	4.7	5.3	6.1	6.7
30-45	4.7	5.5	4.4	4.9	6.5	6.1	6.0

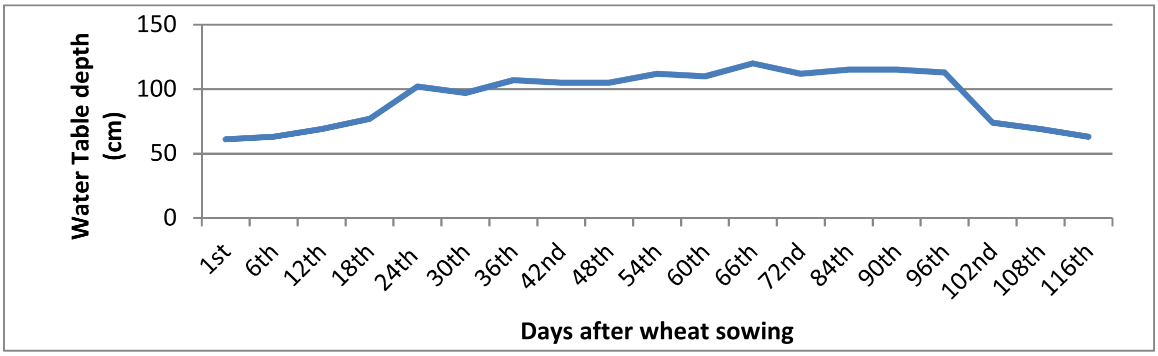

FIG. 2.15. Ground water table depth after wheat sowing in 2016-17.

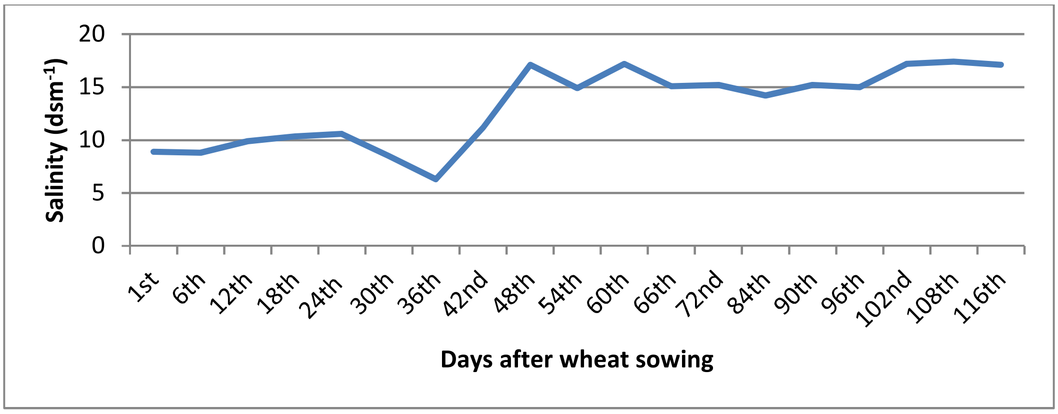

FIG. 2.16. Salinity level of ground water after wheat sowing in 2016-17.

2.3.8.1. Wheat yield

Different soil amendments and N application strategies significantly influenced grain and straw yields of wheat (Fig. 2.17). The highest grain yield of wheat (4.86 t ha^{-1}) was observed for treatment T_5, where soil amendments such as gypsum (100 kg ha^{-1}) and K (additional amount of 90 kg ha^{-1}) were applied along with the recommended dose of NPK fertilizer (N fertilizer was applied in three equal splits at different growth stages of wheat). The lowest grain yield of 2.54 t ha^{-1} was recorded under treatment T_7 where only NPK fertilizers were applied at the recommended dose. Moreover, in T_7 all N fertilizer was applied in a single dose and no soil amendment was added. Like wheat grain, the maximum (5.32 t ha^{-1}) and minimum (2.90 t ha^{-1}) straw yields were observed under treatments T_5 and T_7, respectively.

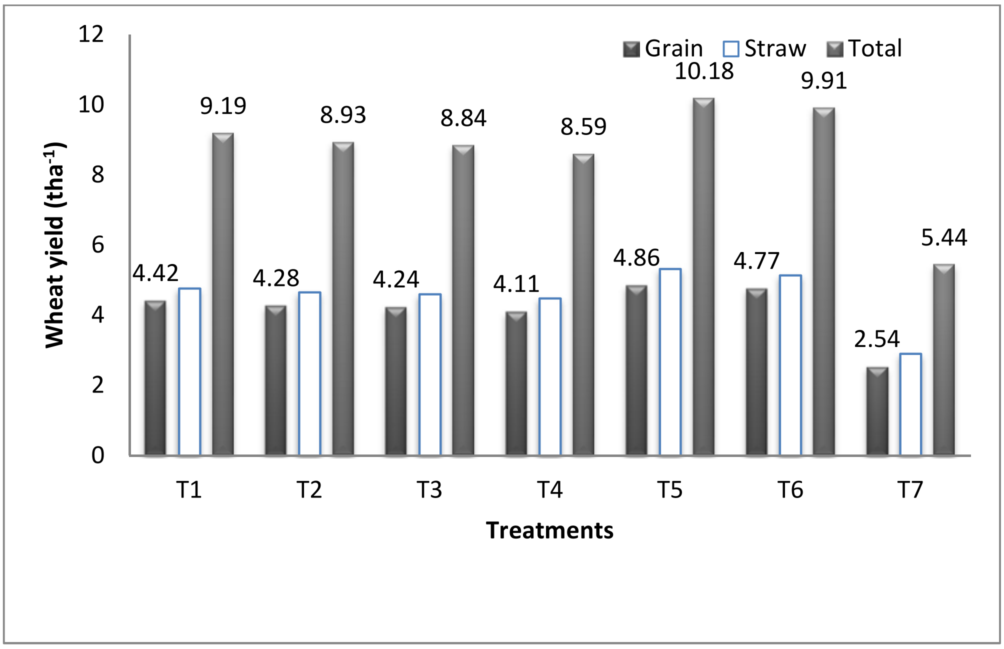

FIG. 2.17. Grain, straw and total yield of wheat during 2016-17. T_1-T_7, Recommended dose of N, P and K; T_1, + application of gypsum @ 150 kg ha^{-1} and N in 3 splits; T_2 + application of gypsum @ 150 kg ha^{-1} and N in 2 splits; T_3 + application of K @ 120 kg ha^{-1} and N in 3 splits; T_4 + application of K @ 120 kg ha^{-1} and N in 2 splits; T_5 + application of K @ 90 kg ha^{-1} + gypsum @ 100 kg $ha^{-1}$and N in 3 splits; T_6 + application of K @ 90 kg ha^{-1} + gypsum @ 100 kg $ha^{-1}$and N in 2 splits.

2.3.8.2. N concentration and N derived from fertilizer and soil

N concentration and N yield (kg ha^{-1}) of wheat grain and straw showed a variation due to the effect of soil amendments and N application strategy (Table 2.13). Among the different treatments the highest concentration of N in wheat grain was found in treatment T_5 (20.8 g kg^{-1}) which yielded 101 kg ha^{-1}, whereas the lowest N content was recorded under T_3 treatment (17.3 g kg^{-1}) and here the N yield was 73 kg ha^{-1}. The results of ^{15}N enrichment, Ndff and Ndfs in wheat grain and straw are presented in Table 2.14 and Fig. 2.18-2.19. The maximum amount of N derived from fertilizer sources in wheat grain occurred under treatment T_5 (Ndff = 46% = 50 kg N ha^{-1}) and the minimum value was recorded for T_7 (Ndff = 23% = 11 kg N ha^{-1}). Similarly, in the case of wheat straw the highest value of Ndff was recorded under the treatment T_5 (Ndff = 23% = 1.5 kg N ha^{-1}) and the minimum value was for treatment T_7 (Ndff = 13% = 0.33 kg N ha^{-1}).

TABLE 2.13 EFFECT OF FERTILIZER STRATEGY ON DRY MATTER YIELD, N CONCENTRATION, ^{15}N ENRICHMENT AND N YIELD OF WHEAT GRAIN AND STRAW IN SALINE SOIL

Treatment[a]	Dry matter ($t\ ha^{-1}$)		N concentration ($g\ kg^{-1}$)		^{15}N enrichment (atom % excess)		N yield ($kg\ ha^{-1}$)	
	Grain	Straw	Grain	Straw	Grain	Straw	Grain	Straw
T_1	4.42	4.76	18.8	5.1	2.05	1.04	83	24
T_2	4.28	4.65	18.0	4.3	1.94	0.86	77	20
T_3	4.24	4.60	17.3	4.0	2.01	0.89	73	18
T_4	4.11	4.48	16.5	3.3	1.82	0.75	68	15
T_5	4.86	5.32	20.8	6.2	2.36	1.20	101	33
T_6	4.77	5.14	20.4	5.5	2.01	0.92	97	28
T_7	2.54	2.90	17.4	3.6	1.22	0.68	44	10

[a] T_1-T_7, Recommended dose of N, P and K; T_1, + application of gypsum @ 150 kg ha^{-1} and N in 3 splits; T_2 + application of gypsum @ 150 kg ha^{-1} and N in 2 splits; T_3 + application of K @ 120 kg ha^{-1} and N in 3 splits; T_4 + application of K @ 120 kg ha^{-1} and N in 2 splits; T_5 + application of K @ 90 kg ha^{-1} + gypsum @ 100 kg $ha^{-1}$and N in 3 splits; T_6 + application of K @ 90 kg ha^{-1} + gypsum @ 100 kg $ha^{-1}$and N in 2 splits

TABLE 2.14 EFFECT OF FERTILIZER STRATEGY ON N DERIVED FROM FERTILIZER AND SOIL OF WHEAT GRAIN AND STRAW IN SALINE SOIL

Treatment[a]	N derived from fertilizer (%)		N derived from soil (%)	
	Grain	Straw	Grain	Straw
T_1	40	20	60	80
T_2	38	17	62	83
T_3	39	17	61	83
T_4	35	15	65	85
T_5	46	23	54	77
T_6	39	18	61	82
T_7	24	13	76	87

[a] T_1-T_7, Recommended dose of N, P and K; T_1, + application of gypsum @ 150 kg ha^{-1} and N in 3 splits; T_2 + application of gypsum @ 150 kg ha^{-1} and N in 2 splits; T_3 + application of K @ 120 kg ha^{-1} and N in 3 splits; T_4 + application of K @ 120 kg ha^{-1} and N in 2 splits; T_5 + application of K @ 90 kg ha^{-1} + gypsum @ 100 kg $ha^{-1}$and N in 3 splits; T_6 + application of K @ 90 kg ha^{-1} + gypsum @ 100 kg $ha^{-1}$and N in 2 splits

2.3.9. Simulation of wheat under different level of salinity – AquaCrop Model Study (2015-16 and 2016-17)

The reference crop evapotranspiration (ETo) values ranged from 1.3 to 5.4 and 1.6 to 5.1 mm day^{-1} throughout the growth period during the year of 2015-16 and 2016-17, respectively (Fig. 2.20-2.21). Observed wheat yield and biomass under optimum (non-stressed) conditions were used in model calibration. The observed and simulated yields for treatments T_1 to T_{10} are provided in Table 2.15 and Fig. 2.22-2.23. The model simulated yields of wheat closely matched with the observed yields for each treatment. For the calibration and validation cases, simulated yields have a very narrow error margin (Root Mean Square Error is 0.21 and 0.15 for the years of 2015-16 and 2016-17, respectively) in comparison with the observed yields. This proves the accuracy of the model to provide practical yield values using field information.

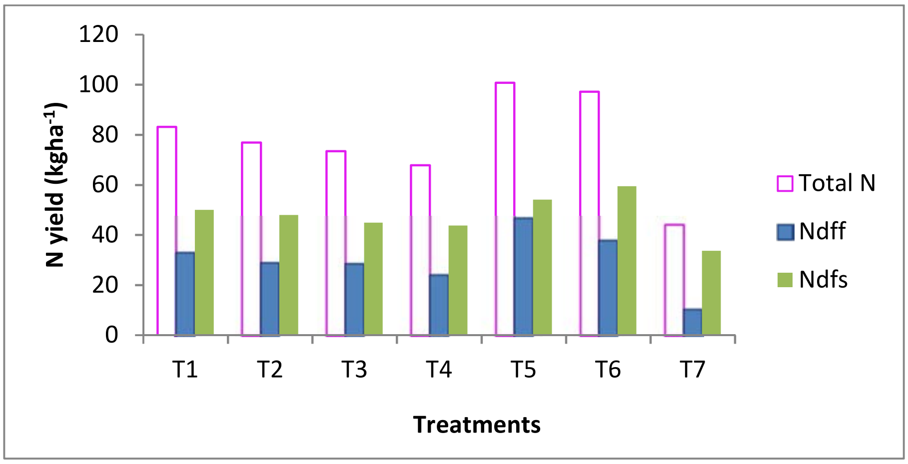

FIG. 2.18. Total N and N derived from fertilizer and soil of wheat grain during 2016-17. T_1-T_7, Recommended dose of N, P and K; T_1, + application of gypsum @ 150 kg ha^{-1} and N in 3 splits; T_2 + application of gypsum @ 150 kg ha^{-1} and N in 2 splits; T_3 + application of K @ 120 kg ha^{-1} and N in 3 splits; T_4 + application of K @ 120 kg ha^{-1} and N in 2 splits; T_5 + application of K @ 90 kg ha^{-1} + gypsum @ 100 kg ha^{-1}and N in 3 splits; T_6 + application of K @ 90 kg ha^{-1} + gypsum @ 100 kg ha^{-1}and N in 2 splits.

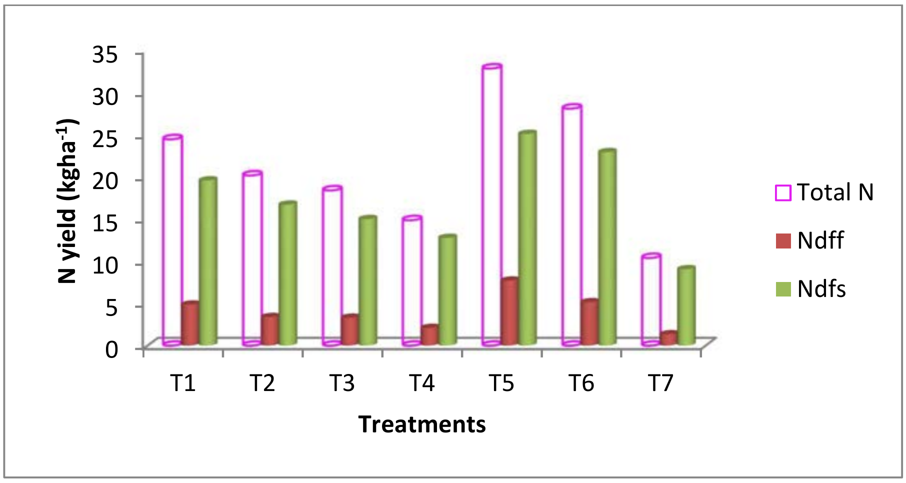

FIG. 2.19. Total N and N derived from fertilizer and soil of wheat straw during 2016-17. T_1-T_7, Recommended dose of N, P and K; T_1, + application of gypsum @ 150 kg ha^{-1} and N in 3 splits; T_2 + application of gypsum @ 150 kg ha^{-1} and N in 2 splits; T_3 + application of K @ 120 kg ha^{-1} and N in 3 splits; T_4 + application of K @ 120 kg ha^{-1} and N in 2 splits; T_5 + application of K @ 90 kg ha^{-1} + gypsum @ 100 kg ha^{-1}and N in 3 splits; T_6 + application of K @ 90 kg ha^{-1} + gypsum @ 100 kg ha^{-1}and N in 2 splits.

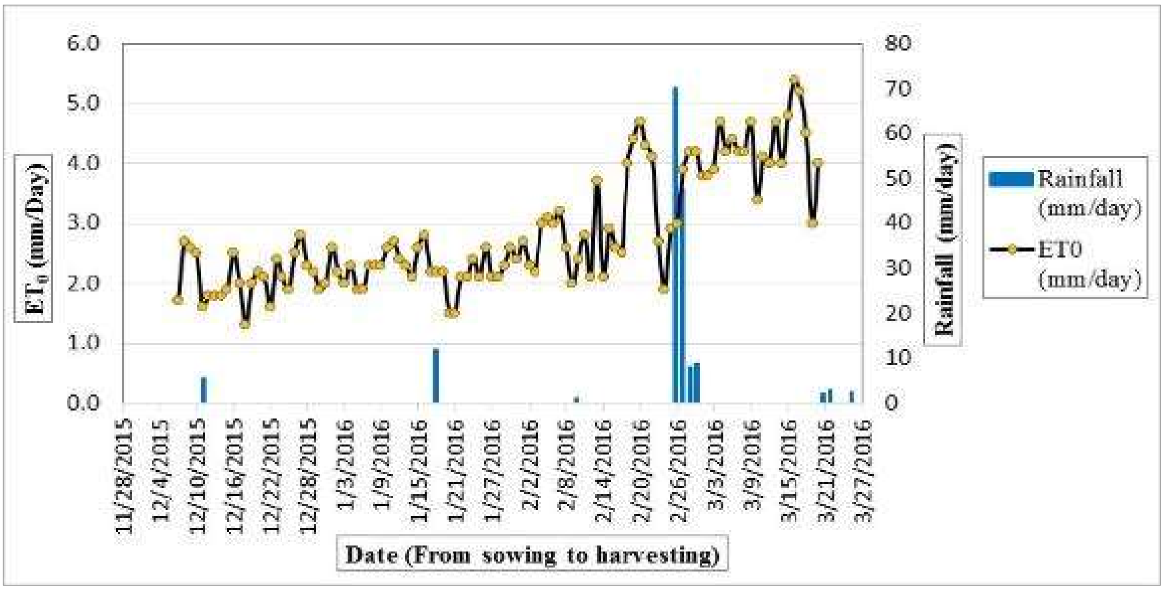

FIG. 2.20. Daily ET_0 and rainfall from sowing to harvest of wheat in 2015-16.

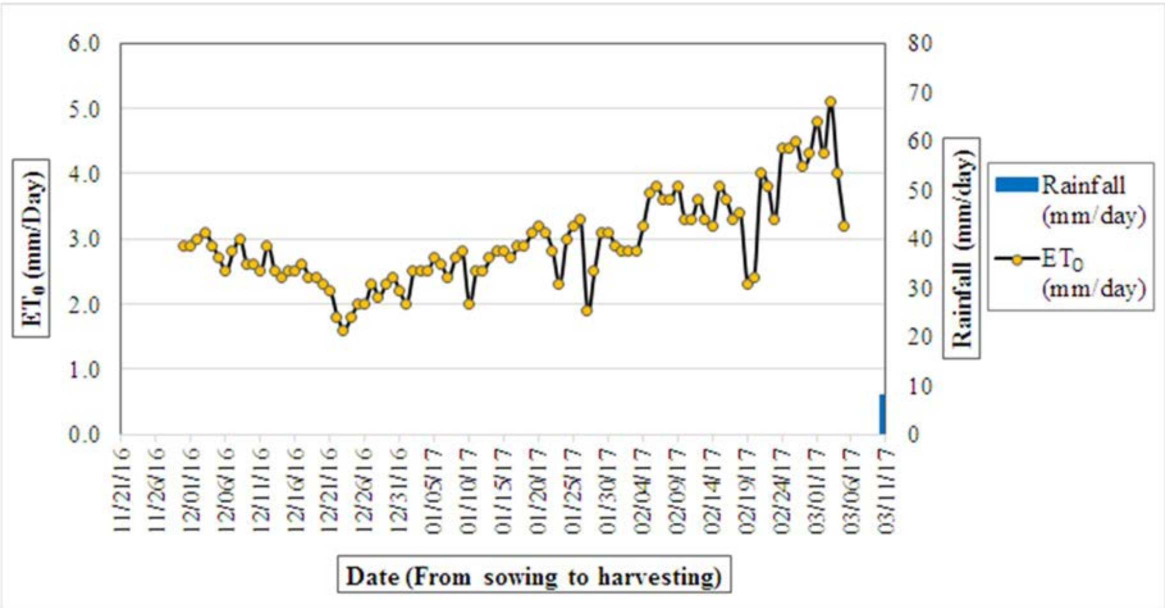

FIG. 2.21. Daily ET_0 and rainfall from sowing to harvest of wheat in 2016-17.

TABLE 2.15 OBSERVED AND MODEL SIMULATED WHEAT YIELDS DURING 2015-16 AND 2016-17

Treatment[a]	Observed yield (t ha^{-1})		Model simulated yield (t ha^{-1})	
	2015-16	2016-17	2015-16	2016-17
T_1	2.43	2.86	2.51	2.87
T_2	2.65	3.51	2.70	3.59
T_3	2.03	3.44	2.07	3.45
T_4	1.90	3.37	1.90	3.40
T_5	2.41	3.57	2.45	3.57
T_6	2.14	3.42	2.19	3.53
T_7	2.16	2.97	2.15	2.97
T_8	2.25	3.06	2.36	3.04
T_9	2.00	2.94	2.12	2.97
T_{10}	1.63	2.62	1.75	2.57

[a] T_1 = Farmer's practice with 3 dS m^{-1} saline water; T_2 = Irrigation at 35% depletion of PAW with 3 dS m^{-1} saline water; T_3 = Irrigation at 35% depletion of PAW with 6 dS m^{-1} saline water; T_4 = Irrigation at 35% depletion of PAW with 9 dS m^{-1} saline water; T_5 = Irrigation at 55% depletion of PAW with 3 dS m^{-1} saline water; T_6 = Irrigation at 55% depletion of PAW with 6 dS m^{-1} saline water; T_7 = Irrigation at 55% depletion of PAW with 9 dS m^{-1} saline water; T_8 = Irrigation at 75% depletion of PAW with 3 dS m^{-1} saline water; T_9 = Irrigation at 75% depletion of PAW with 6 dS m^{-1} saline water; T_{10} = Irrigation at 75% depletion of PAW with 9 dS m^{-1} saline water

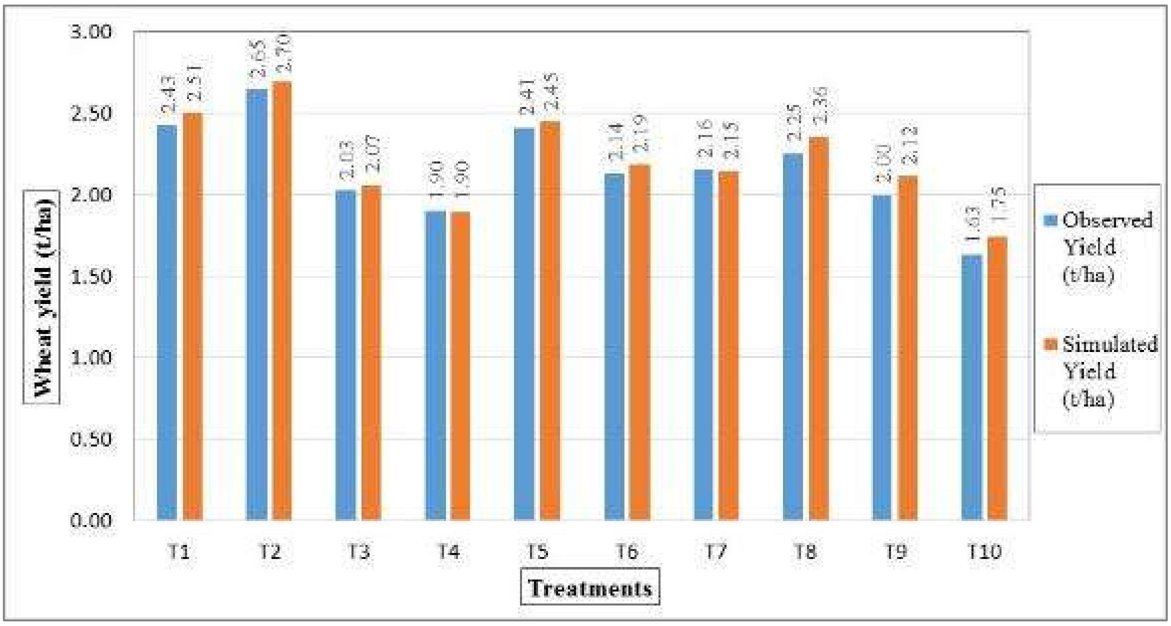

FIG. 2.22. Observed and simulated yields of wheat 2015-16.

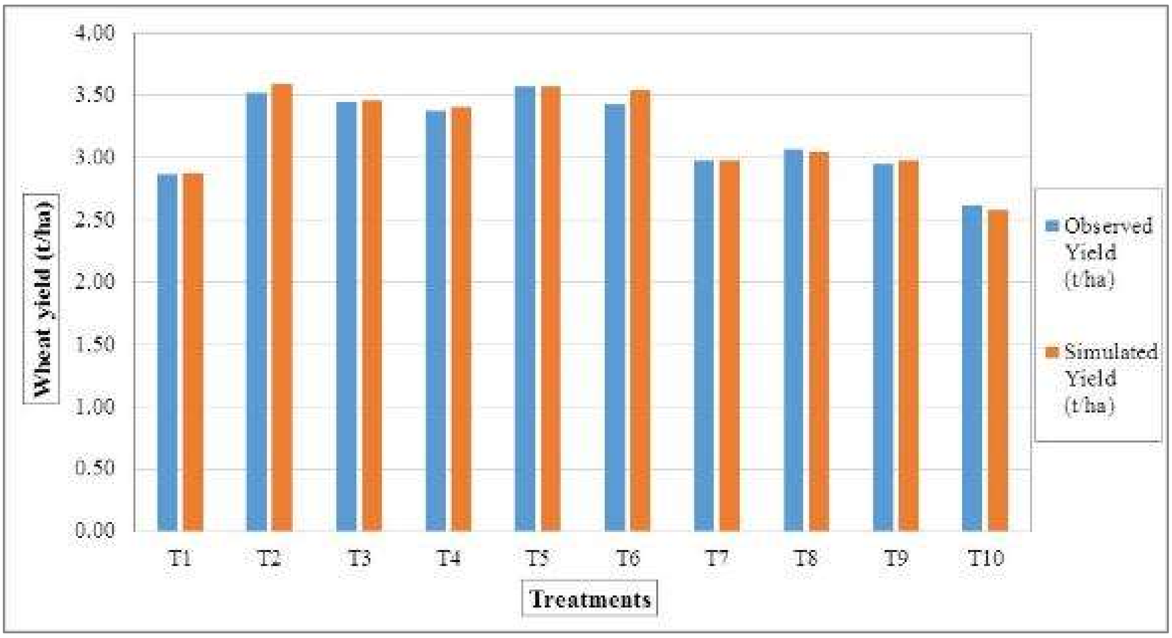

FIG. 2.23. Observed and simulated yields of wheat in 2016-17.

2.4. CONCLUSIONS

During the dry season, soil and water salinity increases with time and reaches the maximum in the months of April–May. Also, the soil water content is reduced during the months of November–May, thus causing difficulties growing cereal crops without irrigation water. The maximum yield of wheat was observed under the irrigation strategy of 35% depletion of soil water content along with the lowest level of salinity. Under a tolerable limit of salinity, a comparatively higher yield was observed when irrigation was done at 55% depletion of soil water content. Considering the different nutrient management practices for wheat cultivation under salt affected / coastal region of Bangladesh, a significant improvement is usually expected in the use of gypsum on saline soils as sources of Ca and S. It can be concluded that application of amendments especially additional gypsum (190 kg ha^{-1}) with the recommended dose of fertilizer improved the yield and yield components of wheat significantly. It was also concluded that wheat crops responded significantly to the applications of N, K and gypsum.

Regarding the nitrogen management for wheat under salt affected areas, it was observed that the split application of N highly influenced the growth and yield. The maximum yield of wheat along with N uptake was noted when the N fertilizer was applied in 3 splits. It is recommended that a dose of NPK + an additional application of K @ 90 kg ha^{-1} + an application of gypsum @ 100 kg ha^{-1} with the N application in 3 splits be given to wheat crops in saline soils (EC = 4.7 to 4.8 dS m^{-1} up to 0-45cm soil depth) in order to get optimum and sustainable yields of wheat with improved N use efficiency.

The FAO model AquaCrop was calibrated by matching observed yield and biomass data, and then validated with independent data sets. Subsequently, the calibrated model was used to simulate grain yield for different irrigation approaches under different salinity levels, and irrigation sequences with a view to develop appropriate irrigation management strategies for wheat. This simulation study clearly showed a decreasing yield trend for wheat under increased salinity along with decreasing the irrigation water frequency. As salinity accumulation due to climate change and upstream withdrawal is a key issue affecting crop production in Bangladesh, the model provides a tool to estimate the impacts of future changes in water and soil salinity as well as climate parameters on wheat yield. The observed and model simulated yields were close matches which indicates the accuracy of the AquaCrop model in simulating wheat yields in different field and management conditions. If calibrated and validated properly, the model can simulate yields of other dry season crops in the saline condition of coastal areas like Bangladesh with variable soil, climatic and hydrological conditions. Also, further analysis can be performed using this model on future wheat yields under future potential climatic scenarios.

ACKNOWLEDGEMENTS

The Project 'Landscape Salinity and Water Management for Improving Agricultural Productivity' was carried out at the Bangladesh Institute of Nuclear Agriculture (BINA), supported by the Institute of Water and Flood Management (IWFM), Bangladesh University of Engineering and Technology (BUET). The project was coordinated and partially funded by FAO/IAEA.

REFERENCES

[1] SRDI, Saline Soils of Bangladesh, A Report published by the Soil Resource Development Institute, SRMAF Project, Ministry of Agriculture, Mrittika Bhaban, Krishikhamar Sarak Farmgate, Dhaka-1215 (2010).

[2] CLARKE, D., et al., Projections of on-farm salinity in coastal Bangladesh, Environ. Sci. Processes Impacts **17** (2015) 1127–1136.

[3] ALLEN, R.G., et al., Crop Evapotranspiration – Guidelines for Computing Crop Water Requirements. FAO Irrigation and Drainage Paper 56, Food and Agriculture Organization of the United Nations, Rome (1998).

[4] ZAMAN, M., et al., Mitigation of ammonia losses from urea applied to a pastoral system: the effect of nBTPT and timing and amount of irrigation, New Zeal. Grass. Assoc. **75** (2013) 121–126.

[5] ZAMAN, M., et al., Effects of urease and nitrification inhibitors on the efficient use of urea for pastoral systems, Soil Sci. Plant Nutr. **59** (2013) 649–659.

[6] ZAMAN, M., et al., Influence of fine particle suspension of urea and urease inhibitor on nitrogen and water use efficiency in grassland using nuclear techniques. In: Heng, L.K., et al. (eds), International Symposium on Managing Soils for Food Security and Climate Change Adaptation and Mitigation, Food and Agriculture Organization of the United Nations, Rome (2014) 29–32.

[7] HENG, L.K., et al., Validating the FAO AquaCrop model for irrigated and water deficient maize, Agron. J. **101** (2009) 488–498.

[8] ARAYA, A., et al., Test of AquaCrop model in simulating biomass and yield of water deficient and irrigated barley (*Hordeum vulgare*), Agric. Water Manage. **97** (2010) 1838–1846.

[9] ARAYA, A., et al., Simulating yield response to water of Teff (*Eragrostis tef*) with FAO's AquaCrop model, Field Crops Res. **116** (2010) 196–204.

[10] GEERTS, S., et al., Simulating yield response of Quinoa to water availability with AquaCrop, Agron. J. **101** (2009) 499–508.

[11] HUSSAIN, F., et al., Simulating cotton yield response to deficit irrigation with the FAO AquaCrop model, Spanish J. Agric. Res. **9** (2011) 1319–1330.

[12] STRICEVIC, R., et al., Assessment of the FAO AquaCrop model in the simulation of rainfed and supplementally irrigated maize, sugar beet and sunflower, Agric. Water Manage. **98** (2011) 1615–1621.

[13] BHATTACHARYA, T., PANDA, R.K., Effect of climate change on rice yield at Kharagpur, West Bengal, IOSR J. Agric. Vet. Sci. **4** (2013) 6–12.

[14] SAM-AMOAH, L.K., et al., Calibration and validation of AquaCrop for full and deficit irrigation of hot pepper, ARPN J. Agric. Biol. Sci. **8** (2013) 175–178.

[15] MONDAL, M.S., et al., Simulating yield response of rice to salinity stress using the AquaCrop model, Environ. Sci. Processes Impacts **17** (2015) 1118–1126.

[16] SAHA, D., MONDAL, M.S., Simulation of rice yield in south-west coastal Bangladesh using the AquaCrop model, Proc. 5th Int. Conf. on Water and Flood Management, Bangladesh (2015) 81–88.

[17] ZAMAN, S., et al., Assessing the potential impacts of climate change on mustard yield using FAO AquaCrop model, Proc. Int. Conf. on Climate Change Impact and Adaptation, Bangladesh (2015) 111–118.

[18] RAES, D., et al., Reference Manual, AquaCrop Version 4.0. FAO, Land and Water Division, Rome (2012).

3. EFFECTS OF ALTERNATE IRRIGATION WITH FRESH AND SALINE WATER ON WHEAT PRODUCTIVITY AND SALINIZATION IN THE NORTH CHINA PLAIN

X.R. MEI
State Engineering Laboratory of Efficient Water Use of Crops and Disaster Loss Mitigation
Beijing, P.R. China

K.R.E. ROMY, D.Z. GONG, H.R. LI
Institute of Environment and Sustainable Development in Agriculture
Chinese Academy of Agricultural Sciences
Beijing, P.R. China

W.Y. ZHANG
Institute of Dryland Agriculture
Hebei Academy of Agriculture and Forest Science
Hengshui, P.R. China

Abstract

In the North China Plain (NCP), sustainable development of agriculture is restricted by freshwater shortage and water quality deterioration. However, there is plenty of saline water in shallow aquifers unutilized due to its negative effects on crop growth and soil salinization. Recently, a new irrigation method for using saline water has been developed, that is to alternately irrigate crops with freshwater at sensitive growth stages and saline water at non-sensitive stages. The experiments were conducted from October 2014 to June 2015 and from October 2015 to June 2016 at the Hengshui Dryland Agriculture Experimental Station to evaluate the effects of alternative irrigation with fresh and saline water (AIFS) on winter wheat productivity and soil salinization.

Five treatments consisting of various combinations of fresh and saline water applied at three growth stages (seedling, turning green-jointing, flowering-filling) were evaluated. Soil water content was measured by the neutron probe, soil electrical conductivity (EC) and pH were analyzed from soil samples, leaf ^{13}C was analyzed by isotope-ratio mass spectrometry and biomass accumulation was weighed manually at different growth stages. At the end of the wheat growing season, the seed yields were measured. The experimental data were used to verify the AquaCrop model and assess the long-term effects AIFS on soil salinization.

There were no significant differences for soil electrical conductivity and pH values among all treatments after two years AIFS, but significant differences were found for soil water dynamics among different treatments. Irrigating winter wheat with saline water at non-sensitive growth stages and freshwater at sensitive stages alleviated the salt stress on biomass accumulation and grain yield and acquired the higher biomass and grain yield among the five treatments. The best irrigation model for alternately irrigating winter wheat with fresh and saline water was AFSI3 (i.e. irrigated with freshwater at the turning green-jointing stage and saline water at the flowering-filling stage) due to higher water use efficiency (WUE) and moderate yields of winter wheat in the North China Plain. However, after AIFS saline water irrigation for a long-term (e.g. 30 years), flood irrigation with a large volume of water (100~150 mm) at intervals of 5~6 years is recommended to move salt in the root zone to deep soil layers

to decrease the effects of soil salinization on crop growth and harvestable yield. AquaCrop is a robust tool to predict crop productivity and salt accumulation of a wheat field irrigated alternately with saline and freshwater at different growth stages and is also used to assess the long-term effects of AIFS on crop productivity and soil salinization.

3.1. INTRODUCTION

Drought and water shortage are major problems facing agriculture in the North China Plain (NCP). The loss of agricultural production each year due to these factors is more than the sum of the losses caused by other factors. Wheat is an important grain crop in NCP, where its water requirement has only been met through over-pumping deep groundwater, resulting in the formation of a groundwater depression. Groundwater depletion from 2002 to 2014 averaged 7.2 ± 1.1 km^3 $year^{-1}$ [1, 2], and its level descended by 0.5~1 m $year^{-1}$. The NCP is becoming one of the greatest global hotspots of groundwater depletion, which can be detected by Gravity Satellite. The scientific estimation explained that after 60 years the deep groundwater reservoir will be empty due to the agricultural, industrial, and domestic development. Moreover, this has been accompanied by serious environmental problems such as land subsidence and seawater intrusion.

The combination of inter-basin water transfer, saline water use, micro-irrigation and drought resistant varieties are strategies that should hinder groundwater depletion and recover its storage in the NCP. There is plenty of saline water in shallow aquifers, but its use is limited due to its negative effects on crop growth and soil salinization. Saline water use mainly includes brackish water (shallow groundwater) and sea ice water. Brackish water (salinity of 2-5 g l^{-1}) can be used to irrigate crops, up to 0.6 km^3 $year^{-1}$ [3] by 2030. This value is close to 8.3% of average annual groundwater depletion from 2002 to 2014. Therefore, utilization of brackish water to irrigate crops provides a potential alternative to reduce deep groundwater depletion in this region.

Recently, a new irrigation method for using saline water has been developed, that is to alternately irrigate crops with freshwater at sensitive growth stages and saline water at non-sensitive stages. Sharma et al. [4] evaluated the effects of using saline drainage water in various combinations with non-saline canal water for irrigation on soil properties and on the yields of wheat and pearl-millet/sorghum grown in rotation under a monsoonal climate in India. According to knowledge of how plants respond to salinity at different growth stages, Murad et al. [5] also identified an appropriate irrigation scheduling method for cultivation of maize in Bangladesh by conjunctively using the limited freshwater and the abundant saline water resources.

It is essential to evaluate the long-term effects of saline water irrigation on soil salinization and crop growth and yield. Kumar et al. [6] simulated salt dynamics in the root zone and yield of a wheat crop under irrigated saline regimes and found that the SWAP model could be used to simulate the salt dynamics in the crop root zone and yield of wheat with acceptable accuracy under the irrigated saline environment. The model performed better for prediction of relative yield of salt tolerant varieties as compared to the non-tolerant variety. Hassanli et al. [7] also evaluated the performance of AquaCrop, SALTMED and SWAP models under cyclic use of saline and non-saline irrigation water for forage maize yield in the Karaj region of Iran.

The Land and Water Division of the Food and Agricultural Organization has developed a crop water productivity model named AquaCrop to ensure efficient use of water and enhance crop water productivity to keep pace with the increasing population of the world. It simulates yield response to water of herbaceous crops with the concept of normalized crop water productivity [8] and is particularly suited to address conditions where water is a key limiting factor in crop production. It attempts to balance accuracy, simplicity, and robustness, which uses a relatively small number of explicit and most-intuitive parameters and input variables requiring simple methods for their determination [8, 9]. Under the water-limited environment in the North China Plain there is a need to maximize crop water productivity and minimize soil salinization by combination of deficit irrigation and saline irrigation. This can be achieved with the help of a validated water productivity model such as AquaCrop.

3.2. MATERIALS AND METHODS

3.2.1. Experimental site and treatments

The experiment was conducted from October 2014 to June 2015, and from October 2015 to June 2016 at the Hengshui Dryland Farming and Agriculture Experimental Station (37.54 °N, 115.42 °E) belonging to the Institute of Dry Farming and Agriculture, Hebei Academy of Agriculture and Forestry Sciences (Fig. 3.1).

FIG. 3.1. Experimental location: Dryland Farming and Water saving Agriculture Station at Hengshui (Hebei).

The station is located in the middle of the Hebei Plain, with a typical continental monsoon climate, adequate light, average frost-free period of 188 d, average annual sunshine of 2600.5 h, annual average temperature of 12.6 ºC, average annual rainfall of 500 mm, with seasonal and inter-annual variations in distribution. The soil texture is silty clay (0-60 cm), soil bulk density was 1.48 g cm^{-3} (0-30 cm), and field volumetric water content was 42.9%. Soil organic matter and nutrient contents are given in Table 3.1.

TABLE 3.1 SOIL PROPERTIES AT THE EXPERIMENTAL SITE

Soil depth (cm)	Organic matter (g·kg^{-1})	Total N (g kg^{-1})	Available nutrient (mg·kg^{-1})		
			N	P	K
0-10	9.3	5.8	77	1.8	115
10-20	9.3	5.0	40	1.5	90
20-30	7.9	4.7	23	1.2	65

Five treatments were applied (Table 3.2). CK was the rainfed control during the whole wheat growth period. AIFS1: wheat received three irrigations with saline water at the seedling stage, freshwater at the turning green-jointing stage and saline water at the flowering-filling stage (Table 3.2); AIFS2: wheat was irrigated with freshwater at the seedling stage, saline water at the turning green-jointing stage, and freshwater at the flowering-filling stage (Table 3.2). AIFS3: no irrigation was applied at the seedling stage, fresh irrigation water at the turning green-joint stage and saline irrigation at the flowering-filling stage. AIFS4: irrigated with saline water at the turning green-joint stage and with freshwater during the flowering-filling stage. All treatments were laid out in a randomized block design in 15 plots of 8 m × 12 m with three replications.

TABLE 3.2 IRRIGATION TIME AND AMOUNT OF ALL TREATMENTS IN WHEAT EXPERIMENTS (2014.10-2015.6; 2015.10-2016.6)

Treatments	Seedling	Turning green jointing	Flowering and filling
CK			
AIFS1	Saline (4.35 dS m^{-1})	Fresh (0.39 dS m^{-1})	Saline (5.42 dS m^{-1})
AIFS2	Fresh (0.34 dS m^{-1})	Saline (4.63 dS m^{-1})	Fresh (0.42 dS m^{-1})
AIFS3		Fresh (0.39 dS m^{-1})	Saline (5.42 dS m^{-1})
AIFS4		Saline (4.63 dS m^{-1})	Fresh (0.46 dS m^{-1})

3.2.2. Measurements of soil water/salt content, EC and weather parameters

Volumetric soil water content (SWC) in the centre of each plot before and after each irrigation, or at least bi-weekly during crop growth and maturation, was measured with a CPN Hydroprobe neutron moisture meter (NMM) at intervals of 20 cm from 20 to 100 cm depth, and with a Minitrase portable time domain reflectometry (TDR) unit in the surface 20 cm. The

NMM was calibrated when the access tubes were installed. Calibration was very consistent over time and space in the plot area. Fresh and saline irrigation water was collected in 500 ml bottles which were kept in the refrigerator at 4 ºC for analysis of pH and EC. Soil samples were also collected in the field and stored in plastics bags for laboratory analysis of pH and EC.

Meteorological data was measured by the standard automatic weather station powered by solar energy. Variables measured included global radiation, air temperature, air humidity, rainfall, and wind speed at 2 m above ground (Fig. 2). Meteorological data were analyzed with Sigma plot.

The mean monthly temperatures were in 2014-2016, 10 ºC in February, 20 ºC for April, and 30 ºC for June. During the growing season, the lowest daily mean temperature was 10 ºC in April 2015 and the highest was 30 ºC in May. The mean monthly humidity ranged from 60 to 80%. The lowest diurnal variation in humidity was 20% in June and the highest was 40% in April.

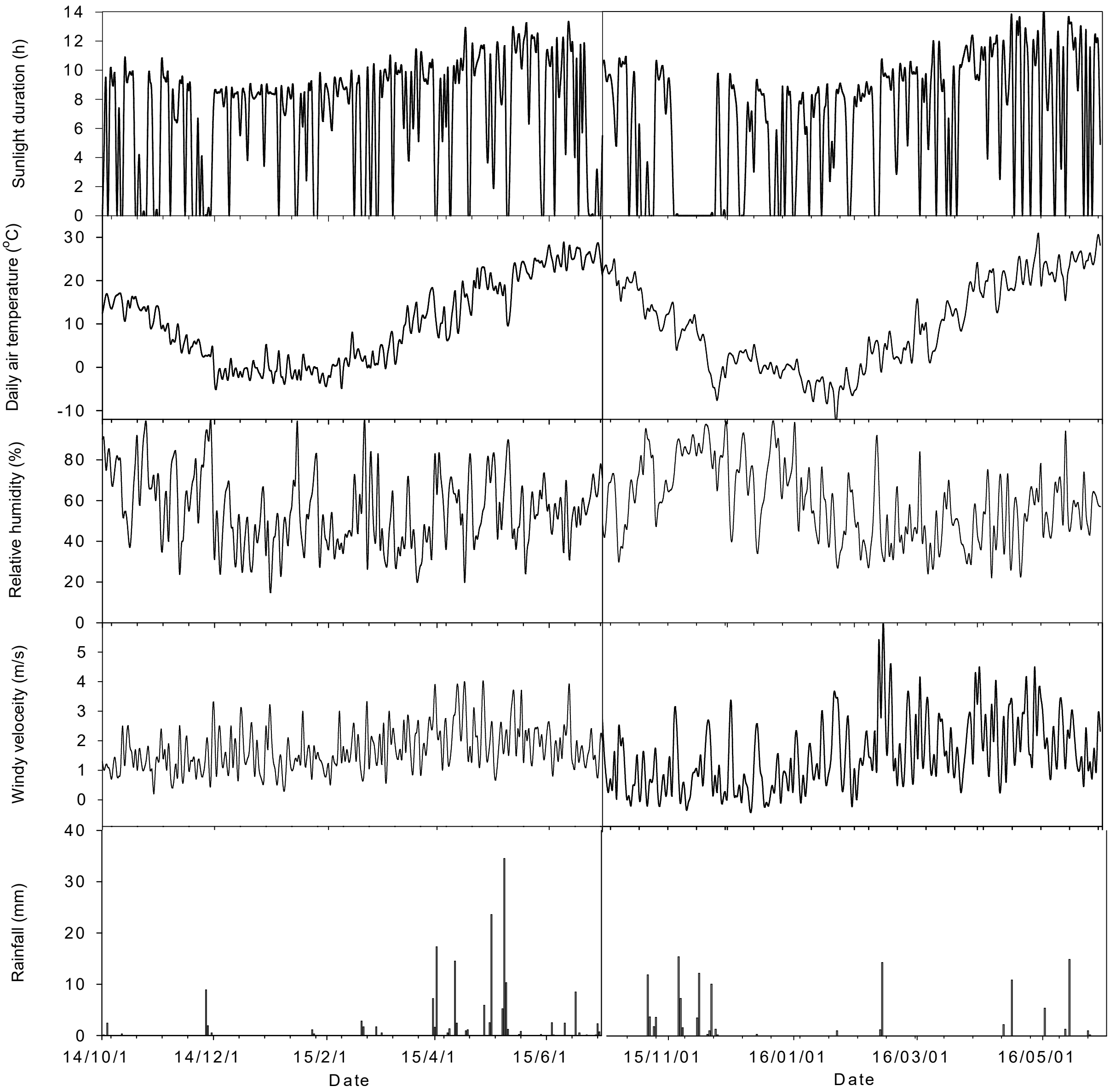

FIG. 3.2. Weather conditions (2014.10-2015.6 and 2015.10-2016.6).

3.2.3. Estimation of crop water use

The Irrigator's Equation (Eq. 1) was used to estimate the depth of water applied.

$$Q \times t = d \times A \quad (1)$$

where Q is the flow rate ($m^3 s^{-1}$); t is the set time or total time of irrigation (hours); d is the depth of water applied (mm) and A is the area irrigated (ha).

ET_a is calculated by the soil water balance as given by Eq. 2:

$$ET_a = P + I + R - D - \Delta S \quad (2)$$

where ET_a is natural crop evapotranspiration (mm day^{-1}); P is precipitation (mm day^{-1}); R is runoff (mm day^{-1}); D is deep water percolation (mm); ΔS is changes of soil water storage (mm).

3.2.3.1. Crop data collection

Plant samples were collected to measure above-ground and below-ground biomass at the different growth stages, i.e. seedling (early February), green-up stage (February-March), jointing stage (late March), elongation stage (early April), booting stage (late April), heading stage (early May), middle stage of maturity (mid-May) and maturity (early June). Fresh and dry plant weights were measured for each sample from each plot.

Carbon isotope (^{13}C) determinations of leaf samplings were performed by isotope ratio mass spectrometry at the stable isotope laboratory, in the Institute of Environment and Sustainable Development in Agriculture, Chinese Academy of Agricultural Sciences.

To estimate the significance level of grain yield difference between the five treatments, in each plot we manually sampled and weighed fresh grain from a subplot approximately 1 m × 1 m in area before harvest by machine. Approximately 10 kg of fresh grain from each plot was sampled and oven-dried to estimate the water content of the fresh grain. The dry grain yield was calculated from the total fresh grain weight in each plot with its water content to estimate the water use efficiency (WUE) of the wheat, which is the ratio of actual yield to crop water consumed. If the crop yield is expressed in kg m^{-2} and the water use is expressed in m^3 m^{-2}, then WUE has units of kg m^{-3} on a unit water volume basis.

3.2.3.2. Calibration and validation of Aqua Crop model

Before the model application, calibration and validation are important steps, which involve a comparison between independent field measurements and output predicted by the model. Soil water content over the root depth, canopy cover, above-ground dry biomass and grain yield were considered for model evaluation. The performance of the calibrated model was evaluated against independent data sets (experimental data of 2014–2015 season) which were not used for model calibration. Different statistical indices including coefficient of determination (r^2), regression 1:1, absolute and normalized root mean square error (RMSE) and agreement (D-index) were employed for comparison of predicted against observed data. The coefficient of determination (r^2) is expressed as percent in Eq. (3):

$$r^2 = \frac{\sum_{i=1}^{n}(O_i - O_{avg})(P_i - P_{avg})}{\sqrt{\sum_{i=1}^{n}(O_i - O_{avg})^2}\sqrt{\sum_{i=1}^{n}(P_i - P_{avg})^2}} \quad (3)$$

where P_i and O_i refer to predicted and observed values of the study variables, respectively, e.g. canopy cover (*Cc*), biomass, grain yield and evaportranspiration. P_{avg} and O_{avg} are the means of the predicted and observed variables, respectively. The normalized RMSE is expressed as percent in Eq. (4).

$$RMSE = \sqrt{\frac{1}{n}\sum_{i=1}^{n}(O_i - P_i)^2} \quad (4)$$

Normalized RMSE gives a measure (%) of the relative difference of simulated versus observed data. The simulation is considered excellent if a normalized RMSE is less than 10%, good if the normalized RMSE is greater than 10% and less than 20%, fair if the normalized RMSE is greater than 20% and less than 30%, and poor if the normalized RMSE is greater than 30%. The index of agreement (D-index) was estimated according to Eq. (5). The closer the index value is to one, the better the agreement between the two variables that are being compared and vice versa:

$$d = 1 - \frac{\sum_{i=1}^{n}(P_i - O_i)^2}{\sum_{i=1}^{n}(|P_i^{'}| + |O_i^{'}|)^2} \quad (5)$$

where P_i the predicted data, O_i is a measured observation, $P_i^{'} = P_i - P_{avg}$ and $O_i^{'} = O_i - O_{avg}$

3.2.3.3. Evaluating long term effects of saline water irrigation with the AquaCrop model

After verification, the AquaCrop model was used to assess long-term effects of alternate irrigation with fresh and saline water on soil salinization and wheat productivity in the North China Plain. The model was used to evaluate the effects of different saline irrigation scenarios (crop growth stages and depth of saline/freshwater applied) on soil salt accumulation and grain yield. Using weather data from the study area from 1971 to 2010, years were classified as: wet (W), normal (N), and dry (D), depending on the amount of annual precipitation (W > third quartile, first quartile < N < third quartile, D < first quartile). The soil characteristics of Hengshui station (Table 3.3) were used for the simulation.

TABLE 3.3 SOIL PHYSICAL CHARACTERISTICS OF THE EXPERIMENTAL SITE

Depth (m)	Moisture content (volume %)			Bulk density (g cm^{-3})	K_{sat} (mm d^{-1})	CN
	Permanent wilting point	Field capacity	Saturation			
0.0-0.3	14.0	32.2	44.1	1.42	230	75
0.3-0.5	15.3	34.3	46.4	1.50	230	
0.5-0.6	13.1	26.7	43.2	1.45	300	
0.6-0.7	18.6	38.4	46.1	1.40	200	
0.7-1.0	16.5	37.1	45.3	1.43	220	

K_{sat}, saturated hydraulic conductivity; CN, curve number of rainfall-runoff

3.3. RESULTS AND DISCUSSION

3.3.1. Effect of alternate irrigation with fresh and saline water on soil water content

During whole growth period soil water content in AIFS1 to AIFS4 treatments was higher than that of CK (Fig. 3.3). Soil water content was distributed with similar patterns at different growth stages among all treatments. The degree of soil water variations from CK were higher than in AIFS1-AIFS4 by 4.2, 4.6, 3.3 and 3.5%, respectively. In the 0-100 cm soil layer the degree of variation of soil water content in CK was less than those of the irrigation treatments.

3.3.2. Effect of AIFS on soil EC and pH

High EC soil readings indicate potential problems with soil salinity that require attention. A good salinity management practice is needed to determine future action for irrigation system design and application of saline water.

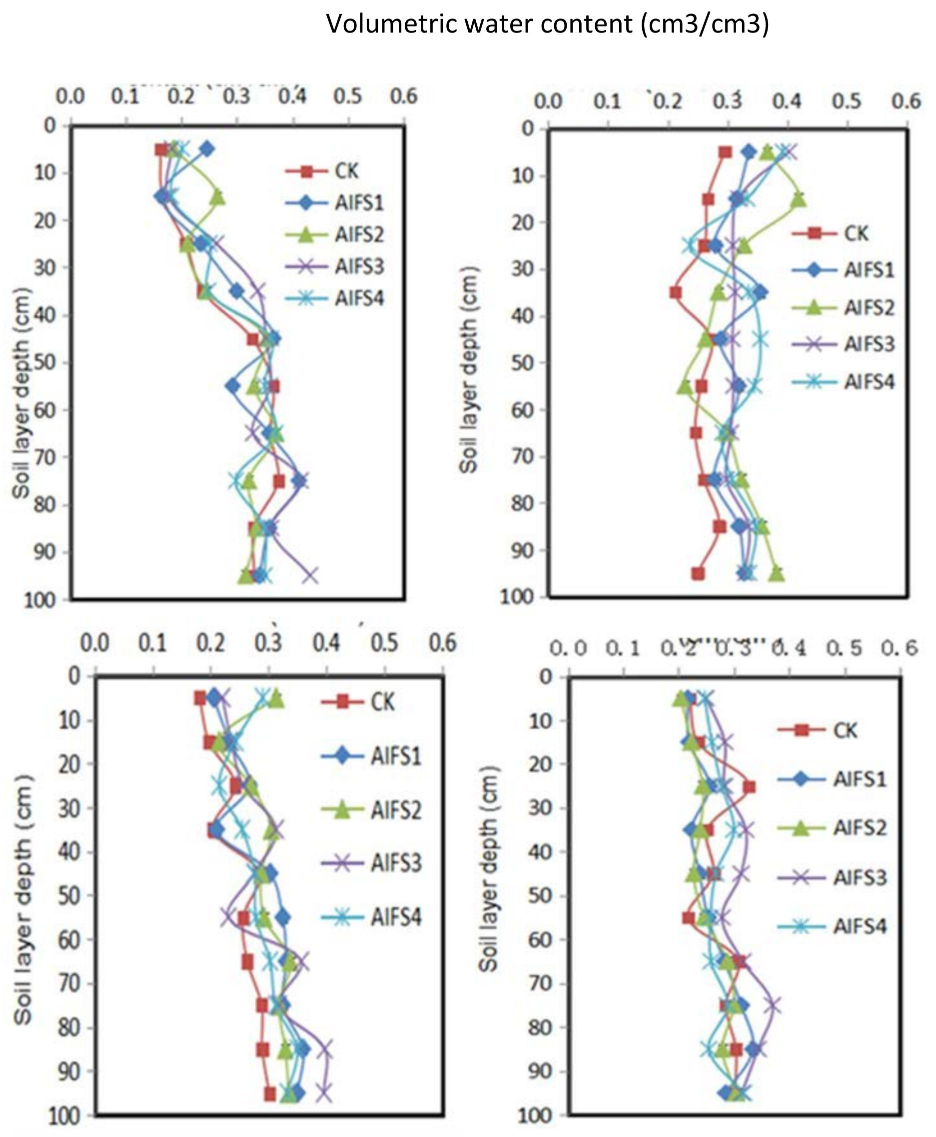

FIG. 3.3. Effects of alternate irrigation with fresh and saline water on volumetric soil water content (2014.10-2015.06 and 2015.10-2016.06).

Soil salt content (electrical conductivity) and pH values of different treatments at different growth stages are shown in Fig. 3.4 and Fig. 3.5, respectively. There were no significant differences for soil electrical conductivity and pH values among all treatments after short-term saline irrigation. During April and May, irrigation with saline water produced some acceptable salt concentrations in the rootzone and increased gradually to the highest values in May (Fig. 3.4), while the average of electrical conductivity showed an increased EC in 2015/04/13. EC decreased in 2015/05/22 after freshwater irrigation.

EC in the topsoil layer increased in AIFS1 compared with the other treatments due to twice irrigation with saline water. Excess salts in the root zone hinder plant roots withdrawing water from surrounding soil [10]. While increasing salinity in the soil solution can produce a positive effect on soil stabilization at high levels, according to Chauhan et al. [11] the data on soil salinity confirm the observation that moisture stress caused a yield decline in treatments with supplemental irrigation with saline water. However, in the AIFS2 treatment the trends of the effect of irrigation water on electrical conductivity (EC) decrease in the 0-100 cm soil layer due to more freshwater moving salt to deeper soil layers, compared with CK. Our results showed the effect of irrigation water salinity on soil EC can be deleted by freshwater washing.

The effect of irrigation water salinity on soil EC values observed during 2014-2015 and 2015-2016 (Fig. 3.4) showed a decrease between planting and the harvest period for the AIFS2 treatment. Full irrigation treatments (AIFS1 and 2) resulted in low EC values at harvest without a significant difference. Higher soil salinity levels were observed for deficit irrigation regimes after harvesting (CK, AIFS3 and 4). Low values of EC should be due to the leaching of soluble salts by freshwater irrigation and rainfall that occurred during the fall and/or winter periods. Thus, alternate irrigation with freshwater and saline water seems to slow down the effects of saline water irrigation on soil salt accumulation, as salts added by saline irrigation are removed from the root zone by freshwater irrigation or rainfall.

In the 0-100 cm soil layer pH was affected by irrigation water salinity. Soil pH increased from 7.5 to 8.5 in all soil depth over 0-100 cm (Fig. 3.5), which may have potentially negative effects on root growth and uptake ability. The average pH covering from 7.0 to 8.5 was maintained by the addition of freshwater to allow the growth of winter wheat. Although wheat has some resistance to some salinity levels, it could lose this tolerance by irrigation with saline water. pH effects in the AFSI treatment were higher in the topsoil layer than the subsurface soil layer (Fig. 3.5).

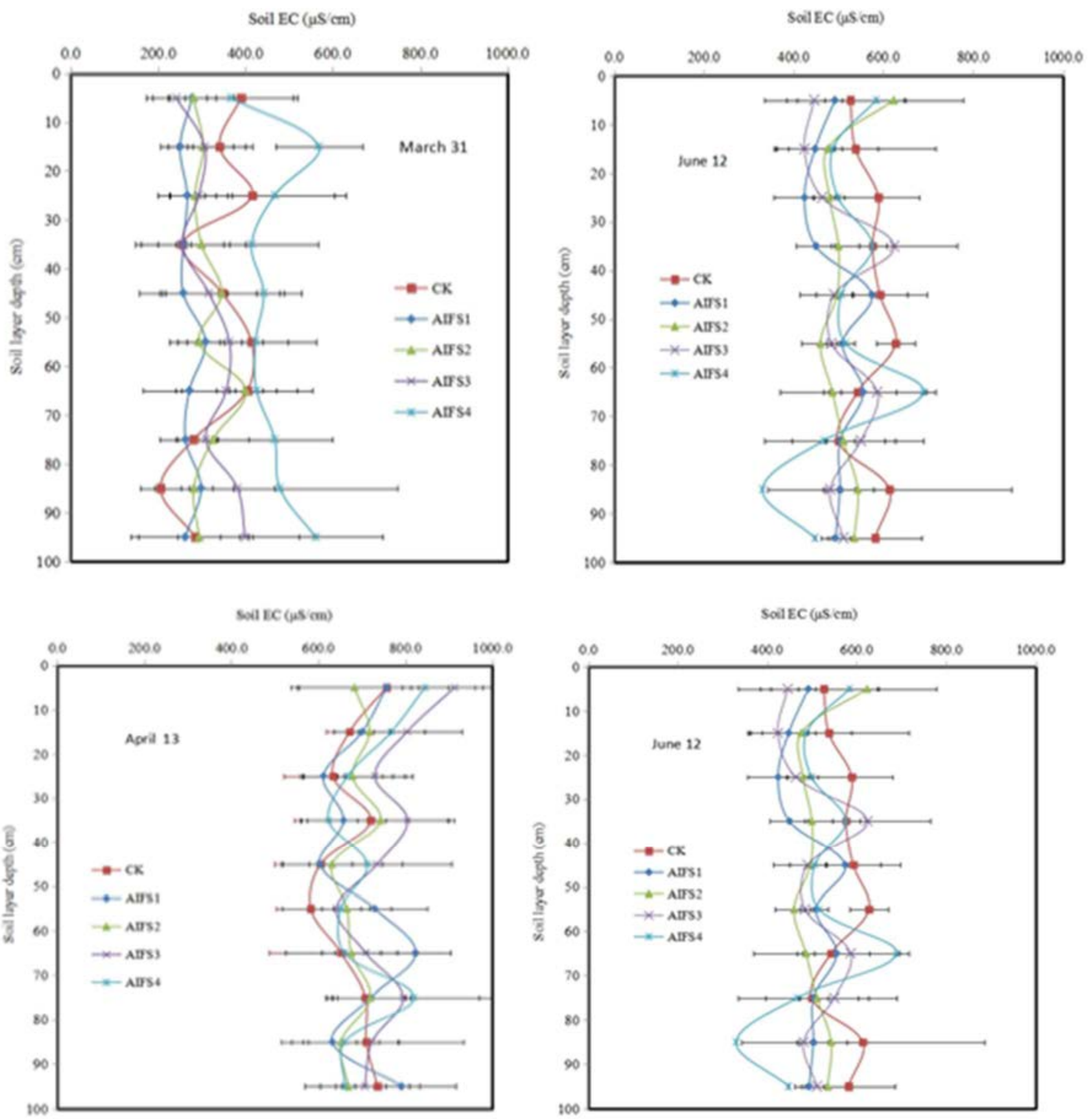

FIG. 3.4. Effects of alternate irrigation with fresh and saline water on soil electrical conductivity (2014.10-2015.06 and 2015.10-2016.06).

Billib et al. [12] reported that efficient water management is one of the key elements in the successful operation of irrigation schemes in arid and semiarid regions. At soil pH values approaching or in excess of 9.0 plants suffer from not only saline stress but also alkaline stress caused by high pH. In fact, all treatments were at a moderately alkaline pH. It was reported by Tyagi [13] that soils that have a high pH in these ranges are often calcareous with a high content of calcium carbonate, and the alkalinity is generally measured in terms of the sodium adsorption ratio (SAR), residual sodium carbonate (RSC) and adjusted SAR. Wheat is moderately susceptible to high pH and may also suffer from nutrient deficiencies on these soils. The increase in exchangeable sodium percentage (ESP) adversely affects soil physical properties, including infiltration and aeration. Soil quality integrates the physical, chemical, and biological components of soil and their interactions.

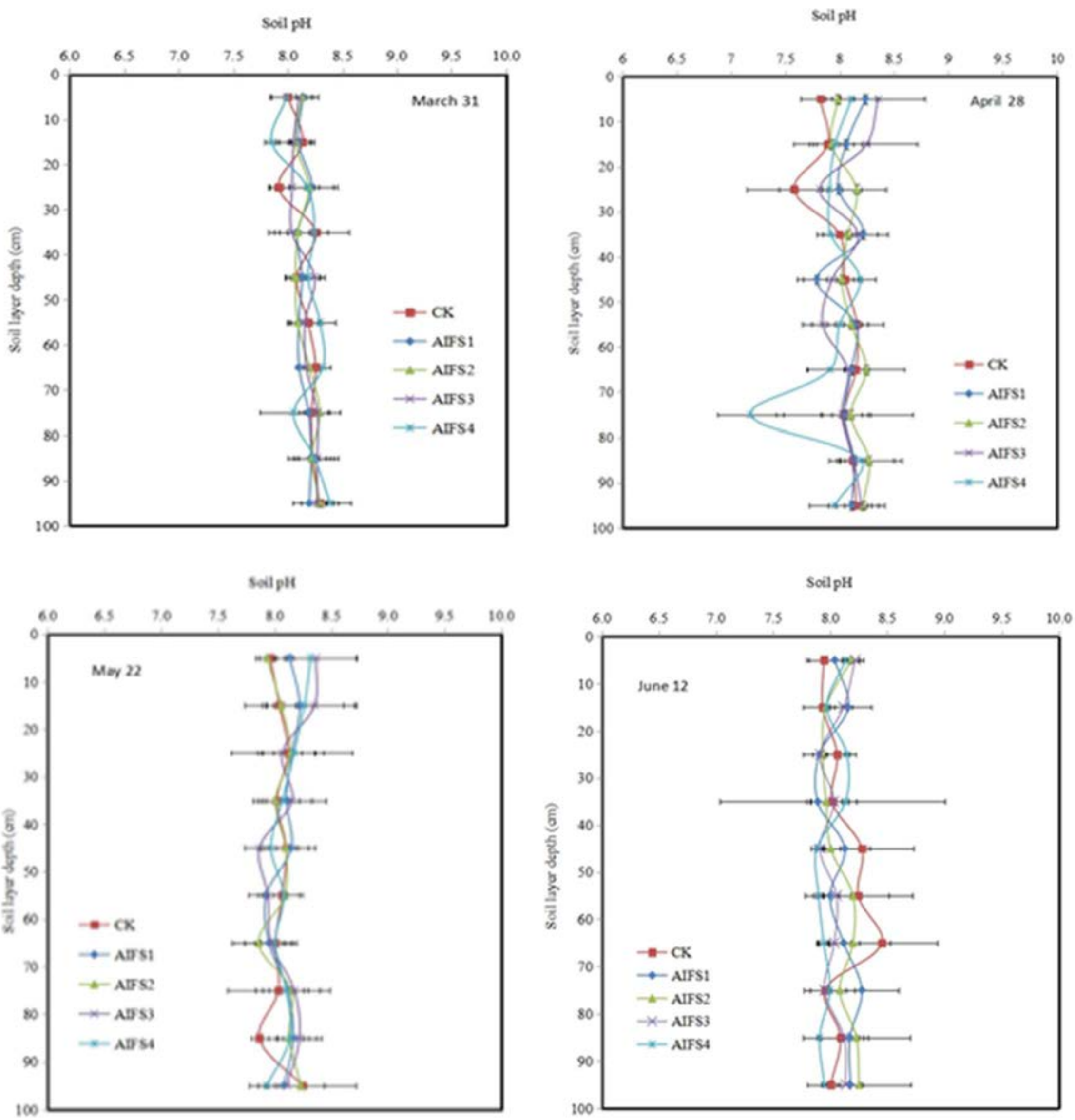

FIG. 3.5. Effect of alternate irrigation with fresh and saline water on soil pH (2014.10-2015.06 and 2015.10-2016.06).

3.3.3. Effect of AIFS on crop biomass accumulation

The effect of alternate irrigation with fresh and saline water on crop biomass accumulation is shown in Fig. 6. At initial and middle stages, the effect of alternate irrigation with fresh and saline water on crop biomass accumulation was not significant. However, differences were significant in the biomass among treatments at maturity. AIFS3 had the highest biomass while CK had the lowest biomass for two experimental seasons. As to below-ground biomass (roots) and above-ground biomass there were similar effects of AIFS. There was a very small difference among treatments at initial and middle stages, but a larger difference among treatments occurred at the maturing stage.

Compared to the CK treatment, the AIFS1, 2, 3 and 4 treatments increased in dry biomass of stem and leaf (60-158 g) for two years (from April, May to June), and the roots had the same response as in March (Fig. 3.6). This was due to the effect in irrigation water salinity on roots and it was indicated by the amount of saline water with EC amounts of 4.35, 4.63, and 5.42 dS m^{-1}. Pearson and Bauder [10] reported that salinity becomes a problem when too much salt accumulates in the root zone to negatively affect plant growth. Excess salts in the root zone hinder plant roots from withdrawing water from surrounding soil. Water deficit and saline water increased the ratio of root to stem biomass for CK and other saline water treatments.

Plants growing in saline soils may appear water stressed [14]. This is because the high salt content of the soil hampers the ability of plants to take up water from the soil. According to Shannon et al. [15] all salinity effects may not be negative, and salinity may have some favourable effects on yield, quality and disease resistance. Yadav et al. [16] reported that the presence of salt in the soil reduces the ability of the plant to take up water, and this leads to a reduction in growth rate, as salt stress affects all the major processes such as growth, water relations, photosynthesis and mineral uptake.

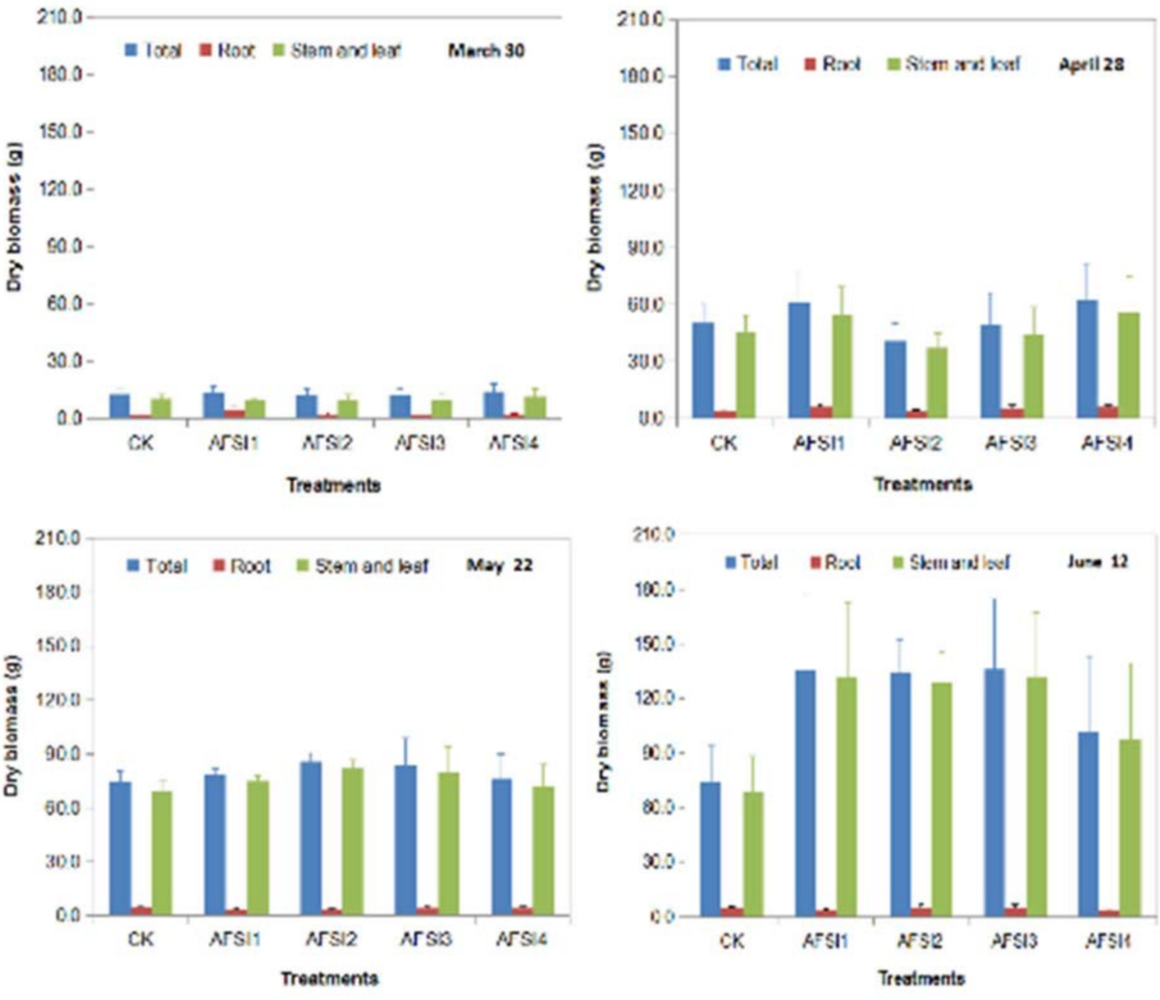

(2014.10-2015.6)

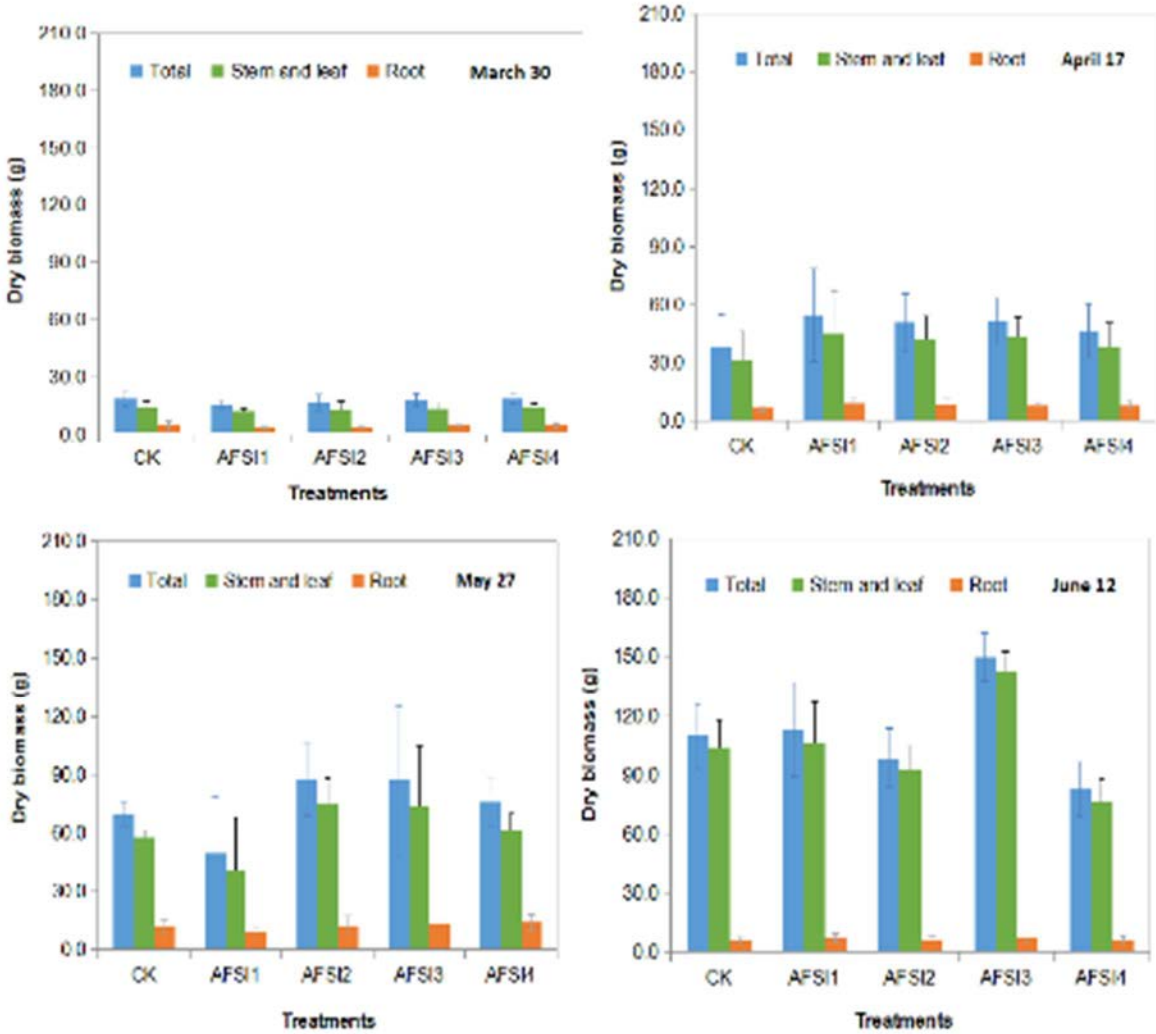

FIG. 3.6. Biomass accumulation under alternate irrigation with fresh and saline water (2014.10-2015.06 and 2015.10-2016.06).

3.3.4. Effect of AIFS on wheat production and water use efficiency (WUE)

Crop water use, yield and WUE for different treatments are shown in Table 3.4. During the experimental period of two years the crop water use and yield of winter wheat was reduced in the rainfed CK treatment. AIFS1 and AIFS2 acquired higher water use and yield than those of AIFS3 and AIFS4 due to more than a single irrigation (90 mm saline or freshwater). Similar results were reported by Fereres and Soriano [17] who found that crop water use efficiency was highest for all crops during dry seasons when deficit irrigation was applied.

Among all treatments AIFS2 had highest yield and AIFS3 had the highest WUE over two years. WUE was considered as an important adaptation to water stress in all treatments (AIFS) with a good yield interaction. All AIFS management treatments improved soil water status and further increased the yields and WUE. During irrigation months, the soil water was maintained at high levels throughout the growth of winter wheat. According to Wan et al. [18] tolerant crops show more or less constant WUE, while sensitive crops show a decrease in WUE with increasing salinity, because of a stronger decrease than evapotranspiration. The best irrigation model for irrigated winter wheat alternating with fresh and saline water was AFSI3 (irrigated with freshwater at the turning green stage and saline water at the flowering-filling stage) due to higher WUE and medium yields.

TABLE 3.4 EFFECTS OF IRRIGATION TREATMENTS ON CROP YIELD AND WUE (2014.10-2015.6 AND 2015.10-2016.6)

Year	Treatments	Irrigation quota (mm)	Water use (mm)	Yield (kg ha^{-1})	WUE (kg m^{-3})
2014.10-2015.6	CK	0	324	6150.0	1.90
	AIFS1	270	453	8139.2	1.80
	AIFS2	270	432	8976.7	2.08
	AIFS3	180	395	8565.8	2.17
	AIFS4	180	387	8096.7	2.09
2015.10-2016.6	CK	0	335	6416.7	1.92
	AIFS1	270	442	7966.7	1.80
	AIFS2	270	446	8583.3	1.92
	AIFS3	180	431	8450.0	1.96
	AIFS4	180	409	7883.3	1.93

According to Tyagi [13] among the various application modes, direct application of saline water can be practiced where the salinity of the water is such that a crop can be grown within acceptable yield levels without adversely affecting soil health. This success, which we could call conventional, can be used with many crops without significant loss of yield. Under such conditions, good drainage management is essential to allow continuous movement of water and salt through the root zone.

There were significant negative linear relationships between WUE and leaf carbon isotope discrimination with coefficients of determination of R^2 of 0.932 (n = 10) under five water levels (Fig. 3.7). These results proved that leaf carbon isotope discrimination could indicate crop water use efficiency [19].

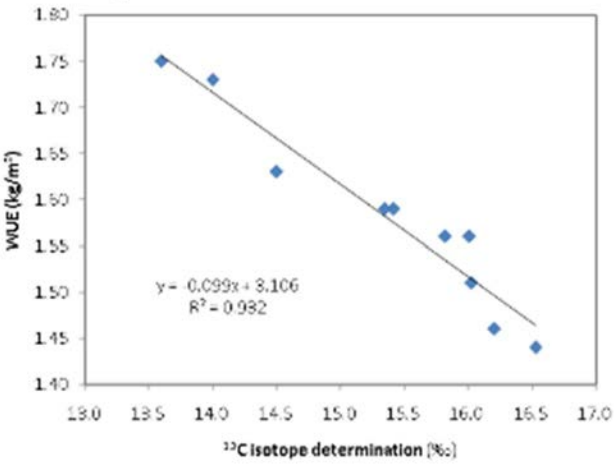

FIG. 3.7. The relationship between water use efficiency and leaf carbon isotope discrimination under five treatments for two growing seasons (2014.10-2015.6, 2015.10-2016.6).

3.3.5. Optimizing deficit irrigation of maize-wheat cropping system with the help of AquaCrop model

3.3.5.1. Verification of the AquaCrop model with experimental data

We verified AquaCrop for winter wheat growth and water productivity with an experimental data set, which included canopy development, soil water dynamics, transpiration and evaporation, biomass accumulation, seed yield and WUE. Soil water changes, canopy development and evapotranspiration were simulated during October 2014 through June 2015 to acquire the validated parameters for the AquaCrop model (Fig. 3.8). There were similar changes and small difference between the simulated and measured data. The simulated and measured data for the final harvest biomass and seed yield and crop water use efficiency are compared in Table 3.5.

3.3.5.2. The application of the verified AquaCrop model to assess the long-term effects of AIFS

The long-term effects of saline water irrigation on soil salt accumulation with the verified AquaCrop model were evaluated. If saline water (4.79 dS m^{-1}) from the shallow aquifer is used to irrigate winter wheat for 30 years, the 0-50 cm root zone salt content will arrive at 8.44~15.36% (Table 3.6). At these values, winter wheat will not germinate. If long-term application of saline water is envisaged, flood irrigation with a huge water amount (100~150 mm) will be required to move salt beyond the root zone to deep soil layers at an interval of 5~6 years.

3.4. CONCLUSIONS

The purpose of this research was to evaluate the effects of alternate irrigation with fresh and saline water on soil salinization, biomass accumulation, crop water use and yield of winter wheat grown in the North Plain China, and then based on these results to validate the AquaCrop model. Finally, the long-term effect of alternate irrigation with fresh and saline water on soil salinization and wheat productivity in the NCP was generated using this verified model and historical meteorological data. Irrigating winter wheat with saline water at non-sensitive growth stages and with freshwater at sensitive stages alleviated the salt stress on crop growth (biomass accumulation) and acquired the highest biomass among five treatments.

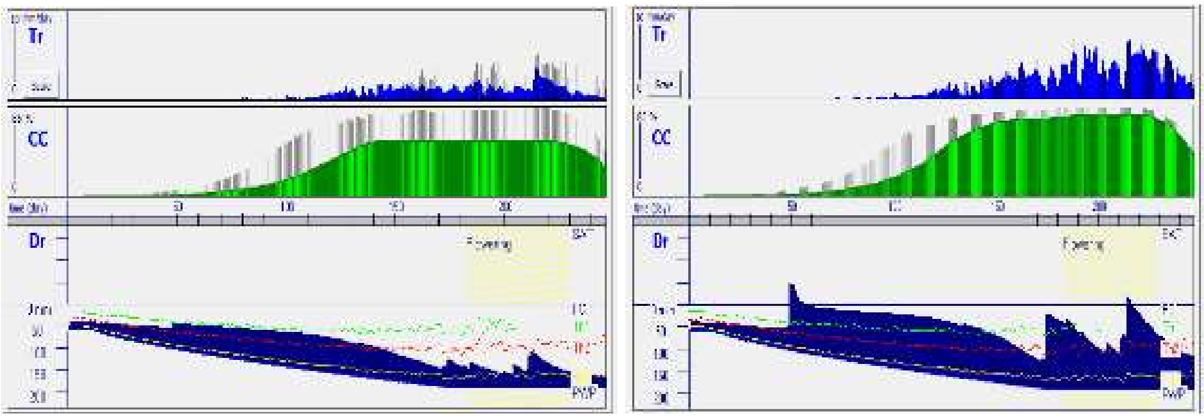

a. CK b. AIFS1

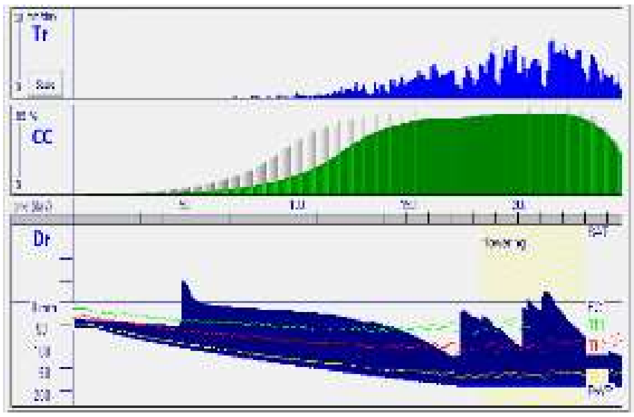

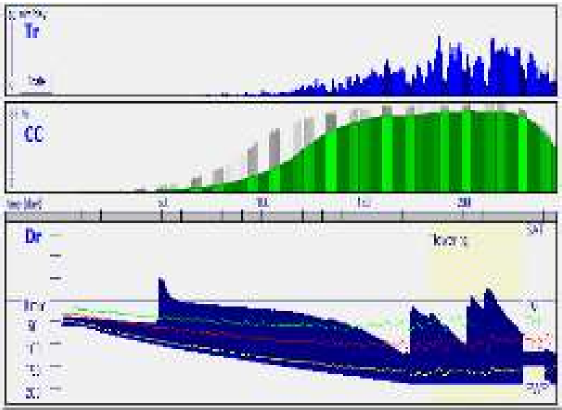

c. AIFS2 d. AIFS3

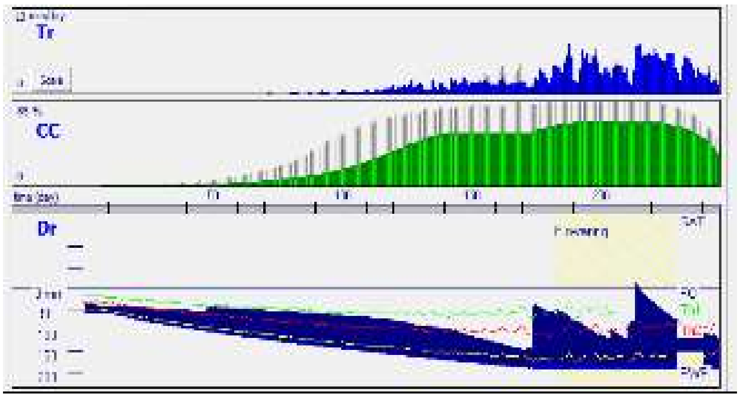

e. AIFS4

FIG. 3.8. Simulation of winter wheat growth and water productivity with AquaCrop; Canopy development; Soil water dynamics; Transpiration and evaporation; Biomass, seed yield and WUE.

TABLE 3.5 COMPARISON BETWEEN THE MEASUREMENTS AND PREDICTED BIOMASS, SEED YIELD AND WATER USE EFFICIENCY (2014.10.10-2015.6.13)

Treatments	Measurements			Predicated values		
	Biomass (t ha^{-1})	Seed yield (t ha^{-1})	WUE (kg m^{-3})	Biomass (t ha^{-1})	Seed yield (t ha^{-1})	WUE (kg m^{-3})
CK	11.60	6.15	1.90	12.50	4.99	1.93
AIFS1	21.90	8.14	1.80	21.40	8.85	1.94
AIFS2	21.40	8.98	2.08	21.20	8.69	1.93
AIFS3	21.90	8.57	2.17	17.30	7.05	1.82
AIFS4	16.30	8.10	2.09	17.40	7.11	1.82

TABLE 3.6 THE LONG-TERM EFFECTS OF SALINE WATER IRRIGATION ON SOIL SALT ACCUMULATION

Treatments	Salt content of water (kg m^{-3})		Irrigation amount (mm)		Topsoil (0-50 cm) salt content (%)		
	Fresh	Saline	Fresh	Saline	10a	20a	30a
CK	0	0	0	0	0	0	0
AIFS1	0.2	3.6	60	120	5.12	10.24	15.36
AIFS2	0.2	3.6	120	60	3.32	6.64	9.96
AIFS3	0.2	3.6	60	60	2.8	5.64	8.44
AIFS4	0.2	3.6	60	60	2.8	5.64	8.44

The best irrigation model for alternate irrigated winter wheat with fresh and saline water was AFSI3 (irrigated with freshwater at the turning green stage and saline water at the flowering-filling stage) due to higher WUE and medium yields. However, for saline water irrigation over the long-term (e.g. 30 y), flooding irrigation with a large volume of water (300-500 mm) will be needed to move salt beyond the root zone to deep soil layers, in order to decrease the effects of soil salinization on crop growth and harvestable yield. This finding may contribute to alleviate the water crisis through increasing the utilization of poor-quality water especially in water-limited regions similar to the NCP.

AquaCrop is a robust tool to predicate crop productivity and salt accumulation of wheat irrigated alternately with saline and freshwater at different growth stages and is also used to assess the long-term effects of AIFS on crop productivity and soil salinization. Therefore, AIFS and AquaCrop have the potential to make a huge contribution to food security improvement in water-limited areas such as the NCP.

ACKNOWLEDGEMENTS

The authors are grateful for the support by the IAEA Research Contracts Programme (No. 18104) and the Chinese National Natural Science Fund (Nos. C31661143011 and 51679243).

REFERENCES

[1] FENG, W., et al., Groundwater storage changes in China from satellite gravity: An overview, Remote Sens. **10** (2018) 674.

[2] FENG, W., et al., Evaluation of groundwater depletion in North China using the Gravity Recovery and Climate Experiment (GRACE) data and ground-based measurements, Water Resour. Res. **49** (2013) 2110–2118.

[3] CAO, G., et al., Use of flow modeling to assess sustainability of groundwater resources in the North China Plain, Water Resour. Res. **49** (2013) 159–175.

[4] SHARMA, D.P., et al., Conjunctive use of saline and non-saline irrigation waters in semi-arid regions, Irrig. Sci. **15** (1994) 25–33.

[5] MURAD, K.F.I., et al., Conjunctive use of saline and freshwater increases the productivity of maize in saline coastal region of Bangladesh, Agric. Water Manage. **204** (2018) 262–270.

[6] KUMAR, P., et al., Simulation of salt dynamics in the root zone and yield of wheat crop under irrigated saline regimes using SWAP model, Agric. Water Manage. **148** (2015) 72–83.

[7] HASSANLI, M., et al., Simulating maize yields when irrigating with saline water, using the Aqua Crop, SALTMED, and SWAP models, Agric. Water Manage. **176** (2016) 91–99.

[8] STEDUTO, P., et al., AquaCrop-The FAO crop model to simulate yield response to water: I. Concepts and underlying principles, Agron. J. **101** (2009) 426–437.

[9] HSIAO, T.C., et al., AquaCrop-The FAO model to simulate yield response to water: III. Parameterization and testing for maize, Agron. J., **101** (2009) 448–459.

[10] PEARSON, K., BAUDER, J., The basics of salinity and sodicity effects on soil physical properties, MSU Extension Water Quality (2006) 1–11.

[11] CHAUHAN, C.P.S., et al., Supplemental irrigation of wheat with saline water, Agric. Water Manage. **95** (2008) 253–258.

[12] BILLIB, M., et al., Integrated water resources management for sustainable irrigation at the basin scale, Chilean J. Agric. Res. **69** (2009) 69–80.

[13] TYAGI, N.K., Managing Saline and Alkaline Water for Higher Productivity, Central Soil Salinity Research Institute (2003) 69–87.

[14] WASKOM, R.M., et al., Diagnosing Saline and Sodic Soil Problems. Crop Series/Soil Fact Sheet (2012) 1–2.

[15] SHANNON, M.C. AND GRIEVE, C.M., Tolerance of vegetable crops to salinity, Sci. Hort. **78** (1998) 5–38.

[16] YADAV, S., et al., Causes of salinity and plant manifestations to salt stress, J. Environ. Biol. **32** (2011) 667–685.

[17] FERERES, E., SORIANO, M.A., Deficit irrigation for reducing agricultural water use, J. Exp. Bot. **58** (2007) 147–159.

[18] WAN, S., et al., Effect of drip irrigation with saline water on tomato (*Lycopersicon esculentum* Mill.) yield and water use in semi-humid area, Agric. Water Manage. **90** (2007) 63–74.

[19] FARQUHAR, G.D., RICHARDS, R.A., Isotopic composition of plant carbon correlates with water use efficiency of wheat genotypes, Aust. J. Plant Physiol. **11** (1984) 539–552.

4. MODELING SOIL WATER AND SALT TRANSPORT UNDER MULCHED DRIP IRRIGATION AND EXPLORING THE CONDITIONS SUITABLE FOR TWO-DIMENSIONAL MODELING USING COMSOL

H. JIAO, Y. CHEN, J. SHI, G. WANG, B. LI
China Agricultural University
Beijing, P.R. China

C. ZHAO, Y. SHENG
Xinjiang Institute of Ecology and Geography
Chinese Academy of Sciences
Urumqi, P.R. China

Abstract

Water shortage and soil salinization increasingly become the main factors constraining sustainable agriculture in southern Xinjiang, China. Mulched drip irrigation, a water-saving irrigation method, has been widely applied in southern Xinjiang for cotton production. In order to evaluate the feasibility of two-dimensional model for simulating soil water and salt dynamics under mulched drip irrigation, numerical simulations employing planar 2-D and 3-D models were conducted and compared with field observations at Aksu, southern Xinjiang. No significant difference was found between the planar 2-D and 3-D simulations for soil water flow, except for the early stage of an irrigation event. The planar 2-D model had a poorer performance in predicting the salt distribution in wide strip during the entire irrigation event. The soil water and salt contents simulated by the planar 2-D model, however, were close to the mean values between two adjacent emitters simulated by the 3-D model, and also coincided with the measurements with corresponding RMSE less than 0.040 cm^3 cm^{-3} and 2.27 g kg^{-1}, indicating that the planar 2-D model was reliable for field irrigation management. Subsequently, hypothetical numerical experiments were further performed considering different irrigation durations and emitter spacings. The results revealed that the planar 2-D model performed better at smaller emitter spacing for delineating soil water and salt transport processes under mulched drip irrigation, and the upper limit value of the emitter spacing suitable for the planar 2-D simulation increased with the prolonged irrigation duration. However, if the effect of solute reaction on retarding solute transport was obvious, the emitter spacing suitable for the planar 2-D simulation should relatively decrease.

4.1. INTRODUCTION

Xinjiang province is located in the inland arid area of China with high evaporation and little rainfall, and hence water shortage and soil salinization are the main concerns restricting the sustainable agricultural development in this area [1]. Mulched drip irrigation, which can save water, raise soil temperature, and restrain salt accumulation on the soil surface [2], has been widely applied in Xinjiang for cotton production. Realizing the full potential of mulched drip irrigation requires knowledge of the precise distributions of soil water and salt during the irrigation period.

Field experiments and process-based numerical models are critical methods to delineate soil water flow and salt transport under irrigation. Field experiments are limited by time, space and manpower, while numerical models can overcome such factors. Especially with the computer speed increasing and more comprehensive numerical models arising, numerical approaches are now increasingly being used for evaluating and optimizing the irrigation strategies [3–5].

Soil water and salt transport under drip irrigation are three-dimensional (3-D) processes, whereas for simplification, two-dimensional (2-D) models are often used for studying these processes [6, 7]. Some studies approximated the drip irrigation process using planar 2-D model with an equivalent line source [2, 8–10] while others simulated the process using an axisymmetric 2-D model with an individual point source [11, 12]. Kandelous et al. [7] discussed the errors of soil water content that are made by the approximation of a 3-D subsurface drip irrigation process into a 2-D one on clay loam soil. Nevertheless, the feasibility of applying a planar 2-D model to delineate the 3-D soil water and salt transport processes under mulched drip irrigation in broader types of soils remains elusive, and further study is needed for uncoupling the possible errors caused by such 2-D simplification and for exploring the irrigation conditions suitable for the 2-D modelling.

COMSOL Multiphysics (COMSOL) is a highly integrated numerical simulation software based on finite element theory, and has been widely used in chemical reaction engineering, structural mechanics, earth science, heat transfer and other fields [13–16]. The subsurface flow module in COMSOL is mainly used for simulating geophysics and environmental phenomena, such as groundwater flow, solute transport, geothermal resources, etc. [17–22]. A considerable advantage of flexible COMSOL is that the user can freely define any types of functions that may describe a material property, source or sink term, and boundary conditions, and these functions can be either temporarily correlated or spatially correlated [17]. In addition, users can define a unique set of partial differential equations (PDEs) to describe the physical phenomena that are not included in the preset modules. COMSOL also provides a large built-in library of meshing tools, numerical solvers, and results visualization capabilities.

In this study, numerical simulations employing 2-D (hereafter, 2-D model refers to the planar 2-D model) and 3-D models were conducted for studying soil water and salt transport processes and were compared with the field observations. On these bases, hypothetical numerical experiments were further performed considering different irrigation durations and emitter spacings for sandy and loamy soils to investigate the irrigation conditions suitable for 2-D modelling of the above processes. With these quantitative simulations, the study would provide broader insight into the irrigation conditions suitable for simulating 3-D mulched drip irrigation processes into 2-D.

4.2. MATERIALS AND METHODS

4.2.1. Site description

The experiment of mulched drip irrigation was conducted in 2015 and 2016 at Aksu National Water Balance Station (40°37′N, 80°45′E, 1028.0 m a.s.l.) in southern Xinjiang, China. The study site is located at a typical cotton production area under a continental arid climate with mean annual temperature of 11.2 °C. The average annual precipitation is 45.7 mm which mostly occurs from June to October, while the average annual evaporation from free water surface is 2500 mm. The average depth of the groundwater table is about 2.75 m and the soil texture is mainly loam and silt loam (Table 4.1).

TABLE 4.1 PARTICLE SIZE FRACTIONS AND CORRESPONDING SOIL HYDRAULIC PARAMETER VALUES USED IN THE MODEL

Soil depth	Particle size fraction (%) in mm range			θ_s	θ_r	α	n	l	K_s (cm day^{-1})
(cm)	<0.002	0.002–0.02	0.02–2	(cm^3 cm^{-3})		(m^{-1})			
0–32	6.90	39.94	53.16	0.45	0.036	1.81	1.47	0.5	34.56
32–100	8.36	55.27	36.37	0.44	0.053	1.10	1.49	0.5	17.28

θ_s is the saturated water content, θ_r is the residual water content, α, n, and l are van Genuchten shape parameters, and K_s is the saturated hydraulic conductivity

4.2.2. Field experiments

Three treatments were conducted with specified irrigation amounts of 46.8 mm (T1), 39.6 mm (T2), and 28.8 mm (T3), with the irrigation interval of about 7 d in 2015 and 2016. As shown in Fig. 4.1, the "narrow mulch" planting mode was employed in 2015 (Fig. 4.1a), and "wide mulch" mode was adopted in 2016 (Fig. 4.1b). Each plot was of 66.5 m × 6 m with four pieces of plastic mulch in 2015 and of 66.5 m × 6.75 m with three pieces of plastic mulch in 2016. In the "narrow mulch" mode, a piece of plastic mulch covered four rows of cotton and one drip tube, and the distance between neighbouring mulches was 60 cm. The widths of wide and narrow strips were 65 cm and 10 cm, respectively. In the "wide mulch" mode, the wider plastic mulch covered six rows of cotton and two drip tubes, and the widths of wide, narrow, and bare strips were consistent with the "narrow mulch" mode.

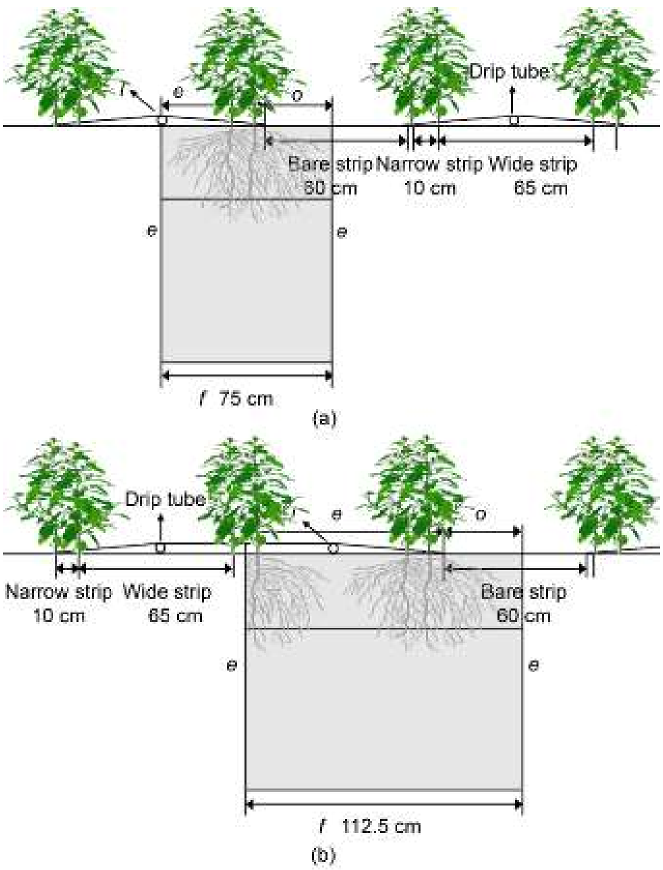

FIG. 4.1. Schematics of the planting modes, modeling domains and boundary conditions for soil water flow in 2015 (a) and in 2016 (b), e is no-flux boundary condition, f is time-variable pressure head boundary condition, o is atmospheric boundary condition, and l is variable flux boundary condition.

Soil samples were collected at every 20 cm depth interval up to 100 cm in wide and bare strips for the measurement of soil water and salt contents. Soil water contents ($cm^3\ cm^{-3}$) were measured twice between two irrigation events using the oven drying method, and soil salt contents ($g\ kg^{-1}$) were measured weekly by drying the 1:5 soil water extract and weighting the solid residue. Meteorological data were collected from the nearby meteorological station.

In 2014, a cosmic ray neutron probe was installed in the cotton field at Aksu Station. To convert neutron counts into soil water content, soil samples at the distances of 25, 75, and 175 m away from the cosmic ray probe, were collected in four directions on July 20 and July 26 (Fig. 4.2). At each sampling point, soil samples were collected at every 10 cm depth interval up to 40 cm in wide and bare strips for the measurement of gravimetric soil water content.

FIG. 4.2. The cosmic ray neutron probe and soil sampling points.

4.2.3. Numerical experiments

COMSOL (version: 5.2, COMSOL Group, Sweden) was used for studying soil water and salt transport processes under mulched drip irrigation. Firstly, the simulations employing 2-D and 3-D models were performed according to the field experimental setup. In addition, to investigate the feasibility of the 2-D simulation for different irrigation conditions, numerical experiments employing 2-D and 3-D models were performed considering different emitter spacings (i.e. from 10 to 60 cm with a 5-cm interval) and irrigation durations (i.e. of 6, 12, 18, and 24 h, with corresponding irrigation amounts of 10.3, 20.6, 30.9, and 41.2 mm, respectively) for sandy and loam soils, respectively. The details of the modeling development are described below.

4.2.3.1. Governing partial differential equations

Soil water flow was simulated in 2-D and 3-D domains in a Cartesian coordinate system. The Richards equation governing soil water flow in a variably saturated domain in the presence of root water uptake is described as,

$$\frac{\partial \theta}{\partial t} = \frac{\partial}{\partial x_i}\left(K(h)\frac{\partial h}{\partial x_i}\right) + \frac{\partial K(h)}{\partial x_1} - S \quad (1)$$

where θ is the volumetric water content, h is the pressure head, t is time, $K(h)$ is the hydraulic conductivity, S is sink term accounting for water uptake by plant roots, and x_i are spatial coordinates ($i = 1, 2$ in the 2-D model, and $i = 1, 2, 3$ in the 3-D model, where x_1 is the vertical space coordinate). Soil hydraulic properties were described using the van Genuchten model [23].

The mobile-immobile (MIM) model is a physically based approach to describe solute transport behavior and separates the porous medium into mobile and immobile regions. The convective-dispersive process is restricted to the mobile zone, and the solute exchange between mobile and immobile regions is described as a first-order process. The solute adsorption by the solid phase is described with a linear adsorption isotherm. Based on the above conceptual model, the equations governing the solute transport in a mobile-immobile domain [24, 25] are described in Eqs. 2 (a-d)

$$\frac{\partial(\varphi_{\mathrm{m}} c_{\mathrm{m}})}{\partial t}+\frac{\partial(\varphi_{\mathrm{im}} c_{\mathrm{im}})}{\partial t}=\frac{\partial}{\partial x_i}\left(\theta_{\mathrm{m}} D_{ij}\frac{\partial c_{\mathrm{m}}}{\partial x_j}\right)-\frac{\partial(u_i\theta_{\mathrm{m}} c_{\mathrm{m}})}{\partial x_i} \tag{2a}$$

$$\frac{\partial(\varphi_{\mathrm{im}} c_{\mathrm{im}})}{\partial t}=\gamma(c_{\mathrm{m}}-c_{\mathrm{im}}) \tag{2b}$$

$$\varphi_{\mathrm{m}}=\theta_{\mathrm{m}}+f_{\mathrm{m}}\rho_{\mathrm{b}}K_{\mathrm{d}} \tag{2c}$$

$$\varphi_{\mathrm{im}}=\theta_{\mathrm{im}}+(1-f_{\mathrm{m}})\rho_{\mathrm{b}}K_{\mathrm{d}} \tag{2d}$$

where $\theta_{\mathrm{m}} = \theta - \theta_{\mathrm{im}}$, $f_{\mathrm{m}} = (\theta_{\mathrm{s}} - \theta_{\mathrm{im}})/\theta_{\mathrm{s}}$, θ_{s} is the saturated water content, θ_{m} and θ_{im} are the mobile and immobile water contents, respectively, f_{m} and $(1 - f_{\mathrm{m}})$ are adsorption fractions in the mobile and immobile regions, respectively, c_{m} and c_{im} are the resident solute concentrations in the mobile and immobile regions, respectively, ρ_{b} is soil bulk density, K_{d} is liquid/solid partitioning coefficient, γ is the first-order exchange coefficient, u_i (i = 1, 2 in the 2-D model, and i = 1, 2, 3 in the 3-D model) is the averaged pore water velocity and $u_i\theta_{\mathrm{m}}$ equals to the flow rate q_i, D_{ij} (i, j = 1, 2 in the 2-D model, and i, j = 1, 2, 3 in the 3-D model) is the dispersion tensor, given by Bear [26],

$$D_{ij}=\delta_{ij}\left(\lambda_{\mathrm{T}}|u|+D\right)+\left(\lambda_{\mathrm{L}}-\lambda_{\mathrm{T}}\right)u_i u_j/|u| \tag{3a}$$

where δ_{ij} is the Kronecker delta ($\delta_{ij} = 1$ if $i = j$ and $\delta_{ij} = 0$ if $i \neq j$), λ_{L} and λ_{T} are the longitudinal and transverse dispersivities, respectively, $|u|=\sqrt{\sum u_i^2}$, D is the effective molecular diffusion coefficient, given by [27],

$$D=D_0\left(\theta^{10/3}/\theta_{\mathrm{s}}^2\right) \tag{3b}$$

where D_0 is the molecular diffusion coefficient in water.

4.2.3.2. Domain geometry, initial and boundary conditions

For 2-D simulation, the domains were set as vertical planes (of 75 cm × 100 cm in 2015 and 112.5 cm × 100 cm in 2016) perpendicular to the drip tube (Fig. 1). For the case in 2015, the 3-D domain has a length of 75 cm, a width of 30 cm (i.e. the distance between the neighboring emitters), and a height of 100 cm.

The initial pressure head and salt concentration values were set as 2-D/3-D interpolation functions based on the measured soil water and salt contents before drip irrigation. In the MIM model, we assumed that a physical equilibrium existed between the mobile and immobile regions, and the initial salt concentrations in the two regions were identical [25].

A time-variable flux boundary condition was applied to the boundary elements representing the emitter. During irrigation, the 3-D model flux was set according to the dripper discharge rate (q), and the 2-D model flux (q') was calculated based on the q, emitter spacing (L_{d}), and the radius of the drip tube (r) [28]. After irrigation, the flux is equal to zero.

$$q'=\frac{q}{\pi L_{\mathrm{d}} r}. \tag{4}$$

Apart from the boundary representing the emitter, the others of 2-D model parameters were identical with those of the 3-D model. A time-variable pressure head boundary condition, which corresponded to the soil water content measured at regular interval, was applied along the bottom boundary for water flow. No-flux condition was established at the lateral boundaries. The upper boundary was divided by the mulch into two parts: mulched and bare soil surface. No-flux boundary condition was imposed at the mulched surface as the plastic mulch prevented passage of evaporation and precipitation, and the time-dependent atmospheric boundary condition was used at the bare soil surface. For solute transport, the irrigation water salinity was taken into account, while the rainwater salinity was neglected due to the small precipitation amount. Third-type Cauchy boundary conditions were used along all domain boundaries.

The potential evaporation and transpiration were calculated based on the meteorological data. Reference crop evapotranspiration (ET_o) was calculated using the FAO Penman-Monteith method, and the potential evapotranspiration of cotton (ET_P) was further obtained by multiplying ET_o with the crop coefficient. The leaf area index was used to divide ET_P into potential evaporation (E_P) and potential transpiration (T_P) using the empirical formula in the CERES model [29].

4.2.3.3. Sink term

The sink term, S, was used to account for root water uptake, which was calculated using the macroscopic approach, described by Šimůnek et al. [30] as follows for the 2-D model:

$$S(h, EC_w, x_1, x_2) = \alpha_1(h)\alpha_2(EC_w)b(x_1, x_2)T_P L_t, \tag{5}$$

where EC_w is the electrical conductivity of soil water, $\alpha_1(h)$ is a water stress response function described according to Feddes et al. [31], $\alpha_2(EC_w)$ is a salinity stress response function described as the threshold-slope model of Maas [32], $b(x_1, x_2)$ is the normalized root density distribution function, and L_t is the width of the soil surface associated with the transpiration process. The parameters for soil salt transport and root water uptake are summarized in Table 4.2.

4.2.3.4. Model calibration and validation

The model was calibrated using the experimental data in 2015 and was further validated using the experimental data in 2016. The calibrated soil hydraulic parameter values are given in Table 4.1. To evaluate the model performance, the mean absolute error (MAE) and the root mean square error (RMSE) were calculated to reflect the correspondence between the simulated and observed values, as given in Eq. 6 and Eq. 7.

TABLE 4.2 PARAMETER VALUES USED IN THE MODEL

Parameter description	Units	Value
Immobile water content, θ_{im}	$cm^3\ cm^{-3}$	0.1
Exchange coefficient, γ	d^{-1}	0.01
Liquid/solid partitioning coefficient, K_d	$m^3\ g^{-1}$	1.79×10^{-6}
Longitudinal dispersivity, λ_L	cm	12
Transverse dispersivity, λ_T	cm	1.2
Solute diffusion coefficient in water, D_0	$cm^2\ d^{-1}$	1.296
Threshold parameter for the Feddes model, h_1	cm	–10
Threshold parameter for the Feddes model, h_2	cm	–25
Threshold parameter for the Feddes model, h_3	cm	–500
Threshold parameter for the Feddes model, h_4	cm	–14000
Threshold value for the Maas model, EC_T	$dS\ m^{-1}$	15.4
Slope value for the Maas model, s	dimensionless	0.026

$$\text{MAE} = \frac{1}{N}\sum_{i=1}^{N}\left|O_i - P_i\right|, \tag{6}$$

$$\text{RMSE} = \sqrt{\frac{\sum_{i=1}^{N}\left(O_i - P_i\right)^2}{N}}, \tag{7}$$

where O_i and P_i are observed and simulated values, respectively, N is the number of observations.

4.3. RESULTS AND DISCUSSION

4.3.1. Soil water contents measured by the cosmic ray neutron probe

The soil water contents measured by the cosmic ray neutron probe are shown in Fig. 4.3. The cosmic ray neutron probe is a convenient and non-destructive method to monitor soil moisture fluctuations in a small region (with a radius of about 300 m). As irrigation amount and time were different for each field at the Aksu station, two fields (i.e., the probe installation field and the flood irrigation field) were selected to analyze the effect of irrigation on the probe measured data. The soil water contents ranged from 0.07 to 0.39 g g^{-1} and increased with the irrigation and precipitation. The cosmic ray neutron probe responded well to the irrigation and precipitation.

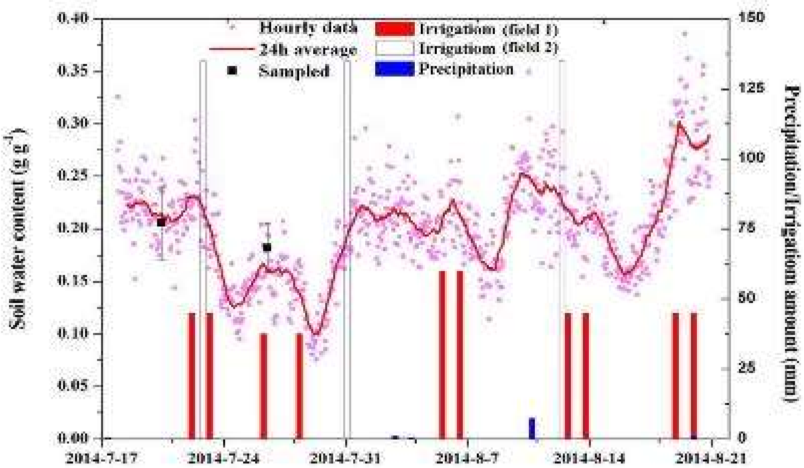

FIG. 4.3. The cosmic ray neutron probe measured soil water content.

4.3.2. Error analysis caused by simplifying 3-D mulched drip irrigation processes into 2-D ones

The changes of soil water distribution during the 24-h irrigation event for T1 are shown in Fig. 4.4a. Soil around each emitter was firstly wetted as a hemisphere, and then the wetting patterns of two adjacent emitters began to gradually overlap. With the irrigation proceeding, the overlap area of two wetting patterns extended, and the water distribution between two adjacent emitters became relatively uniform after a 12-h irrigation.

Similarly, soil salt content started to decrease at the beginning of the irrigation event within a small region, and the size of the desalination area gradually increased with the irrigation proceeding (Fig. 4.4b). However, the remaining soil salt did not become uniform between two adjacent emitters during the entire 24-h irrigation event, and its content increased with increasing distance from the emitter. In addition, the desalination area was smaller than the wetting pattern, and the horizontal radius of the desalinated region at the end of the irrigation event was less than 20 cm.

To compare the 2-D and 3-D simulated results, soil water and salt contents at the vertical cross-section under the drip tube in the 3-D domain (marked as cross-section A) were compared with those at the corresponding vertical line under the emitter in the 2-D domain (marked as line A). In addition, the simulated values at three vertical lines at distances of 0, $L_d/4$, and $L_d/2$ away from the emitter (marked as lines A1, A2, and A3, respectively) were compared for the cross-section A in the 3-D domain. As shown in Fig. 4.5, soil water contents at A1, A2, and A3 were different at the 0−20 cm layer after 2-h irrigation, but then tended to uniformity at the 0−100 cm layer after 12-h irrigation. Soil salt contents at A1, A2, and A3 were different at the 0−10 cm layer after 2-h irrigation. Surprisingly, the difference in soil salt contents among A1, A2, and A3 always existed, and appeared at the 0−26 cm layer after 24-h irrigation. In addition, the 2-D model simulated values were close to the mean values of the 3-D simulation (i.e., the mean values of A1, A2, and A3) across the irrigation event.

The results suggested that soil water infiltration process at the beginning of a mulched drip irrigation event was different from that of a line-source one. Such difference diminished over the propagating wetting fronts and nearly vanished upon a complete merging of two adjacent wetting patterns, when the 2-D model was able to describe the soil water dynamics under the mulched drip irrigation. However, the 2-D model couldn't precisely describe soil salt content for the wide strip across the entire irrigation event. In addition, the 2-D model simulated soil water and salt distributions were close to the average between two adjacent emitters.

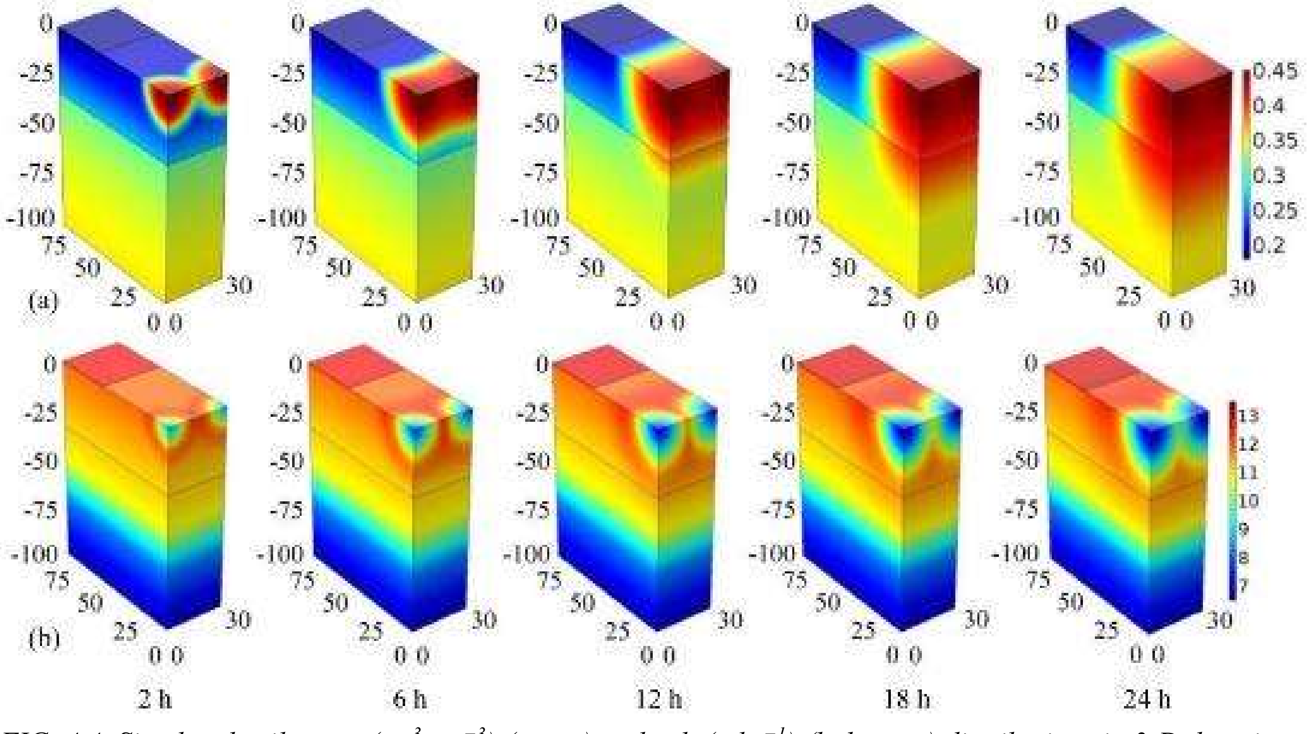

FIG. 4.4. Simulated soil water (cm^3 cm^{-3}) (a, top) and salt (g kg^{-1}) (b, bottom) distributions in 3-D domain (75 cm × 30 cm × 90 cm) along an entire irrigation event, with sampling time from left to right of 2, 6, 12, 18, and 24 h. Values of soil water and soil salinity were given in the legends on the right.

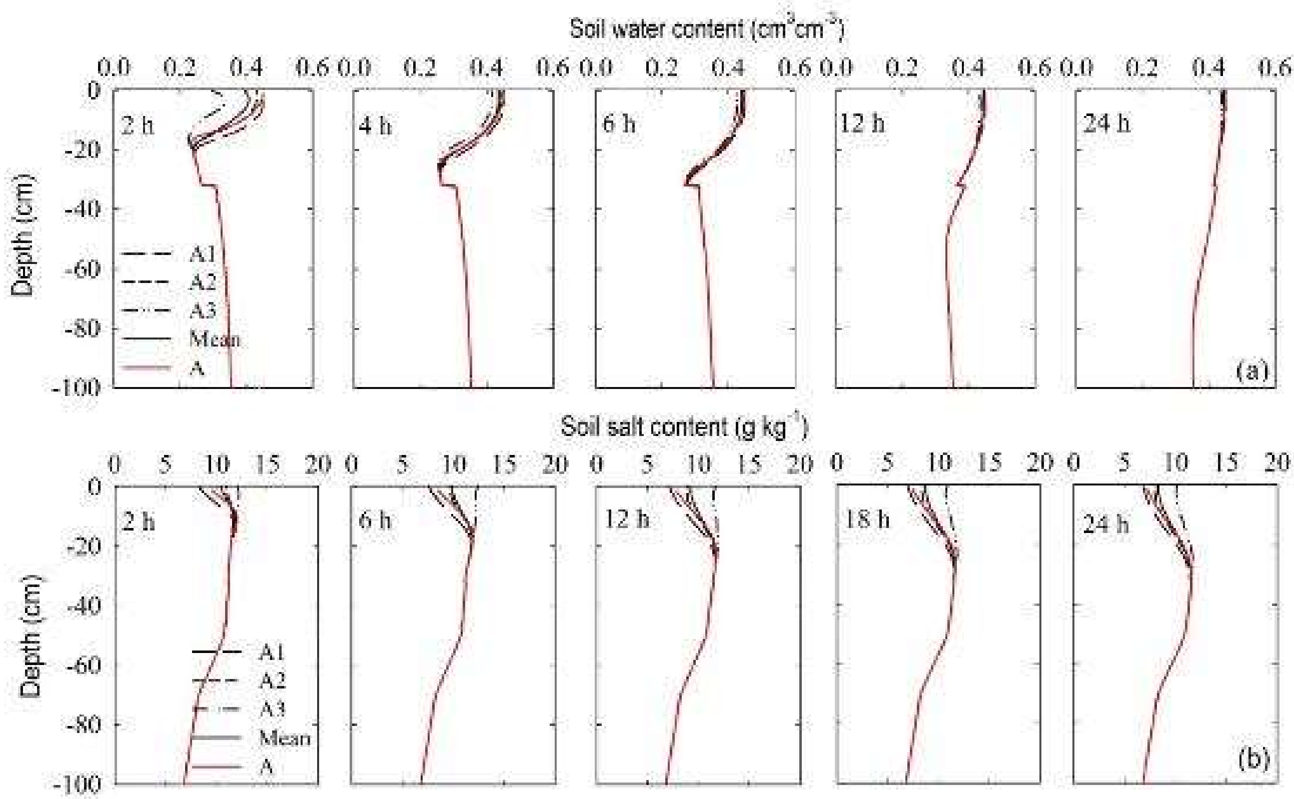

FIG. 4.5. Comparison of simulated soil water (a) and salt (b) contents using 3-D (black lines) and 2-D (red lines) models along a continuous irrigation event. The blank dash lines represent the simulated results of A1, A2, and A3 in 3-D domain, respectively, and the blank solid lines are the average results of the three lines. Red lines mark the simulated results of A in 2-D domain.

4.3.3. Comparison of the 2-D model simulated and measured values

The 2-D model simulated soil water contents were compared with the measured values at different observation points, and the results of T1 in 2016 are shown in Fig. 4.6. The simulated fluctuations of soil water content were more drastic in the upper layer as compared with those of the lower layers, and in wide strip as compared with those of the bare strip due to irrigation, evaporation, and transpiration. The MAE and RMSE values between the measured and simulated soil water contents are summarized in Table 3. The MAE values ranged from 0.023 to 0.033 cm^3 cm^{-3}, and RMSE values ranged from 0.030 to 0.040 cm^3 cm^{-3}, indicating a good agreement between the measured and simulated soil water contents. Other studies [9, 33, 34] also showed a similar magnitude of difference between measured and simulated soil water contents.

The comparison between simulated and measured soil salt contents at different sampling times of T1 in 2016 is shown in Fig. 4.7. Since a small quantity of irrigation water reached to the bare strip, the irrigation-driven salt leaching mainly occurred under the mulch. Evaporation took place at the exposed soil surface, which led to the salt accumulation in the bare strip. The salinity difference between the mulched and exposed areas was found mainly within 40 cm below the soil surface. The MAE values between simulated and measured soil salt contents ranged from 0.78 to 1.89 g kg^{-1}, and the RMSE values ranged from 1.14 to 2.27 g kg^{-1}, which are acceptable for a complex and highly dynamic soil system. These statistical results indicated that the calibrated model implemented by COMSOL could describe soil water and salt transport under the mulched drip irrigation.

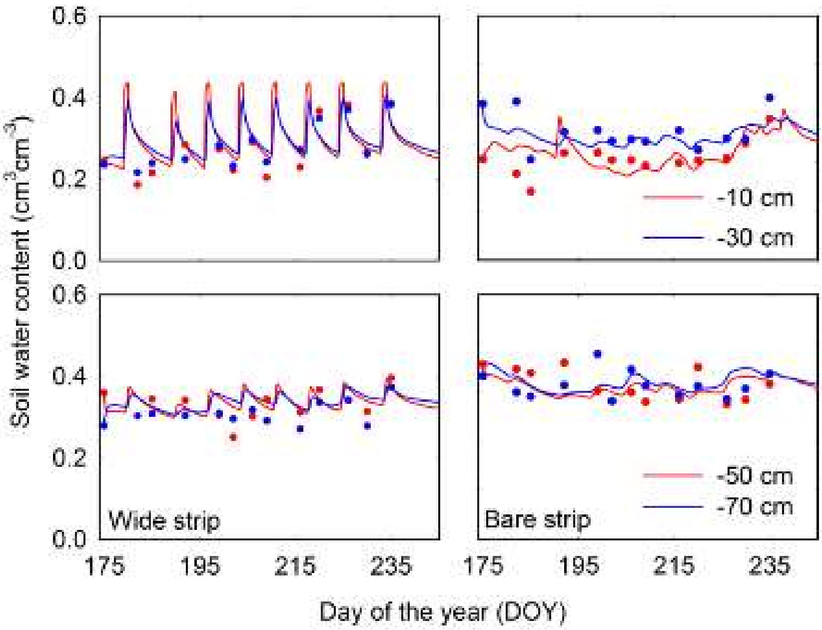

FIG. 4.6. Measured (dots) and simulated (lines) soil water contents for wide and bare strips at different depths for T1 in 2016.

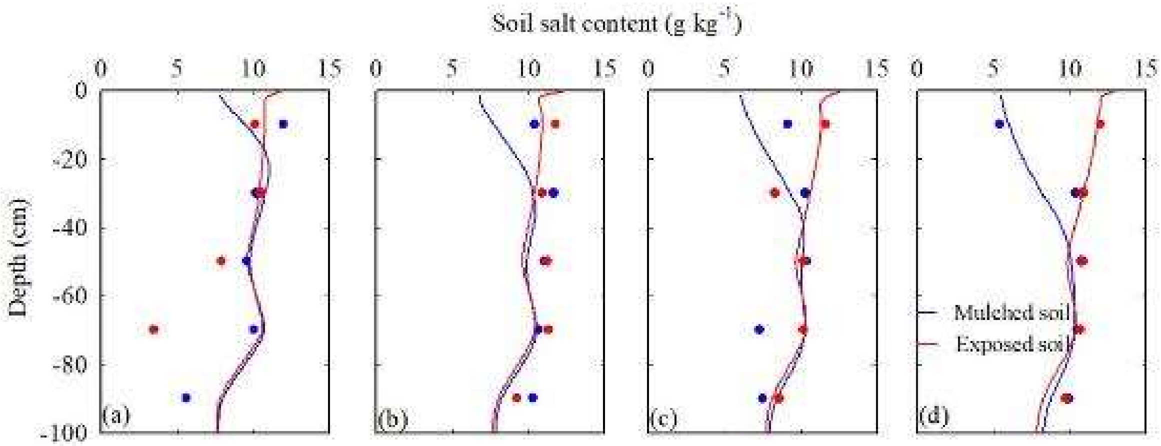

FIG. 4.7. Measured (dots) and simulated (lines) soil salt contents for T1 on (a) July 1, (b) July 21, (c) August 4, and (d) August 23, 2016.

TABLE 4.3 STATISTICAL COMPARISON OF OBSERVED AND SIMULATED VALUES IN 2015 AND 2016

Year	Treatment	Soil water content (cm^3 cm^{-3})		Soil salt content (g kg^{-1})	
		MAE	RMSE	MAE	RMSE
2015	T1	0.032	0.037	1.89	2.27
	T2	0.026	0.032	0.97	1.35
	T3	0.033	0.040	1.82	2.18
2016	T1	0.029	0.034	1.26	1.69
	T2	0.023	0.030	0.78	1.54
	T3	0.026	0.032	0.83	1.14

4.3.4. Analysis of irrigation conditions suitable for the 2-D simulation

To investigate the feasibility of the 2-D simulation for different irrigation conditions, numerical experiments were performed considering different emitter spacings and irrigation durations, respectively. In the 3-D domain, three sets of observation nodes were located at three horizontal positions between two emitters (i.e., 0, $L_d/4$, and $L_d/2$ away from the emitter, denoted as 3-D1, 3-D2, and 3-D3, respectively) and at the depths of 0, 10, 20, 30, and 40 cm, which corresponded to a set of observation nodes at the same depths under emitters in the 2-D domain to obtain soil water and salt contents. The RMSE values between the simulated soil water contents of 3-D1 and 3-D3 were calculated to quantify the uniformity of soil water distributions between two emitters in the 3-D domain, and those between the 2-D simulated soil water contents and the mean values of the 3-D domain (i.e., the average results of the simulated values of 3-D1, 3-D2, and 3-D3) were used to quantify the correspondence between the simulated results of 2-D and 3-D models. In addition, mean relative error (MRE) values [35] were used to quantify these comparisons for soil salt content.

4.3.4.1. Soil water flow

The statistical comparisons between the simulated soil water contents using 3-D and 2-D models for two types of soils, five emitter spacings (only a portion was listed) and four irrigation durations are summarized in Table 4.4. The RMSE values between 3-D1 and 3-D3 for the sandy soil were generally larger than those for the loam soil under the same irrigation conditions. It was primarily due to the higher hydraulic conductivity of the sandy soil, which increased the horizontal heterogeneity of the soil water distribution. As the emitter spacing increased, whether for sandy or loam soil, the RMSE values between 3-D1 and 3-D3 increased. When irrigation duration increased, the RMSE values between 3-D1 and 3-D3 gradually decreased as the 3-D water flow under mulched drip irrigation became similar with the infiltration process under a line source. The changing pattern of the RMSE values between 3-D and 2-D models was similar with that between 3-D1 and 3-D3 as the relatively uniform water distribution between two emitters is beneficial to the simplified 2-D simulation. For each case, however, the RMSE values between 3-D and 2-D models were much smaller than those between 3-D1 and 3-D3.

The results indicated that the 2-D model performed better at smaller emitter spacing for describing the soil water distribution under mulched drip irrigation, and the upper limit value of emitter spacing suitable for 2-D simulation increased with the prolonged irrigation duration. In addition, the 2-D model could, to some extent, predict the average soil moisture condition in the mulched drip irrigated field. Specifically, the RMSE values for both comparisons were less than 0.05 $cm^3\ cm^{-3}$ when emitter spacings were shorter than 15 cm for the sandy soil and 35 cm for the loam soil, even for the short irrigation duration, evidencing a reliable simplified simulation using the 2-D model.

TABLE 4.4 STATISTICAL COMPARISON OF SIMULATED SOIL WATER CONTENTS USING 3-D AND 2-D MODELS AT THE END OF THE NUMERICAL EXPERIMENTS WITH DIFFERENT EMITTER SPACINGS AND IRRIGATION DURATIONS

Soil texture	Emitter spacing (cm)	Comparison	RMSE (cm^3 cm^{-3}) at hour			
			6	12	18	24
Sand	15	3-D1 with 3-D3[a]	0.047	0.046	0.046	0.046
		3-D with 2-D[b]	0.004	0.003	0.003	0.003
	20	3-D1 with 3-D3	0.052	0.051	0.051	0.051
		3-D with 2-D	0.007	0.006	0.006	0.006
	30	3-D1 with 3-D3	0.064	0.062	0.061	0.061
		3-D with 2-D	0.012	0.011	0.011	0.011
	40	3-D1 with 3-D3	0.076	0.072	0.072	0.071
		3-D with 2-D	0.017	0.016	0.016	0.015
	50	3-D1 with 3-D3	0.092	0.084	0.082	0.082
		3-D with 2-D	0.022	0.020	0.019	0.019
Loam	20	3-D1 with 3-D3	0.017	0.013	0.012	0.011
		3-D with 2-D	0.006	0.005	0.004	0.004
	35	3-D1 with 3-D3	0.038	0.025	0.021	0.019
		3-D with 2-D	0.012	0.009	0.008	0.007
	40	3-D1 with 3-D3	0.053	0.030	0.025	0.022
		3-D with 2-D	0.015	0.010	0.009	0.008
	50	3-D1 with 3-D3	0.095	0.047	0.035	0.030
		3-D with 2-D	0.024	0.014	0.011	0.010
	60	3-D1 with 3-D3	0.144	0.074	0.050	0.038
		3-D with 2-D	0.040	0.019	0.014	0.012

[a] 3-D1 with 3-D3, the comparison between the simulated values under the emitter and halfway between two emitters in 3-D domain. [b] 3-D with 2-D, the comparison between the simulated mean values of 3-D domain and the simulated values of 2-D domain.

4.3.4.2. Soil salt transport

For soil salt transport, each case was considered in two situations: in the presence of solute reaction (e.g., adsorption and precipitation) or not. The statistical comparison of soil salt content for five emitter spacings (only a portion was listed) and four irrigation durations is shown in Table 4.5. Similar to the soil water flow, the MRE values for soil salt content between 3-D1 and 3-D3 or between 3-D and 2-D models both increased with the increasing emitter spacings. However, different changing patterns of MRE values could be observed with the increasing irrigation duration. For example, when the emitter spacing was 35 cm for the loam soil, the MRE values gradually decreased without consideration of solute reaction, but gradually increased in the presence of solute reaction. It was primarily because adsorption or precipitation would likely retard the salt leaching process.

The 2-D model performed better at smaller emitter spacing for describing the soil salt distribution under mulched drip irrigation. Specifically, the degree of solute reaction should be taken into account for the feasibility of the 2-D simulation. In the cases without consideration of solute reaction, the MRE values for both comparisons were less than 10% when emitter spacing were shorter than 20 cm for the sandy soil and 30 cm for the loam soil, respectively. However, the upper limit value of the emitter spacing suitable for the 2-D simulation reduced when the solute reaction was obvious.

TABLE 4.5 STATISTICAL COMPARISON OF SIMULATED SOIL SALT CONTENTS USING 3-D AND 2-D MODELS AT THE END OF THE NUMERICAL EXPERIMENTS WITH DIFFERENT EMITTER SPACINGS AND IRRIGATION DURATIONS

Soil texture	Emitter spacing (cm)	Comparison	MRE (%) at h (without solute reaction)				MRE (%) at h (with solute reaction)			
			6	12	18	24	6	12	18	24
Sand	20	3-D1 with 3-D3	6.0	3.9	2.8	2.1	11.9	11.4	10.3	9.3
		3-D with 2-D	1.3	1.3	0.8	1.1	3.0	2.7	2.8	2.0
	25	3-D1 with 3-D3	11.7	8.6	6.2	4.4	14.8	16.6	16.4	15.8
		3-D with 2-D	1.9	1.8	1.1	0.8	3.7	4.0	4.2	3.4
	30	3-D1 with 3-D3	19.0	15.2	11.2	8.5	16.8	20.7	22.1	22.4
		3-D with 2-D	3.1	2.5	2.0	1.3	4.1	5.0	5.5	4.9
	40	3-D1 with 3-D3	34.4	34.1	28.2	22.8	17.7	23.8	28.9	30.8
		3-D with 2-D	6.8	6.3	4.7	5.1	4.6	5.8	7.2	7.5
	50	3-D1 with 3-D3	46.6	55.7	51.6	44.1	18.7	25.5	30.9	35.0
		3-D with 2-D	9.9	11.5	10.2	9.8	5.1	6.3	7.5	8.2
Loam	20	3-D1 with 3-D3	4.4	3.1	2.3	1.8	10.4	9.4	8.3	7.5
		3-D with 2-D	0.9	0.6	0.4	0.3	2.1	1.9	1.5	1.3
	30	3-D1 with 3-D3	9.7	8.5	7.1	6.0	14.9	17.4	17.7	17.4
		3-D with 2-D	1.7	1.2	0.9	0.7	3.2	3.9	3.9	3.7
	35	3-D1 with 3-D3	12.3	12.3	10.5	9.0	15.3	19.0	20.6	21.0
		3-D with 2-D	2.1	1.4	0.9	0.6	3.0	4.0	4.4	4.4
	40	3-D1 with 3-D3	14.13	16.6	14.8	13.04	16.2	20.9	23.4	24.9
		3-D with 2-D	3.48	2.7	2.0	1.73	3.8	4.8	5.5	5.7
	50	3-D1 with 3-D3	17.01	25.0	23.9	22.35	17.1	22.6	26.4	29.2
		3-D with 2-D	5.07	4.8	4.1	3.67	4.3	5.3	6.4	6.9

4.4. CONCLUSIONS

The planar 2-D model was able to precisely describe the 3-D soil water flow under mulched drip irrigation, except for the early stage of an irrigation event. However, the planar 2-D model had a poorer performance in predicting the salt distribution in wide strip during the entire irrigation event. In addition, the planar 2-D model could, to some extent, predict the averaged soil moisture and salinity conditions in the mulched drip irrigated field.

The planar 2-D model performed better at smaller emitter spacings for delineating soil water and salt transport processes under mulched drip irrigation, and the upper limit value of the emitter spacing suitable for the planar 2-D simulation increased with the prolonged irrigation duration. If the effect of solute reaction on retarding solute transport was obvious, the emitter spacing suitable for the planar 2-D simulation should relatively decrease.

REFERENCES

[1] WANG, R., et al., Salt distribution and the growth of cotton under different drip irrigation regimes in a saline area, Agric. Water Manage. **100** (2011) 58–69.

[2] NING, S., et al., Generalization of the root length density distribution of cotton under film mulched drip irrigation, Field Crops Res. **177** (2015) 125–136.

[3] GONCALVES, M.C., et al., Multicomponent solute transport in soil lysimeters irrigated with waters of different quality, Water Resour. Res. **42** (2006) W08401.

[4] DABACH, S., et al., Numerical investigation of irrigation scheduling based on soil water status, Irrig. Sci. **31**(2013) 27–36.

[5] KUMAR, P., et al., Simulation of salt dynamics in the root zone and yield of wheat crop under irrigated saline regimes using SWAP model, Agric. Water Manage. **148** (2015) 72–83.

[6] RUSSO, D., et al., Water uptake, active root volume, and solute leaching under drip irrigation: a numerical study, Water Resour. Res. **45** (2009) W12413.

[7] KANDELOUS, M.M., et al., Soil water content distributions between two emitters of a subsurface drip irrigation system, Soil Sci. Soc. Am. J. **75** (2011)488–497.

[8] ROBERTS, T., et al., Modeling salt accumulation with subsurface drip irrigation using HYDRUS-2D, Soil Sci. Soc. Am. J. **73** (2009) 233–240.

[9] PHOGAT, V., et al., Modelling soil water and salt dynamics under pulsed and continuous surface drip irrigation of almond and implications of system design, Irrig. Sci. **30** (2012) 315–333.

[10] WANG, Z., Jet al., Evaluation of mulched drip irrigation for cotton in arid Northwest China, Irrig. Sci. **32** (2014) 15–27.

[11] KANDELOUS, M.M., ŠIMŮNEK, J., Comparison of numerical, analytical and empirical models to estimate wetting pattern for surface and subsurface drip irrigation, Irrig. Sci. **28** (2010) 435–444.

[12] CHEN, L., et al., A bidirectional model for simulating soil water flow and salt transport under mulched drip irrigation with saline water, Agric. Water Manage. **146** (2014) 24–33.

[13] SUAREZ, V., et al., Study of the heat transfer in solids using infrared photothermal radiometry and simulation by COMSOL Multiphysics, Appl. Radiat. Isotop. **83** (2014) 260–263.

[14] BUTLER, S.L., ZHANG, Z., Forward modeling of geophysical electromagnetic methods using Comsol, Comput. Geosci. **87** (2016) 1–10.

[15] JU, Y., et al., On the thermal spalling mechanism of reactive powder concrete exposed to high temperature: Numerical and experimental studies, Int. J. Heat Mass Transf. **98** (2016) 493–507.

[16] KHAJEPOUR, A., RAHMANI, F., An approach to design a ^{90}Sr radioisotope thermoelectric generator using analytical and Monte Carlo methods with ANSYS, COMSOL, and MCNP, Appl. Radiat. Isot. **119** (2017) 51–59.

[17] WISSMEIER, L., BARRY, D.A., Simulation tool for variably saturated flow with comprehensive geochemical reactions in two- and three-dimensional domains, Environ. Model. Softw. **26** (2011) 210–218.

[18] ZHOU, J., LI, D., 2012. Numerical analysis of coupled water, heat and stress in saturated freezing soil, Cold Reg. Sci. Technol. **72** (2012) 43–49.

[19] SAEID, S., et al., An efficient computational model for deep low-enthalpy geothermal systems, Comput. Geosci. **51** (2013) 400–409.

[20] SAKAKI, T., et al., Airflow pathway development as affected by soil moisture variability in heterogeneous soils, Vadose Zone J. **12** (2013)

[21] SHAO, W., et al., How to use COMSOL Multiphysics for coupled dual-permeability hydrological and slope stability modeling, Procedia Earth Planet. Sci. **9** (2014) 83–90.
[22] BORTONE, I., et al., Design of permeable adsorptive barriers (PABs) for groundwater remediation by COMSOL Multi-physics simulations, Desalin. Water Treat. **55** (2015) 3231–3240.
[23] VAN GENUCHTEN, M.T., A closed-form equation for predicting the hydraulic conductivity of unsaturated soils, Soil Sci. Soc. Am. J. **44** (1980) 892–898.
[24] VAN GENUCHTEN, M.T., WIERENGA, P.J., Mass transfer studies in sorbing porous media I. Analytical solutions, Soil Sci. Soc. Am. J. **40** (1976) 473–480.
[25] RUSSO, D., et al., On the mechanism of field-scale solute transport: Insights from numerical simulations and field observations, Water Resour. Res. **50** (2014) 7484–7504.
[26] BEAR, J., Dynamics of Fluids in Porous Media, Elsevier, NY (1972).
[27] MILLINGTON, R.J., QUIRK, J.M., Permeability of porous solids, Trans. Faraday Soc. **57** (1961) 1200–1207.
[28] BUFON, V.B., et al., Soil water content on drip irrigated cotton: comparison of measured and simulated values obtained with the Hydrus 2-D model, Irrig. Sci. **30** (2012) 259–273.
[29] JONES, C.A., et al., CERES-Maize: A simulation model of maize growth and development. Texas A&M University Press, College Station, Texas (1986).
[30] ŠIMŮNEK, J., et al., The Hydrus software package for simulating two- and three-dimensional movement of water, heat, and multiple solutes in variably-saturated media. Technical Manual, Version 1.0, PC Progress, Prague (2006).
[31] FEDDES, R.A., et al., Simulation of field water use and crop yield, Simulation monographs. Pudoc, Wageningen (1978).
[32] MAAS, E.V., Crop salt tolerance. In: TANJI, K.K. (Ed.), Agricultural Salinity Assessment and Management, Manual Engineering Practice 71, Am. Soc. Civ. Eng., Reston, VA, (1990) 262–304.
[33] PHOGAT, V., et al., Seasonal simulation of water, salinity and nitrate dynamics under drip irrigated mandarin (*Citrus reticulata*) and assessing management options for drainage and nitrate leaching, J. Hydrol. **513** (2014) 504–516.
[34] RAMOS, T.B., et al., Two-dimensional modeling of water and nitrogen fate from sweet sorghum irrigated with fresh and blended saline waters, Agric. Water Manage. **111** (2012) 87–104.
[35] LI, X., et al., Modeling soil water dynamics in a drip-irrigated intercropping field under plastic mulch, Irrig. Sci. **33** (2015) 289–302.

5. COPING WITH SOIL AND WATER SALINITY FOR IMPROVING AGRICULTURAL PRODUCTIVITY IN IRRIGATED WHEAT

R. MIRKHANI
Nuclear Science and Technology Research Institute
Tehran, Islamic Republic of Iran

L.K. HENG, M. ZAMAN
International Atomic Energy Agency
Vienna, Austria

M. MIRZAEI, L. JAHANBAZI
University of Tehran,
Tehran, Islamic Republic of Iran

Abstract

Salinization of land and water scarcity is a big threat to food security and agriculture in the Zayandeh Rood Basin of Islamic Republic of Iran. Developing best practices for sustainable and efficient use of land and water resources in this area is critical to avoid desertification. Accurate crop development models are important tools in evaluating the effects of different irrigation scenarios on crop yield or productivity and predicting yields to optimize irrigation under limited available water for enhanced sustainability and profitable production. A field study using a randomized complete block design with a split plot arrangement in three replications was established. The main plots were 35, 55 and 75% Soil Moisture Depletions (SMD) and the sub-plots were five wheat cultivars. The objectives of this study were to investigate the effect of different scenarios of irrigation (crop growth stages) on wheat yield, to separate evaporation (E) and transpiration (T) using isotopic techniques. Different soil moisture depletion levels had significant ($p<0.001$) effects on wheat grain yield. The maximum harvest index occurred at 55% soil moisture depletion and the lowest HI % was observed at 75% soil moisture depletion. A sensitivity analysis of the model was conducted. AquaCrop model successfully simulated grain yield and biomass in saline-sodic conditions with high accuracy. Average values of normalized root mean square error (NRMSE), index of agreement (d), and coefficient of determination (R^2) of simulated grain yield were 6.2%, 0.91, and 0.89, respectively while these indices were 3.8%, 0.94, and 0.92, respectively for biomass. The highest yield loss was simulated in scenarios where saline water for irrigation was used at sowing, tillering and booting stages. Salinity stress at these stages is likely to affect leaf growth, tiller generation, canopy development and other crop traits which resulted in decreasing biomass production and final grain yield. For simulation of soil water content, the average value of NRMSE was 13.7%, while for the simulation of soil salinity it was 27.6%. Therefore, the error of the model in simulating soil salinity is greater than that in simulating soil water content. The proportion of evaporation to total evapotranspiration was smaller when wheat was sown in early November. Adjusting planting date by AquaCrop model indicated that higher biomass and grain yield are likely to be obtained when winter wheat is sown in early November than in October possibly due to better crop canopy cover.

5.1. INTRODUCTION

Land degradation by salinization and alkalization and scarcity of water are the major problems affecting food security and agriculture in central parts of Islamic Republic of Iran. In these areas, soluble salts accumulate in soil, resulting in a gradual decline of crop production [1]. Isfahan province, which is situated in the center of Islamic Republic of Iran (Fig. 5.1), has more than 60 000 ha of agricultural lands affected by different forms of salinity. The main reasons for such high scale soil salinization include dry climatic conditions, high temperature, high wind speed, high evaporation, low rainfall, and poor farming practices [2]. The steady growth of the region, coupled with the onset of climate change, have taken their respective tolls, leading to increasing water scarcity. The increasing water demand in this area is putting pressure on the Zayandeh Rud's water resources as well as having negative impacts on the livelihood of the people and ecosystems. As a result of climate change, temperatures have been rising constantly, while annual rainfall has been declining and changing in this area. The increasing water demand by different water users is leading to increased competition [3]. Farmers in this area are uncertain about the use of land and availability of water resources for future agricultural activities.

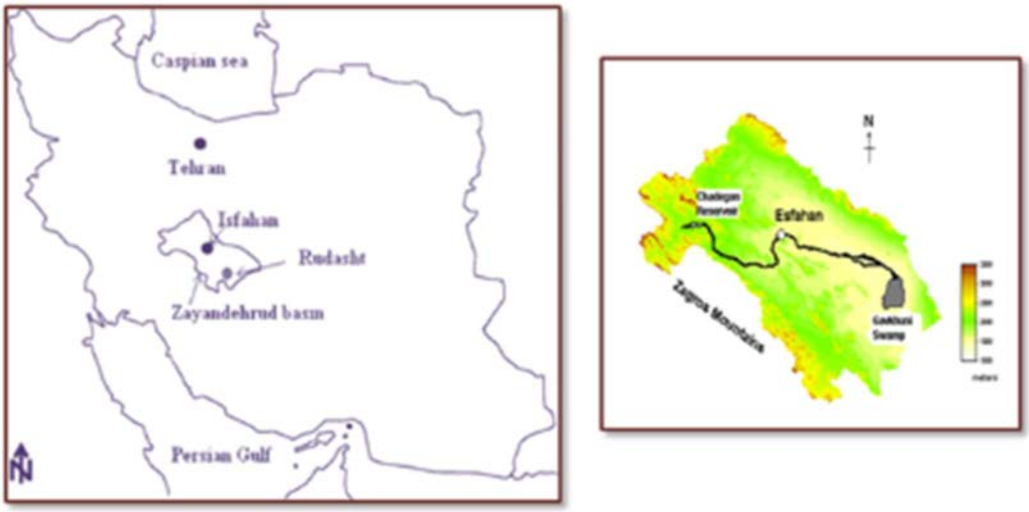

FIG. 5.1. Map of the study area

In Islamic Republic of Iran, the Zayandeh Rud River is regarded as a special resource and it means "the life-giving river". This river originates in the Zagros Mountains with a cold and humid climate, which passes 405 km from the west to the east, providing irrigation water to agricultural lands of Isfahan, and finally reaches the Gavkhuni marshes that are located 140 km south-east of the city of Isfahan, with an arid climate. Thus, the average annual precipitation ranges from 1,500 mm at the Zagros Mountains, where the Zayandeh Rud River originates, to only 80 mm near the desert [3].

Sustainable use of freshwater resources and their conservation is important in this area because of the increasing water demand by the humans, industrial and municipal sectors. Due to increased water demand by all sectors, water availability for agriculture is becoming limited, thus affecting agricultural production and livelihoods of farmers in the area. Due to the limited availability of freshwater, farmers mainly rely on using saline water for agriculture. Using saline water for irrigation may lead to a decrease in crop yield and salinity build-up in the long run. Studying the effect of using saline water for irrigation during sensitive growth stages under field conditions is laborious as well as expensive. In such scenario, a modeling approach including the AquaCrop model which has the most potential as a useful tool to develop best irrigation strategies. In this study, the AquaCrop model version 6.1, developed in 2018, was applied to evaluate the effects of different irrigation scenarios on grain yield and water productivity of wheat under a dry climate with saline-sodic soils. The soil moisture neutron probe (SMNP) was used to measure soil water contents for irrigation scheduling in this study.

The agricultural sector in Islamic Republic of Iran is one of the most important economic sectors, but limited water availability has a negative impact on the production of many crops including wheat. More than 90 percent of the renewable water in the country is used for agriculture, but this can't meet the country's water demand for irrigation because Islamic Republic of Iran is situated in one of the most arid regions of the world. The average annual precipitation is 252 mm (one-third of the world's average precipitation), where 179 mm (71% of the total annual rainfall) is lost through unproductive water use (evaporation) [4]. To develop best practices for efficient use of water on-farm, one needs individual assessment of water losses by evaporation (E) and transpiration (T). At the farm level, evapotranspiration (ET) can be measured using conventional methods such as Bowen ratio, eddy covariance, gradient systems and weighting macro-lysimeters, but these methods can't differentiate between E and T, which are controlled by different biotic and abiotic factors [5–8].

Two isotopic methods have been developed to separate E and T, including isotope mass balance (IMB) and the Keeling Plot. Compared to the Keeling Plot, IMB is a relatively simple technique for assessing time-averaged fluxes of E and T under field condition. IMB is also a simple method to partition between E and T, because of its reliance on mass balance of the amount (mass) and isotopes of water. Meanwhile, it is also simple in operation and can be used for plot experiments in the field, because it does not measure the isotopic composition of water vapor, which is generally difficult under field conditions. However, it only provides a time-averaged estimation of soil evaporation for a given period within the entire crop [9–11]. In our study, the IMB method was applied to separate E and T from ET for analyzing the evapotranspiration components.

5.2. MATERIALS AND METHODS

5.2.1. Study site

The Roudasht region (32º 29' N, 52º 10' E and elevation of about 1,560 m above mean sea level) is located in the southeast area of Isfahan, in the central part of Iran, with about 50,000 ha of salt affected soils. This area comprises fertile agricultural land with a relatively flat topography and medium to heavy textured soils. The climate is dry with low annual rainfall (< 100 mm) and high evapotranspiration demand (>1,500 mm). Agriculture is the main economic activity of the region. Since there is insufficient rainfall (less than 100 mm per year) to leach salts from the soil profile, soluble salts accumulate in the soil. The soil was classified as fine, mixed, thermic, typic Haplosalids with ochric epipedon and salic horizon, containing sporadic carbonates and small amounts of gypsum.

5.2.2. Experimental design

A randomized complete block design with split plot arrangement in three replications was used in our study. The main plots were 35, 55 and 75% Soil Moisture Depletions (SMD) (I_1, I_2, and I_3) and the sub-plots were five wheat cultivars namely: Parsi (V_1), Arg (V_2), Bam (V_3), Roshan (V_4) and Ofogh (V_5) (Fig. 5.2).

In the region, wheat production varies with the quality and quantity of irrigation water. Usual agronomic practices include, plowing and levelling field plots, applying triple super phosphate (100 kg ha^{-1}) as base fertilizer, followed by sowing wheat at 250 kg seed ha^{-1}. Urea fertilizer was applied at 200 kg N ha^{-1} in 3 split applications. Irrigation water was applied using the surface flood method (basin irrigation) without runoff. Weeds were effectively controlled, and no pests or disease were observed during the growing seasons.

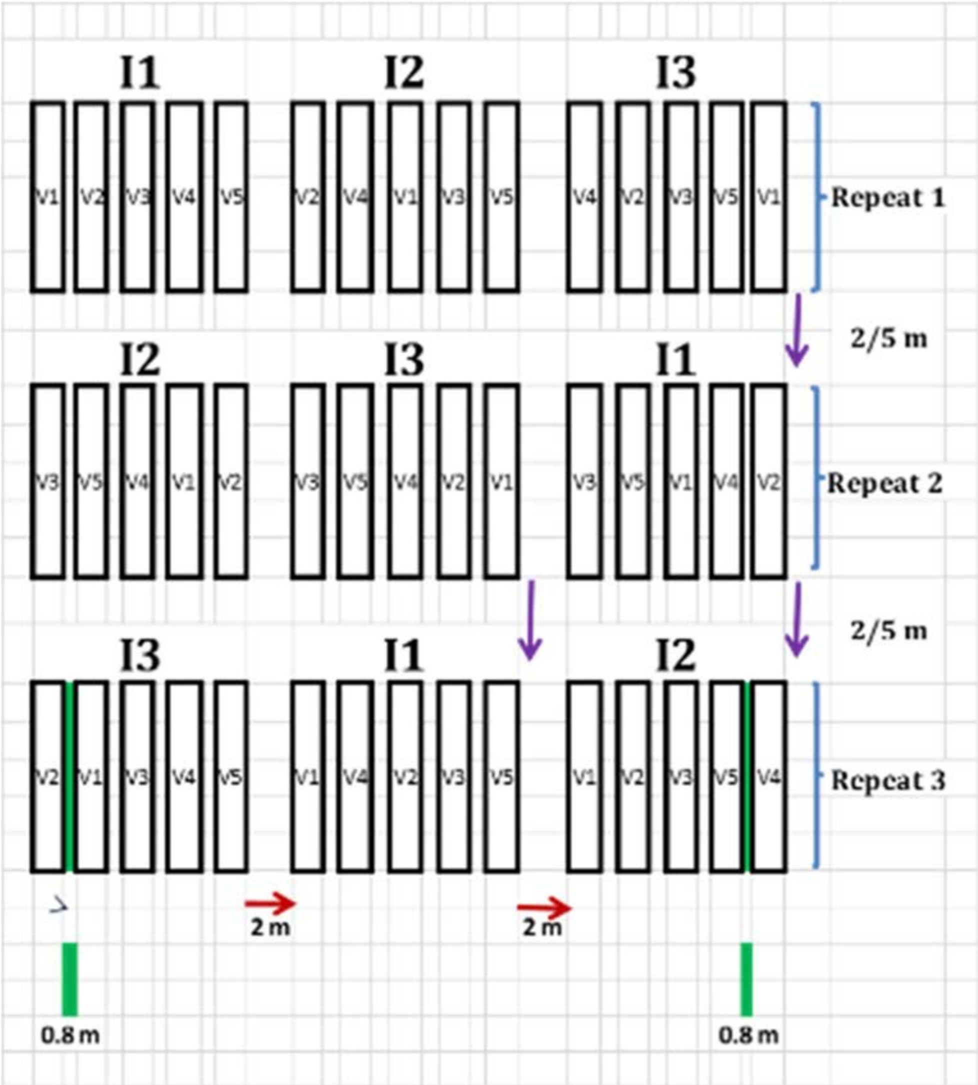

FIG. 5.2 Layout of the experiment

5.2.3. Physical and chemical characteristics of the soil

Soil samples were collected from four depths (0-30, 30-60, 60-90 and 90-120 cm) to determine key soil physical properties. Particle size analyses were determined using the hydrometer method. To determine bulk density, undisturbed soil samples were taken and mass of dry soil was divided by the bulk volume of soil. Field capacity (FC) and permanent wilting point (PWP) were measured using the pressure plate method (Table 5.1). Soils in the area are alluvial deposits and are fine textured. The groundwater level is around 6.5 m below the surface.

TABLE 5.1 PHYSICAL CHARACTERISTICS OF THE SOIL AT THE STUDY SITE

Depth	Distribution ($g\ kg^{-1}$)			Texture	Moisture (volume %)			ρ_b	K_{sat}
(cm)	Clay	Silt	Sand		Sat	FC	PWP	($g\ cm^{-3}$)	($mm\ day^{-1}$)
0-30	390	430	180	Silty clay loam	49	36	21	1.3	72
30-60	550	380	70	Clay	52	32	22	1.4	51
60-90	610	340	50	Clay	47	36	23	1.5	21
90-120	490	420	90	Silty clay	43	34	21	1.6	30
>120	350	550	100	Silty clay loam	42	32	19	1.8	37

Sat, saturation; FC, field capacity; PWP, permanent wilting point

Composite soil samples taken from 0-30 and 30-60 cm depths before planting were used to determine chemical properties. Soil electrical conductivity (EC) was measured by an EC meter in the soil-saturated paste extract, and soil pH was measured by a glass electrode in the soil-saturated paste. Water-soluble Na was determined in the saturation extract using a flame photometer. Water-soluble Ca and Mg were measured by Atomic Absorption Spectrophotometry. HCO_3^- and SO_4^{2-} were measured by titration and acetone methods. Chloride concentration was measured using titration with $AgNO_3$. Soil organic carbon (C) was determined using the Walkley-Black method. Total soil nitrogen was measured by the Kjeldahl method. Available P was measured by the Olsen method, and available K by the ammonium acetate method adjusted at pH 7. The sodium adsorption ratio (SAR) was calculated (Table 5.2).

TABLE 5.2 CHEMICAL CHARACTERISTICS OF THE SOIL AT THE STUDY SITE

Depth	EC	pH	Ions ($meq\ l^{-1}$)						($mg\ kg^{-1}$)		Ions (ppm)		SAR
(cm)	($dS\ m^{-1}$)		Ca	Mg	Na	HCO_3^-	Cl^-	SO_4^{2-}	N	OM	K	P	
0-30	12.7	7.6	26	26	94	2.8	83	60	0.8	8.7	248	6.4	18.6
30-60	9.6	7.6	18	16	73	2.8	50	54	0.6	6.0	300	3.4	17.6

EC, electrical conductivity; OM, organic matter; SAR, sodium adsorption ratio

5.2.4. Soil moisture measurement using neutron probe

Soil moisture measurements are critical in studies of soil-plant-water relationships. A moisture neutron probe is a quick and less sensitive device to measure soil water content under saline condition.

To calibrate the SMNP, aluminium access tubes were installed in the field to 2.2 m depth. Wet site plots were established by irrigating to field capacity by berming the area and ponding water until the wetting front descended below the bottom of the access tubes, and then waiting until the soil drained to field capacity. Also, soil samples were taken close to each access tube at each depth of reading (Fig. 5.3). For the surface soil, the equation for the 10 cm soil depth was different from the equations for deeper layers. Reasonable calibration equations were obtained separately for 10-60, 60-100, and 100-200 cm depth ranges (Table 5.3).

FIG. 5.3. Images of SMNP calibration

TABLE 5.3 CALIBRATION EQUATIONS FOR THE SOIL LAYERS

Row	Soil layer (cm)	Equation*	R^2	RMSE (m^3 m^{-3})
1	0-10	$\theta = 0.826\left(\frac{C}{Cs}\right) + 0.074$	0.92	0.025
2	10-60	$\theta = 0.841\left(\frac{C}{Cs}\right) - 0.017$	0.91	0.005
3	60-100	$\theta = 1.127\left(\frac{C}{Cs}\right) - 0.171$	0.88	0.009
4	100-200	$\theta = 0.979\left(\frac{C}{Cs}\right) - 0.092$	0.83	0.006

* where C and Cs referred to neutron probe counts and standard counts, respectively.

5.2.5. Isotope mass balance method

Soil pits were excavated, and soil samples were removed from different depths. Soil samples were sealed and stored frozen until analysis for soil-water was carried out. High-speed centrifugation was used for deeper layers soils, while for surface soil, vacuum distillation was used to extract the water from the soil, and samples were analyzed with a laser spectrometer.

5.2.6. Yield data

After harvest, data including the number of fertile and infertile tillers per square meter, grain, straw and total yields (t ha^{-1}), weight of a thousand seeds (g), plant height (cm), spike, peduncle and awn lengths (cm), numbers of nodes, grains per spike and tillers per plant were measured for 35, 55 and 75% Soil Moisture Depletions (SMD) in different wheat cultivars.

Analysis of variance (ANOVA) using the mixed Model in SAS 9.4 was carried out to determine the effect of different treatments. Tukey's Honestly Significant Difference (HSD) values at ($P<0.05$) were calculated when the treatment effect was found to be statistically significant.

5.2.7. Calibration and validation of the AquaCrop model

The performance of the calibrated model was evaluated against the experimental data of 2014–2015 and 2017–2018 cropping seasons which were not used for model calibration (Table 5.4). After model validation, the model was used to evaluate the effects of different scenarios on grain yield and water use efficiency.

TABLE 5.4 CALIBRATION AND VALIDATION OF THE AQUACROP MODEL

Calibration	Validation
2013-2014	2014-2015
2015-2016	2017-2018

5.2.8. Remote sensing indices

Soil salinization, a dynamic phenomenon, is extremely variable (both spatially and temporally), thus posing the greatest challenge to researchers to accurately predict salinization. Using conventional methods of salinity assessment is challenging and time consuming. Therefore, finding an effective and robust method is essential for salinity assessment, monitoring and mapping. Many researchers emphasize remotely sensed data techniques such as airborne imagery, in-situ spectroradiometry and also combining spectral indices derived from various sensors with the geochemical laboratory measurements for salinity measurement [12, 13]. Remote sensing methods are reliable, cost effective (spatially in large areas), easy to use in different time and spatial scales [14]. Currently, the most used source of imagery for salinity detection remains multispectral remote sensing with the Landsat series sensors [15, 16]. Salinity researchers usually apply remote sensing as a tool for computing the Salinity Index (SI). The different salinity indices can be calculated by the infrared and visible spectral reflective bands in the electromagnetic spectrum [17].

We used three indices; Normalized Difference Vegetation Index (NDVI), Normalized Difference Salinity Index (NDSI) and Normalized Difference Water Index (NDWI). Multi-spectral LANDSAT series of 1994, 1998, 2014 and 2017 were applied. The semi-automatic classification plugin of QGIS was employed for satellite data pre-processing, namely the radiometric calibration and the atmospheric correction. Due to using multi-temporal images of different sensors, we were faced with changing sensor characteristics, atmospheric conditions and acquisition characteristics which caused radiometric inconstancy [18, 19]. To reduce these effects and increase the sensitivity, correction is necessary. As the study area is in Isfahan Province, Iran, the path/row of the acquired satellite data is 163 and 38 (WRS-2). Landsat 5 was used for 1994 and 1998, and Landsat 8 for 2014 and 2017; the NDVI, NDSI and NDWI indices during the month of April in the mentioned periods were applied to monitor salinity, water and vegetation status, and then to delineate the salt affected soil.

Salt affected soils usually have poor vegetation due to osmotic and ion imbalance. Among several vegetation indices, Normalized Difference Vegetation Index (NDVI) was used to characterize crop growth conditions influenced by salinity. NDVI is the most common vegetation index, but it also has its limitation, affected by the soil substrates and its brightness

[20]. Dry soil generally has high reflectance and no absorption in the red spectrum; the unmixed pixel is reported to be the main issue in dry lands for calculation of NDVI.

The NDVI was calculated via the following equation [20]:

$$\mathrm{NDVI} = \frac{\mathrm{NIR} - \mathrm{Red}}{\mathrm{NIR} + \mathrm{Red}}$$

where Red and NIR are the surface reflectance values in the red and near-infrared bands [21]; they are bands of 5 and 4 in Landsat 8 (OLI), but bands 4 and 3 in Landsat 5, respectively.

The Normalized Difference Salinity Index (NDSI) as a salinity index is the ratio of the difference of two short-wave infrared (SWIR) bands divided by their sums [22, 23].

$$\mathrm{NDSI} = \frac{\mathrm{SWIR1} - \mathrm{SWIR2}}{\mathrm{SWIR1} + \mathrm{SWIR2}}$$

- Landsat 8: SWIR1 = B6, SWIR2 = B7
- Landsat 5: SWIR1 = B5, SWIR2 = B7

The Normalized Difference Water Index (NDWI) is the ratio of the difference of the near-infrared and short-wave infrared (SWIR) bands divided by the summation of the two bands [24].

$$\mathrm{NDWI} = \frac{\mathrm{NIR} - \mathrm{SWIR2}}{\mathrm{NIR} + \mathrm{SWIR2}}$$

- Landsat 8: SWIR2 = B7, NIR = B5
- Landsat 5: SWIR2 = B7, NIR = B4

5.3. RESULTS AND DISCUSSION

5.3.1. Vegetation status

According to NDVI results, vegetation cover decreased from 1994 to 2017 (Fig. 5.4), with the area with low vegetation completely converting to bare land. This can be attributed to climate change, high evapotranspiration and low precipitation, in these years. On the other hand, deficiency of suitable water for irrigation caused salt accumulation as a result of vegetation degradation.

5.3.2. Salinity status

The high salinity area decreased from 1994 to 2017, while saline land increased moderately (Fig. 5.5). Vegetation, as shown in the NDVI results, changed with salinity variation. For instance, the area with low salinity and low vegetation in 1994 converted to moderately saline land with no vegetation in 2017.

5.3.3. Water content of vegetation

NDWI computation showed that dry lands increased from 1994 to 2017 (Fig. 5.6). In general, it can be concluded that low vegetation as well as salinity is in coincidence with low water index which can be investigated clearly in the 2014 evaluated indices.

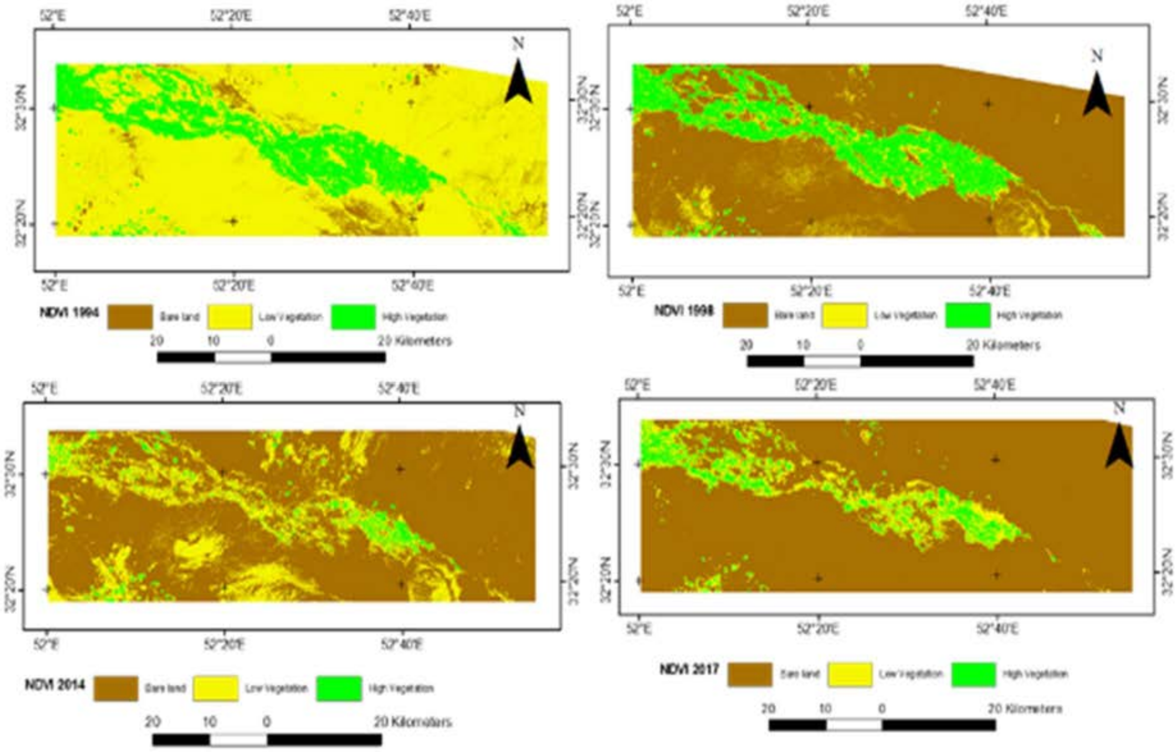

FIG. 5.4. Normalized Difference Vegetation Index (NDVI) in different years.

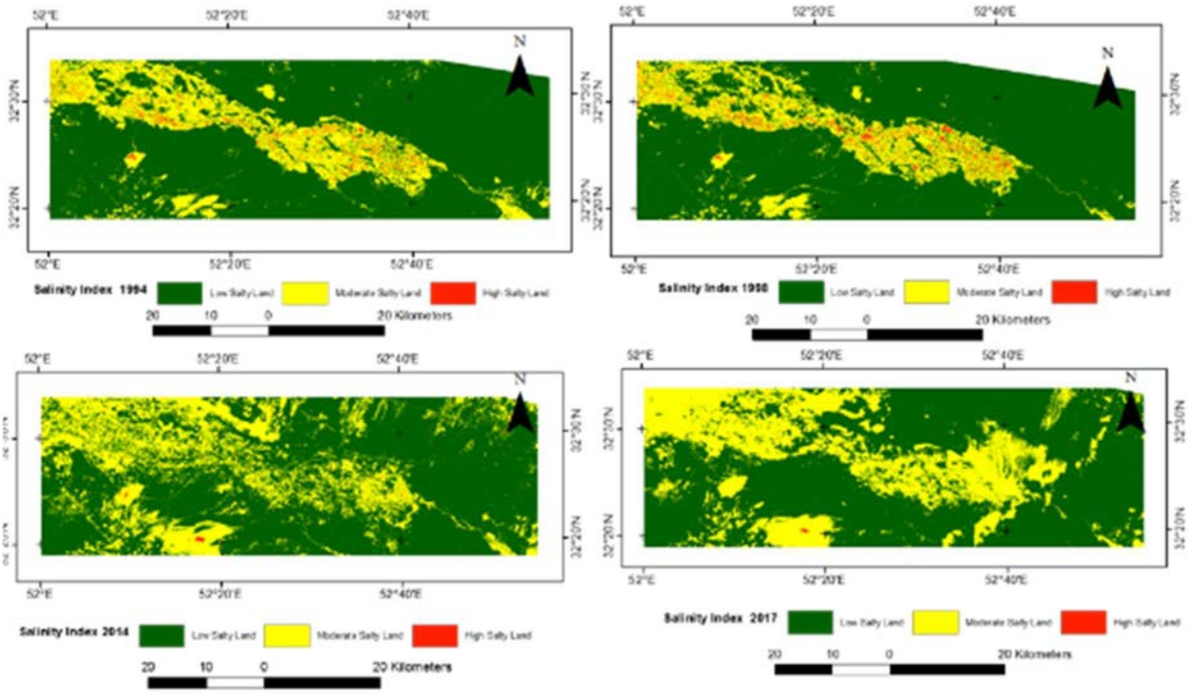

FIG. 5.5. Normalized Difference Salinity Index (NDSI) in different years.

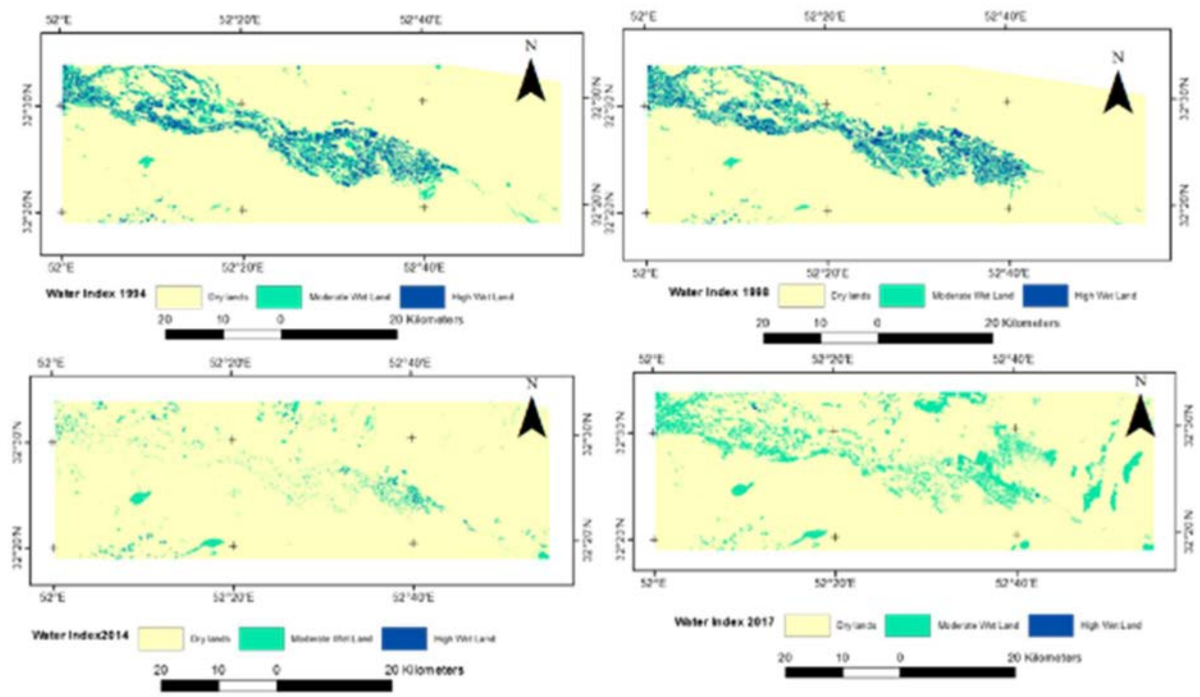

FIG. 5.6. Normalized Difference Water Index (NDWI) in different years.

5.3.4. Harvest data analysis

Analyses of variance (ANOVA) of harvest data are given in Tables 5.5 and 5.6.

TABLE 5.5 ANALYSIS OF VARIANCE OF YIELD AND AGRONOMIC PARAMETERS

Source of variation	df	Yield (t ha^{-1})			Grains spike^{-1}	Tillers plant^{-1}	1000-grain weight (g)	HI (%)
		Grain	Straw	Total				
Year (Y)	3	107^{**}	106^{**}	412^{**}	337^{**}	8.6^{ns}	3172^{**}	338^{**}
Y × Rep (R)	8	0.27	4.5	5.9	11.3	2.8	5.6	27
Irrigation (I)	2	67^{**}	48^{**}	226^{**}	209^{**}	12.8^{**}	640^{**}	226^{**}
Y× I	6	3.9^{**}	0.48^{ns}	6.8^{ns}	30^{ns}	1.89^{*}	69^{**}	30^{**}
Y × I × R	16	0.71	1.11	3.3	13.1	0.58	7.6	2.1
Variety (V)	4	16.7^{**}	1.24^{ns}	22.3^{**}	1192^{**}	1.88^{**}	311^{**}	232^{**}
V × I	8	3.66^{**}	5.7^{**}	17.1^{**}	54^{**}	0.45^{ns}	42^{**}	17.6^{**}
Y × V	12	0.92^{ns}	0.26^{ns}	1.06^{ns}	10.4^{ns}	0.21^{ns}	14.2^{**}	10.9^{*}
Y × V × I	24	0.83^{ns}	1.19^{ns}	5.0^{ns}	13.8^{ns}	0.11^{ns}	3.8^{ns}	1.4^{ns}
Error	96	0.66	1.30	4.8	17	0.39	3.25	5.7
CV (%)	-	12.1	12.9	5.2	12.3	16.1	11.6	5.6

TABLE 5.6 ANALYSIS OF VARIANCE OF PHYSIOLOGICAL PARAMETERS

Source of variation	df	No. of tillers (m^{-2})		Plant height (cm)	Length (cm)			No. of nodes
		Fertile	Infertile		Spike	Peduncle	Awn	
Y (Y)	3	816807^{**}	300^{**}	2832^{**}	138^{**}	272^{**}	25.5^{**}	2.4^{**}
Y × Rep (R)	8	31239	3.4	56	1.6	3.0	0.50	0.08
Irrigation (I)	2	27605^{ns}	1251^{**}	812^{**}	13^{**}	203^{**}	0.92^{ns}	0.09^{ns}
Y × I	6	5468^{**}	42^{**}	24^{ns}	0.85^{ns}	6.2^{ns}	0.005^{ns}	0.004^{ns}
Y × I × R	16	17958	4.2	23	0.51	5.8	0.27	0.04
Variety (V)	4	49302^{**}	14.4^{**}	2968^{**}	60^{**}	448^{**}	182^{**}	1.7^{**}
V × I	8	19013^{*}	20.0^{**}	56^{ns}	0.66^{ns}	7.4^{ns}	0.26^{ns}	0.03^{ns}
Y × V	12	1418^{ns}	8.4^{*}	27^{ns}	5.8^{**}	13.8^{**}	0.76^{**}	0.12^{**}
Y × V × I	24	570^{ns}	10.4^{**}	8.0^{ns}	0.11^{ns}	2.8^{ns}	0.05^{ns}	0.02^{ns}
Error	96	1523	3.7	31	0.34	5.7	0.15	0.04
CV (%)	-	12.9	10.5	6.8	5.3	7.5	7.9	5.9

The analysis of variance indicates that in all traits, except the number of tillers, there was a significant difference between two different years (α = 0.01). Also, the triple interactions between factors of year, irrigation and variety of all traits are not significant except for the number of infertile spikes m^{-2} (α = 0.01). In addition, the interaction between irrigation and variety showed significant differences for the traits of fertile and infertile spikes, grain and straw yields, 1000-grain weight, number of grains $spike^{-1}$, total yield and harvest index (α = 0.01).

Among the five wheat cultivars (Fig. 5.7-8)), V_4 (Roshan) produced the lowest grain yield (Table 5.7). The grain yield decreased 16.2, 19.1, 25.0 and 17.4% in V_4 (Roshan), respectively, compared to those of V_1 (Parsi), V_2 (Arg), V_3 (Bam) and V_5 (Ofogh). The highest number of grains per spike was observed in the V_5 (Ofogh) cultivar. Different wheat cultivars showed significant effects in 1000-seed weight, which decreased significantly in V_5 (Ofogh) compared to the other cultivars. The Roshan cultivar (V_4) had the lowest HI % compared to the other wheat cultivars due to low grain yield. Cultivars V_4 (Roshan) had the highest plant height and lowest awn and spike lengths (Table 5.8).

TABLE 5.7 GRAIN, STRAW AND TOTAL YIELDS, NUMBERS OF GRAINS PER SPIKE AND TILLERS PER PLANT, WEIGHT OF A THOUSAND SEED AND HARVEST INDEX OF WHEAT CULTIVARS

Treatments	Yield ($t\ ha^{-1}$)			Grain $spike^{-1}$	Tillers $plant^{-1}$	1000-grain weight (g)	HI (%)
	Grain	Straw	Total				
V_1	6.68 b	8.85 a	15.53 abc	31.6 b	3.9 ab	43.4 a	42.7 b
V_2	6.92 b	8.78 a	15.70 ab	33.2 b	3.5 b	43.0 a	43.7 ab
V_3	7.47 a	9.12 a	16.59 a	33.7 b	3.8 ab	42.7 a	44.6 a
V_4	5.60 c	8.79 a	14.39 c	27.2 c	4.2 a	43.5 a	38.2 c
V_5	6.78 b	8.61 a	15.39 bc	42.9 a	3.8 ab	36.6 b	43.8 ab

HI, harvest index; Data within a column followed by different lowercase letters are significantly different ($P < 0.05$)

TABLE 5.8 THE MEAN NUMBER OF FERTILE AND INFERTILE TILLERS PER SQUARE METER, PLANT HEIGHT, SPIKE, PEDUNCLE AND AWN LENGTHS AND NUMBER OF NODES OF WHEAT CULTIVARS

Treatments	No. of tillers (m^{-2})		Plant height (cm)	Length (cm)			No. of nodes
	Fertile	Infertile		Spike	Peduncle	Awn	
V_1	657 b	17.3 b	76 c	11.9 a	28.1 c	6.9 a	3.2 c
V_2	715 ab	18.8 a	80 b	11.2 c	33.4 b	5.3 b	3.2 c
V_3	679 b	18.9 a	79bc	11.5 bc	33.5 b	5.6 b	2.9 c
V_4	750 a	18.0 ab	98 a	8.7 d	36.3 a	1.0 c	3.6 a
V_5	679 b	18.2 ab	78 bc	11.7 ab	28.4 c	5.5 b	3.4 b

Data within a column followed by different lowercase letters are significantly different ($P < 0.05$)

The applied water led to significant reductions in grain, straw and total yields and weight of thousand seed in the I_3 treatment (75% soil moisture depletion) compared to I_1 and I_2 treatments (35 and 55% soil moisture depletions) (Table 5.9). Such decreases were attributed to using long intervals between irrigation at the time when evapotranspiration was very high.

TABLE 5.9 THE EFFECT OF DIFFERENT SOIL MOISTURE DEPLETIONS ON GRAIN, STRAW AND TOTAL YIELDS, NUMBERS OF GRAINS PER SPIKE AND TILLERS PER PLANT, WEIGHT OF A THOUSAND SEED AND HARVEST INDEX

Treatments	Yield (t ha^{-1})			Grains spike^{-1}	Tillers plant^{-1}	1000-grain weight (g)	HI (%)
	Grain	Straw	Total				
I_1	7.20 a	9.50 a	16.70 a	34.89 a	3.70 b	43.31 a	42.72 b
I_2	7.39 a	9.18 a	16.58 a	34.74 a	4.36 a	44.13 a	44.51 a
I_3	5.47 b	7.80 b	13.28 b	31.58 b	3.48 b	38.11 b	40.64 c

Data within a column followed by different lowercase letters are significantly different ($P < 0.05$)

The number of tillers per plant in I_1 and I_3 treatments decreased about 15.1 and 20.2 % compared to the I_2 treatment (Table 5.10). In the 75% soil moisture depletion treatment, the number of grains per spike decreased significantly by about 9.5 and 9.1%, respectively, compared to 35 and 55% soil moisture depletion treatments (Table 5.10). The maximum harvest index was exhibited at 55% soil moisture depletion and the lowest in the 75% soil moisture depletion treatment.

TABLE 5.10 THE EFFECT OF DIFFERENT SOIL MOISTURE DEPLETIONS ON NUMBER OF FERTILE AND INFERTILE TILLERS PER SQUARE METER, PLANT HEIGHT, SPIKE, PEDUNCLE AND AWN LENGTHS AND NUMBER OF NODES

Treatments	No. of tillers (m^{-2})		Plant height (cm)	Length (cm)			No. of nodes
	Fertile	Unfertile		Spike	Peduncle	Awn	
I_1	720 a	14.1 c	85 a	10.9 b	32.7 a	4.9 a	3.3 a
I_2	688 a	17.5 b	84 a	11.5 a	33.3 a	5.0 a	3.3 a
I_3	679 a	23.1 a	78 b	10.6 b	29.8 b	4.7 a	3.2 a

Data within a column followed by different lowercase letters are significantly different ($P < 0.05$)

FIG. 5.7. Different varieties of wheat

5.3.5. Sensitivity analysis of the AquaCrop model

A qualitative sensitivity analysis was conducted, following the method of Geerts et al. [25] which provides guidelines for the model calibration, and allows for a better interpretation of the simulation results. The results of this analysis can be considered in the planning of further field experiments. The classes low, moderate and high correspond to changes in the model response of less than 2%, 2 to 20%, and more than 20%. The agronomic, soil and meteorological data as well as irrigation management data were considered for sensitivity analysis. The results of SA for input parameters to simulate grain yield are presented in Table 5.11.

Normalized water productivity (WP*) and reference harvest index (HI_o) had a high influence on the simulated yield; this is logical as Normalized water productivity is the proportionality factor that allows derivation of biomass production from transpiration, and HI_0 is the proportionality factor used to derive yield from biomass. Also, the maximum rooting depth is a critical parameter in AquaCrop. The crop coefficient for transpiration, planting date, canopy growth coefficient and maximum canopy cover had a moderate influence on crop simulations. The canopy decline coefficient (CDC) had only a small influence on the simulation results. The soil water content at saturation had a low influence on the model output. It has been proposed as a redundant parameter that could be removed from AquaCrop for model simplification [26]. Saturated hydraulic conductivity (K_{sat}) had no noticeable influence on our simulation results. Model outputs were highly sensitive to the water salinity, SWC at FC and EC of the saturated soil paste extract. The maximum air temperature had a moderate influence on crop simulations.

TABLE 5.11. SENSITIVITY CLASSES OF AQUACROP INPUTS FOR WINTER WHEAT

Input parameter	High sensitivity	Moderate sensitivity	Low sensitivity
Crop parameters	Normalized water productivity (WP^*)	Crop coefficient for transpiration (Kc_{Tr})	Canopy decline coefficient (CDC)
	Reference harvest index (HI_0)	Planting date	
	Maximum rooting depth	Canopy growth coefficient (CGC)	
		Maximum canopy cover (CC_X)	
Soil parameters	SWC at field capacity	SWC at permanent wilting point	SWC at saturation
	Saturated soil paste extract (EC_e)		Saturated hydraulic conductivity (K_{sat})
Management irrigation	Water salinity		
Climate parameters		Maximum air temperature	

5.3.6. Application of the AquaCrop model to simulate the biomass and yield

The simulated grain and biomass yields showed good agreement with the measured wheat yields. The AquaCrop model could very well predict biomass and grain yield of winter wheat. Biomass was better simulated by the model than grain yield. The simulated grain yield varied from 5 to 8.8 t ha^{-1}, while the measured yield varied from 4.8 to 8.7 t ha^{-1} in both cropping seasons. The low NRMSE values and the relatively high index of agreement (d) for grain yield and biomass confirm the performance of the model in simulating biomass and grain yield under saline-sodic conditions (Table 5.12).

TABLE 5.12 THE PERFORMANCE OF THE AQUACROP MODEL IN PREDICTING GRAIN YIELD AND BIOMASS

Cropping year	Treatment	Biomass (t ha^{-1})		Grain yield (t ha^{-1})	
		Predicted	Observed	Predicted	Observed
	I_1	20.1	19.8	8.8	8.4
2014-2015	I_2	19.7	20.1	8.1	8.7
	I_3	18.1	18.2	7.7	7.9
	I_1	17.3	16.9	6.7	6.3
2017-2018	I_2	17.0	17.2	6.3	6.7
	I_3	16.5	16.0	6.1	5.8
Index					
NRMSE (%)		3.8		6.2	
d		0.94		0.91	
R^2		0.92		0.89	

5.3.7. Application of the AquaCrop model to simulate soil moisture water content and soil salinity

The average electrical conductivity of the saturation soil extract (EC_e) was determined in each 0.2 m layer up to 0.8 m depth five times after sowing in all treatments. Statistical comparison of observed and predicted soil water content and salinity are presented in Table 5.13. The model's accuracy for simulation of soil water content was higher than the accuracy for simulation of soil salinity. For simulation of soil water content, the average value of normalized root mean square error (NRMSE) was 13.7%, while for simulation of soil salinity it was 27.6 %. Therefore, the error of the model in simulating soil salinity is greater than that in simulating soil water content. The coefficient of the residual mass (CRM) values for soil salinity simulation were positive, which indicated underestimation of soil salinity by the model. However, the model tended to overestimate the soil water content, which could be attributed to evaporation through the soil cracks which was not detected by the model. The AquaCrop model is based on the Convection-Diffusion Equation (CDE). The processes of sorption of salts, degradation and sedimentation are not considered in soils with accumulations of gypsum and lime.

TABLE 5.13 OBSERVED AND PREDICTED SOIL WATER CONTENT AND SALINITY

Parameter	Method	NRMSE (%)	*d*	CRM	R^2
Soil water content	Calibration	13.1	0.79	–0.08	0.75
	Validation	14.3	0.73	–0.09	0.71
Soil salinity	Calibration	27.2	0.60	0.24	0.56
	Validation	28.1	0.55	0.26	0.51

Statistical comparisons of measured and simulated soil water content and salinity at different depths are presented in Table 5.14. The NRMSE is reduced with increasing depth for simulation of soil water content and soil salinity.

TABLE 5.14. MEASURED AND SIMULATED SOIL WATER CONTENT AND SALINITY AT DIFFERENT DEPTHS

Parameter	Depth (cm)	NRMSE (%)	*d*	CRM	R^2
Soil water content	0 - 20	16.1	0.63	–0.09	0.58
	20 - 40	14.4	0.69	–0.09	0.67
	40 - 60	13.7	0.78	–0.08	0.76
	60 - 80	12.8	0.85	–0.08	0.79
Soil salinity	0 - 20	29.4	0.50	0.27	0.48
	20 - 40	28.2	0.56	0.26	0.51
	40 - 60	27.7	0.54	0.26	0.52
	60 - 80	27.0	0.58	0.25	0.54

5.3.8. Model application for irrigation management scenarios

The AquaCrop model was used to simulate different scenarios. The highest yield loss was simulated in scenarios where saline water for irrigation was used at sowing, tillering and booting stages. Salinity stress at these stages can affect leaf growth, tiller generation, canopy development and other crop traits which resulted in decreasing biomass production and final grain yield. For the studied area, it can be concluded that using about 700 mm of irrigation with an average water salinity level of 4 dS m^{-1}, crop yields for winter wheat are expected to be around 70% of the yield potential of 10-ton ha^{-1}. The analysis of different scenarios showed that the highest grain yield could be obtained by applying eight irrigations and using freshwater three times until April. A further salinization of irrigation water to 8 dS m^{-1}, will decrease the crop yield for winter wheat to 80% of potential obtainable.

FIG. 5.8. Winter wheat in saline-sodic soil

5.3.9. Adjusting planting date by the AquaCrop model

Winter wheat obtained higher biomass and grain yield when planted in early November than in October due to better crop canopy cover (Fig. 5.9). The crop canopy cover affects the rate of transpiration and consequently biological yield and grain yield accumulation.

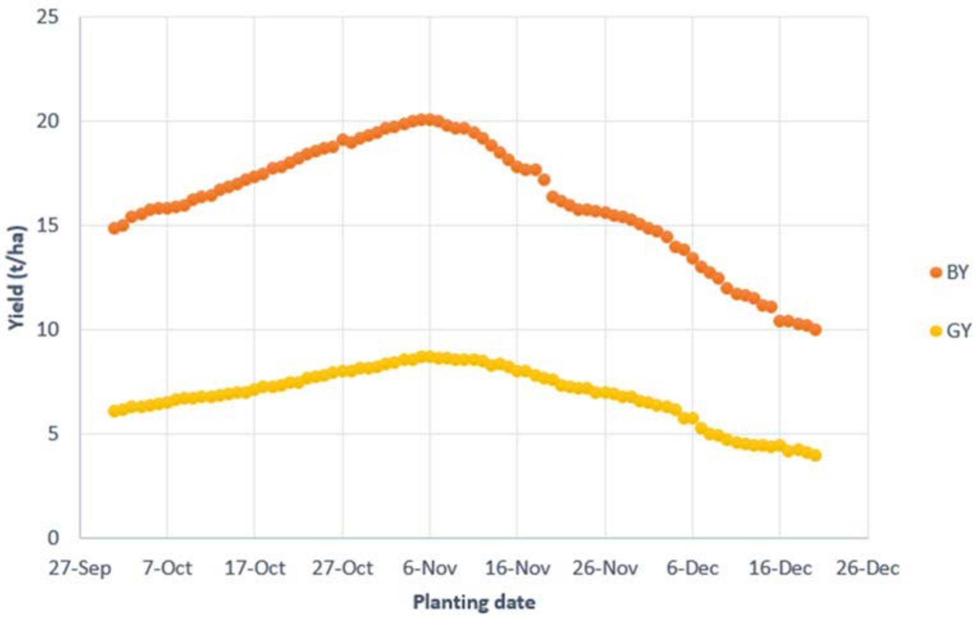

FIG. 5.9. Adjusting planting date by the AquaCrop model.

5.3.9.1. Isotope mass balance method

The isotope mass balance method was applied to determine the fractions of water lost through soil evaporation and leaf-transpiration under different management strategies. The proportion of evaporation to total evapotranspiration was smaller when the crop was planted in early November (Table 5.15), indicating that the AquaCrop model gives good results for adjusting planting date in this region.

TABLE 5.15 THE RATIO OF SOIL EVAPORATION TO EVAPOTRANSPIATION (E/ET) AND THE DURATION OF GROWTH STAGES FOR WINTER WHEAT

Year	Planting date	E/ET	Emergence	Tillering	Stem elongation	Booting	Total
2013-2014	December 11	E/ET	0.33	0.64	0.43	0.38	0.44
		Time period	31/12/13 06/01/14	26/02/14 04/03/14	25/03/14 31/03/14	25/04/14 01/05/14	
2014-2015	November 9	E/ET	0.37	0.45	0.30	0.25	0.34
		Time period	19/11/14 25/11/14	26/01/15 01/02/15	02/03/15 08/03/15	29/03/15 04/04/15	
2015-2016	November 23	E/ET	0.37	0.48	0.34	0.29	0.37
		Time period	02/12/15 08/12/15	08/02/16 14/02/16	14/03/16 20/03/16	10/04/16 16/04/16	

5.4. CONCLUSIONS

The AquaCrop model can be a vital tool to improve water productivity and crop yields under saline-sodic conditions. The sensitivity analysis of the model under local conditions provided useful information about the needed parameters and input variables for model predictions. The highest yield loss was simulated in scenarios where saline water for irrigation was used at sowing, tilling and booting stages, while the highest grain yield could be obtained by applying eight irrigations and using freshwater for three times till April. Winter wheat obtained higher biomass and grain yield when planted in early November than in October or December due to better crop canopy cover. The crop canopy cover affects the rate of transpiration and consequently total and grain yield accumulation. For the studied area, it is concluded that with proper management of water, crop yields for winter wheat are expected to be around 70% of the yield potential, otherwise soil degradation will occur. It seems that more inputs of soil characteristics are needed to improve AquaCrop estimations. Adding CEC seems necessary. In soils with different amounts of sodium, the negative effects of sodium may be affected by other salts. If the concentration of other salts is not high, adding % ESP to the model is essential, but warrants further testing.

ACKNOWLEDGEMENTS

This work was funded by the International Atomic Energy Agency (IAEA), Vienna through a Coordinated Research Project [Landscape Salinity and Water Management for Improving Agricultural Productivity (17658)] of the Soil and Water Management & Crop Nutrition Section, Joint FAO/IAEA Division of Nuclear Techniques in Food and Agriculture.

REFERENCES

[1] FARIFTEH, J., et al., Assessing salt-affected soils using remote sensing, solute modelling, and geophysics, Geoderma **130** (2006) 191–206.

[2] BARZANI, M.M., KHAIRULMAINI, O.S., Desertification risk mapping of the Zayandeh Rood Basin in Iran, J. Earth Syst. Sci. **122** (2013) 1269–1282.

[3] MOHAJERI, S., Integrated water resources management Zayandeh Rud, German-Iranian research and development cooperation for a better future, Part I (2015) www.iwrm-zayandehrud.com

[4] ESKANDARIE, B., Country report on history and status of soil survey in Iran (The Islamic Republic of Iran Ministry of Jihad-e Agriculture), Report on Iran's Soil and Agricultural status (2012).

[5] ANGUS, D.E., WATTS, P.J., Evapotranspiration–how good is the Bowen ratio method, Agric. Water Manage. **8** (1984) 133–150.

[6] WILSON, K.B., et al., A comparison of methods for determining forest evapotranspiration and its components: sap-flow, soil water budget, eddy covariance and catchment water balance, Agric. For. Meteorol. **106** (2001) 153–168.

[7] LIU, C.M., et al., Determination of daily evaporation and evapotranspiration of winter wheat and maize by large-scale weighing lysimeter and microlysimeter, Agric. For. Meteorol. **111** (2002) 109–120.

[8] RAZ-YASEEF, N., et al., Dynamics of evapotranspiration partitioning in a semi-arid forest as affected by temporal rainfall patterns, Agric. For. Meteorol. **157** (2012) 77–85.

[9] HSIEH, J.C.C., et al., Oxygen isotopic composition of soil water: implications for partitioning evapotranspiration, Geoderma **82** (1998) 269–293

[10] FERRETTI, D.F., et al., Partitioning evapotranspiration fluxes from a Colorado grassland using stable isotopes: Seasonal variations and ecosystem implications of elevated atmospheric CO_2, Plant Soil, **254** (2003) 291–303.

[11] WILLIAMS, D.G., et al., Components of evapotranspiration determined by stable isotope, sap flow and eddy covariance techniques, Agric. For. Meteorol. **125** (2004) 241–258.

[12] ABBAS, A., et al., Characterizing soil salinity in irrigated agriculture using a remote sensing approach, Phys. Chem. Earth Part A/B/C (2013) 43–52.

[13] ALLBED, A., et al., Mapping and modeling spatial variation in soil salinity in the Al Hassa Oasis based on remote sensing indicators and regression techniques, Remote Sens. **6** (2014) 1137–1157.

[14] ZINCK, J.A., Monitoring soil salinity from remote sensing data. From the 1st workshop EARSel special interest group on remote sensing for developing countries, (2000) 359–368.

[15] JOSHI, D.C., et al., Spectral reflectance characteristics of Na-Carbonate irrigated arid secondary sodic soil, Arid Land Res. Manage. **16** (2002) 161–176.

[16] SCUDIERO, E., et al., Regional-scale soil salinity assessment using Landsat ETM+ canopy reflectance, Remote Sens. Environ. **169** (2015) 335–343.

[17] BANNARI, A., et al., Salt-affected soil mapping in an arid environment using semi-empirical model and Landsat-OLI data, Adv. Remote Sens. **6** (2017) 260–291.

[18] DU, Y., et al., Radiometric normalization of multitemporal high-resolution satellite images with quality control for land cover change detection, Remote Sens. Environ. **82** (2002) 123–134.

[19] HADJIMITSIS, D.G., et al., The use of selected pseudo-invariant targets for the application of atmospheric correction in multi-temporal studies using satellite remotely sensed imagery, Int. J. Appl. Earth Obs. Geoinf. **11** (2009) 192–200.

[20] HUETE, A.R., et al., Spectral response of a plant canopy with different soil backgrounds, Remote Sens. Environ. **17** (1985) 37–53.
[21] CHO, K.H., et al., Dynamics of soil salinity and vegetation in a reclaimed area in Saemangeum, Republic of Korea, Geoderma, **321** (2018) 42–51.
[22] RICHARDSON, A.D., et al., An evaluation of noninvasive methods to estimate foliar chlorophyll content, New Phytol. **153** (2002) 185–194.
[23] AL-KHAIER, F., Soil salinity detection using satellite remotes sensing. Master thesis, International institute for Geo-information science and earth observation, Enscheda, (2003) 61 p.
[24] CECCATO, P., et al., Designing a spectral index to estimate vegetation water content from remote sensing data: Part 1: Theoretical approach, Remote Sens.Environ. **82** (2002) 188–197.
[25] GEERTS, S., et al., Simulating yield response of quinoa to water availability with AquaCrop, Agron. J. **101** (2009) 499–508.
[26] VANUYTRECHT, E., et al., Global sensitivity analysis of yield output from the water productivity model, Environ. Model. Software **51** (2014) 323–332.

6. APPLICATION OF ISOTOPIC TECHNIQUES FOR ASSESSMENT OF SALT TOLERANCE AND N_2-FIXATION BY TREES IN A MULTI-SPECIES AFFORESTATION PROJECT

A. KHAMZINA
Korea University, Seoul
Republic of Korea

Abstract

In Central Asia, decades of intensive irrigation led to the desiccation of the Aral Sea as well as elevated groundwater tables in irrigated agricultural areas, resulting in ubiquitous soil salinization and an adverse impact on crop production. As an alternative to water-intensive reclamation by leaching of highly salinized croplands, some degraded landscapes can be converted to tree plantations of salt-tolerant species. The 12-year continuous monitoring in a multi-species afforestation site established on degraded, highly salinized cropland shows that water availability does not preclude the afforestation due to effective utilization of shallow saline groundwater by trees. However, soil salinity increased significantly as the tree plantations matured under non-irrigated conditions, requiring occasional salt leaching at the plantation sites which therefore are not entirely independent of irrigation. Monitoring of foliar $\delta^{13}C$ appears promising for interpreting the relative salt tolerance among the tree species, given the consistent $\delta^{13}C$ variations for tree species and the responsiveness of $\delta^{13}C$ values to salt leaching.

The efficient N_2-fixation by actinorhizal *E. angustifolia* greatly contributed to self-sufficiency in nitrogen nutrition of the afforestation system under non-fertilized conditions. Including *E. angustifolia* as a nursing plant in tree plantations may assist in restoration of *P. euphratica* dominated native riparian forests and in revegetation of degraded croplands. The ^{15}N natural abundance method allows quantification of biological nitrogen fixation in trees but the results need to be carefully interpreted considering the sampling material used (foliar or whole-plant), plant age, and reference species due to the confounding of ^{15}N signals during the successional changes in tree stands over time.

Long-term studies provide an appropriate timeframe for understanding tree community dynamics under changing environmental conditions in afforestation schemes and for devising appropriate management options to inform land restoration practices. Therefore, further monitoring is required including the use of C and N isotopic methodologies effective in revealing important physiological responses of the candidate afforestation species to prevailing salinity and nutrient deficiency stresses in degraded croplands.

6.1. INTRODUCTION

In Central Asia, up to 50% of the irrigated land is affected by degradation, mostly due to soil salinization and waterlogging. Agricultural yields reportedly declined by 20–30%, resulting in annual losses of agricultural production as high as $2 billion from soil salinization alone [1]. In the downstream area of Uzbekistan, where natural outflow of the groundwater is restricted due to the low-lying land with a flat relief, a shallow groundwater table is reported on over 80% of the cropland [2]. The salinity has been exacerbated by intensive irrigation which, in the absence of appropriate drainage, raises the groundwater table, thus causing movement of salts through capillary rise and their accumulation in the crop rooting zone [3].

The common measure to cope with soil salinity is salt leaching and engineering drainage. Such a practice requires a high input of freshwater and might be uneconomical for severely degraded arid areas in view of precarious water supplies further reduced by upstream water utilization and climate change. An alternative to the water-intensive reclamation by leaching is an adaptive option of converting highly salinized cropland into multi-purpose systems of salt-tolerant trees [4, 5]. The impact of afforestation on soil salinity is not uniform and depends on a variety of factors, including hydro-geological conditions of the landscape, strategies for tree planting and management as well as tree species characteristics, such as salt tolerance and transpiration rates [6].

There is a body of published research indicating a reduction in soil salinity due to the bio-drainage by trees, whereas studies in groundwater discharge zones reported a gradual increase in salinity of the afforested soils due to the accumulation of salts excluded from the root water uptake by salt-tolerant tree species [7]. This may eventually result in salinity stress for tree plantations thus reducing their biomass production and supply of important ecosystem services. Analyzing the mutual impact of soil salinity and tree growth is of interest for decisions about appropriate silvicultural management i.e. rotation period, need for occasional leaching, species choice. Soil salinity *per se* might not explain biomass yield variations, as plants differ in salt tolerance which, particularly in perennial vegetation, also depends on growth stage. It was argued by [8] that $\delta^{13}C$ of plants, which reflects the cumulative salinity impact experienced by plants over time, might be a more robust indicator for salinity stress.

Next to salt tolerance and phreatophytic features (ability to effectively utilize shallow saline groundwater) of candidate species used in re- and afforestation, their success is influenced by the ability to re-establish on degraded soil depleted of essential nutrients. Tree species associated with salt-tolerant N_2-fixing bacteria [9, 10] might therefore be useful in re-vegetating poor soils, enhancing organic matter and in consequence, facilitating the successional development of vegetation on lands after decades in agricultural use. Quantification of biological nitrogen fixation via actinorhizal symbioses, most common in tree species, over time horizons beyond the seedling stage remains scarce in contemporary published research. Such information based on continuous observations is essential for quantifying the role of N_2-fixing tree pioneers in rehabilitation of degraded forest and agricultural sites. Besides the logistical difficulty of sampling large-sized plants there are methodological shortcomings in field applications that ensue as the tree stands mature. The ^{15}N natural abundance method is considered most reliable for N_2-fixation estimation of woody perennials, large scale and field grown [11].

This report is focused on studies relying on the use of isotopic methodologies [12] for the analysis of salinity-induced stress and of biological nitrogen fixation in afforestation species under saline conditions. These studies particularly concern the question of long-term sustainability of tree plantations established on nutrient-poor and salinized cropland soils. Specific CRP-related objectives included the monitoring of soil salinity and moisture as well as plant carbon and nitrogen parameters since tree planting and over 12 consecutive growing seasons (2003–2014) for the assessment of:

- Root-zone soil water and salt dynamics in afforested plots;
- Changes in ^{13}C discrimination in afforestation species as a proxy of salt stress;
- Efficiency of N_2-fixation in afforestation species using the ^{15}N natural abundance method.

6.2. MATERIAL AND METHODS

6.2.1. Description of the study region and research site

The study area is located in the Aral Sea Basin of northern Uzbekistan and covers irrigated croplands of the Khorezm region and southern part of the autonomous Republic of Karakalpakstan in the lower reaches of the Amudarya River. The total area is 854,500 ha, with the irrigated cropland occupying about 410,000 ha. The study area is characterized by an extremely arid, continental climate. The annual average air temperature is 13.4 °C with seasonal temperatures ranging between 40 °C in summer to freezing in winter. Average precipitation totals approximately 100 mm per year and occurs mostly outside the crop growing season (April-October). Crop cultivation therefore is entirely dependent on irrigation, with the Amu Darya River as the principal water source. The major crops are cotton, grown in rotation with winter wheat on most of the territory, followed by rice and maize. Land degradation due to secondary soil salinization is particularly widespread in these lowland areas, mainly due to inefficient irrigation and drainage practices which cause a rise in groundwater tables and threaten crop yields [3].

6.2.2. Plantation and tree species characteristics

The study was conducted on a ~2.5 ha tree plantation (41°65′ N, 60°62′ E, 102 m a.s.l.) established as an afforestation trial in March 2003 on a strongly salinized cropland in the Khorezm region of Uzbekistan. The plantation was established on former riparian forest land that had been cultivated with annual crops for about 20 years until the severe loss in land productivity due to soil salinization. Two leaching events were performed at the site, prior to tree planting in February-March 2003 and in the 9th year of afforestation in February 2012. At each event about 1,500 mm of fresh to slightly saline water ($\leq$2 dS m^{-1}) was applied. The trees received 80–160 mm year^{-1} of irrigation (via drip or furrow) during the first two growing seasons and thereafter relied entirely on the groundwater [13].

The winter-deciduous tree species of the afforestation experiment are two native species: actinorhizal *Elaeagnus angustifolia* L. *(Elaeagnaceae*), principal species of native riparian forest *Populus euphratica* Oliv. (*Salicaceae*), and an introduced timber species *Ulmus pumila* L. *(Ulmaceae*). At the onset of the experiment, one-year-old saplings were arranged in 36 mono-specific, completely randomized plots (12 plots per species, 36 plots in total), spaced 3.5 m from each other. Each experimental plot initially included 70 one-year-old planted saplings. Subsequently, over the period of 2003–2014, the plots were gradually thinned from 5,714 to less than 4,000 trees ha^{-1}. Survival rates of *E. angustifolia*, *U. pumila*, and *P. euphratica* respectively averaged 97, 92%, and 57% during 2003–2005. Thereafter no further mortality was observed but a vigorous vegetative and sexual propagation of *P. euphratica* via root suckers and wind-dispersed seeds was recorded in its own as well as in the neighbouring species plots.

Soils at the experimental site are old-irrigated meadow alluvial soils classified as salic Fluvisols of a predominantly silt loamy texture with a high $CaCO_3$ content ($\approx$ 16%), slightly alkaline reaction (pH $\approx$ 8) and a high water-holding capacity (available water content $\approx$ 190 mm) [4, 13]. Initial concentration of total N and available P (in fall 2003) were low, averaging respectively 0.52 g kg^{-1} and 3.8 mg kg^{-1}, but in subsequent years a build-up of the nutrients was observed, particularly in plots of *E. angustifolia* [9]. Irrigation activities in surrounding cropland regulated the groundwater level fluctuations and impacted the soil water-salt regime in afforestation sites [14]. The concentrations of major nutrients in the groundwater, measured at the end of the growing seasons, were low except for several peaks due to the short-term presence of mineral fertilizer leached from neighbouring cropping fields during fertilization events [9].

6.2.3. Plant sampling for dry matter measurements

The initial size of saplings i.e., dry matter of stem, twigs, coarse and fine roots, was measured on 30 individuals of each species prior to planting. Over the course of the study, every second row in each of the 7-row plots (i.e. 1-10 trees) was gradually harvested for measurements of the biomass accumulation at the end of the growing seasons 2006, 2007, 2009, and 2011, 2013, and 2014 (when trees grew from five to thirteen years of age). At harvest, the trees were felled at ground level and separated according to the biological stem, branch fractions of various diameter classes, woody necromass, foliage, and reproductive fractions. Coarse roots were completely excavated by hand tools, separated and grouped by diameter and washed free of soil. For the above-ground biomass fractions, the total dry matter (DM) was estimated from the total and sub-sample fresh weights at harvest and the sub-sample dry weight. Due to the prolonged time required for root excavations and associated moisture loss from roots, the dry weights of entire root systems were measured. All plant parts were dried at 103 °C to constant mass.

6.2.4. Plant isotopic analyses

Foliar sampling was conducted before the leaf fall (September-October) to provide the most stable measure of isotopic signals accumulated at the end of the growing season [9, 15]. Sub-samples of about 200 g of fresh weight were collected at harvest from one tree per plot. These sub-samples were collected from the total tree biomass and bulked for each of the major fractions (i.e. leaves, stem, branch, coarse roots, fine roots, nodules, and fruits) to account for the within-tree variations. In case of foliage, only healthy, green, fully unfolded leaves were selected. In addition, the foliage of root suckers of *P. euphratica* was sampled from all native and invaded plots. The samples were dried at 60 °C for 72 h, finely ground (<2mm) and analyzed for C and N concentration, ^{15}N natural abundance and ^{13}C discrimination with a stable isotope mass spectrometer (ANCA-SL/20-20, SerCon, UK). The isotopic analyses were conducted with 2−5 replicates per sample, depending on the within-sample variability. Several samples showing a coefficient of variability above 10% after five replicated measurements were suspected of contamination and omitted from the data analysis.

To determine N concentration and ^{15}N natural abundance, samples collected during 2003−2005 were stored and analyzed all at the same time in 2005, afterwards, during 2006-2014 the samples were analyzed in the same year of collection in the field. The analysis of foliar C concentration and ^{13}C discrimination was performed in 2014 on same samples as measured for the N-related parameters. Before this analysis, the samples were stored in zip-bags in a cool, dry room. However, the oldest of the samples, collected in 2003–2007, had been already destroyed due to laboratory maintenance, restricting the analysis of C-related parameters to the remaining samples, originating from years 2008–2014.

6.2.5. Quantification of N2-fixation by E. angustifolia

Fixation of N_2 by *E. angustifolia* was quantified by the ^{15}N natural abundance technique according to [16]:

$$\%Ndfa = \left[\frac{(\delta^{15}N_{ref} - \delta^{15}N_{fixing})}{(\delta^{15}N_{ref} - B)} \right] \cdot 100 \qquad (1)$$

where %Ndfa is the proportion of N derived from atmospheric N_2, $\delta^{15}N_{ref}$ is the ^{15}N natural abundance of the reference (non-fixing) species *P. euphratica* or *U. pumila*, $\delta^{15}N_{fixing}$ is the $\delta^{15}N$ of the N_2-fixing *E. angustifolia*, and *B* is the ^{15}N value of the same N_2-fixing species grown with N_2 as the sole nitrogen source.

For years 2006, 2007, 2009, and 2011, 2013, and 2014 the efficiency of N_2-fixation (%Ndfa) was calculated using a weighted mean of $\delta^{15}N$ based on whole-plant samples and whole-plant *B* values previously determined for actinorhizal species [15, 17], ranging from values of –1.4 to –2.0‰. Based solely in foliar ^{15}N signatures, the %Ndfa was quantified for the entire observation period 2003–2014. The published *B*-values exceeded the foliar $\delta^{15}N$ values of *E. angustifolia* trees in the afforestation trial, rendering the %Ndfa estimations unvalid. Therefore, to determine the %Ndfa based solely on the foliar $\delta^{15}N$ approach [18] was followed, using the minimal field-observed foliar $\delta^{15}N$ (measuring –2.5 in September 2007) as the *B*-value.

6.2.6. Soil and groundwater sampling and analyses

In September–October of each growing season, soil (in 20 cm layers down to 1 m depth) and groundwater were sampled from all experimental plots. The groundwater level was monitored through a network of 36 observation wells installed at a depth of 3 m at each experimental plot. Samples for the analysis of soil EC and water content were collected with an auger every 15–30 days in all plots, 0.3 m distant from a tree stem, down to 1 m depth in 20 cm layers. Electrical conductivity of the soil-water suspension ($EC_{1:1}$) was measured with an EC meter. The $EC_{1:1}$ values were converted to ECe based on the relationship ECe = 3.6$EC_{1:1}$ [19]. Soil water content was measured gravimetrically (103 °C) and converted to volumetric values based on soil bulk density [13].

6.3. RESULTS AND DISCUSSION

6.3.1. Root-zone soil salinity dynamics

The groundwater table level remained shallow over the growing seasons (April–October) during 2003–2014, on average fluctuating within 133–193 cm below the ground surface. Groundwater salinity ranged between 0.7 and 5.1 dS m^{-1} during the growing seasons, peaking in May 2011 but at all times showing a slight to moderate degree of salinity [20]. Due to the shallow groundwater table, the mean root-zone water content exhibited little variation and was close to field capacity, which ranged from 27 to 38% within the soil profile of 0–100 cm. Therefore, the soil water availability was not a constraint for plant growth. In contrast, the degree of soil salinity [21] has risen significantly as evidenced by the ECe measurements over the 12 growing seasons (Fig. 6.1).

The highest ECe level, above the threshold for a very strong degree of soil salinity (>16 dS m^{-1}), was observed prior to establishing the tree plantation. Following the pre-planting salt leaching in winter 2003, the soil salinity declined to the moderate degree (4–8 dS m^{-1}) and mostly remained within this range over two subsequent growing seasons, when irrigation was applied, and for another season after the irrigation was discontinued. However, a gradual increase in salinity occurred under non-irrigated conditions in the following years, typically peaking at the end of each growing season. The second leaching event was only marginally successful due to the malfunctioning of the on-farm drainage system that was not able to effectively convey the effluent off the site. As a result, after a temporary drop the salt load was restored in the soil profile in the course of the next three years, approaching the pre-leaching level. The differences in the root-zone soil salinity among the three species were statistically insignificant, suggesting that salinity was largely controlled by the shallow saline groundwater dynamics despite the appreciable differences in water/ solute uptake by the species [4, 14].

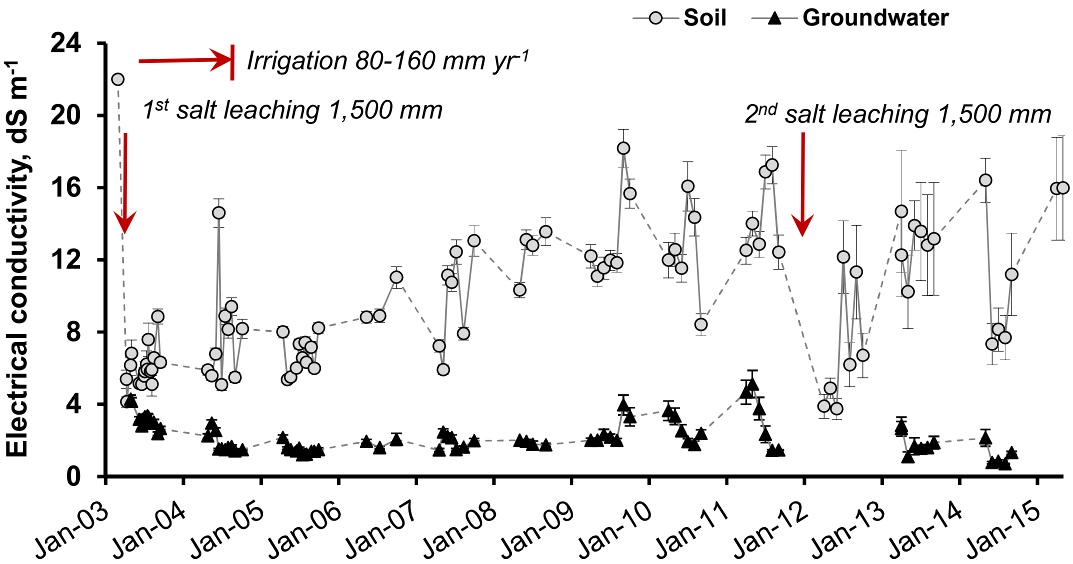

FIG. 6.1. Root-zone electrical conductivity measured in 0–100 cm soil profile during 12 consecutive growing seasons (April–October) in 2003–2014. Bars represent standard errors of the mean of 36 values measured at the experimental afforestation plots. Connecting lines are for viewing aid only. Red lines signify the duration of the irrigation period and timing of two salt leaching events.

6.3.2. Dynamics of $\delta^{13}C$ in plant tissues

Foliar $\delta^{13}C$ values measured during 2008–2014 ranged from –27.4 to –30.4, with highly significant variations for species. Specifically, *P. euphratica* showed most negative values at each observation while the values of the two other species were either only marginally different from each other or were more negative in *E. angustifolia* (Fig. 6.2).

These differences among the species are indicative of their relative salinity tolerance [8], suggesting that *P. euphratica* experienced the least salt stress despite the considerable presence of salts in the soil profile at the afforestation site (Fig. 1). Visual comparison suggests the similarity between soil salinity and foliar $\delta^{13}C$ trends in that for all species the values tended to increase over time, temporarily dropped after the salt leaching event in 2012 and went on increasing thereafter. However, statistical comparison of the trends did not reveal significant relationships between the soil ECe and foliar $\delta^{13}C$, possibly because (i) variations in the plant isotopic signature were consistent among the tree species whereas the species differences were lacking for soil salinity dynamics; (ii) soil ECe showed high variability within each growing season whereas the plant parameters were not captured with the same frequency, which compromised the correlation analysis.

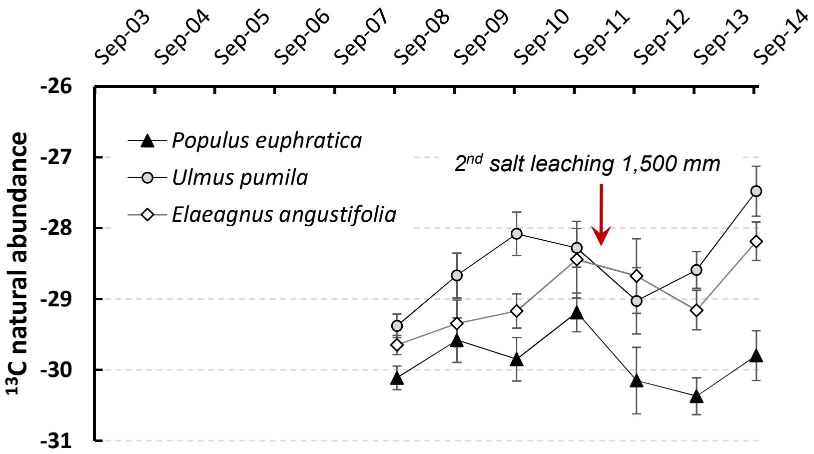

FIG. 6.2. Dynamics of foliar $\delta^{13}C$ in three afforestation species on saline soil and subjected to a salt leaching event in the 9th year after tree planting. Bars represent standard errors of the mean of 36. values measured at the experimental afforestation plots. Connecting lines are for viewing aid only. Red arrow indicates the time of the leaching event.

6.3.3. Dynamics of ^{15}N signals of plant tissues

Besides the greater salt tolerance and efficient uptake of groundwater [4], the dominance of *P. euphratica* was reflected in its vigorous self-propagation across the afforestation plots, which might be attributed to an increased soil N stock and availability measured by [9]. Some N might have been supplied via the groundwater due to leaching of fertilizers when they were applied on the neighboring cropland [9]. However, the more reliable N supply was probably provided through the N_2-fixation by *E. angustifolia*, as suggested by the long-term changes in the species ^{15}N signatures.

Except in 2003, the 1st year after planting, foliar ^{15}N signals of the non-N_2-fixing species (*P. euphratica* and *U. pumila*) were virtually identical until 2009 when the deviation was first observed, persisted and increased over the subsequent years (Fig. 6.3). The ^{15}N abundance of both non-fixing species tended to decline from highly positive values (ranging from +2‰ to +5‰) in 2003 towards nil or negative values during 2009–2014. There was little $\delta^{15}N$ variation during early growth of N_2-fixing *E. angustifolia* (except in the transplanted seedlings) until year 2010, when foliar ^{15}N values rose from −2 to −1‰. Consequently, due to the ^{15}N depletion of the non-fixing plants, on the one hand, and ^{15}N enrichment of the N_2-fixer, on the other hand, the difference in foliar values between *E. angustifolia* and *U. pumila* reduced from about 4‰ to less than 2‰, while no significant differences were any longer detected between *E. angustifolia* and *P. euphratica* at the end of the study period. The foliar $\delta^{15}N$ of *P. euphratica* root suckers invading its own and the other species plots increased from −2‰ since the first measurement in 2012 to about 0‰ in 2014.

In comparison to the foliar values, largely similar patterns were observed in aboveground woody fractions (stem and branches) but with some time lag and different magnitude of values. In contrast, ^{15}N discrimination of coarse roots of *E. angustifolia* did not show a clear temporal trend and root nodules remained significantly depleted in ^{15}N. The belowground ^{15}N signatures of the non-fixing species tended to decline, less obviously so in *U. pumila,* in which case significant differences with the N_2-fixer persisted. The weighted mean of all fractions (calculated for the period from 2006 to 2014) was greatly influenced by the values measured in aboveground wood fractions, which constituted the bulk of the total biomass (Fig. 6.3).

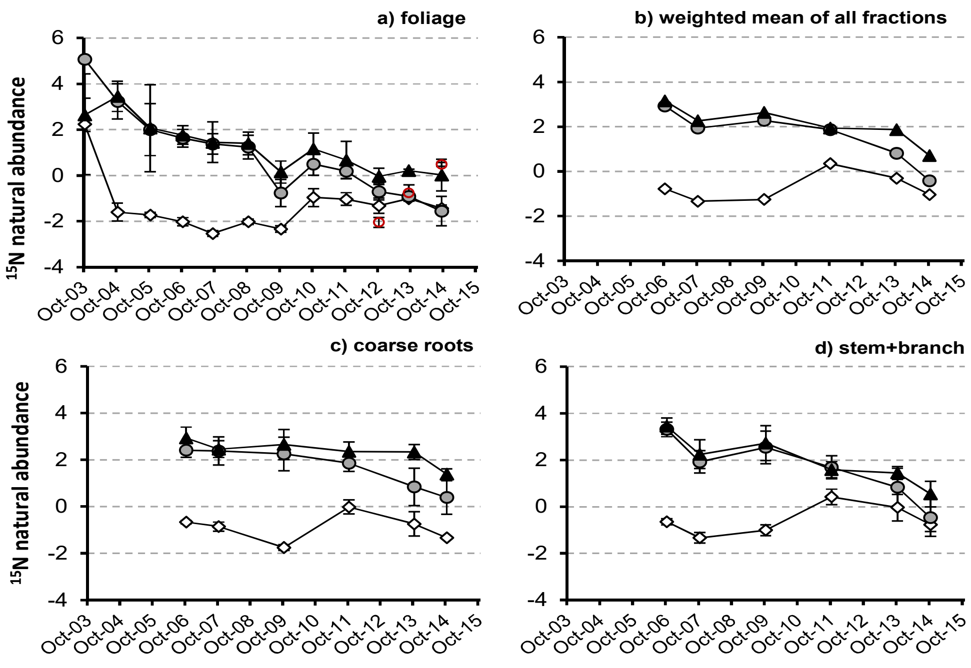

FIG. 6.3. ^{15}N natural abundance in three tree species in individual fractions and as a weighted mean in September–October 2003–2014. Legend: ◇ E. angustifolia; ● P. euphratica; ▲ U. pumila, ○ foliage of root sprouts of P. euphratica. Bars indicate standard errors of the mean. Connecting lines between points are for viewing aid only.

6.3.4. %Ndfa of Elaeagnus angustifolia

The lack of required differences in ^{15}N signals (at least 2‰) [22] between the reference and N_2-fixing plants impose restrictions for %Ndfa estimates when using *P. euphratica* as a reference for the later growth stage of the plantation, particularly if the estimations were based solely on the $\delta^{15}N$ of foliage. However, the differences in whole-plant weighted $\delta^{15}N$ remained sufficiently large to allow for the %Ndfa estimates using *U. pumila* signals as reference over the entire observation period. During the 12 consecutive growing seasons following the afforestation, %Ndfa fluctuated from 22 to 100% depending on tree age and the measuring technique (Fig. 6.4).

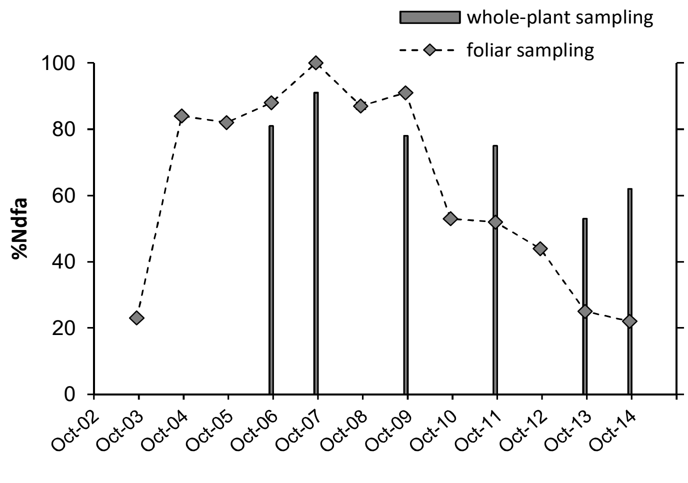

FIG. 6.4. The efficiency of N_2-fixation (%Ndfa) by E. angustifolia using U. pumila as the reference plant and based on whole-tree weighted mean and sole foliar ^{15}N natural abundance measurements during 12 consecutive growing seasons since the afforestation.

The ^{15}N natural abundance method revealed efficient N_2-fixation of 75–100% by young trees (except transplanted seedlings in 2003), but a significant tendency towards decline was observed as the plantation matured, particularly if judged by the %Ndfa values estimated through solely foliar ^{15}N signatures. The divergence between %Ndfa estimations based on foliar and whole-tree ^{15}N measurements were subtle in the early growth stage of trees but increased almost 3-fold over time. The declining %Ndfa in the older tree stand might be attributed to increasing soil N stocks and availability [9] due to nutrient release from decomposing leaf litter and belowground residues [23]. The increasing soil nutrient availability in older stands reduces the need for the physiologically costly process of biological nitrogen fixation. However, the apparent decline in N_2-fixation can be at least partly attributed to the limitations of the ^{15}N natural abundance method due to the apparent confounding of ^{15}N signals in mature, mixed-species tree stands [24].

The gradual confounding ^{15}N signals is evident through visual comparisons of the spatio-temporal variations in foliar $\delta^{15}N$ (‰) observed at the experimental site during 2007–2014 (Fig. 6.5). The comparisons reveal a decreasing range of values over time while the spatial distribution of ^{15}N natural abundance tended to homogenize throughout the afforestation site. Although the experimental plots were initially segregated according to the species, the encroachment of *P. euphratica* in plots of *E. angustifolia* (and *U. pumila*) could have resulted in the uptake by *P. euphratica* of soil N as affected by the decomposing litter of N_2-fixing *E. angustifolia* [23]. This was reflected in the increasing convergence between the $\delta^{15}N$ of the two reference species and declining ^{15}N values in both of them, with *U. pumila* being less affected than *P. euphratica* (Fig. 6.3). The dominance of *P. euphratica* over the other afforestation species is consistent with its relative abundance in the native riparian forests [25] and reflects the natural forest successional process that was assisted by the afforestation in the experimental site.

Despite the recognized limitations, the ^{15}N natural abundance method is still considered the only appropriate technique for quantifying biological nitrogen fixation by trees in a shallow groundwater environment. In particular for older trees, the method is superior to the ^{15}N dilution method which could only be applied to saplings in lysimeters, restricting the tree root growth over time [26]. The total N-difference method also showed low applicability for older trees due to higher N yields of the reference species *P. euphratica* [9].

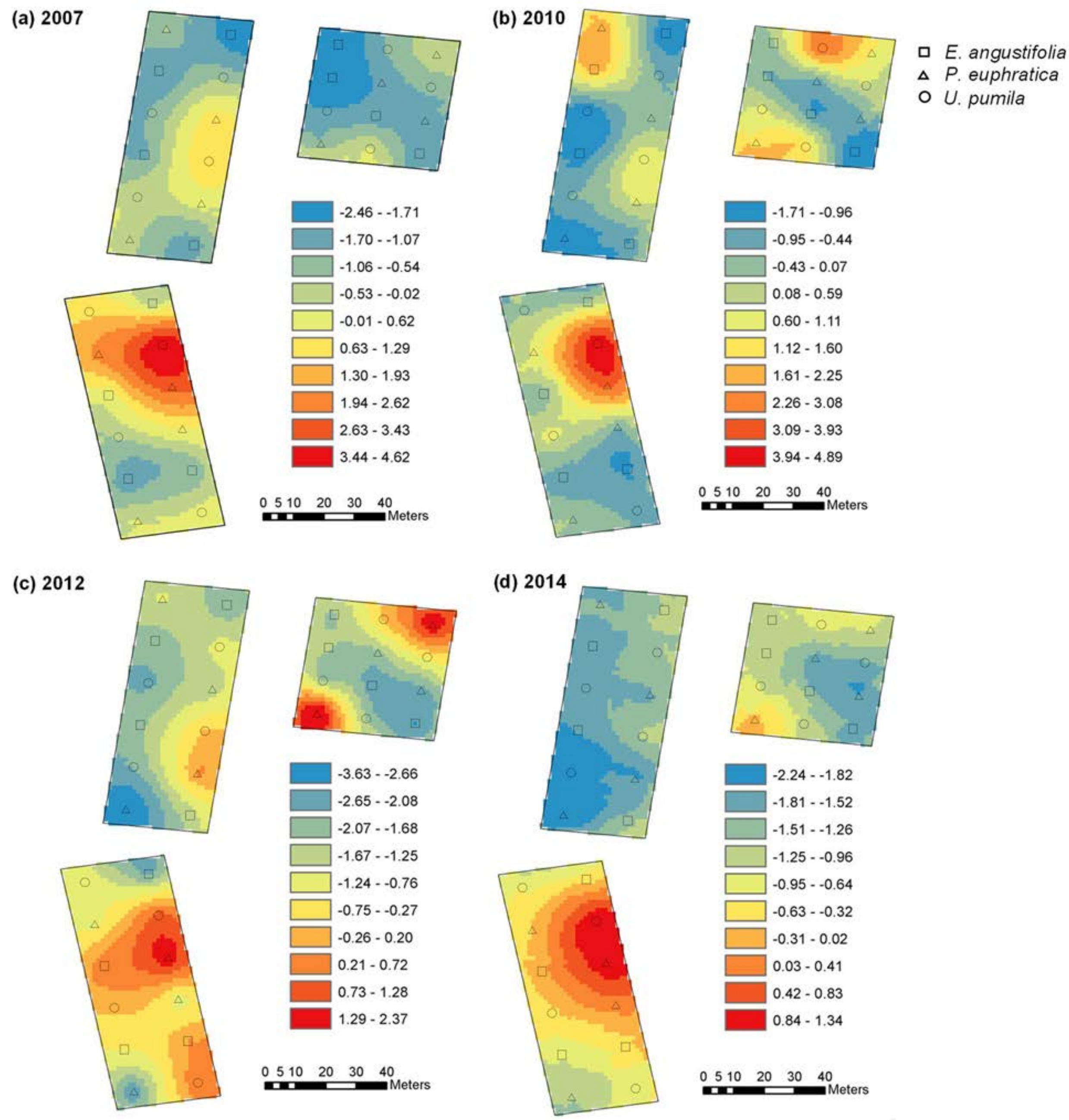

FIG. 6.5. Spatio-temporal patterns of foliar ^{15}N natural abundance (‰) resulting from the interpolation of values measured at the individual species plots (n=36, indicated by symbols) at the experimental afforestation site in the fall of 2007, 2010, 2012, and 2014. The dimension of the mono-specific plots are 105 m^2 spaced 3.5m from each other.

6.4. CONCLUSIONS

The 12-year continuous monitoring in the afforestation site established on degraded, highly salinized cropland shows that water availability does not appear a constraint for growing tree plantations due to the contribution from the shallow saline groundwater table. However, soil salinity increased significantly as the tree plantations matured under non-irrigated conditions. The salinity levels exceeded salt tolerance of many non-halophytic plant species, requiring occasional salt leaching at the plantation sites which therefore are not entirely independent of irrigation. Among the studied species, *P. euphratica* seems most well-adapted to the environmental conditions at the plantation site in the long-run and should be included in tree planting efforts on degraded lands. Monitoring of $\delta^{13}C$ is a promising approach for interpreting the relative salt tolerance among the tree species, given the consistent $\delta^{13}C$ variations observed for the three tree species and the responsiveness of $\delta^{13}C$ values to salt leaching. Future studies should analyze ^{13}C patterns in other afforestation sites covering greater soil salt and water gradients and multiple tree species, to aid in further interpretation of $\delta^{13}C$ values as an indicator of the salinity-related growth stress. Due to high temporal variability in soil salinity and plant $\delta^{13}C$ values, both parameters need to be measured simultaneously and with the same frequency.

The efficient N_2-fixation by actinorhizal *E. angustifolia* greatly contributed to self-sufficiency in nitrogen nutrition of the afforestation system under non-fertilized conditions. Including *E. angustifolia* as a nursing plant in tree plantations may assist in restoration of *P. euphratica* native riparian forests and in revegetation of degraded croplands. The ^{15}N natural abundance method allowed the evaluation of the efficiency of biological nitrogen fixation but the results need to be carefully interpreted considering the sampling material used (foliar or whole-plant), plant age, and reference species due to the spatial interference of ^{15}N signals during the successional changes (encroachment of *P. euphratica*) in tree stands over time.

Long-term studies provide an appropriate timeframe for understanding tree community dynamics under changing environmental conditions in afforestation schemes and for devising appropriate management options to inform land restoration practices. Therefore, further monitoring is required including the use of C and N isotopic methodologies, effective in revealing important physiological responses of the candidate afforestation species to prevailing salinity and nutrient deficiency stresses in degraded croplands.

REFERENCES

[1] ASIAN DEVELOPMENT BANK (ADB), Central Asian countries initiative for land management multicountry partnership framework support project, Tashkent (2008).

[2] WORLD BANK FOR RECONSTRUCTION AND DEVELOPMENT (WORLDBANK), Global condition of environment, Tashkent (2002).

[3] IBRAKHIMOV, M., et al., Groundwater table and salinity: Spatial and temporal distribution and influence on soil salinization in Khorezm region (Uzbekistan, Aral Sea Basin), Irrig. Drain. Syst. **21** (2007) 219–236.

[4] KHAMZINA, A., et al., Transpiration and early growth of tree plantations established on degraded cropland over shallow saline groundwater table in northwest Uzbekistan, Agric. For. Meteorol. **149** (2009) 1865–1874.

[5] KHAMZINA, A., et al., Conversion of degraded cropland to tree plantations for ecosystem and livelihood benefits, In: MARTIUS, C., et al., Eds, Cotton, Water, Salts and Soums - Economic and Ecological Restructuring in Khorezm, Uzbekistan, Springer Science + Business Media, B.V. (2012) 235–248.

[6] HEUPERMAN, A., et al., Biodrainage - principles, experiences and applications, Food and Agriculture Organization of the United Nations (FAO), Rome (2002).

[7] THORBURN, P.J., Interactions between plants and shallow, saline water tables: Implications for the management of salinity in Australian agriculture, Agric. Water Manage. **39** (1999) 89–90.

[8] VAN GROENIGEN, J.W., VAN KESSEL, C., Salinity-induced patterns of natural abundance carbon-13 and nitrogen-15 in plant and soil, Soil Sci. Soc. Am. J. **66** (2002) 489–498.

[9] KHAMZINA, A., et al., Nitrogen fixation by *Elaeagnus angustifolia* L. in the reclamation of degraded croplands of Central Asia. Tree Physiol. **29** (2009) 799–808.

[10] DJUMAEVA, D., et al., The benefits of phosphorus fertilization of trees grown on salinized croplands in the lower reaches of Amu Darya, Uzbekistan, Agrofor. Syst. **87** (2013) 555–569.

[11] BODDEY, R.M., et al., Use of the ^{15}N natural abundance technique to quantify biological nitrogen fixation by woody perennials, Nutr. Cycl. Agroecosys. **57** (2000) 235–270.

[12] INTERNATIONAL ATOMIC ENERGY AGENCY (IAEA), Use of isotope and radiation methods in soil and water management and crop nutrition, IAEA, Vienna, (2001) 247 p.

[13] KHAMZINA, A., et al., Tree establishment under deficit irrigation on degraded agricultural land in the lower Amu Darya River region, Aral Sea Basin, For. Ecol. Manage. **255** (2008) 168–178.

[14] KHAMZINA, A., et al., Evaluation of young and adult tree plantations for biodrainage management in the lower Amudarya River Region, Uzbekistan. In: Proc. ICID 21st European Regional Conference Integrated Land and Water Resources Management: Towards Sustainable Rural Development, Frankfurt (Oder) and Slubice - Germany and Poland, 15–19 May (2005) 11 p.

[15] DOMENACH, A.-M., et al., Estimation of symbiotic dinitrogen fixation in alder forest by the method based on natural ^{15}N abundance, Plant Soil **118** (1989) 51–59.

[16] SHEARER, G., KOHL, D.H. N_2-fixation in field settings: estimations based on natural ^{15}N abundance, Aust. J. Plant Physiol. **13** (1986) 699–756.

[17] TJEPKEMA, J.D., et al., Natural abundance of ^{15}N in actinorhizal plants and nodules, Plant Soil **219** (2000) 285–289.

[18] PEOPLES, M.B., et al., Quantification of nitrogen fixation, In: Nitrogen Fixation at the Millennium, LEIGH, G.J. (Ed.). Elsevier Science, Amsterdam (2002) 357–389.

[19] SHIROKOVA, Y.I., et al., Use of electrical conductivity instead of soluble salts for soil salinity monitoring in Central Asia, Irrig. Drain. Syst. **14** (2000) 199–205.
[20] RHOADES, J.D., et al., The use of saline waters for crop production, FAO Irrigation and Drainage Paper **48,** FAO, Rome (1992).
[21] ABROL, I.P., et al., Salt-affected soils and their management, FAO Soils Bulletin **39,** FAO, Rome (1988) 1–131.
[22] UNKOVICH, M.J., et al., Measuring plant-associated nitrogen fixation in agricultural systems, ACIAR Monograph **136** (2008) 258 p.
[23] KHAMZINA, A., et al., Above- and below-ground litter stocks and decay at a multi-species afforestation site on arid, saline soil, Nutr. Cycl. Agroecosyst. **104** (2016) 187–199.
[24] GEHRING, C., VLEK, P.L.G., Limitations of the ^{15}N natural abundance method for estimating biological nitrogen fixation in Amazonian forest legumes, Basic Appl. Ecol. **5** (2004) 567–580.
[25] KUZ'MINA, Z.V., TRESHKIN, S.E., Riparian forests and the possibility of their modern restoration, Arid Ecosyst. **2** (2012) 165–176.
[26] DJUMAEVA, D., et al., Quantification of symbiotic nitrogen fixation by *Elaeagnus angustifolia* L. on salt-affected irrigated croplands using two ^{15}N isotopic methods, Nutr. Cycl. Agroecosyst. **88** (2010) 329–339.

7. CALIBRATION AND EVALUATION OF AQUACROP FOR SIMULATING BARLEY YIELD AND WATER USE EFFICIENCY UNDER SALINE SOIL AND IRRIGATION WATER SALINITY IN A SEMI-ARID ENVIRONMENT

WAJID ISHAQUE, MUHAMMAD ATIF RIAZ
Nuclear Institute for Agriculture and Biology
Faisalabad, Pakistan

LEE KHENG HENG, MOHAMMAD ZAMAN
International Atomic Energy Agency
Vienna, Austria

Abstract

Crop growth modeling can be used to assess various crop management options and water productivity for higher crop production under different environments. In the present study, FAO's AquaCrop model was calibrated and evaluated to simulate the effect of irrigation water quality / strategies on barley yield and water use efficiency grown on saline soil in the semi-arid environment of Pakka Anna, Pakistan. The model was calibrated using two years (2016-17 and 2017-18) datasets measured from different combinations of soil and irrigation water salinity. The data of soil moisture (measured using neutron moisture probe), in-season biomass and canopy cover, biomass, grain yield at harvest and water use efficiency based on biomass and grain yield was used to calibrate the model. The calibrated model was then evaluated using three years (214-15, 2105-16 and 2016-17) independent datasets measured from the experiments involving saline soil and different irrigation regimes. Evaluation with the measured data showed that performance of the model was realistic as indicated by the acceptable %D, RMSE, nRMSE and d-index between measured and simulated values of soil moisture, biomass and grain yield at harvest. However, the performance was less satisfactory for high soil moisture stress applied to the crop grown under higher soil and irrigation water salinity.

7.1. INTRODUCTION

Salinization of agricultural soils is one of the major processes resulting in low crop productivity. Yokoi et al. [1] estimated that 50% of agricultural land is salt stressed in the arid and semi-arid regions of the world, which is a serious threat limiting crop production [2]. Scarcity of freshwater and its non-availability for agricultural production is the main impediment that leads to secondary salinization of prime agricultural lands. African and South Asian countries contain 183 M ha of salt-affected land [3], of which 91 M ha has electrical conductivity of the saturation extract (ECe) levels of 1500 mS m^{-1} within the upper 0.75 to 1.25 m of soil. Pakistan is no exception where 6.8 million hectares of land is reported to be affected by salinity to varying degrees. The groundwater in most of the agricultural areas is also brackish and thus unfit for irrigation. Reclamation of vast areas of saline lands is impractical due to several factors such as scarcity of good quality water, higher costs of drainage systems and expensive energy inputs required to operate such schemes. Therefore, alternate options for utilization of saline land and saline water resources need to be explored.

Qureshi and Barrett [4] have provided a comprehensive review of the salinity problems and management options for productive use of salt-affected lands by growing salt tolerant plants with saline water. Among crop plants, barley is rated as salt tolerant and is suitable for grain as well as forage production on saline soils [5].

Besides salt tolerance of plants, water quality and availability are a major constraint to plant productivity in saline environments. Due to higher salt contents, higher irrigation inputs are recommended to leach the salts from the root zone that in turn add more salts to the soil. On the other hand, lower inputs of saline irrigation water lead to accumulation of salts in the topsoil. Therefore, cautious practices are necessary to manage saline irrigation to sustain productivity of farming systems particularly in salt-affected environments.

To evaluate various crop management options under a saline environment for higher crop production and productivity, it is necessary to integrate these factors into a comprehensive cropping system approach. Crop growth models may provide an efficient way to study such complex mechanism of crop production, and to develop appropriate crop management strategies. This technique supports decision making to develop optimal crop management strategies in varied soil, water and environmental conditions. Various crop models have been developed during past decades. AquaCrop is a crop growth model developed by the Food and Agriculture Organization of the United Nations that has the ability to simulate both salinity and irrigation water stress independently and in combination [6]. It can simulate growth and development in a daily time step from planting to harvest based on physiological processes which describe the response of the crop to soil-weather conditions and management options. The model can synthesize results and provide alternatives for extrapolation of results to other areas with different soil characteristics and climatic conditions. The application domain of AquaCrop has evolved significantly and includes the evaluation for dry land wheat [7], irrigation management [8], estimation of wheat yield at field and district scales [9], rice development and water balance [10], deficit or optimal irrigation [11, 12] and regional crop information [13]. However, few studies have tested the model under saline conditions. Moreover, in Pakistan, application of crop growth models as decision support tools is limited and there is a general scarcity of literature related to the use of crop growth models applied under saline soil and irrigation water supply conditions.

The study presented here was a part of three-years (2014-2017) of experiments conducted to assess the impact of soil and water salinity on barley yield and productivity and to devise crop management strategies for sustainable crop production. Thus, the objective of this study was to calibrate and evaluate the AquaCrop model for barley grown on normal and saline soil, irrigated with fresh and saline water under different irrigation regimes for its further use at the landscape level.

7.2. MATERIAL AND METHODS

Data from barley (*Hordeum vulgare* L.) experiments conducted to determine the response of barley grown under optimal and sub-optimal irrigation application, quality of soil and irrigation water were used in this study. These experiments were conducted at the Bio-saline Research Station (BSRS), Pakka Anna, Pakistan (longitude 73°05'E and latitude 31°24'N, 190 m above sea level). The climate is semi-arid (BWh) in the Köppen–Geiger classification with an annual average rainfall of 325 mm, most of which (about 80%) falls during the monsoon (July - September). Normal monthly rainfall (P; mm) at BSRS, Pakka Anna during the barley growing months of November, December, January, February, March and April is 7, 9, 20, 34, 32 and 33 mm, respectively. Average monthly maximum temperature (T_{max}) during the barley growing season in the present study was 27 °C, which is similar to the normal T_{max} in this area. However, the mean T_{max} for the crop growing months of November, December, January, February, March and April during the study period was 28±3, 22±2, 20±2, 23±3, 30±4 and 36±3 °C. The mean minimum temperature (T_{min}) for November, December, January, February, March and April was 13±3, 8±2, 6±2, 9±2, 15±3 and 21±2 ºC, respectively during the study period; whereas the mean T_{min} for these months is 14, 8, 7, 6 12 and 18 ºC, respectively.

7.2.1. Soil and water resources of the study site

The major constraint for crop production is unavailability of freshwater resources. Presently, the study area has no fresh/surface water supplies and the groundwater is commonly used for irrigation. The water quality used in the current study is presented in Table 7.1 which shows that the water quality is not fit for irrigation.

TABLE 7.1. CHEMICAL ANALYSIS OF IRRIGATION WATER USED AT BSRS PAKKA ANNA

Characteristics	Value
EC_w (dS m^{-1})	6.6
pH	8.6
CO_3 (meq L^{-1})	1.5
HCO_3 (meq L^{-1})	24.5
$Ca^{2+} + Mg^{2+}$ (meq L^{-1})	3.21
SAR	40.8
RSC	22.4
Na^+ (meq L^{-1})	51.8
K^+ (meq L^{-1})	0.6
Cl^- (meq L^{-1})	14.2
SO_4 (meq L^{-1})	15.3

The soil of the area is saline-sodic to sodic with medium to light texture. Soil salinity is highly variable; electrical conductivity (EC_e) ranges from <5 dS m^{-1} in the sandy patches to >50 dS m^{-1} but is mostly between 10 to 20 dS m^{-1}. The $CaCO_3$ content ranges from 1.2 to 2.3% in the 0–30 cm soil depth. Higher spatial variability of the soil EC_e necessitated initial soil sampling from 0-25 and 25-50 cm soil depth from 5.0 hectare to select a suitable area for the field experiments. The selection criterion was based on minimum difference between the EC_e levels. After selecting an area of 0.3 ha, detailed analysis of the experimental field was performed by exposing the soil profiles up to 2.0 m (2 m × 3 m × 3 m) at three different points. Soil samples (in triplicate) were taken from each depth and sampling point using a bulk density corer from different depths (25 to 200 cm) to determine bulk density and soil texture. In-situ hydraulic conductivity at different depths was measured using a constant head permeameter (Guelph Permeameter). Water-retention characteristics were determined with the pressure-plate apparatus (Table 7.2).

7.2.2. AquaCrop calibration

Data from the experiments conducted during crop seasons 2016-17 and 2017-18 were used to calibrate AquaCrop model. The data collected for barley production and water use efficiency under different combinations of soil and water salinity was used for this purpose.

The calibration treatments included (1) Normal soil applied with good quality irrigation water (S_1W_1), (2) Saline soil applied with good quality irrigation water (S_2 W_1), (3) Normal soil applied with poor quality ground water (S_1W_2) and (4) Saline soil irrigated with poor quality ground water (S_2 W_2).

TABLE 7.2. SOIL PROPERTIES OF DIFFERENT LAYERS OF EXPERIMENTAL FIELD AT BSRS, PAKKA ANNA

Soil depth (cm)	Sand (g kg^{-1})	Clay	EC_e (dS m^{-1})	BD (g cm^{-3})	Sat. (volume %)	FC	WP	Ksat (mm day^{-1})
0-25	670	140	7.6	1.52	41	23	09	1200
25-75	420	80	8.1	1.53	46	27	10	575
75-100	500	320	13.4	1.42	47	25	12	225
100-125	210	120	14.4	1.44	46	26	13	575
125-200	850	140	10.8	1.52	41	22	10	1200

1. EC_e, electrical conducitivity; Sat., saturation; FC, field capacity; WP, wilting point; Ksat, saturated hydraulic conductivity

Prior to establishing the experiment, the leaching requirements of the experimental plots which were selected on the basis of lower/similar EC_e values and used for good soil conditions was calculated. Salts were leached from the soil profile up to 1 m soil depth through application of canal water using water tankers. Initial conditions of soil EC_e and soil moisture at crop planting in both the crop seasons are presented in Table 7.3. The quality of ground water used for saline irrigation water treatment is provided in Table 7.1.

TABLE 7.3. INITIAL CONDITIONS OF SOIL MOISTURE (SMC; MM) AND EC_E (DS M^{-1}) AT CROP SOWING IN CROP SEASON 2016-17 AND 2017-18

Soil depth (cm)	Crop Season 2016-17 Low EC_e (S1) ECe	SMC	High EC_e (S2) ECe	SMC	2017-18 Low EC_e (S1) ECe	SMC	High EC_e (S2) ECe	SMC
0-25	3.8	16.4	6.2	17.0	3.3	16.7	7.2	16.5
25-50	4.0	13.8	6.1	14.3	4.2	19.4	8.0	18.0
50-75	4.5	14.2	6.4	13.7	4.4	22.2	8.3	20.4
75-100	4.8	13.5	6.0	14.4	4.5	19.6	9.5	21.0

Individual values are mean of 9 samples (3 samples collected each replicate)

Barley cultivar Haider-93 was planted at a seed rate of 125 kg ha^{-1}, pre -treated with fungicide and placed at 4–5 cm soil depth with a row-to-row spacing of 15 cm using a tractor mounted seed drill. Phosphorus as single super phosphate (SSP, 80 kg P_2O_5 ha^{-1}) was applied at seedbed preparation. Nitrogen as urea (100 kg N ha^{-1}) was applied in two equal splits at planting and with the 2nd irrigation. All other agronomic practices (except irrigation treatments/soil moisture) such as weeding, intercultural practices and plant protection measures were kept uniform in all experimental plots and crop seasons. Soil moisture measurements were taken approximately at 10-day interval using the neutron moisture probe. Irrigation was applied with water collected in a water tanker and attached with a flow meter to measure the quantity of irrigation applied to each treatment plot.

For growth analysis, a randomly selected area of 1 m^2 was harvested from each replicate plot and dried to constant weight at 70 °C for 48 hours. In-season canopy growth was determined with duplicate photographs taken 1–1.5 m above the canopy to include a fair number of plants with the viewing plane of the camera parallel to the ground surface. The photographs were taken between 12:00-13:30 hours and digitized using a JAVA Program (Image-J) for calculation of canopy cover. The crop was harvested at physiological maturity, and total biomass and grain yield were determined.

The model calibration was started with the basic information for the barley cultivar provided within the model. The adjustments in the crop parameters were made sequentially, starting with phenology including days to flowering and maturity. After achieving appropriate adjustments for phenology, adjustments for biomass, canopy growth and crop yield parameters, i.e., accumulated biomass and grain yield were made. The simulated results were compared with observed data and the calibration process was repeated until further possibilities for improvement in the simulated versus measured values were negligible.

7.2.3. Model evaluation

After calibration, AquaCrop was evaluated with the data collected from the experiments comprising four levels of irrigation water application that corresponded to 120, 100, 80 and 60 % of crop requirement in cropping season 2014-15 and five levels i.e., 150, 125, 100, 75 and 50 % of the ET_c in both 2015-16 and 2016-17 cropping seasons (Table 7.4).

TABLE 7.4. IRRIGATION TREATMENTS AND SOWING DATE OF BARLEY USED FOR AQUACROP CALIBRATION

Study Year	Date of Sowing	Irrigation treatments (% of ET_c)				
2014-15	22.11.2.14	120	100	80	60	
2015-16	25.11.2015	150	125	100	75	50
2016-17	11.11.2016	150	125	100	75	50

Irrigation water applied to other treatments was calculated using 100% of ET_c irrigation level as the reference. Irrigation was scheduled when 50 mm of moisture from the field capacity had been depleted from the 0-100 cm soil depth in 100% of the ET_c treatment. Irrigation water applied to other treatments calculated using 100% ET_c irrigation level as the reference. To assess the changes in soil moisture content in the root zone during active crop growth, moisture status at different soil depths was measured using on-site calibrated neutron moisture meter (NMM).

At maturity, the whole of the treatment/replicate sub-plot was harvested and aboveground biomass was air dried to constant weight. After computing total aboveground biomass (straw and grain), grain was thrashed manually and subsequently measured. Harvest index (HI) was calculated as grain percentage of total biomass. Water use efficiency for both biomass production (WUE_b) and grain yield (WUE_g) as affected by different irrigation treatments were calculated as a ratio of biomass or grain yield produced per unit of water evapo-transpired (ET_c) in the respective treatment. Initial conditions of soil moisture and soil salinity measured at crop planting and used for model evaluation are presented in Table 7.5.

7.2.4. Statistical analysis

The field data collected for biomass, grain yield, HI, WUE_b and WUE_g were subjected to statistical analysis using computer based Statistix 8.1 software. The goodness of fit between simulated and observed values for biomass at harvest and grain yield was determined with the percent deviations (%D) within 15%. A negative %D indicates an under prediction while a positive %D indicates an over prediction. Values for %D were calculated using the following formula [14].

TABLE 7.5. SOIL EC_E AND SOIL MOISTURE DISTRIBUTION IN DIFFERENT SOIL LAYERS AT CROP SOWING IN THREE SEASONS USED FOR MODEL EVALUATION

Soil depth	EC_e (dS m^{-1})			Initial SMC (% volume)		
(cm)	2014-15	2015-16	2016-17	2014-15	2015-16	2016-17
0-25	8.3	5.0	9.6	0.13	0.17	0.19
25-50	8.5	6.0	8.7	0.19	0.16	0.20
50-75	9.8	7.1	8.2	0.24	0.24	0.24
75-100	12.6	13.6	14.0	0.28	0.21	0.21
100-125	14.1	15.1	13.9	0.27	0.21	0.21
125-150	11.3	12.2	14.1	0.18	0.23	0.17
150-175	10.4	10.5	10.4	0.13	0.20	0.17
175-200	8.8	9.4	10.5	0.10	0.17	0.15

$$\%\mathrm{D} = 100 \times \frac{Simulated - Measured}{Measured}$$

Correlation coefficient (r) and coefficient of determination (R^2) are used to determine the association between simulated and measured values. Average error estimates in measured and simulated in-season biomass growth, biomass at harvest and grain yield were calculated using root mean square error (RMSE) and normalized root mean square error (nRMSE), as suggested by Wallach and Goffinet [15] and Loague and Green [16], respectively, using the following relationships.

$$RMSE = \sqrt{\frac{\sum_{i=1}^{n}(S_i - O_i)^2}{n}}$$

$$NRMSE = \sqrt{\frac{\sum_{i=1}^{n}(S_i - O_i)^2}{n}} \times \frac{100}{M}$$

where S_i and O_i are the simulated and measured values for studied variables, M is the mean of measured values and n is the number of observations. The relative size of the average difference and nature of the difference in time course simulation, widely used descriptive measure for cross comparison, i.e., Willmott index of agreement (d) [17, 18] was used in this study.

$$d = 1 - \frac{\sum_{i=1}^{n}(S_i - O_i)^2}{\sum_{i=1}^{n}(|S_i - M| + |O_i - M|)^2}$$

Model performance improved as the d value approaches unity while RMSE reaches zero. NRMSE gives a percent measure of the relative difference between simulated and measured values. The simulation was considered excellent when NRMSE values were less than 10%, good with values greater than 10% but less than 20% and poor with nRMSE greater than 30% [19].

7.3. RESULTS AND DISCUSSION

7.3.1. AquaCrop calibration

7.3.1.1. Root-zone soil moisture and crop evapotranspiration

Time series analysis of root-zone moisture during the barley growing season and the relationships between simulated and measured soil moisture contents (mm) under different irrigation treatments are presented in Fig. 7.1.

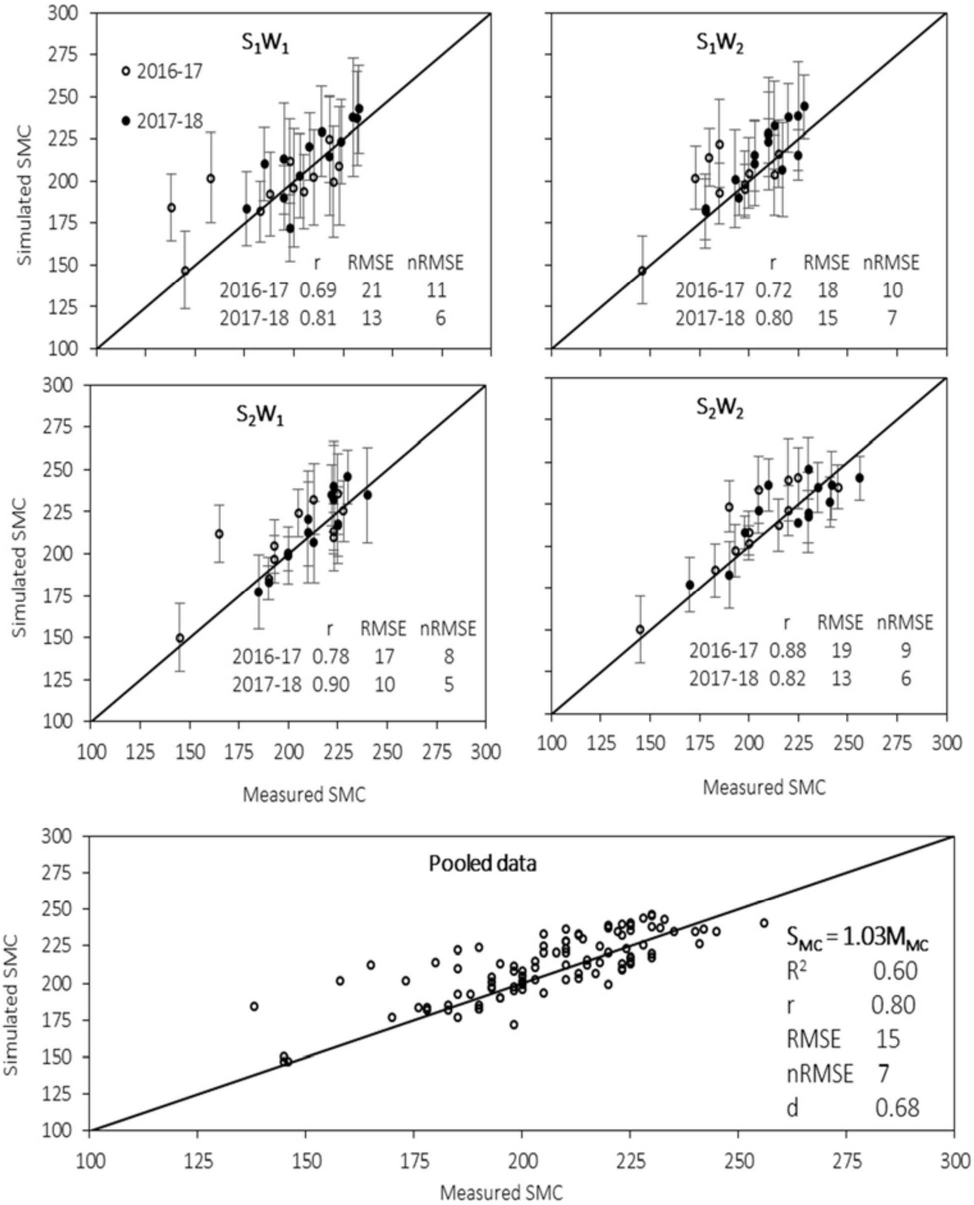

FIG. 7.1. Simulated and measured soil moisture contents as affected by different combinations of soil and irrigation water salinity.

Among individual crop growing seasons, model simulation for soil moisture was comparatively better for growing season 2017-18 with nRMSE ranging from 5-7%. For crop season 2016-17, the range of r and RMSE was from 0.69-0.88 and 17-21 mm, respectively. The slope of regression lines for the pooled data of simulated and measured values (n = 99) was 1.03 when intercept was set to zero. Generally, the model slightly over predicted SMC but the overall statistical indicators of R^2, r, RMSE and nRMSE showed excellent model predictions to simulate soil moisture contents.

Crop evapotranspiration (ET_c) was measured using the water balance approach for all irrigation treatments for both study years. To calculate simulated ET_c, the model outputs for evaporation from the soil surface and transpiration from the plant canopy was added. The simulated and measured data of crop evapotranspiration is presented in Table 7.6. The measured crop evapotranspiration in the 2016-17 season was 280, 248, 244 and 227 mm for S1W1, S1W2, S2W1 and S2W2 treatments, respectively, with corresponding simulated ET_c of 239, 219, 211 and 194 mm. Similarly, in crop season 2017-18, the measured and simulated ET_c for S1W1, S1W2, S2W1 and S2W2 was 264, 269, 257, 232 mm and 286, 252, 232 and 195 mm, respectively. The correlations (Pearson; r) between simulated and measured ETc was calculated as 0.77 with NRME and nRMSE of 31 mm and 12%, respectively, indicating a good relationship between simulated and measured ETc values.

TABLE 7.6. SIMULATED AND MEASURED CROP EVAPOTRANSPIRATION (ETC) OF BARLEY GROWN IN CROP SEASON 2016-17 AND 2017-18 AT BSRS, PAKKA ANNA

Input	Measured water balance				Aquacrop water balance				Difference (%)
	I[a]	R	Δ	ET_c	E	T	D	ET_c	
					2016-17				
S1W1	225	47	8	280	55	181	-	239	–14
S1W2	225	47	–24	248	66	153	-	219	–18
S2W1	225	47	–28	244	78	133	-	211	–14
S2W2	225	47	–45	227	9	103	-	194	–14
					2017-18				
S1W1	250	17	–3	264	44	242	-	286	8
S1W2	250	17	2	269	51	201	-	252	–6
S2W1	250	17	–10	257	68	164	10	232	–10
S2W2	250	17	–35	232	75	120	33	195	–16

[a] I = Irrigation (mm), R = Rainfall (mm), Δ = change in soil moisture at sowing and at harvest, E = Evaporation from soil, T = crop transpiration, D = Drainage below 1 m of soil depth

7.3.1.2. In-season biomass and canopy cover

AquaCrop was calibrated for in-season biomass production (t ha^{-1}) and comparison was made between measured and simulated values on a daily basis for all the studied treatments (Fig. 7.2). In-season biomass production was accurately simulated by the model. This is shown by the high index of agreement (d = 0.99) and satisfactory nRMSE (9% ≤ nRMSE ≤ 16%) in different crop growing seasons and treatments. Similarly, for percent canopy cover (Fig. 7.3), model predictions were good for both the crop seasons and irrigation treatments. Correlations (r) between simulated and measured CC ranged from 0.93 to 0.99 and index of agreement 0.98-0.99. The range of RMSE (2.4% ≤ RMSE ≤ 10%) and nRMSE (9% ≤ nRMSE ≤ 16%) for years and treatments showed satisfactory behaviour of the model to predict in-season canopy growth.

Simulated and measured in-season biomass data pooled across the evaluation years, closely followed a 1:1 line of perfect agreement (Fig. 7.4). Generally, the model under predicted in-season biomass growth with the linear relationship of $S_b = 0.92M_b + 0.27$ (where S_b and M_b are simulated and measured in-season biomass). The slope of the line (0.92) closer to unity indicates an excellent relationship between the two while a positive y-intercept shows model under prediction of 0.27 t ha^{-1}. However, the higher coefficient of determination (R^2, 0.98) along with the two year mean r, RMSE, nRMSE and d of 0.98, 0.71 t ha^{-1}, 12% and 0.95 respectively, shows satisfactory behaviour of the model to predict in-season biomass.

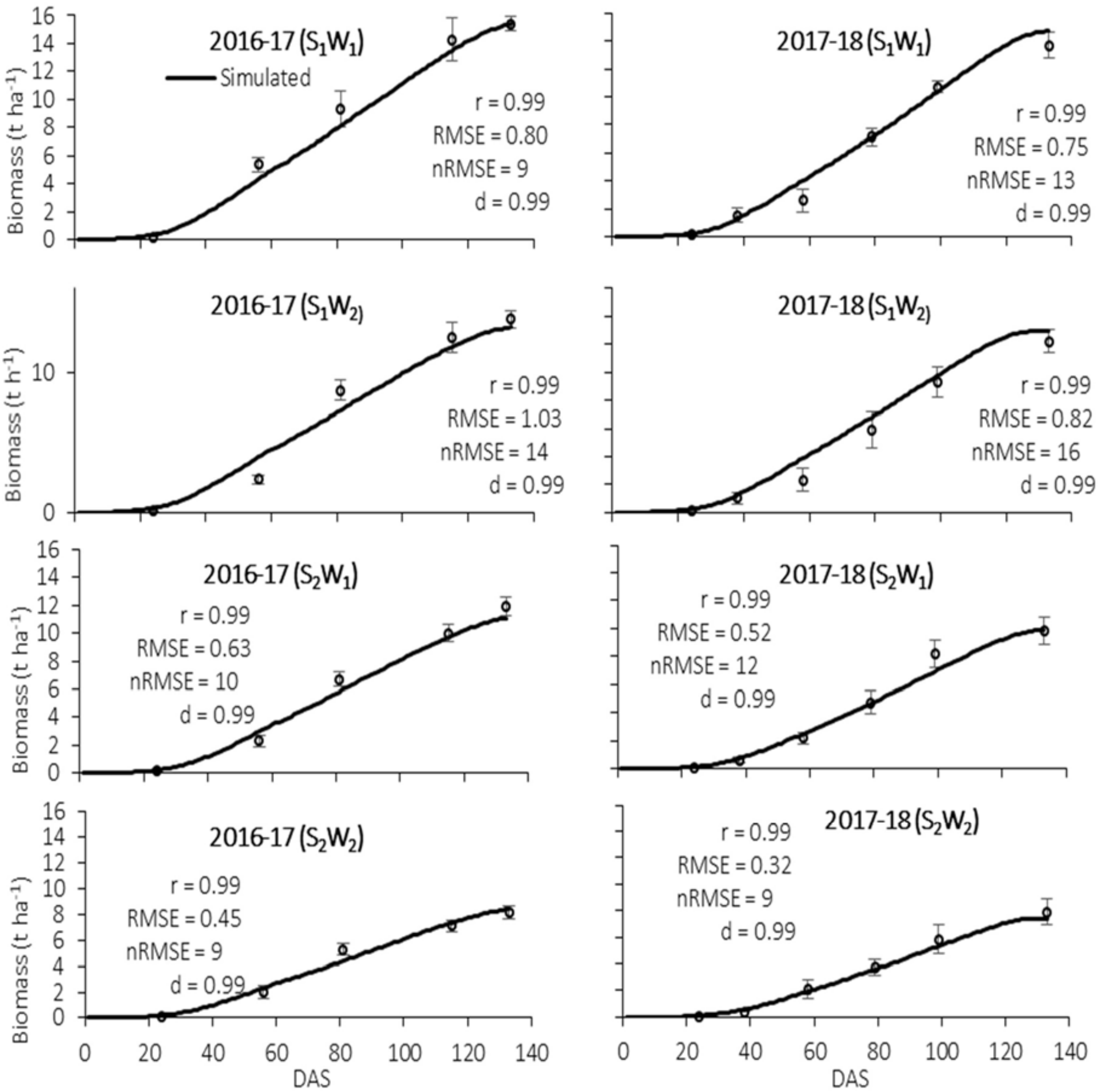

FIG. 7.2. Simulated (line) and measured (symbol with SD) in-season biomass (n = 3) of barley as affected by different combinations of soil and irrigation water salinity during crop season 2016-17 (left) and 2017-18 (right).

Model- predicted %CC showed good agreement with the observed data. Simulated and measured canopy growth values pooled across study years closely followed a 1:1 line. Generally, the model under predicted %CC. The linear equation relating simulated and measured canopy cover (Scc = 0.90Mcc + 9) showed lower simulated compared to measured CC. Nevertheless, the higher coefficient of determination (R^2) of 0.90 for %CC along with two year mean values of r, RMSE, nRMSE and d of 0.88, 6, 11% and 0.87, respectively, indicated an excellent performance of the model to predict canopy growth.

7.3.1.3. Biomass and grain yield at harvest

Among individual study years (Table 7.7) and for crop season 2016-17, the percent difference (%D) between simulated and measured biomass ranged between −2 to 3%. The model over predicted biomass in saline soil applied with saline irrigation water (S2W2). A similar trend was observed for grain yield with 9, 8 and 6% under prediction in S1W1, S1W2 and S2W1 treatments, while 5% over prediction for the S2W2 treatment. However, the trend was opposite for the crop season 2017-18 with over prediction in S1W1 (7%), S1W2 (8%) and

S2W1 (1%) and under estimation for S2W2 (6%). Approximately the same trend was observed for grain yield in crop season 2017-18. Nevertheless, overall model simulations were in good agreement with measured data as indicated by high r (0.98-0.99), nRMSE (4-11%) and sufficient d index (0.82-0.9).

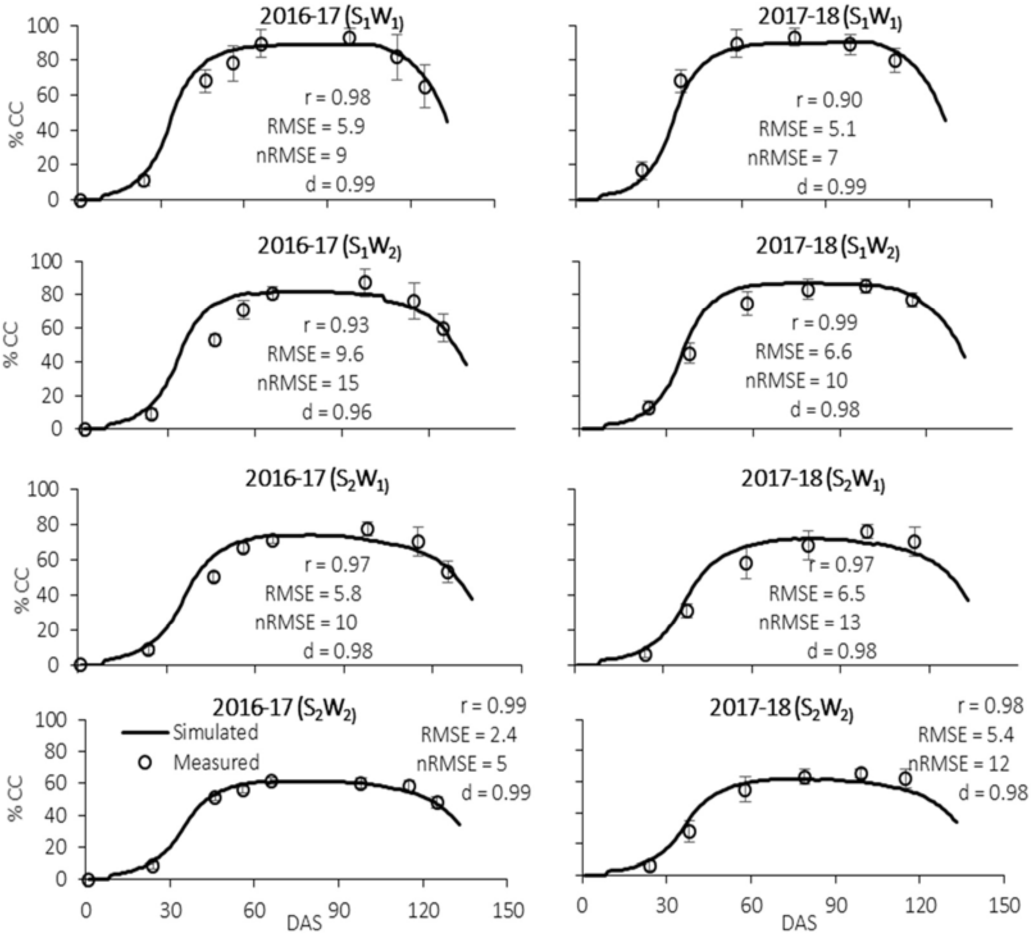

FIG. 7.3. Simulated (line) and measured (symbol with SD) percent canopy cover (CC, n = 9) of barley as affected by different combinations of soil and irrigation water salinity during crop season 2016-17 (left) and 2017-18 (right).

Averaged across treatments, measured above-ground biomass of barley varied significantly among years with average biomass of 12.5 t ha^{-1} in crop season 2016-17 and 10.9 t ha^{-1} in crop season 2017-18 (Fig. 7.5). Similarly, measured grain yield was 3.5 and 2.9 t ha^{-1} in crop season 2016-17 and 2017-18, respectively. Mean simulated biomass and grain yield in crop season 2016-17 and 2017-18 were 12.1, 11.3 t $ha^{-1}$and 3.3, 3.1 t ha^{-1}, respectively. The overall percent difference in simulated and measured biomass averaged across treatments was −3 and 3% with respective grain yield differences of −5 and 7%.

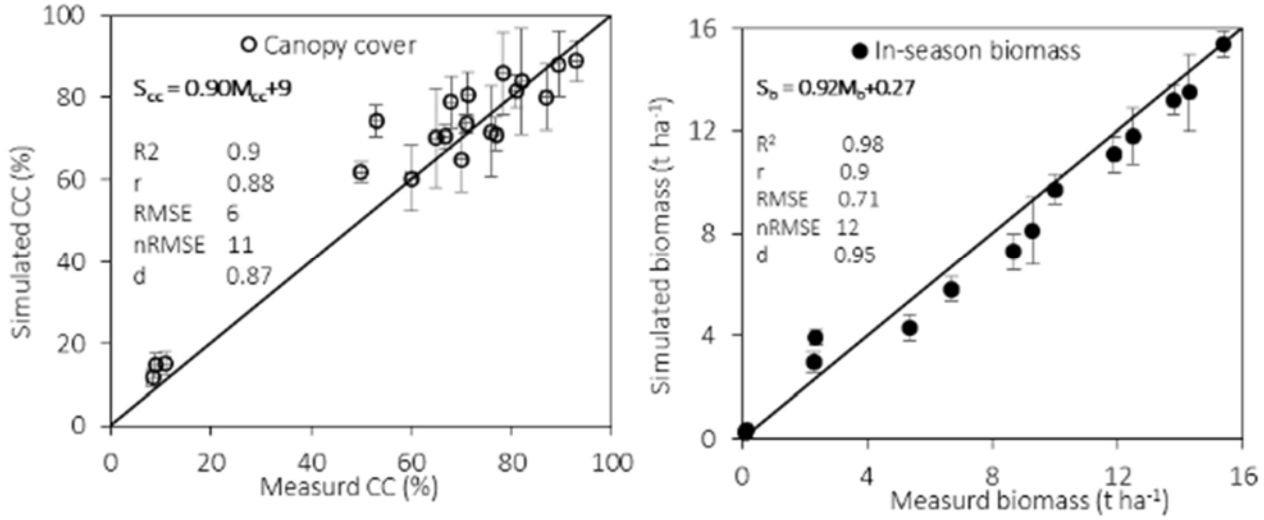

FIG. 7.4. The relationship between overall simulated vs. measured values of in-season biomass (n =40) and canopy cover (n= 52).

TABLE. 7.7. SIMULATED AND MEASURED BIOMASS AND GRAIN YIELD AT HARVEST IN BARLEY GROWING SEASONS 2016-17 AND 2017-18 AT BSRS, PAKKA ANNA

Treatment	2016-17						2017-18					
	Biomass			Grain yield			Biomass			Grain yield		
	M[a]	S	%D	M	S	%D	M	S	%D	M	S	%D
S1W1	15.7	15.4	−2	4.6	4.2	−9	13.7	14.7	7	4.1	4	−2
S1W2	14	13.3	−5	4	3.7	−8	12	13	8	3.3	3.7	12
S2W1	11.9	11.4	−4	3.3	3.1	−6	9.8	9.9	1	2.3	2.7	17
S2W2	8.2	8.4	3	2.2	2.3	5	7.9	7.4	−6	1.8	2	−13
r		0.99			0.99			0.99			0.98	
RMSE		0.47			0.27			0.75			0.3	
nRMSE		4			8			7			11	
D		0.9			0.82			0.85			0.82	

[a] M = measured value; S = Simulated value; %D = 100 × (S-M) / M

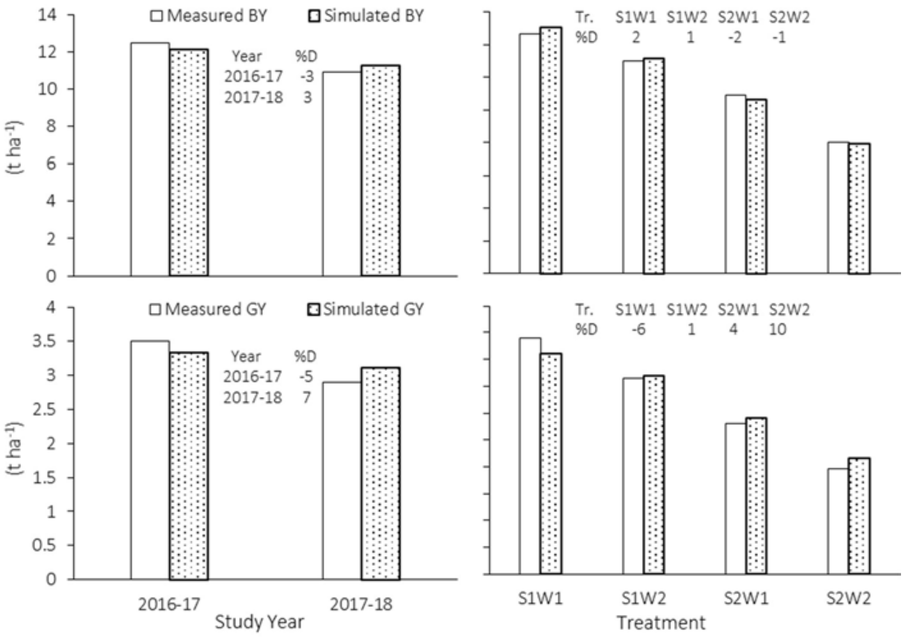

FIG. 7.5. Simulated and measured biomass and grain yield of barley grown in crop season 2016-17 and 2017-18 at BSRS, Pakka Anna.

Among irrigation treatments, the overall biomass production averaged across years was significantly higher for S1W1 (14.7 t ha^{-1}) followed by S1W2 (13.1 t ha^{-1}), S2W1 (10.9 t ha^{-1}) and lowest for S2W2 (8.03 t ha^{-1}). The model was able to predict the same trend of higher biomass production in S1W1 (15.1 t ha^{-1}) followed by 13.2, 10.7 and 7.9 t ha^{-1} for S1W2, S2W1 and S2W2 treatments, respectively. The overall percent difference between simulated and measured biomass was 2, 1, −2 and −1 % for S1W1, S1W2, S2W1 and S2W2 treatments, respectively. The model was able to predict accurately the grain yield with respective simulated and measured values of 4.1, 3.7, 2.9, 2.2 t ha^{-1} and 4.3, 3.7, 2.9 and 2.0 t ha^{-1}.

7.3.1.4. Water use efficiency based on biomass and grain yield at harvest

Simulated and measured water use efficiency for biomass (WUE_b; kg ha^{-1} mm^{-1}) and grain yield (WUE_g; kg ha^{-1} mm^{-1}) calculated using simulated and observed biomass, grain yield (Table 7.7) and crop evapotranspiration (Table 7.6) is presented in Table 7.8.

TABLE.7.8. SIMULATED AND MEASURED WATER USE EFFICIENCY (KG HA^{-1} MM^{-1}) OF BARLEY FOR CROP SEASON 2016-17 AND 2017-18 AT BSRS, PAKKA ANNA

Treatment	2016-17						2017-18					
	WUE_b			WUE_g			WUE_b			WUE_g		
	*M	S	%D	M	S	%D	M	S	%D	M	S	%D
S1W1	56	64	15	16	18	10	52	51	−1	15	14	−6
S1W2	57	61	7	17	17	-	45	52	15	12	15	22
S2W1	48	54	13	13	15	13	38	43	12	9	12	29
S2W2	36	43	20	9	12	32	34	38	12	7	10	47
r		0.97			0.96			0.93			0.89	
RMSE		7			2			5			3	
nRMSE		13			13			11			23	
d		0.6			0.70			0.67			0.5	

Among individual crop growing seasons and irrigation treatments, percent difference between measured and simulated WUE_b in crop season 2016-17 was comparatively higher for S2W2 (20%) compared to S1W1, S1W2 and S2W1 with respective values of 15, 7 and 13%. Similarly, in crop season 2017-18 the respective %D for S1W1, S1W2, S2W1 and S2W2 was −1, 15, 12 and 12%. An approximately similar trend was observed for WUE_g values. The model generally over predicted the WUE values under high soil and irrigation water salinity levels as indicated by high nRMSE and lower d-index values.

Depending on measured biomass and ETc, measured WUE_b averaged across irrigation treatments (Fig. 7.6) varied non-significantly between crop seasons with mean values of 49 and 42 kg ha^{-1} mm^{-1} for crop seasons 2016-17 and 2017-18.

Similar differences were observed for WUE_g (14 kg ha^{-1} mm^{-1} for crop season 2016-17 and 11 kg ha^{-1} mm^{-1} for 2017-18). The AquaCrop simulated WUE_b value for crop season 2016-17 (56 kg ha^{-1} mm^{-1}) was 16% higher than crop season 2017-18 (47 kg ha^{-1} mm^{-1}). Similarly, simulated WUE_g for crop season 2016-17 (15 kg ha^{-1} mm^{-1}) was 13% higher compared to crop season 2017-18 (13 kg ha^{-1} mm^{-1}). The overall percent difference between simulated and measured WUE_b was 15% for crop season 2016-17 and 11% for 2017-18. Moreover, the %D between simulated and measured WUEg was higher (17%) for crop season 2017-18 than calculated for 2016-17 (10%).

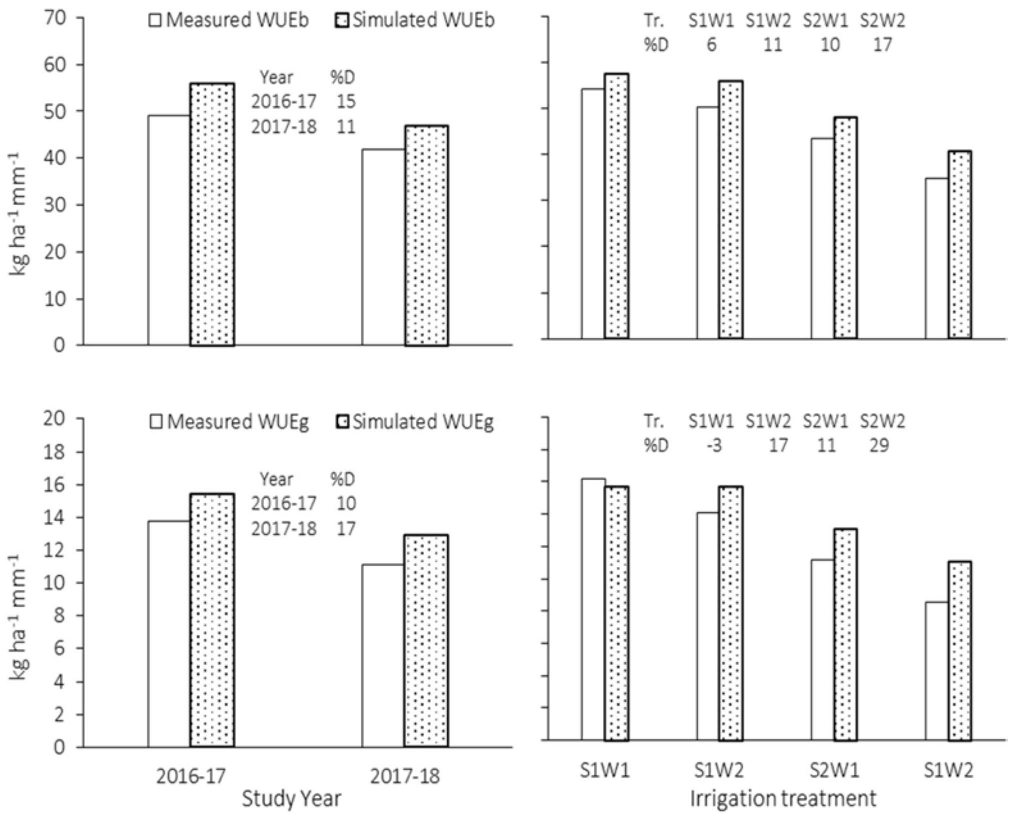

FIG. 7.6. Simulated and measured water use efficiency for biomass (WUE_b) and grain production (WUE_g) of barley grown in crop seasons 2016-17 and 2017-18 at BSRS, Pakka Anna.

Averaged across study years, measured WUE_b was not significantly different for S1W1 (54 kg ha^{-1} mm^{-1}) and S1W2 (51 kg ha^{-1} mm^{-1}). However, significantly lower values were observed for S2W1 and S2W2 with mean values of 43 and 35 kg ha^{-1} mm^{-1}. A similar trend was observed for WUE_g with mean values of 16, 14, 11 and 8 kg ha^{-1} mm^{-1} in S1W1, S1W2, S2W1 and S2W2 treatments, respectively.

Analysis of the pooled data of both crop seasons showed satisfactory performance of the model to predict water use efficiency (Fig. 7.7). Overall mean r, RMSE, nRMSE and d for WUE_b was calculated as 0.95, 6.0 kg ha^{-1} mm^{-1}, 13% and 0.98, respectively. Similarly, the values of r (0.92), RMSE (1.98 kg ha^{-1} mm^{-1}), nRMSE (16%) and d (0.97) showed satisfactory performance of the model to predict WUE under saline soil and irrigation water supply conditions.

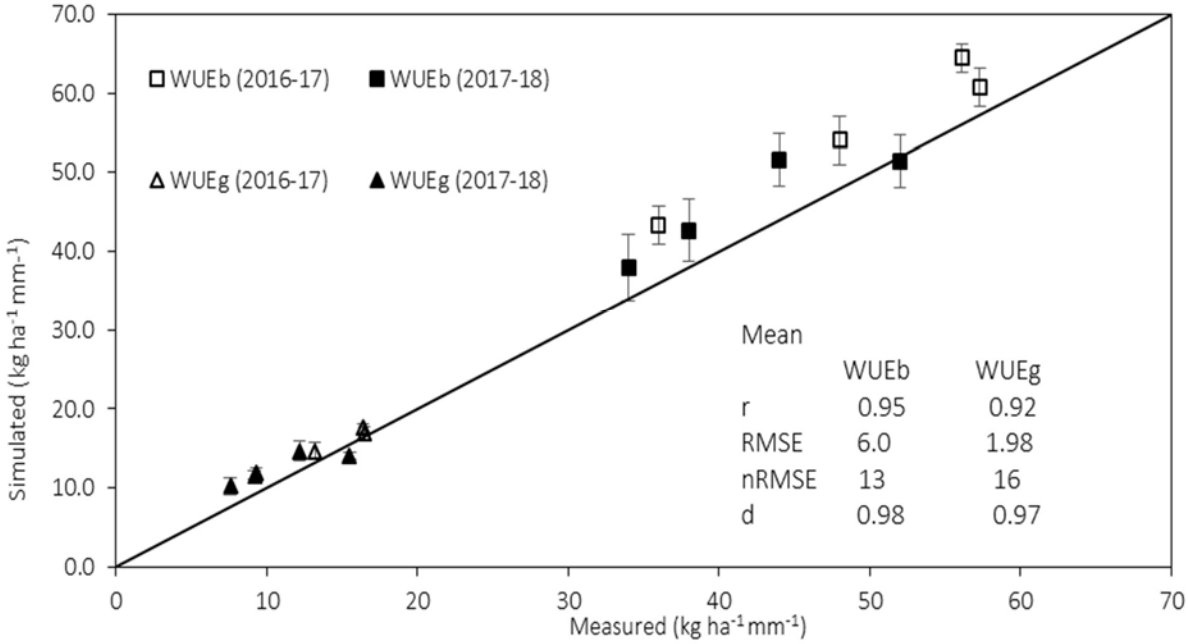

FIG. 7.7. Simulated and measured water use efficiency (kg ha^{-1} mm^{-1}) of barley for crop seasons 2016-17 and 2017-18.

The comparison of simulated and measured values for soil moisture, crop evapotranspiration, in-season biomass and canopy growth, above-ground biomass and grain yield at harvest and finally water use efficiency based on biomass and grain yield shows a satisfactory calibration of the AquaCrop model. Final values of different parameters after calibration are given in Table 7.9.

7.3.1.5. AquaCrop evaluation

After achieving a reliable agreement between simulated and measured values during calibration, evaluation of the model was performed with data other than that used in calibration. The process involved 14 independent data sets collected over 3 years (2004-15 to 2016-17) at the same experimental field. The performance of the model was evaluated from its ability to predict soil moisture contents, biomass and grain yield at harvest.

7.3.1.6. Soil moisture content

The measured soil moisture using the NMM during the crop growing period in different years and irrigation treatments was compared with model predicted soil moisture contents. The model performance to simulate soil moisture during evaluation was satisfactory with acceptable nRMSE ranging from 3.1 to 21.6% (Table 7.10).

The overall efficiency of the model to simulate root zone soil moisture was satisfactory for crop seasons 2014-15 and 2015-16. The mean nRMSE ≤ 10% of different irrigation treatments in these years shows excellent performance of the model to predict soil moisture contents. However, for crop season 2015-16 a higher difference between simulated and measured soil moisture was observed (RMSE = 34.4-36.2 mm). Nevertheless, model performance was satisfactory on the basis of nRMSE (17.3-21.6%).

TABLE 7.9. CALIBRATION PARAMETERS OF AQUACROP FOR BARLEY UNDER SALINE SOIL AND WATER QUALITY OF BSRS, PAKKA ANNA, PAKISTAN

Number of plants	160 plants m^{-2}	ECe thresholds	
Canopy size (seedling)	1.5 cm^2 $plant^{-1}$	Upper	4 dS m^{-1}
Time to emergence	8 days	Lower	15 dS m^{-1}
Time to maximum canopy	60 days		
Maximum canopy cover	90%	Water	
Maximum effective rooting depth	0.6 m	p (upper)	0.15
Time to maximum rooting depth	67 days	p (lower)	0.60
Time to flowering	91 days	Shape factor	3.0
Flowering Duration	8 days		
Senescence	107 days		
Canopy decline	34 days		
Maturity	133 days		
Water productivity	16 g m^{-2}		
Harvest Index	27%		

TABLE 7.10. STATISTICAL INDICATORS OF MODEL PERFORMANCE TO SIMULATE SOIL MOISTURE IN DIFFERENT STUDY YEARS AND IRRIGATION TREATMENTS DURING MODEL CALIBRATION

Season	Treatment (% of ET_c)	RMSE (mm)	nRMSE (%)	D
2014-15	120	14.5	5.1	0.55
	100	14.1	4.9	0.57
	80	18.5	6.6	0.41
	60	18.4	6.5	0.50
2015-16	150	36.2	18.1	0.46
	125	34.4	17.3	0.47
	100	40.0	21.6	0.33
	75	36.4	20.4	0.29
	50	35.9	21.4	0.30
2016-17	150	8.3	3.1	0.94
	125	10.1	3.9	0.89
	100	12.3	4.8	0.86
	75	20.7	8.2	0.63
	50	21.3	8.6	0.55

7.3.1.7. Biomass and grain yield at harvest

Measured above-ground biomass of barley was significantly different among years and irrigation treatments. However, the difference between irrigation treatments in different years was variable due to growing season rainfall and initial soil salinity levels at crop sowing. Comparatively higher rainfall in crop season 2014-15 (125 mm) and 2015-16 (133 mm) resulted in lesser differences among irrigation treatments. AquaCrop was able to simulate this trend in biomass and yield production well (Fig. 7.8).

Overall measured biomass in crop season 2014-15 was 13.4, 12.5, 11.2 and 9.8 t ha^{-1} compared to simulated values of 12.9, 12.0, 11.7 and 11.5 t ha^{-1} for 125, 100, 75 and 50% of ET_c treatments, respectively. The percent difference (%D) in simulated and measured biomass was 4, 6, –4 and –17 % for 120, 100, 80 and 60 % of ET_c treatment. The model was able to predict accurately the grain yield (3.6 t ha^{-1}) in the 120% ET_c treatment for crop season 2014-15. However, like biomass the model under predicted the grain yield by –14 and –63 % for irrigation treatment 80 and 60 % of ET_c. Overall statistical indicators of r, RMSE and nRMSE for biomass i.e., 0.83, 0.98 and 8% and grain yield (0.7, 0.64 and 21%) indicated appropriate simulation by the model for crop season 2014-15.

In crop season 2015-16, %D between simulated and measured biomass was 2, 6, 4, –8 and –9%, whereas for grain yield it was 10, –1, 1, –19 and –37% for 150, 125, 100, 75 and 50 %ET_c treatments, respectively. The model generally under predicted the grain yield for water stressed conditions. However, analysis of pooled data indicated good relationships between simulated and measured values with r, RMS and nRMS of 0.96, 0.58 kg ha^{-1}, and 5%, respectively, for biomass and 0.98, 0.29 kg ha^{-1} and 10% for grain yield in crop season 2015-16. A similar trend was observed for simulated and measured biomass for crop season 2016-17. However, the overall model predictions were better in crop season 2016-17 compared to 2015-16 with better r, RMSE and nRMSE. The overall effect of irrigation treatment with mean data of crop seasons 2015-16 and 2016-17, showed appropriate simulations made by the model for irrigation application. In general, the model under predicted the biomass and grain yield from 13 to 31% under water stressed conditions. Nevertheless, the statistical indicators showed appropriate simulations by the model to predict biomass and grain yield at varying irrigation levels.

Crop growth models are an organization of processes controlled by different specific genetic encryptions with its context-related expressions. Lack of understanding and inherent complexity of processes involved limits the capabilities of these models to provide a full description of specific process under investigation. However, the model should be able to simulate/predict the behaviour or process close enough to the real values before its application to test any hypotheses. After certain specific adjustments i.e., calibration, the capability of the model to predict the real system can be evaluated by comparing the experimental data collected under similar conditions before its application to test the hypothesis under study i.e., model application.

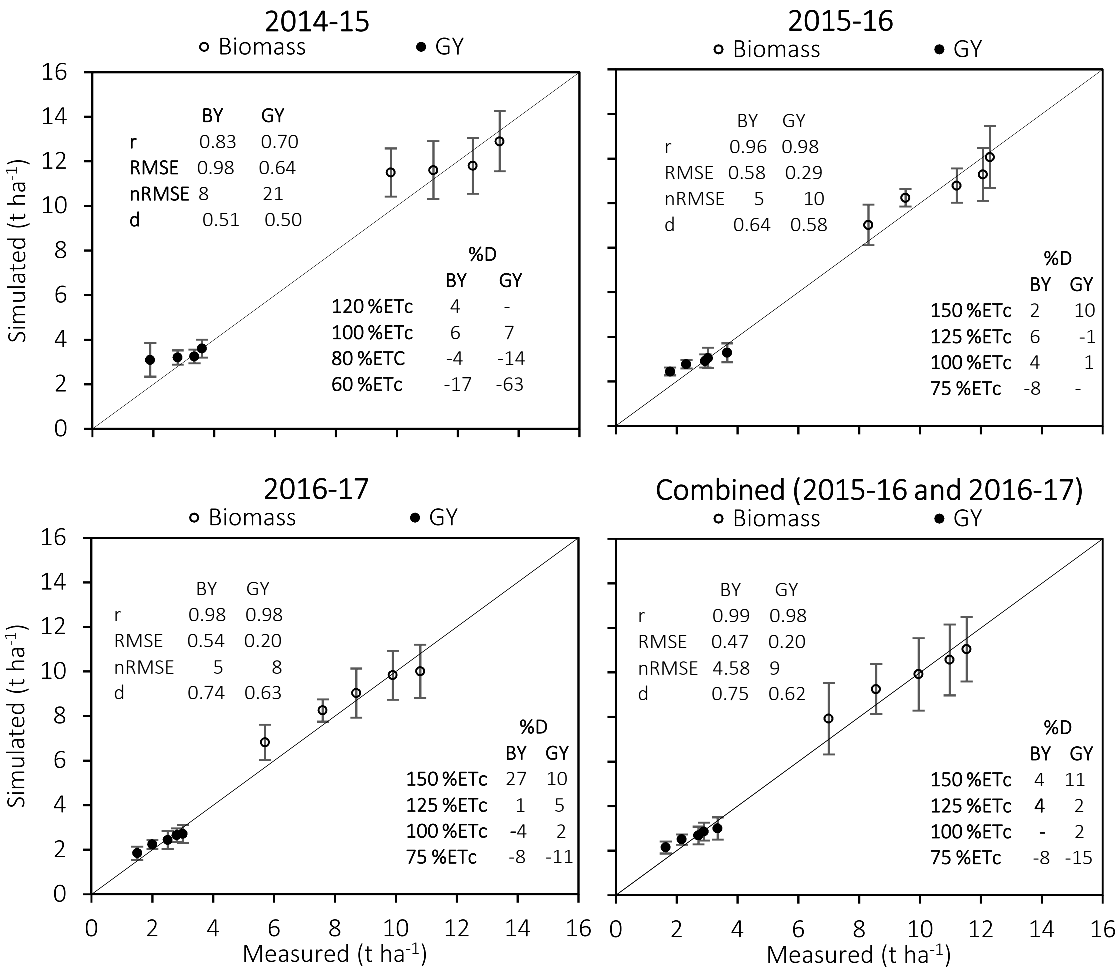

FIG. 7.8. Simulated and measured biomass and grain yield of barley in different years and irrigation treatments.

7.4. CONCLUSIONS

This three-year field study conducted on barley indicated that barley yield was affected by soil, irrigation water salinity and irrigation regimes. Generally, soil salinity had higher impact on barley biomass (32% reduction) and grain yield (21% reduction) compared to irrigation water salinity (21% reduction). In the experiments with the crop grown on saline soil and applied with saline irrigation water under different irrigation regimes, barley grain yields obtained under higher soil moisture stressed conditions were significantly lower than those obtained with 100 %ET_c and higher irrigation levels. The results indicated deficit irrigation with saline ground water may reduce the growth and yield due to the compounded effect of water deficit and soil/irrigation water salinity. The water use efficiency for biomass and grain yield were also affected by irrigation treatments and soil/irrigation water quality. The FAO AquaCrop model predicted accurately soil moisture contents, crop evapotranspiration, in-season biomass (9% ≤ nRMSE ≤ 16%) and canopy growth (9% ≤ nRMSE ≤ 16%), yield (8% ≤ nRMSE ≤ 11%) and water use efficiency (13% ≤ nRMSE ≤ 23%) during model calibration. However, the performance of the model during evaluation was comparatively less satisfactory to simulate yield under higher soil moisture stressed conditions of the 60%ETc treatment (D = 63%) for crop season 2014-15. The model generally under-predicted biomass and grain yield under water stressed conditions. However, this under prediction was 8% for biomass and 15% for grain yield for the pooled data of crop seasons 2015-16 and 2016-17 for the 75 %ET_c treatment. These results confirm that AquaCrop was able to simulate with acceptable accuracy barley yield under saline conditions and limited irrigation water. As a result of this research, full irrigation or 25% higher than crop water requirement is recommended for irrigation of barley crop under saline soil and irrigation water supply conditions. However, it may accelerate secondary salinization if a sufficient amount of rainfall or a minimum amount of freshwater to leach the salts below the root zone is not available. In case of water scarcity, the irrigation application may be reduced by 75-80% of full crop water requirements.

REFERENCES

[1] YOKOI, S., et al., Salt Stress Tolerance of Plants. JIRCAS Working Report, Center for Environmental Stress Physiology, Purdue University, West Lafayette, IN, USA (2002) 25–33.

[2] MUNNS, R., Comparative physiology of salt and water stress, Plant Cell Environ. **25** (2002) 239–250.

[3] KHAN, M.J., GLENN, E.P., Yield and evapotranspiration of two barley varieties as affected by sodium chloride salinity and leaching fraction in lysimeter tanks, Comm. Soil Sci. Plant Anal. **27** (1996) 157–177.

[4] QURESHI, R.H., BARRETT, L., Saline Agriculture for Irrigated Land in Pakistan: a Handbook (1998).

[5] MAHMOOD, K., Salinity tolerance in barley (*Hordeum vulgare* L.): Effects of varying NaCl, K+ / Na+ and $NaHCO_3$ levels on cultivars differing in tolerance, Pak. J. Bot. **43** (2011) 1651–1654.

[6] RAES, D., et al., Aquacrop the FAO crop model to simulate yield response to water: II. Main algorithms and software description, Agron. J. **101** (2009) 438–447.

[7] KHALILI, N., et al., Simulation of rainfed wheat yield using AquaCrop model, case study: Sisab Rainfed Researches Station, Northern Khorasan, Majallah-i āb va Khāk **28** (2015) 9030.

[8] ARAYA, A., et al., Test of AquaCrop model in simulating biomass and yield of water deficient and irrigated barley (*Hordeum vulgare*). Agric. Water Manage. **97** (2010) 1838–1846.

[9] SILVESTRO, P., et al., Estimating wheat yield in China at the field and district scale from the assimilation of satellite data into the Aquacrop and simple algorithm for yield (SAFY) models, Remote Sens. **9** (2017) 509.

[10] XU, J., et al., Modeling rice development and field water balance using AquaCrop model under drying-wetting cycle condition in eastern China, Agric. Water Manage. **213** (2019) 289–297.

[11] GARCIA-VILA, M., et al., Deficit irrigation optimization of cotton with AquaCrop, Agron. J. **101** (2009) 477–487.

[12] SALEMI, H.M.A., et al., Application of AquaCrop model in deficit irrigation management of winter wheat in arid region, Afr. J. Agric. Res. **610** (2011) 2204–2215.

[13] KIM, D., KALUARACHCHI, J., Validating FAO AquaCrop using Landsat images and regional crop information. Agric. Water Manage. **149** (2015) 143–155.

[14] HSIAO, T.C., et al., AquaCrop—The FAO crop model to simulate yield response to water: III. Parameterization and testing for maize, Agron. J. **101** (2009) 448–459.

[15] WALLACH, D., GOFFINET, B., Mean squared error of prediction as a criterion for evaluating and comparing system models, Ecol. Model. **44** (1989) 299–306.

[16] LOAGUE, K., GREEN, R.E., Statistical and graphical methods for evaluating solute transport models: Overview and application, J. Contam. Hydrol. **7** (1991) 51–73.

[17] WILLMOTT, C.J., Some comments on the evaluation of model performance, Bull. Am. Meteorol. Soc. **63** (1982) 1309–1313.

[18] WILLMOTT, C.J., et al., Statistics for the evaluation and comparison of models. J. Geophys. Res. Oceans (1978–2012) **90** (1985) 8995–9005.

[19] JAMIESON, P.D., et al., A test of the computer simulation model ARCWHEAT1 on wheat crops grown in New Zealand, Field Crops Res. **27** (1991) 337–350.

8. SOIL WATER AND BULK ELECTRICAL CONDUCTIVITY SENSOR TECHNOLOGIES FOR IRRIGATION AND SALINITY MANAGEMENT

R.C. SCHWARTZ, S.R. EVETT
USDA Agricultural Research Service
Conservation and Production Research Laboratory
Bushland, Texas, USA

A. DOMÍNGUEZ, B.C. LÉLLIS, J.J. PARDO
Regional Center for Water Research (CREA)
Dept. Agriculture and Forestry Engineering
University of Castilla-La Mancha
Albacete, Spain

Abstract

Assessment of the soil water content, bulk electrical conductivity, and pore water electrical conductivity is critical in the evaluation and management of irrigation and leaching regimes for crop production in salt-affected soils. Soil water content sensing systems based on electromagnetic (EM) properties of water are problematic in salt-affected soils due to severe interference from the bulk electrical conductivity, which can vary greatly throughout an irrigation season and across a field. In these soils, capacitance-based EM measurements have been shown to be nearly useless whereas the neutron probe can provide accurate soil water sensing but is labor intensive and subject to regulations. We investigated several new technologies suitable for evaluation of field soil water contents including (i) time domain reflectometry (TDR) probes with pulse generation directly-coupled to the electrodes (ii) prototypes of profiling soil water sensors based on directly-coupled TDR and (iii) a cosmic ray neutron probe (CRNP) that senses background fast neutrons generated by cosmic rays as well as background thermal neutrons. Laboratory investigations of the directly coupled TDR probes demonstrated that they can estimate soil water contents with accuracies of ≤ 0.03 $m^3 m^{-3}$ at bulk electrical conductivities up to 2.5 to 3.0 dS m^{-1} in fine textured soils (clay ≤ 400 g kg^{-1}) with a soil specific calibration. In coarser textured soils, accurate estimation of soil water content using these sensors is feasible up to a bulk electrical conductivity of ~5 dS m^{-1}. The corresponding electrical conductivity of the pore water at saturation would range from 5 to 10 dS m^{-1}. Several prototypes of the profiling soil water sensor were designed, evaluated, and found to be satisfactory. However, the principal difficulty was achieving a structural design that could withstand the forces of installation while keeping manufacturing costs reasonable. The CRNP was evaluated during two seasons and found to respond positively to elevated near-surface atmospheric humidity and be sensitive only to water within a shallow soil depth (<0.3 m). Consequently, the CRNP data would have little relevance for irrigation management for the field crops commonly grown in the Southern Great Plains. Field evaluations of arrays of EM sensors deployed at multiple depths demonstrated that sensed changes in stored profile water could resolve daily changes in evapotranspiration (ET) and correlated strongly with changes in storage determined with the neutron probe. This indicates the possibility that properly deployed EM sensors of the types used here could provide change in storage data accurate enough to determine ET from the soil water balance.

8.1. INTRODUCTION

Existing in-situ soil water content sensing systems based on electromagnetic (EM) properties of water are problematic in salt-affected soils due to severe interference from the bulk or apparent electrical conductivity (EC), which can vary greatly throughout an irrigation season and across a field. In particular, the systems based on capacitance measurements have been shown to be nearly useless in such soils [1–3]. At the same time, it is important to be able to assess the soil water content, bulk electrical conductivity, and pore water electrical conductivity in order to effectively manage irrigation and leaching regimes and to study effects of irrigation management and water quality on crop production. The neutron probe is capable of accurate water content sensing in salt-affected soils but has the disadvantages of (i) being labor intensive, (ii) not able to be left unattended in the field, (iii) subject to onerous regulations and (iv) unable to sense salinity. There are, however, two new technologies that are promising. One is the profiling soil water sensor or waveguide-on-access-tube (WOAT) system based on time domain reflectometry (TDR) principles [4]. This system may be less sensitive to interference from soil bulk EC than are conventional TDR systems, and it makes accurate measurements of both soil water content and bulk EC from the soil surface to user-chosen depths exceeding 2 m. The other technology is the Cosmic Ray Neutron Probe (CRNP) which is a method for detecting soil water content by sensing fast neutrons generated by cosmic rays and also sensing the thermal neutrons resulting from collisions with hydrogen [5]. Because it is based on neutron detection, the CRNP is relatively immune to salinity effects. It responds to the soil water content in the surface layers and to the near-surface atmospheric humidity and vegetation water content over a large area (radius of approximately 165 m) [6].

The profiling EM soil water sensor, while carefully evaluated [7–11], is a newly introduced system that requires design improvements to facilitate manufacturability and reduce cost as well as testing for irrigation and salinity management. The direct-coupled TDR circuits developed by Acclima Inc.[4] were concurrently being developed for both the profiling soil water sensor and for individual probes similar to conventional TDR technology. Although with pulse generation and waveform capture in the probe head and directly coupled to the waveguide electrodes. The quality and interpretability of TDR waveforms acquired from both the profiling and stand-alone TDR soil water sensors, especially in lossy media, is a key consideration for their accuracy in a range of soils and their usefulness in assessing soil water balance. The CRNP has a limited effective measurement depth that can change with soil and environmental conditions, which potentially confounds its usefulness for irrigation management. The objectives of this research were to (i) develop and further evaluate the WOAT for soil water monitoring in irrigation management (ii) evaluate individual TDR and other sensors in the laboratory and field for use in soil water and bulk EC monitoring with some consideration of the useful range in salt affected soils and (iii) evaluate the CRNP in assessing field soil water balance in an agricultural setting with irrigation.

[4] The use of trade, firm, or corporation names in this article is for the information and convenience of the reader. Such use does not constitute an official endorsement or approval by the United States Department of Agriculture or the Agricultural Research Service of any product or service to the exclusion of others that may be suitable. It also does not imply any intention to infringe proprietary rights, nor should it be construed as an endorsement or recommendation on the part of the IAEA.

8.2. MATERIALS AND METHODS

8.2.1. Profiling soil water sensor

The profiling soil water sensor that is being developed by Acclima Inc. in collaboration with USDA-ARS Scientists at Bushland, Texas, initially consisted of a tube with a series of 0.20-m long electrodes mounted longitudinally on the exterior surface and corresponding electronic circuitry for acquiring time domain reflectometry (TDR) waveforms for the determination of soil water content and bulk electrical conductivity. A patent for the apparatus [4] was granted on 3 Feb 2015. These prototypes consist of a tube of varying length with electrodes and circuitry for the acquisition of individual TDR waveforms at 0.3-m depth increments, oftentimes with a pair of modules for every depth increment on opposite sides of the tube (Fig. 8.1). The unit is controlled by an SDI-12 data recorder wired to the tube head, and there are plans to incorporate access via wireless communications. The electronic circuitry, consisting of a pulse generator and voltage receiver for capturing waveforms, and the associated firmware for evaluating travel time, water content and bulk electrical conductivity were similar to circuitry later developed for the TDR-315 and TDR-315L standalone TDR probes (described below). The principal challenge remaining has been achieving a structural design associated with the mounting of the transmission rods and embedding of electronics that can withstand the forces of installation while keeping manufacturing costs reasonable.

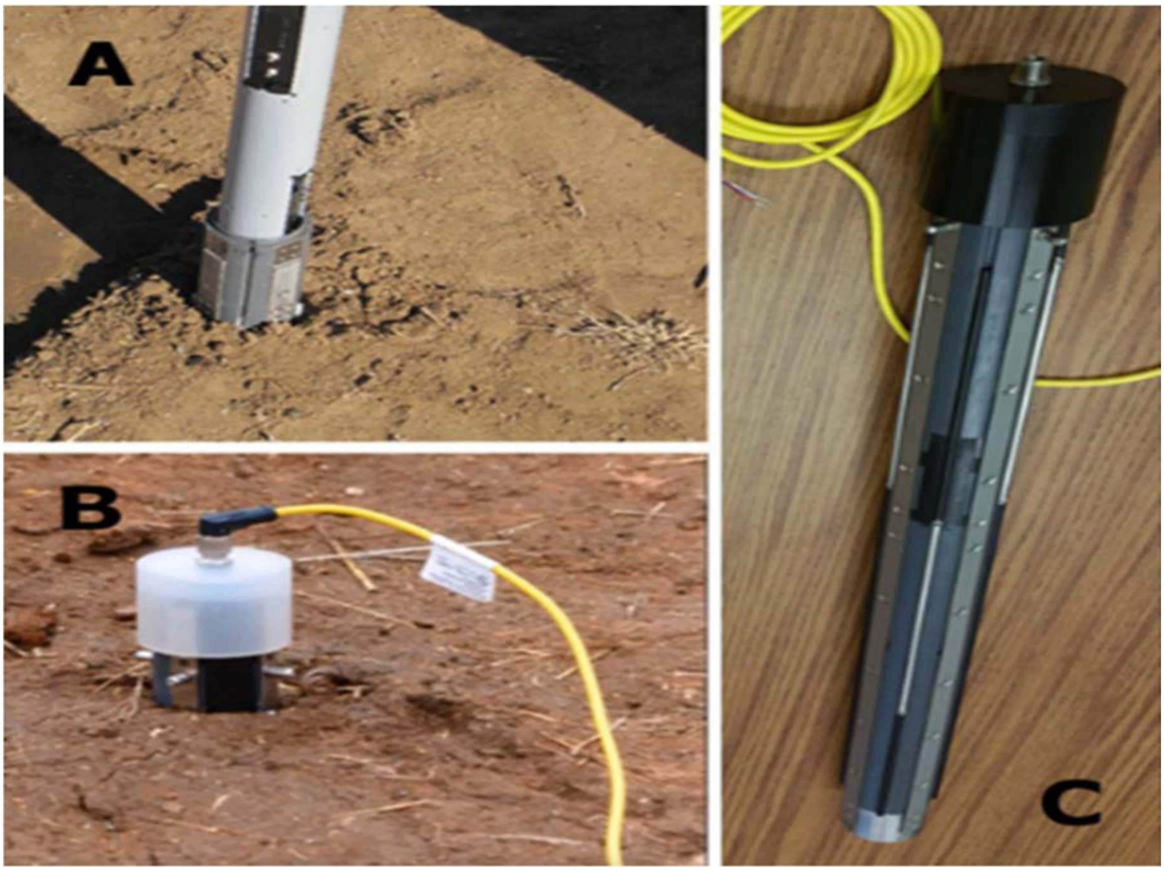

FIG. 8.1. Prototypes profiling soil water sensors included (A) one evaluated in January 2015 showing the TDR circuits being inserted into the body installed into the soil, another prototype (B) installed into the soil in September 2015 and the prototype (C) used for laboratory investigations.

On 15 January 2015, a prototype WOAT was installed in Bushland, Texas, to evaluate the structural design (Fig. 8.1A). This prototype consisted of a 1.2 m exterior tube installed by auguring within and a separate and removable core consisting of 12 TDR modules inserted into the exterior tube after installation. A field test of the second WOAT prototype with Acclima Inc. was carried out in September 2015 at Bushland, Texas. The WOAT (total length = 1.5 m) consisted of six 0.20-m segments, each with a single TDR circuit and rods. In contrast to the previous prototype, the TDR circuits were mounted directly into the body of the WOAT and potted in epoxy (Fig. 8.1B). The unit was installed using a hydraulic push probe mounted on a tractor. The WOAT was incrementally pushed into the soil after augering within the tube each time to remove excess soil at the bottom. The WOAT was removed using the hydraulics of the push probe and reinstalled using a gasoline powered T-post driver again while augering within the tube. After each installation process, the TDR circuits were tested.

A 0.40-m WOAT prototype similar to the field version but modified to accommodate two TDR units per 0.20-m depth, was also evaluated in the laboratory in January 2016. We note that, unlike TDR-315 probes, measured travel time with the profiling probe depends not only on the soil permittivity but also the permittivity of a portion of the plastic body to which the electrodes are attached. A specialized approach is therefore required for calibrations that remove the effects of the probe body. In this prototype, four stainless steel straps run along the length of the probe to fasten individual 0.20-m units together and also serve as ground rods (Fig. 8.1C). The WOAT was evaluated in a cylindrical test chamber that isolated the two 0.2-m segments from the lower portion so that mass changes in the soil volume would only be reflected in the depth increments where water content (i.e. travel time) was being measured.

8.2.2. Directly coupled time domain reflectometry evaluations

The Acclima TDR-315 is a standalone digital TDR sensor with all electronics required for pulse generation and waveform acquisition embedded in the probe handle. We evaluated this sensor in early 2015 prior to it being commercially available in June 2015. Operationally, a step function triggered by a timing generator launches a series of step pulses down a 0.15 m transmission line and samples the reflections to construct a digitized waveform consisting of amplitudes at successive time increments. A voltage comparator is used to digitize the amplitude of the analog signal compared with reference amplitude at a given time offset. The sensors employ a ~3.5 GHz step pulse with a 10 – 90% rise time of 100 ps (20 – 80% rise time of 64 ps). In comparison, the Tektronix 1502C cable tester typically used for conventional TDR measurements has a 1.75 GHz bandwidth with a 10 – 90% rise time of 200 ps. Because conventional TDR uses interconnects, cables, and multiplexers to transmit the pulse to the transmission rods of the probe, the effective bandwidth of the transmitted and reflected pulses is typically less than 1.0 GHz [12]. Bulk electrical conductivity (σ_a) can dominate the low frequency dielectric loss spectrum in soils, causing changes in the real permittivity and errors in estimated water content. Maintaining a bandwidth of greater than 1.0 GHz is necessary to minimize the bulk EC dependency of apparent permittivity important for accurate water content measurements in salt affected soils [3].

In the spring of 2015, 10 prototype TDR-315 sensors provided by Acclima Inc. were evaluated and compared with conventional TDR. The TDR-315 sensors consisted of a planar three-conductor transmission line with rod diameters of 3.2 mm, an outer rod separation distance of 38 mm, and were approximately 150 mm in length. The TDR-315 sensors were compared with two conventional TDR probes (each with a 8.5-m low-loss coaxial cable), with rod diameters of 3.2 mm, an outer rod separation distance of 60 mm, and a length of 150 mm. Waveforms were acquired from conventional TDR probes using a cable tester (model 1502C, Tektronix, Beaverton, OR). A coaxial cable length of 8.5 m was used in this study because it more properly represented the attenuated signal used to acquire travel times for estimation of soil water contents in the field than would an arbitrarily short cable.

The TDR-315 sensors were calibrated for apparent permittivity (K_a) using waveforms acquired at 20 ps intervals in air and deionized water. Conventional TDR was also calibrated in the same manner using 251-point waveforms in air and water (13.5 and 53.4 ps intervals, respectively). Amplitudes, V, acquired from the TDR-315 were converted to reflection coefficients, ρ as

$$\rho = \frac{2 \cdot V - V_0}{V_0}$$

where V_0 is the measured amplitude at long times (20 ns) in air (open circuit). Short circuit measurements with the TDR-315 invariably yielded an amplitude of zero at long times.

Water content calibrations of the Ap horizon (0 – 0.15 m) of the Pullman clay loam were carried out for six TDR-315 probes and two conventional TDR probes. Packed columns (0.101 cm inside diameter by 0.20 m long Schedule 40 rigid polyvinyl chloride) were prepared using soil sieved through a 12.7-mm by 12.7-mm mesh screen. A range of volumetric water contents were achieved by combining air-dry soil with different ratios of deionized water, thoroughly mixing to achieve uniformity, and packing the mixture into the columns in 20-mm increments. Four replicate waveforms were acquired at room temperature (20°C), a refrigerator (6°C), and in a water-jacketed incubator (40°C) after permitting the columns to equilibrate for one day at each temperature regime. The refractive mixing model [13] was fitted to measured apparent permittivity using measured volumetric water contents.

Bulk EC calibrations were completed for two TDR-315 sensors and conventional TDR with the σ_a estimated using the longtime amplitudes at 3 µs and based on the Giese and Tiemann thin section approach [14]. Calibrations were evaluated using $CaCl_2$ solutions with conductivities ranging from 1 µS cm^{-1} (deionized water) to 7.3 dS m^{-1}. Electrical conductivity of solutions was measured using a bench top meter with conductivity reported at ambient temperatures (20°C ± 2°C). Bulk electrical conductivity (σ_a) using the conventional TDR probes was determined [15] with open (air) and short circuit measurements to evaluate the scaled reflection coefficient ρ_{scale} at 3 µs.

We also examined the dependence of measured apparent permittivity (K_a) on σ_a in soil using both conventional TDR and the TDR-315 during near saturated solute displacement experiments. Sensors were installed in columns packed with Pullman clay loam. Displacement experiments were completed by first equilibrating columns with 0.25 dS m^{-1} $CaCl_2$, introducing a step pulse of 7.3 dS m^{-1} $CaCl_2$ and, after equilibration, displacing the resident solution with 0.25 dS m^{-1} $CaCl_2$.

In all of the experimental evaluations, waveforms acquired from the TDR-315 probes and Tektronix 1502C using conventional TDR were evaluated for travel time using the AWIGF algorithm [16]. Travel time estimated using AWIGF was also compared with the firmware determined travel time. Further details of the methodologies of this study are described in [17].

The electronics for measuring soil water content (i.e. travel time) were redesigned by Acclima Inc. to use lower cost silicon chips for the step-pulse generator instead of the silicongermanium technology used by the TDR-315. These sensors (TDR-315L) have approximately a 20% lower power requirement than their predecessors. The new probe has a 10 – 90% rise time of 360 ps that yields an approximate bandwidth of 1 GHz. In February through April 2016, the TDR-315L was evaluated in air, water, and Pullman soil (40% clay) saturated with 1 and 7 dS m^{-1} $CaCl_2$ solutions and compared with the TDR-315 sensors. Methodologies were similar to that reported for the TDR315.

8.2.3. Cosmic ray neutron probe evaluation

A cosmic ray neutron probe (CRNP) was installed at the Bushland USDA-ARS Laboratory in 2012 at the northeast (NE) large weighing lysimeter (35° 11' N, 102° 06' W, 1170 m elevation above MSL), which is centered in a 4.4 ha, 210 m × 210 m field. The soil is a Pullman silty clay loam (fine, mixed, superactive, thermic Torrertic Paleustoll). The field is subsurface drip irrigated with drip lateral lines buried at 0.30 to 0.34 m depth with a 1.52 m lateral spacing that placed a drip lateral in the center of every other interrow. Drip laterals and row crops were placed using GPS guided tractors with an average accuracy of ± 2 cm. The field slope is less than 0.3%. The large (3 m × 3 m × 2.4-m deep) precision weighing lysimeter is at the field's center. It was calibrated using masses traceable to NIST (RMSE of calibration = 0.04 mm equivalent water depth). Lysimeter ET and precipitation amounts were calculated [18,19].

In 2013 a maize (*Zea mays* L.) crop was planted on 22-23 May and subsurface drip irrigation (SDI) was applied to meet crop water requirements not otherwise met by precipitation. Plant height, leaf area index (LAI) and above-ground biomass (wet and dried) were measured periodically in order to assess the effect on the CRNP of green biomass accumulation over time and eventual senescence of the crop. Microclimatological measurements were made at the lysimeter and at an immediately adjacent research weather station over mowed grass. Field water contents and soil profile water storage were determined by neutron probe (NP) weekly during the crop growing season using eight NP access tubes to 2.4-m depth with measurements in increments of 0.2 m beginning at 0.1-m depth using a depth control stand to ensure accuracy at the 0.1-m depth. The eight access tubes were arranged in a grid around the weighing lysimeter as illustrated in Fig. 8.2. Irrigation amounts were measured using a total flow meter for the entire field and individual flow meters for each of the 20 SDI zones.

A wireless sensor network consisting of 40 CS655 sensors (Campbell Scientific Inc., Logan, Utah) was installed, with five sensors adjacent to each NP access tube. At each access tube, sensors were installed horizontally in the side of a pit at depths of 0.05, 0.10, 0.15, 0.20 and 0.25 m in order to monitor the rise of water from the SDI system, the infiltration of water from precipitation, and to monitor the drying of the surface layers of the soil after irrigation and precipitation events. The sensors were inserted into the soil in a direction perpendicular to the crop row so that the electrodes of each sensor were centered under the row (0.38 m horizontal offset from the drip tape). Data recorded from the CS655 sensors were the soil apparent permittivity, bulk electrical conductivity and temperature. Apparent permittivity was corrected using the linear relationship between CS655 permittivity values and those determined by conventional TDR [20], and corrected values were then used to estimate soil water content (RMSE = 0.01 m^3 m^{-3}, and r^2 = 0.973) using the Pullman Ap horizon time domain reflectometer (TDR) calibration [21]. Depth weighted mean profile water content in the 0-0.30 m deep profile at hourly intervals was calculated from the five CS655 sensors at each NP location. CRNP soil water content (θ_{CRNP}, m^3 m^{-3}) data were acquired on an hourly basis and were smoothed using a 12-hour boxcar filter. Filtered water content data from the CRNP were compared with data from the neutron probes, wireless CS655 network, and lysimeter. The CRNP installed at the weighing lysimeter location sensed the entire 4.4-ha field and likely beyond into adjacent irrigated fields, although sensitivity beyond the field perimeter was likely much reduced [6].

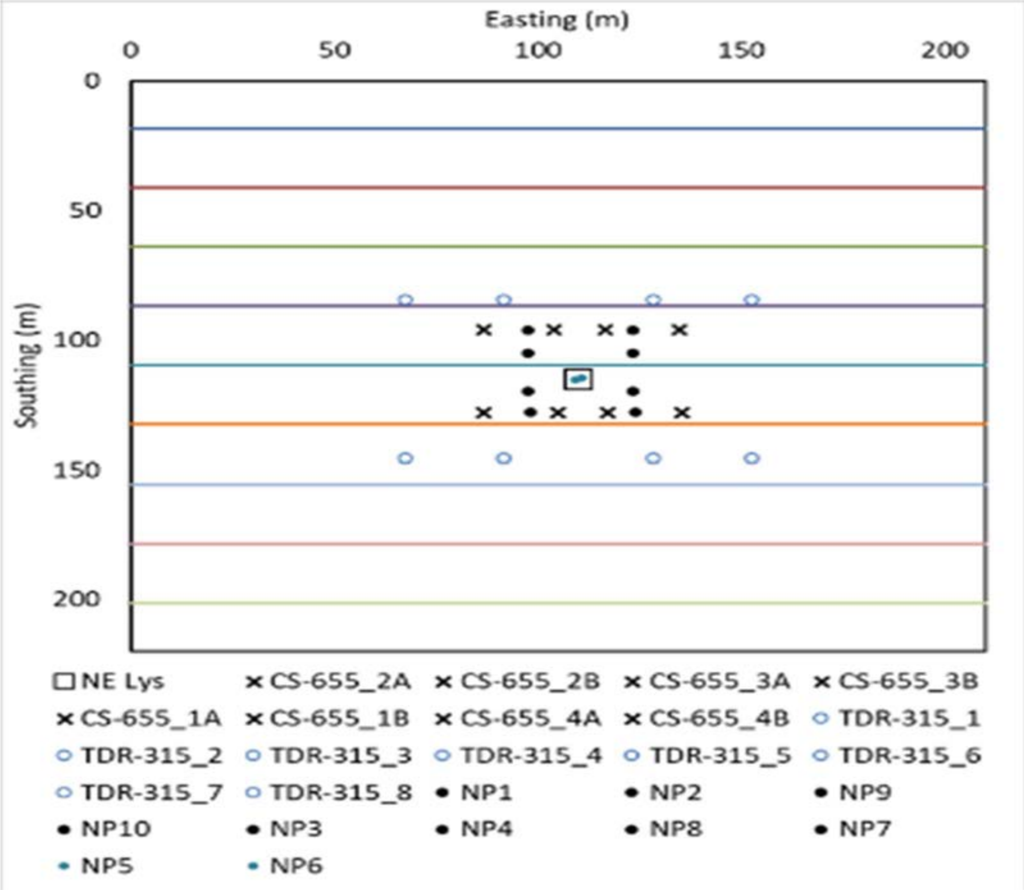

FIG. 8.2. Locations where electro-magnetic (EM) soil water sensors were installed in the lysimeter field. The cosmic ray neutron probe was located 2 m east of the lysimeter. Eight locations had CS655 sensors installed, six at each location in; and eight locations had TDR-315L sensors installed only in 2017, six at each location. Depths of installation were 0.05, 0.10, 0.15, 0.20 and 0.25 m in 2013 and 0.06, 0.20, 0.35, 0.50, 0.70 and 1.00 m in 2017. Eight neutron probe (NP) access tubes were installed in the field and read periodically (usually weekly) at center depths of 0.10 to 2.30 m in 0.20-m increments. Two NP access tubes were installed in the lysimeter and read in the same depth increments to 1.9 m.

In 2017, soybeans (*Glycine max*), were planted in the field surrounding the CRNP, but a hailstorm on 2 July (DOY 183) destroyed the young soybean crop, and the field was plowed to terminate the remaining crop. Thereafter, the field remained in fallow for the duration of the summer. During this year, EM sensors were installed at 16 locations in the field surrounding the lysimeter, with six sensors at each location (Fig. 8.2). Half the sensors were model CS655 (Campbell Scientific, Inc., Logan, Utah) and half were model TDR-315L (Acclima Inc., Meridian, Idaho). At each location, sensors were installed at depths of 0.06, 0.20, 0.35, 0.50, 0.70 and 1.00 m. The top two sensors were installed horizontally whereas the bottom four sensors were installed vertically so that the installation depth was halfway along the length of the electrodes. The deepest three sensors were installed into the bottoms of individual auger holes and re-packed using the removed soil. Sensors were installed midway between the drip lateral and the crop row, that is, approximately 0.19 m from the drip lateral and 0.19 m from the crop row. Sensors were connected to dataloggers (model 206X, Campbell Scientific, Inc., Logan, Utah) and readings of apparent permittivity, soil temperature and bulk electrical conductivity were made every hour. The TDR-315L EM sensor arrays began recording data on day of year (DOY) 170 in 2017, with the CS655 arrays starting nine days later, and both continued recording until DOY 349 when the dataloggers were removed from the field. Soil water contents were based on calibrations described for the 2013 season but with a change in the intercept for both horizons to the value of –0.176 $m^3 m^{-3}$ obtained for a range of soils [22].

8.2.4. Field evaluation of soil water sensors

An estimation of soil water depletion and pore water electrical conductivity is necessary to evaluate crop response to water and salinity stress, schedule irrigations, and forecast optimal water distribution to irrigated crops. These assessments are being made within the framework of MOPECO, an economic optimization model for irrigation water management [23]. The principal objectives of this evaluation are to (i) compare sensor technologies, (ii) evaluate soil profile changes in water content resulting from irrigations and daily evapotranspiration.

Experimental field plots were established and planted to purple garlic (*Allium sativum*) to evaluate the effect of deficit irrigation strategies on soil water depletion, crop development, and yield. The field plots were located near Aguas Nuevas, Albacete, Spain, and were equipped with mini-lysimeters and a surface drip irrigation system. The soils in the experimental field plots are Petrocalcic Calcixerepts with a petrocalic horizon at approximately 0.50 m and a clay loam texture. Eighteen experimental plots in a randomized complete block design were established to examine five irrigation treatments in which the crop received a volume of irrigation water equal to at 70, 80, 90, and 100 percent of typical crop irrigation requirements in the area, and full irrigation as the control, with irrigation scheduling determined using MOPECO [24]. Lateral drip lines with a 0.5 m emitter spacing were placed between each of the rows, and flow meters recorded applied irrigation to each of the plot replicates. All irrigations were completed during nighttime. Further details of the study can be found in [25].

Soil water sensors (TDR-315; Acclima Inc., Meridian, Idaho) were installed on March 2017 during garlic dormancy at 0.1, 0.2, 0.3, and 0.4 m below the surface with probes oriented perpendicular to the rows and between the dripline and the rows. Two sensor arrays were installed in one of the plot replicates of the 70, 80, 90, and 100% irrigation treatments. Besides the TDR-315, WaterMark (Irrometer, Inc., Riverside, California) granular matrix sensors (0.2 and 0.4 m depths; 8-hour measurement frequency), MPS6 (Meter Group, Inc., Pullman, Washintton) granular matrix sensors (0.2 and 0.4 m depths; 1-hour measurement frequency), and the PR2/4 (Delta-T Devices, Cambridge, UK) profiling capacitance sensor (0.1, 0.2, 0.3, and 0.4 m depths; 1-hour measurement frequency) were also installed in the plots. Within each of the plot replicates, one profile each of the WaterMark, MPS6, and PR2/4 were installed all in close proximity to one another and the two TDR-315 arrays (<5 m). The factory calibration was used to estimate soil water content using apparent permittivity measurements for the TDR-315. Water contents estimated using the TDR-315 and the PR2/4 sensors were integrated with depth to obtain profile water contents to 0.45 m depth. Applied irrigation and rainfall depths were estimated using TDR-315-measured soil water contents by evaluating change in storage (0-0.45 m) and assuming a soil water content at the surface of 0.09 $m^3 m^{-3}$ prior to wetting. This water content represents approximately the mean lower limit of water contents recorded at 0.1 m among all plots during the study.

8.3. RESULTS AND DISCUSSION

8.3.1. Profiling soil water sensor

The installation of the initial prototype of profiling soil water sensor in January 2015 was successful and high-quality waveforms were acquired from the TDR circuits after installation. However, the manufacturability of this prototype was prohibitively costly for widespread use. The installation of the prototype in September 2015 using a hydraulic push probe and the T-post driver was successful. After each installation process, the TDR circuitries were tested and found to be operational. Waveforms obtained from this installed prototype (Fig. 8.3) were high quality and interpretable for travel time estimation.

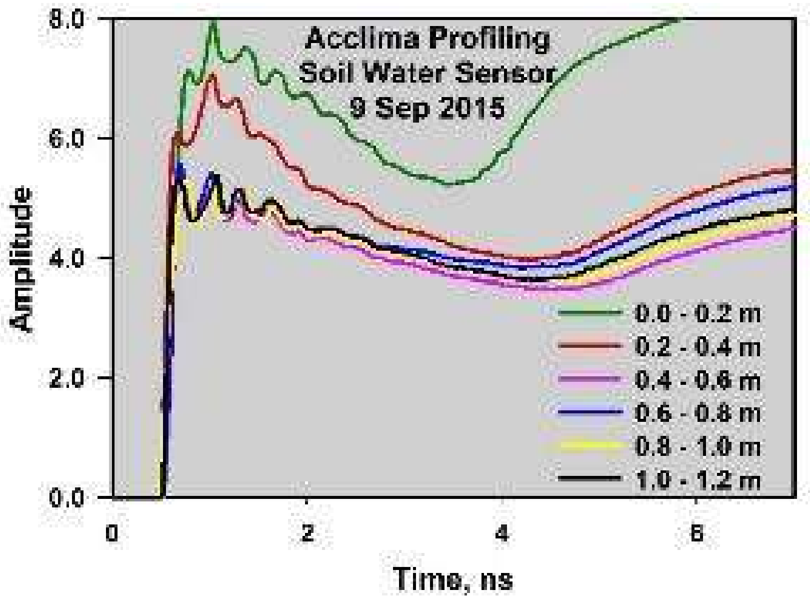

FIG. 8.3. Waveforms acquired from the Acclima profiling soil water sensor prototype installed in September 2015 in Bushland, Texas for each of the TDR circuits that sampled the six depth increments in the soil profile

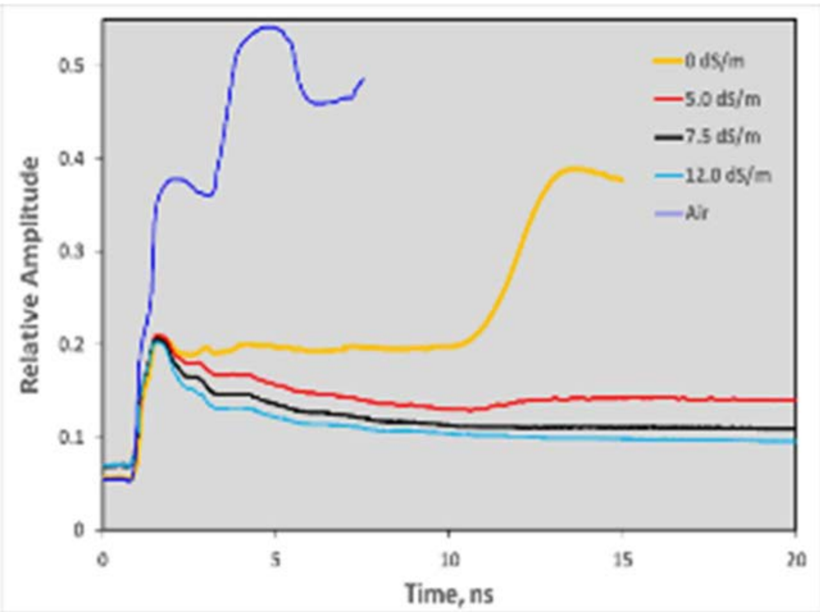

FIG. 8.4. Waveforms of the one of the TDR circuits of the profiling soil water sensor acquired in air and water for range of electrical conductivities.

Each individual TDR unit of the 0.40-m WOAT prototype yielded similar waveforms and travel times in water, air, and $CaCl_2$ solution up to 15 dS m^{-1}. Waveform interpretation for travel time estimation was easily evaluated using AWIGF [16] and stable up to an electrical conductivity of 5 dS m^{-1} above which attenuation made it difficult to find the reflection at the end of each electrode triplet (Fig. 8.4). Signal to noise ratios were lower in these units compared with the TDR-315 but significantly improved compared with earlier circuit designs [10]. Calibration of this probe in air, water, and ethylene glycol and further testing in soils was planned but not pursued because water began to leak through into the surface below the stainless-steel straps and thence into the interior of the tube. We note that although the water entry did not affect the circuitry, it does influence the measured travel time because water inside the cylinder is within the electromagnetic field associated with permittivity measurements.

Because of the design problems associated with maintaining a watertight seal during installation of the profiling soil water sensor, we were unable to evaluate the sensor under field conditions as planned. In addition, manufacturing costs of these prototypes were still too high for a commercially acceptable product. Acclima Inc. has been involved in redesign efforts during the past two years to address these problems. The current design consists of an access tube made of extruded plastic with channels for the TDR electronics formed into the wall of the tube.

8.3.2. Directly coupled time domain reflectometry evaluations

Waveforms in air and water for TDR-315 sensors are similar to conventional TDR (not shown) except that t_1, the time at which the signal enters the media, is offset from the time of the pulse launch t_{x1} rather than the transition between the coaxial cable and the probe handle. Electrical length L_e and offset t_c for permittivity calibrations of the TDR-315 and conventional TDR are remarkably similar (see [17]). Variations in calibrated L_e and t_c among TDR-315 probes result from small variations in the physical rod length and the timing circuit but are dealt with during factory calibration of each individual sensor.

The fitted water content calibration derived from AWIGF K_a estimates using the TDR-315 corresponded closely to the conventional TDR calibration also using AWIGF to evaluate travel time (Fig. 8.5). The firmware calculated K_a averaged 95% of the TDR-315 AWIGF calculated K_a and the two estimates were closely correlated (r^2 = 0.997). Consequently, the water content calibration obtained from the firmware estimate of K_a was remarkably similar to the AWIGF derived calibrations (Fig. 8.5). The firmware water content calibration tended to underestimate soil water content and had a root mean square error of 0.0324 m^3 m^{-3} compared with 0.0173 to 0.020 m^3 m^{-3} obtained for the soil specific calibrations (Fig. 8.5).

Apparent permittivity measured using conventional TDR was sensitive to bulk EC, increasing from 32 to 40 after introduction of the 7.3 dS m^{-1} $CaCl_2$ step pulse (Fig 8.5). In contrast, K_a measured using the TDR-315 and evaluated using AWIGF was insensitive to bulk EC (Fig. 8.6). Both of the above AWIGF-derived estimates of K_a use the default method whereby t_2 is conditionally evaluated using the maximum of the second derivative [16]. Firmware estimates of K_a were slightly sensitive to bulk EC and were subject to reduced precision at $\sigma_a > 2$ dS m^{-1} (Fig. 6). Algorithms used for waveform interpretation can influence the sensitivity to EC of TDR permittivity and water content estimation [16, 26). We note that the firmware algorithm used to estimated t_2 has been modified since the initial commercial availability of the TDR315 in 2016.

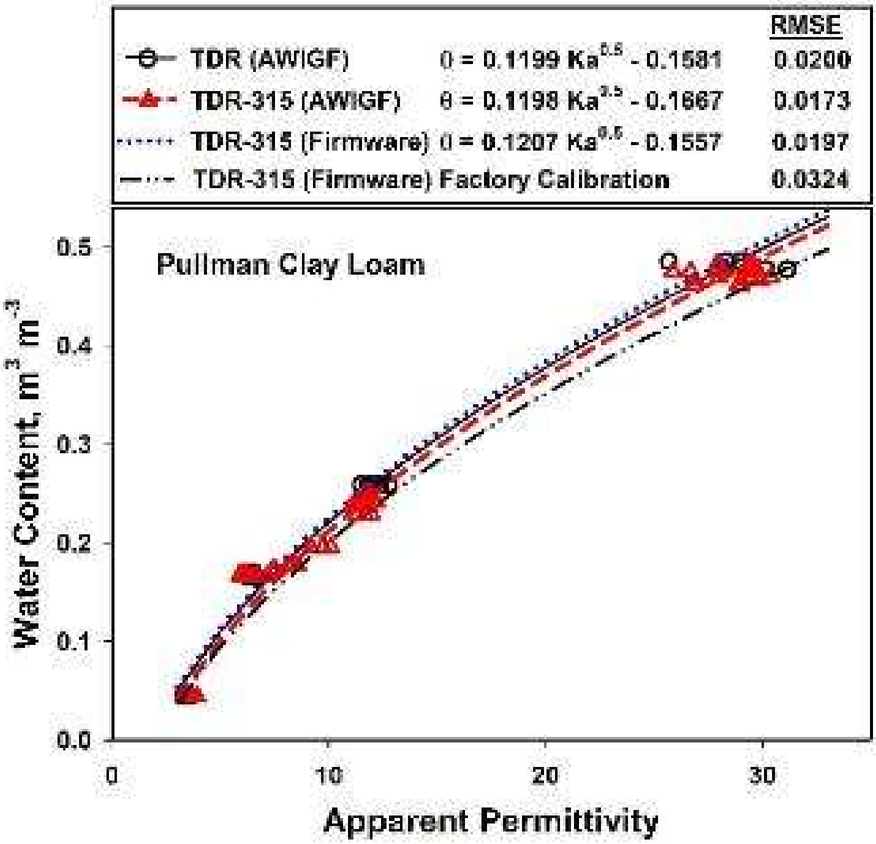

FIG. 8.5. Refractive mixing model soil water content calibrations of the Pullman clay loam (0.0 to 0.15 m) for conventional TDR and TDR-315 using AWIGF-estimated travel times and the calibration and the TDR-315 using firmware estimated apparent permittivity (K_a). Also shown is the Acclima factory soil water content calibration.

The cause of the insensitivity of the TDR-315 measured permittivity to bulk EC compared with conventional TDR is evident from the waveforms of these two sensors at a high bulk EC (2.8 dS m^{-1}). The slope of the reflection at the termination of the rods is significantly larger for the TDR-315 waveform compared with conventional TDR indicating that a greater proportion of the high frequency component has been preserved (Fig. 8.7). This signifies that water contents measured by the TDR-315 are less sensitive to salinity fluctuations compared with conventional TDR.

The electrical conductivity calibrations for both the TDR-315 and conventional TDR were linear with similar slopes, thus validating the thin-section approach [14] for using these sensors. Long time reflection coefficients evaluated from the 3 μs amplitudes reported by the firmware of the newer probes departed from a linear response at electrical conductivities greater than 3 dS m^{-1}. Initial firmware for the TDR-315 estimated electrical conductivity based on a long-time amplitude with the timing based on microprocessor cycles [17]. Because of the nonlinearity problems identified above, Acclima has incorporated a dual time base in all subsequent sensors so that long time amplitudes could be measured using a precise controller at 100 ns and independent of the travel time measurements.

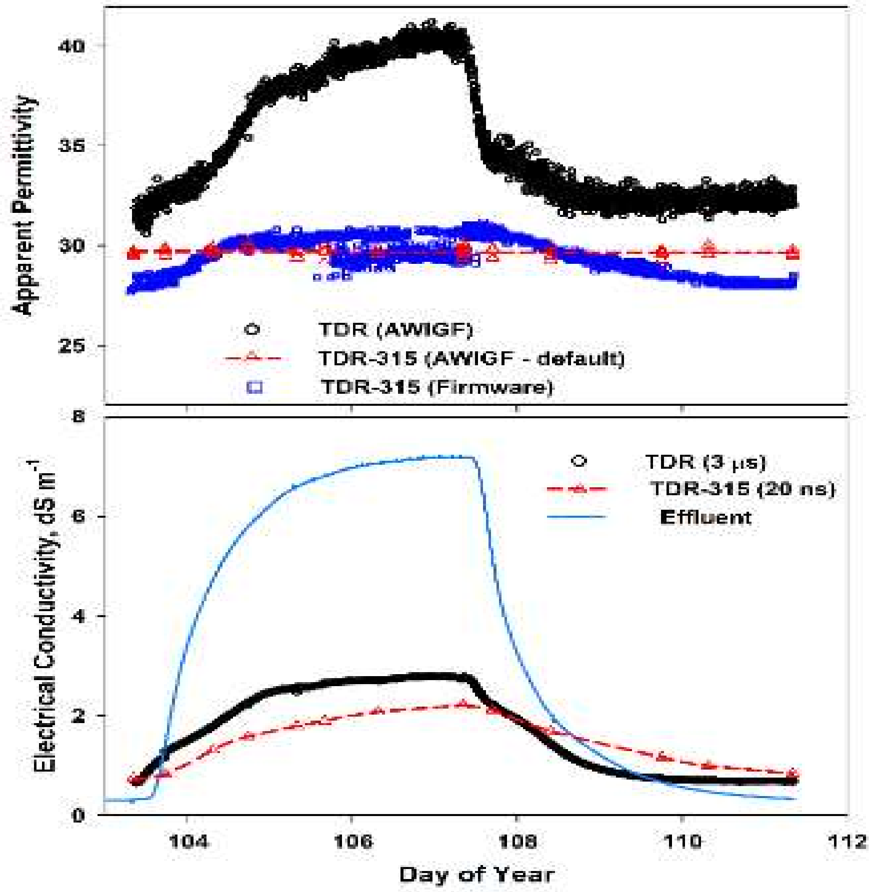

FIG. 8.6. Response of electrical conductivity and apparent permittivity during column displacement for conventional TDR and TDR-315 sensors in a Pullman clay loam. Apparent permittivities for the TDR-315 are plotted using the default AWIGF methodology to estimate the time at which the pulse arrives at the end of the transmission line. In addition, firmware-calculated apparent permittivities are also plotted. A lag in the TDR-315 response compared with conventional TDR is due to differing heights within the soil column.

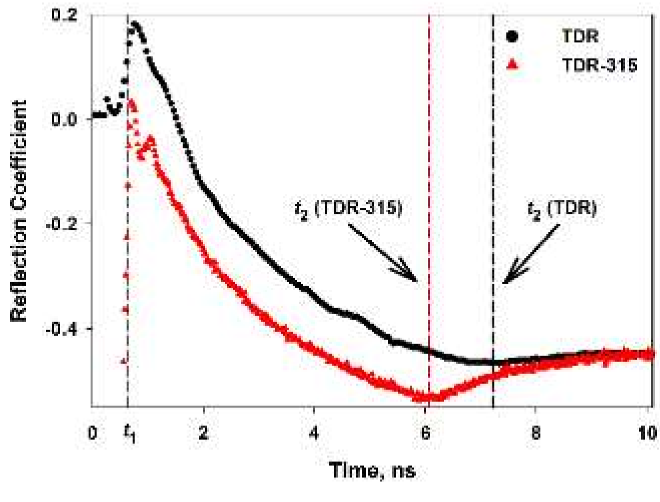

FIG. 8.7. Waveforms of conventional TDR and the TDR-315 at a bulk electrical conductivity (σ_a) of 2.8 dS m^{-1} and the AWIGF-evaluated time at which the pulse arrives at the end of the transmission line (t_2). The waveforms have been horizontally adjusted in time so that the time at which the step pulse enters the media (t_1) is identical.

A challenge in managing soil salinity under irrigated crop production is the estimation or measurement of the pore water electrical conductivity (σ_w). This quantity is required both in approximating the leaching fraction for the soil profile and estimating the conductivity of the saturated paste extract to evaluate yield response to salinity [27]. The TDR-315 measures the apparent bulk electrical conductivity (σ_a) of the soil, which can be used to approximate σ_w using the Hilhorst model [28] or others. Errors in estimated σ_w can be considerable (e.g. [29]) and may partly arise from the presence of significant bound water and surface conductance in high surface area clays and because all sensors measure apparent permittivity rather than a real permittivity. Using TDR-315 measurements obtained from the column displacement experiments for a near saturated Pullman clay loam, the Hilhorst model overestimated σ_w by 30% at a measured σ_w of 7 dS m^{-1}, with error increasing as σ_w declined. It is clear that a soil specific calibration across a range of water contents and salinities will be required to accurately assess changes in σ_w for this soil using TDR-315 measurements.

Despite the slower step pulse, interpretation of TDR-315L waveforms indicated its response was similar to that of the TDR-315 for the media tested. Because of an unavoidable impedance mismatch at low permittivities for the newer design, there is a discontinuity in waveform at about 1450 ps just after the launch of the signal (Fig. 8.8). This aberration, however, was found not to interfere with the detection of the end reflection in air or dry soil.

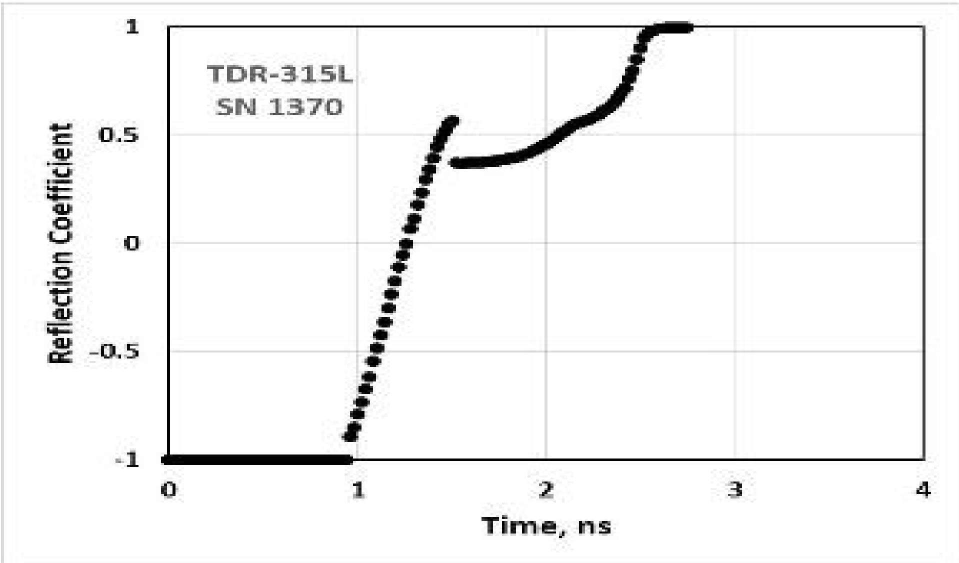

FIG. 8.8. Acquired waveform from the TDR-315L sensor in air showing the discontinuity caused by an impedance mismatch.

Accurate travel time measurements were obtained for both technologies in air and water up to and including 5 dS m^{-1} $CaCl_2$ solutions (Fig. 8.9). At 7 dS m^{-1} $CaCl_2$, attenuation of waveforms in both sensor technologies was too great to reliably evaluate the time associated with the reflection at the termination of the rods and, consequently, travel time. Waveforms acquired with both technologies in the Pullman soil saturated exhibited similar responses as the saturating solution increased from 1 to 7 dS m^{-1} $CaCl_2$ (Fig. 8.10). The scaled slopes of the rising limb of the reflection at the end of the rods (important for travel time evaluation) were similar over a range of electrical conductivities for the TDR-315L and the TDR-315. At high attenuation levels, the signal to noise ratios were smaller for the TDR-315L compared with the TDR-315. However, this was found not to influence the standard deviation of the permittivity measurements in water over a range of electrical conductivities less than or equal to 5 dS m^{-1}.

Because of slightly greater noise, greater smoothing was used for analysis of these TDR-315L waveforms using AWIGF. Both the TDR-315 and TDR-315L yielded accurate water content measurements (within 0.03 m^3 m^{-3}) using a previous calibration [17] in the saturated Pullman soil which had a maximum bulk EC of 3.3 dS m^{-1}.

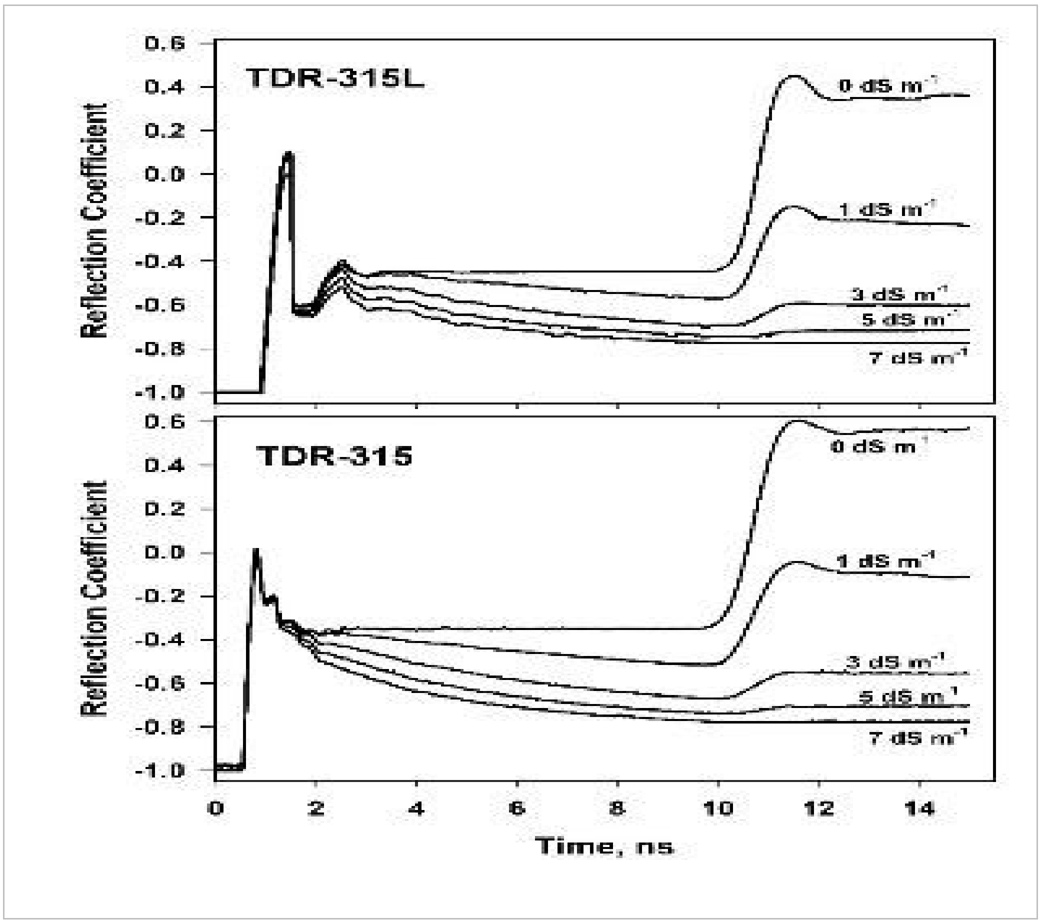

FIG. 8.9. Waveforms for the TDR-315 and TDR-315L sensors acquired in water for range of electrical conductivities.

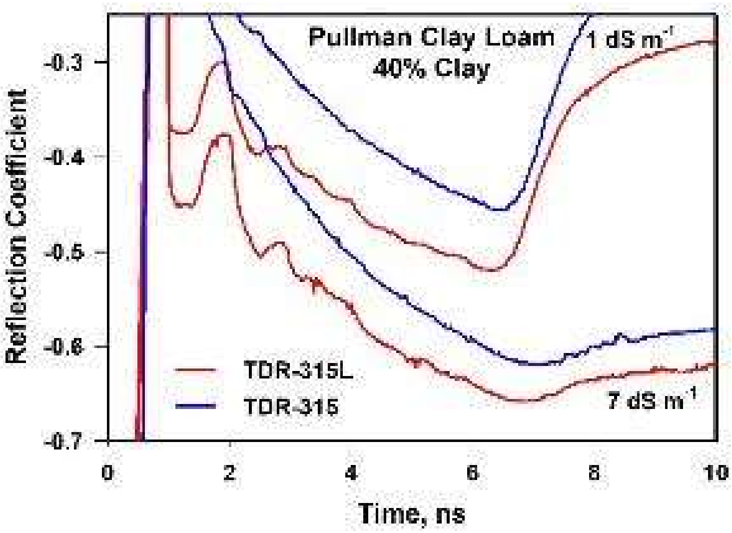

FIG. 8.10. Waveforms for the TDR-315 and TDR-315L sensors acquired in a Pullman clay loam soil saturated with 1 and 7 dS m-1 CaCl2 solutions. The waveforms have been horizontally adjusted in time so that the time at which the step pulse enters the media is identical.

8.3.3. Cosmic ray neutron probe evaluation

In 2013, leaf area index (LAI) of the maize exceeded 4 m^2 m^{-2} by 22 July (DOY 203), and the equivalent depth of water stored in the above ground biomass reached a maximum of 5 mm by 21 August 2013 (DOY 233). The crop was completely senesced by 27 Sept 2013 after which time the water content of biomass was practically zero. Data from the CS655 sensors (θ_{CS655}, m^3 m^{-3}) were recorded beginning on DOY 190 (9 July 2013) when field mean LAI was 3.0, so early comparison of CS655 and CRNP water contents were carried out when green biomass was present.

Trends in the CRNP water contents during the growing season were similar to the mean 0-0.30 m profile water contents reported by the CS655 sensor (Fig. 8.11). However, compared with mean CS655 profile water contents, CRNP-reported water contents were clearly biased by green biomass as evidenced by greater and lower values prior to and subsequent to senescence, respectively, with a clear crossover during the week of 27 Sept 2013 (Fig. 8.11).

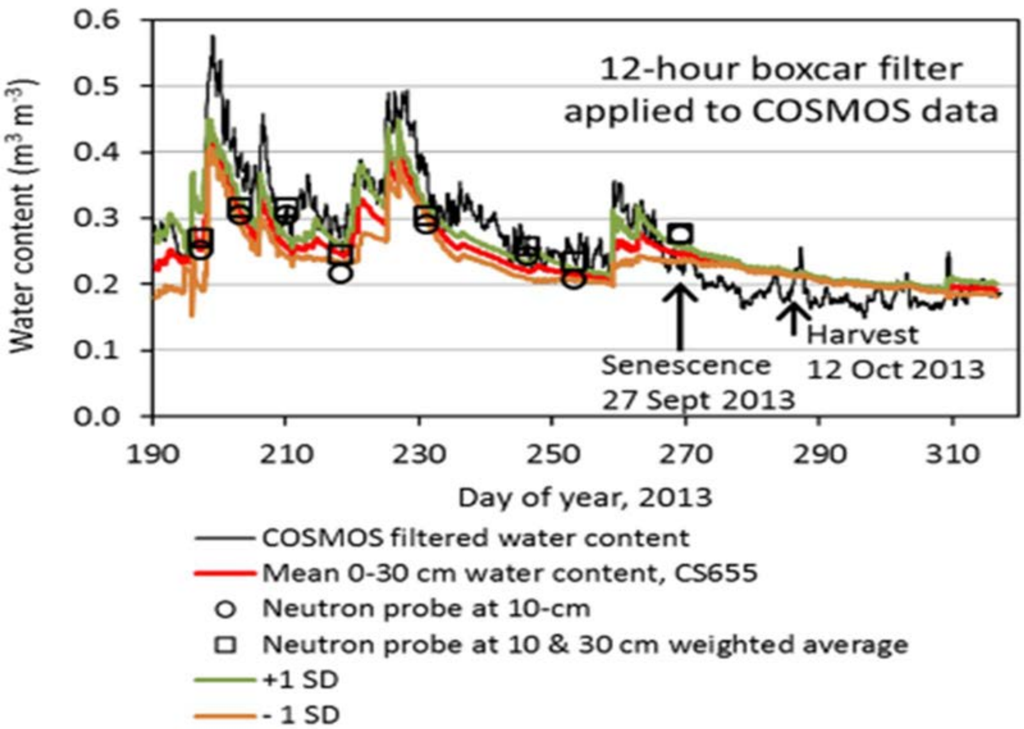

FIG. 8.11. Soil water content as reported by the CRNP (COSMOS) compared with the mean 0-0.30 m profile water content as sensed by the CS655 sensor network from day of year 190 when leaf area index was at 3.0 through day of year 317 when leaf area index was zero after senescence. Also plotted are the +/- 1 standard deviation of mean CS655 profile water content and the neutron probe reported water content for 0.10-m depth and the weighted average of 0.10 and 0.30-m depth neutron probe readings for the 0-0.30-m profile water content.

Despite being filtered, the CRNP-reported water contents were noisier than the CS655 data. The NP water contents generally were closer to the CS655 data except for DOY 210 and 231, both of which are unexplained. At senescence, the NP reported water content larger than that reported by either the CRNP or the CS655 sensors, likely due to rapid drying of the soil surface and the influence of deep soil water on the NP readings due to its increasing volume of sensing as soil dries.

The greater water content reported by the CRNP relative to that reported by the CS655 and NP sensors can also be explained as a sensitivity to the humidity of the air within the inter-canopy space or after precipitation events that humidify the air. For example, in Fig. 8.12A, the CRNP data appear to respond to the rainfall event, which causes an increase in lysimeter storage, but then further increase to a maximum of 20 mm more than that reported by the lysimeter. The largest increase in CRNP reported water storage occurred after the rainfall ended and was very likely due to humidification of the near-surface air due to rapid evaporation of water from the soil surface (Fig. 8.12B).

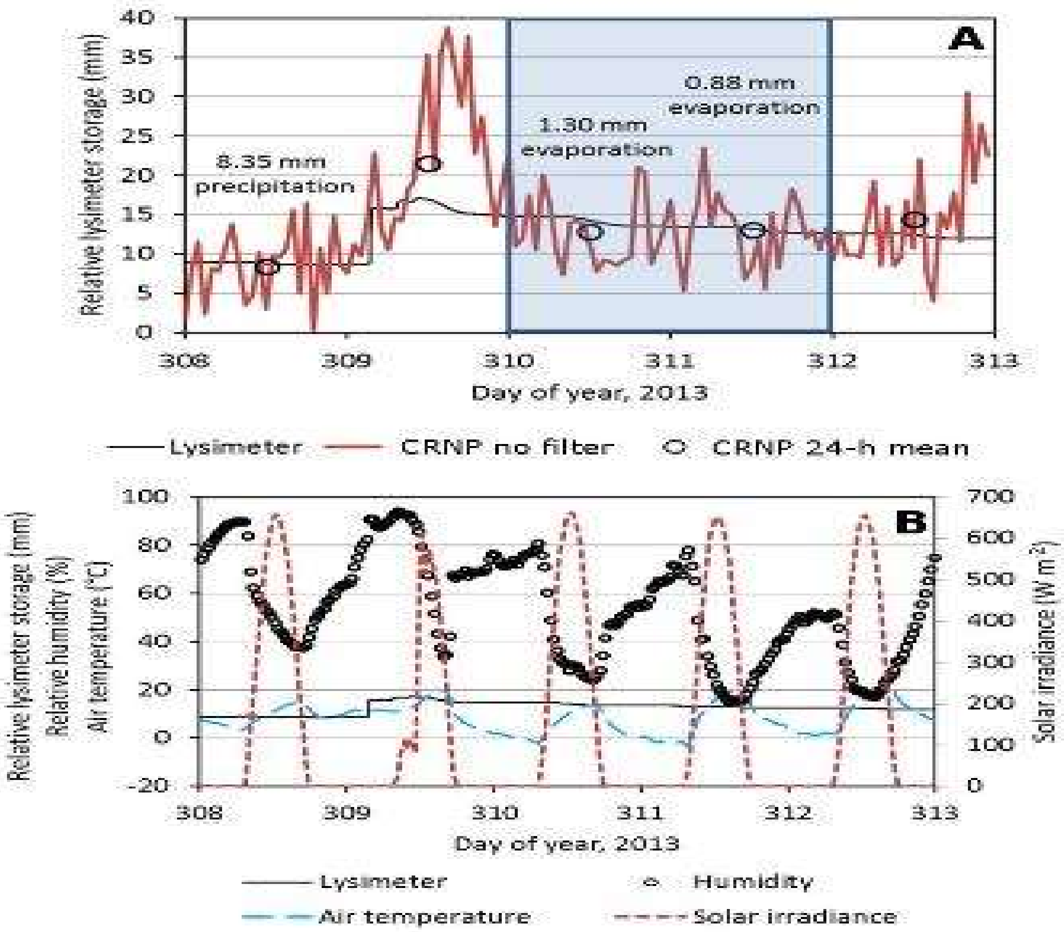

FIG. 8.12. (A) Comparison of the cosmic ray neutron probe (CRNP) reported water storage variation with relative water storage on the large weighing lysimeter before, during, and after an 8.4 mm precipitation event. Relative lysimeter storage was adjusted by a constant amount to match that from the CRNP before the precipitation event. Circles are 24-hour mean values from the CRNP system. (B) Relative humidity (%), air temperature (°C) and solar irradiance (W m^{-2}) during the event. Shown for reference is the lysimeter storage.

The CRNP water content data for the entire period (DOY 190-317) were well correlated with the mean 0-0.30 m profile water content sensed using the CS655 network, but with considerable bias (Fig. 8.13). The correlation was progressively reduced as the deeper CS655 data were progressively excluded from the data used to calculate profile water storage. These results indicate that the CRNP was sensitive to soil water content at depths between zero and 0.3 m. The lack of CS655 sensors below 0.30-m depth precluded investigating if sensitivity extended below that depth during this year.

In 2017, the combination of plentiful precipitation and lack of plant cover allowed the soil profile to become very wet (Fig. 8.14). Below 0.06 m depth, soil water contents remained near field capacity. The CRNP station reported a few faults after DOY 170 but began reporting more numerous faults on DOY 220. On DOY 272, faults became numerous, so CRNP data after DOY 271 were not used. Faults were associated with a power supply instability. Level 3 CRNP data were used in the initial analyses without site-specific calibration. In addition to the screening completed by the University of Arizona, CRNP data between DOY 170 and 272 were carefully screened for physically unrealistic values and those were excluded from analysis. CRNP data, filtered using an 11-h boxcar function, were obviously correlated to precipitation events that increased surface water content as sensed by the EM sensors (Fig. 8.15).

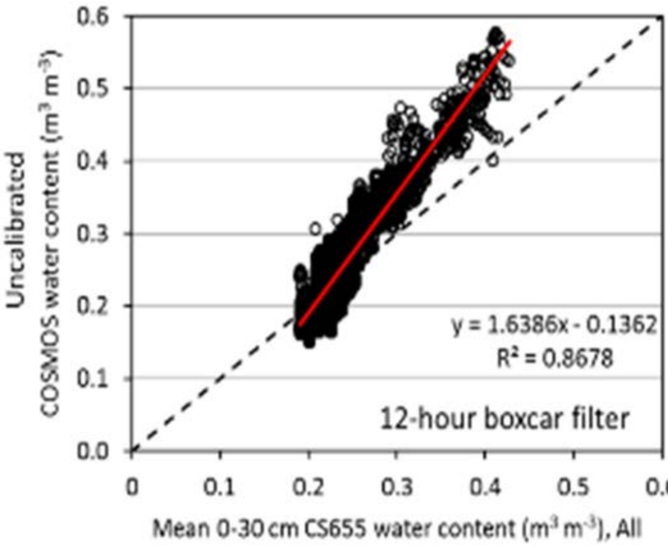

FIG. 8.13. Cosmic ray neutron probe uncalibrated water content compared with mean 0-0.30 m profile water content determined using the CS655.

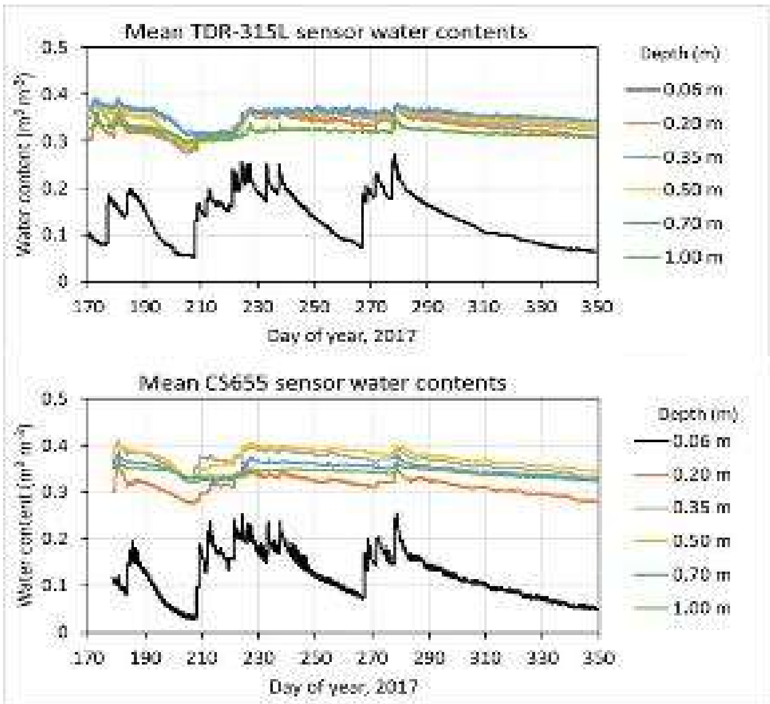

FIG. 8.14. Mean soil water contents at each measurement depth from TDR-315L sensor locations (top) and CS655 sensor locations (bottom).

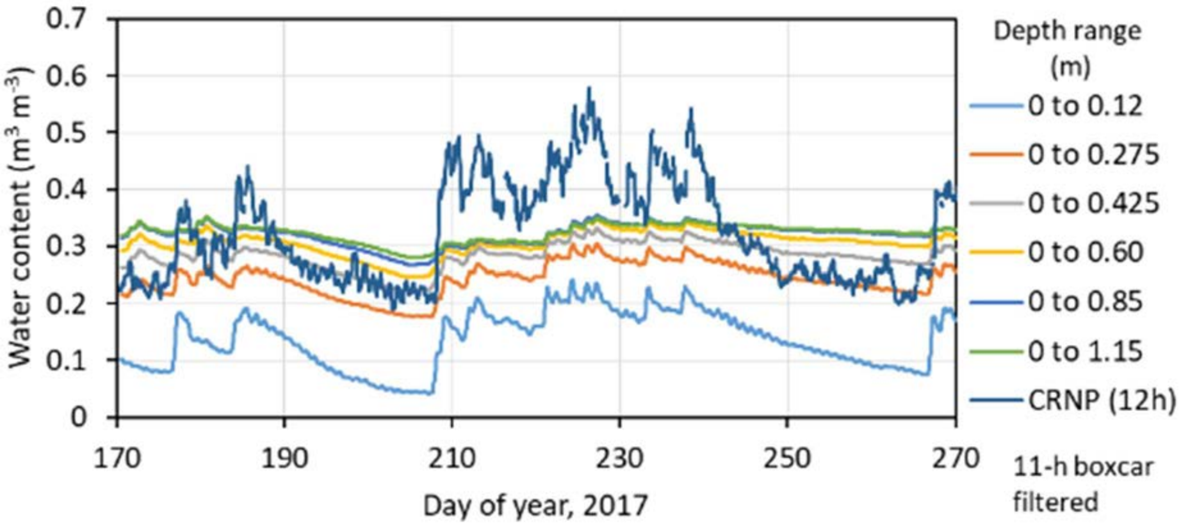

FIG. 8.15. Hourly CRNP data compared with mean EM sensor data water contents calculated for soil profiles of several depths ranging from the surface (0) to 0.12 m depth to the 0 to 1.15 m depth (bottom). CRNP data were filtered with a 12-h boxcar filter and the EM sensor data were filtered with an 11-h boxcar filter.

Regressing the filtered CNRP data against the profile water contents from the EM sensor sensors showed that correlation was greatest with the 0-0.12 m profile data, and that correlation steadily decreased as the depth of the soil profile considered was increased. The correlation coefficient of determination was largest (0.80), slope was closest to unity (1.57) and intercept was closest to zero (0.11 m^3 m^{-3}) for correlations of CRNP data versus the EM sensor water content for the shallowest profile considered (0-0.12 m). The insensitivity of CRNP data to soil water content at depths of 0.20 m and greater is consistent with the result of neutron transport studies by Köhli et al. [6], which predicted a penetration depth of 0.21 m directly under the sensor for uniform soil water content of 0.30 m^3 m^{-3} and a penetration depth of ~0.15 m at a radial distance of 50 m for that water content.

Examination of Fig. 8.15 indicates that there is a delay between soil wetting events and the CRNP response similar to the observed response in 2013 after precipitation events. To investigate the strength of this delayed response, we regressed CRNP data against EM sensor data offset in time from one day before to 0.5 days after the CRNP data in one-hour increments. In the cases considered, the r^2 of the offset CRNP data was greater than that obtained for zero offset time. For EM water contents averaged over 0.12 m and shallower, maximal correlation occurred at negative values indicating a delayed response of the CRNP. This observation and a moderate to strong correlation with absolute humidity (r^2 = 0.70) suggests that soil water evaporation humidifying the atmosphere after a wetting event had a strong effect on the CRNP data.

Schwartz et al. [30] discusses the importance of ensuring that soil water contents estimated using EM sensors are integrated with depth to correctly compare with NP-estimated water contents, which have a measurement volume approximately two orders of magnitude greater than EM sensors. Comparison of the NP data to the EM sensor data over the same 0-1.15 m depth range showed that while mean profile water contents were only moderately strongly correlated (r^2 = 0.75, Fig. 8.16A), which was likely due to spatial variability, the change in storage between NP measurement dates was well correlated ($r^2 = 0.94$) and linear with a slope of 1.02 (Fig. 8.16B), which was likely due to relatively uniform ET across the field.

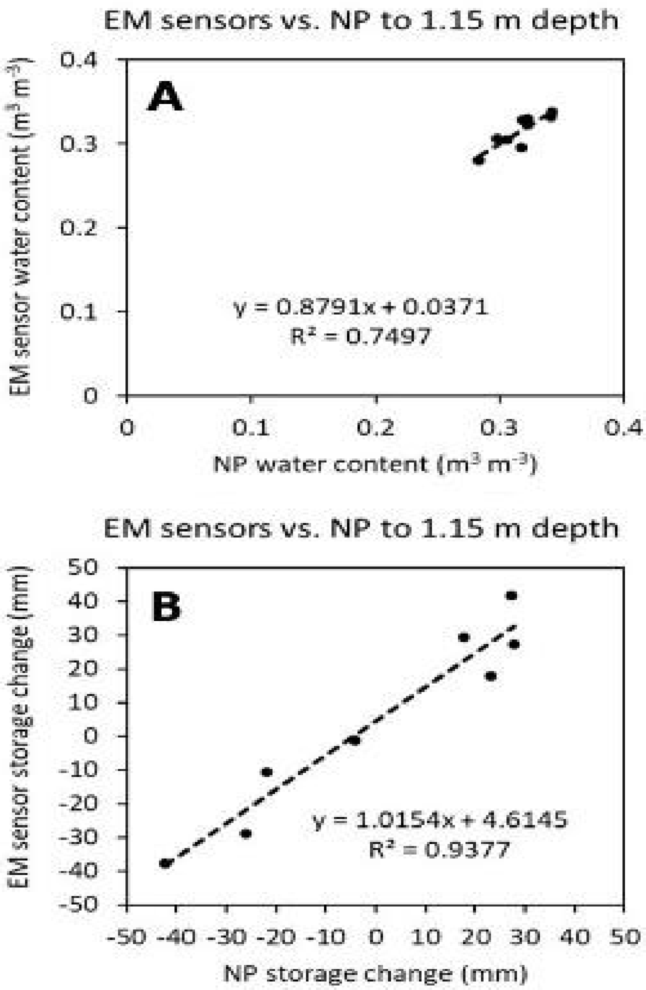

FIG. 8.16. (A) Linear correlation of profile water content to 1.15 m depth as calculated from EM sensor data compared to profile water content calculated from NP data. (B) Linear correlation of change in soil water storage in the 1.15 m deep profile as calculated from the EM sensor data compared to that calculated from the NP data. In both graphs, data are for the same eight periods from day of year 178 (July 5, 2017) through day of year 349 (December 14, 2017).

8.3.4. Field evaluation of soil water sensors

Water contents measured throughout the growing season in Spain with the TDR-315 probes (Fig. 8.17) ranged from 0.08 to 0.39 $m^3\ m^{-3}$ and exhibited the expected range for this clay loam soil. Saturation (~0.48 $m^3\ m^{-3}$) was never attained most likely because of the manner in which the plots were irrigated with a line source drip tape. Water contents measured throughout the growing season with the Delta-T PR2/4 profiling probe (Fig. 8.18) ranged from 0.30 $m^3\ m^{-3}$ to greater than 0.70 $m^3\ m^{-3}$ and, based on an estimated porosity of 0.48 $m^3\ m^{-3}$, were noticeably overestimated. In addition, there were strong temperature dependencies in the PR2/4 reported soil water content (Fig. 8.19) that oscillated with an amplitude of ± 0.025 $m^3\ m^{-3}$. Soil specific calibrations that include measured temperature may improve the accuracy of the probe, although problems associated with poor representation of spatial and temporal behavior of soil water [31] indicate the PR2/4 is unsuitable in fine-textured soils.

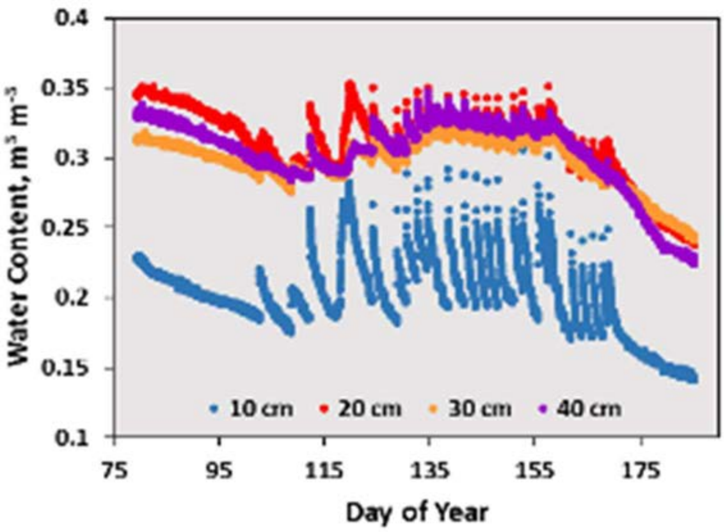

FIG. 8.17. Mean soil water contents (n = 2) measured with TDR-315 probes throughout the growing season in Aguas Nuevas, Albacete, Spain (Plot 7, 80% Irrigation Level).

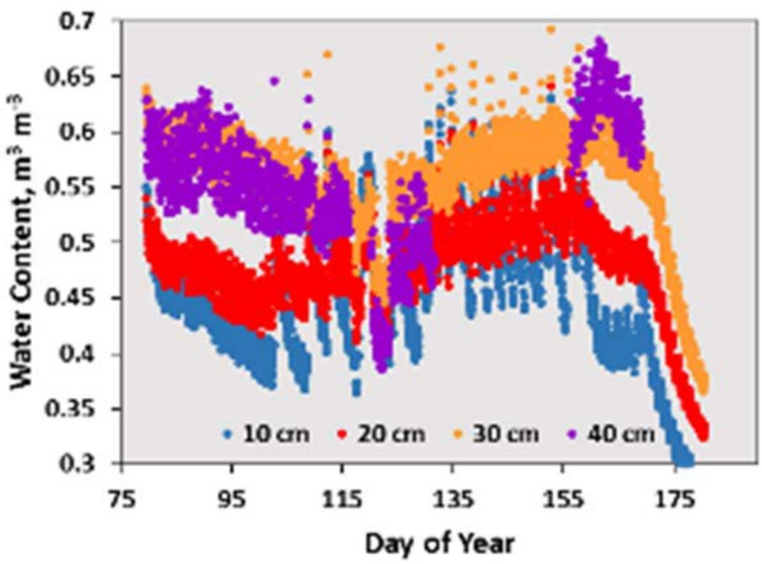

FIG. 8.18. Soil water contents measured with the Delta-T PR2/4 profiling probe throughout the growing season (Plot 7, 80% Irrigation Level) in Aguas Nuevas, Albacete, Spain. Some data for the 40-cm segment was omitted because of signal problems that yielded unrealistic water contents.

Stored soil profile water (0-0.45 m) estimated using the TDR-315 sensors (Fig. 8.20) varied with treatment although not in the manner expected based on the irrigation regime. Evaluation of the change in storage during irrigation showed that this accounted for only 77% of the applied water under the 100% irrigation treatment and 154% under the 80% level with the other two irrigation levels exhibiting stored water changes nearly equivalent to irrigation levels. We hypothesize that the variability in storage changes after irrigation is a result of the varying distance of the emitter from the TDR-315 arrays leading to smaller storage changes and progressively greater lag times as this distance increases. In contrast, changes in stored soil water during a precipitation event on day of year (DOY) 117-118 exhibited similar responses among treatments with changes ranging from 90 to 102% of measured precipitation depth (18.4 mm).

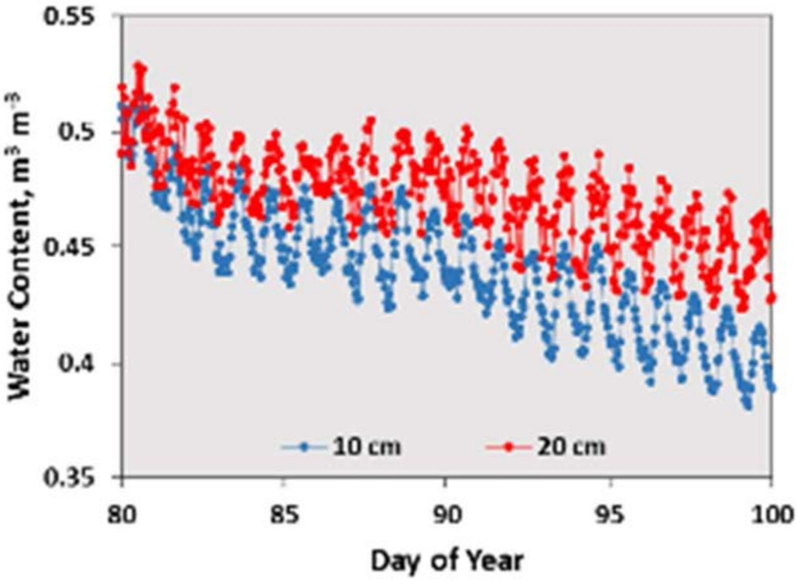

FIG. 8.19. Soil water contents measured with the Delta-T PR2/4 profiling probe exhibiting temperature dependencies in Aguas Nuevas, Albacete, Spain (Plot 7, 80% Irrigation Level).

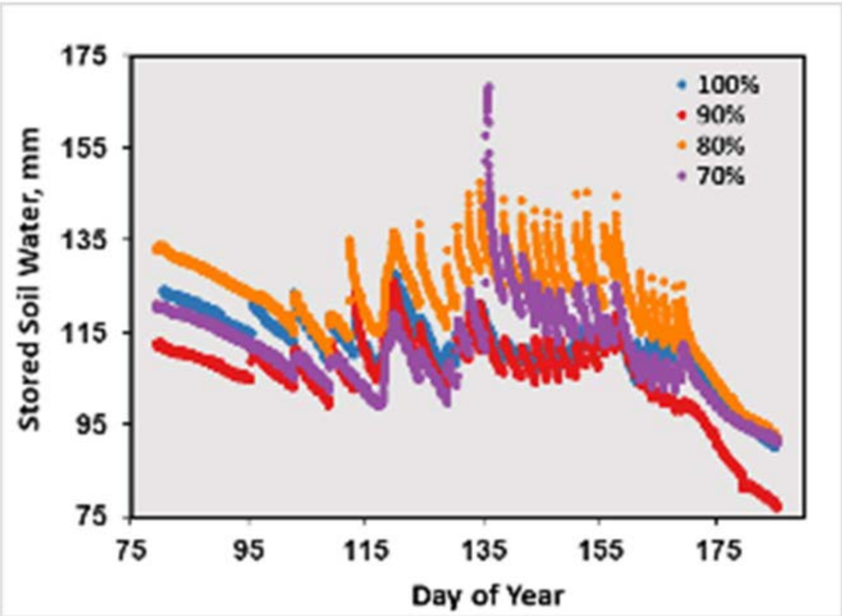

FIG. 8.20. Mean stored soil water in the 0 to 0.45 m profile estimated with the arrays of TDR-315 probes throughout the growing season for each of the irrigation treatments in Aguas Nuevas, Albacete, Spain.

Daily changes in profile water content estimated using the TDR-315 clearly exhibit water loss patterns associated with crop ET of about 4 to 7 mm d^{-1} (Fig. 8.21). These fluxes likely reflect some drainage out of the profile as evidenced by nighttime changes in stored soil water that successively decline and become negligible on the third day after irrigation. During the first day after irrigation, these changes may also reflect lateral water fluxes into and out of the volume sensed by the TDR-315 probes, depending on the proximity of the emitter, thereby confounding evaluations of vertical water fluxes associated with ET and drainage. All other sensing technologies would suffer the same difficulties in assessing soil water contents and fluxes. For comparison purposes, daily changes in profile water storage calculated using the PR2/4 profiling probe are shown in Fig. 8.22 and exhibit increases in storage during the morning hours and decreases in storage during the afternoon that reflect the instruments strong sensitivity to temperature as well as soil water content.

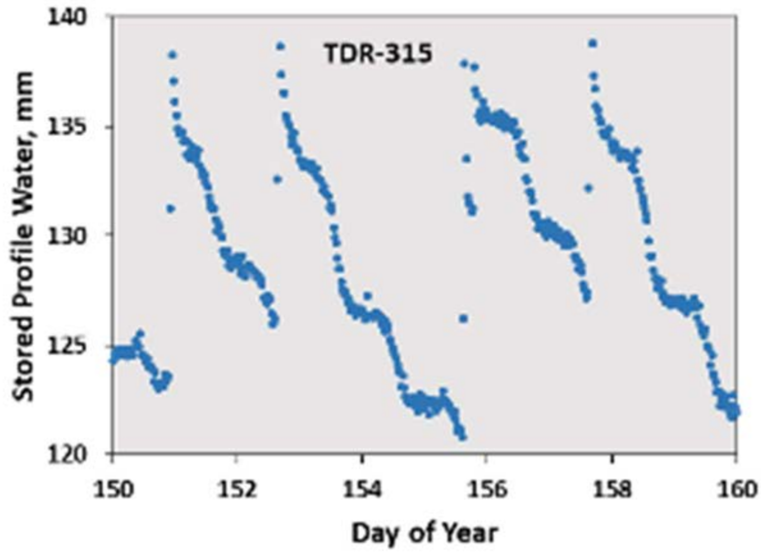

FIG. 8.21. Mean stored soil water in the 0 to 0.45 m profile estimated with the two arrays of TDR-315 probes showing daily changes in estimated storage resulting from ET (and potentially drainage) after irrigation (Plot 7, 80% Irrigation Level) in Aguas Nuevas, Albacete, Spain.

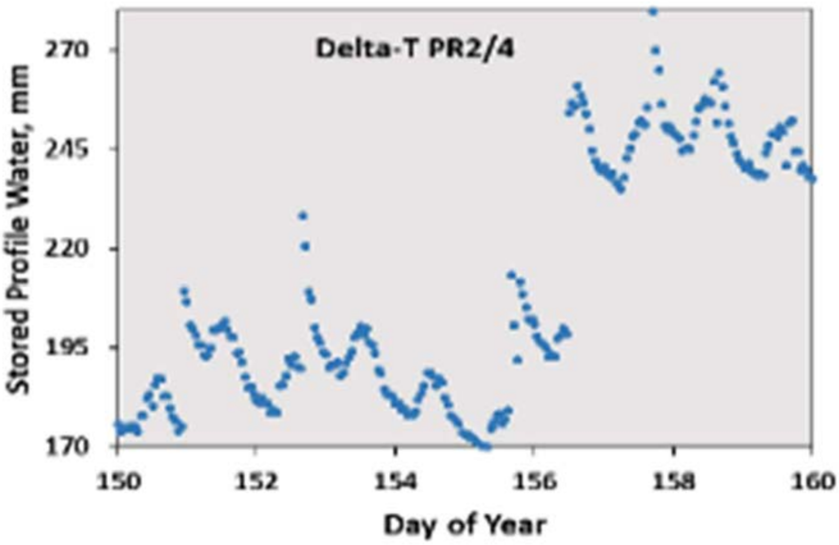

FIG. 8.22. Mean stored soil water in the 0 to 0.45 m profile estimated with the PR2/4 profiling probe showing daily changes in estimated storage (Plot 7, 80% Irrigation Level) in Aguas Nuevas, Albacete, Spain.

8.4. CONCLUSIONS

We examined several sensing technologies for use in assessing the soil water content and bulk electrical conductivity, soil water balance, and their potential for management of irrigation and soil salinity. Detailed investigations of the TDR-315 and TDR-315L demonstrated that they can accurately estimate apparent permittivity at bulk electrical conductivities up to 2.5 to 3.0 dS m^{-1} in soils with a large clay fraction (e.g. 400 g kg^{-1}) of which a considerable proportion consists of high surface area layer silicates. For these types of soils, accurate (error less than 0.03 m^3 m^{-3}) soil water content estimation usually requires a soil specific calibration, which could include bulk electrical conductivity as well as permittivity as dependent variables. In coarser textured soils, accurate estimation of soil water content using these sensors is feasible up to a bulk electrical conductivity of ~5 dS m^{-1}. The corresponding measurement limits in saturated soils for electrical conductivity of the pore water would range from 5 to 10 dS m^{-1} depending on the bulk density and clay content related to solid phase electrical conductivity. The performance of the CS-655 was similar to the TDR-315L in field investigations, although this sensor exhibited greater temperature sensitivity and noise in the permittivity measurements in a clay textured soil.

When calibrated for the Pullman soil in Bushland, Texas and deployed at depths of 0.06, 0.20, 0.35, 0.50, 0.70 and 1.00 m at 16 locations, the model TDR-315L and CS-655 electromagnetic soil water sensors produced profile water contents that were well correlated with neutron probe data over the same depth range (0 to 1.15 m). Changes in stored profile water content calculated from the EM sensor data were even more strongly correlated (r^2 = 0.94) with change in storage determined with the neutron probe. This indicates the possibility that properly deployed EM sensors of the types used here could provide change in storage data accurate enough to determine ET from the soil water balance.

Many of the electromagnetic sensors can measure apparent or bulk electrical conductivity and therefore are useful for irrigation management of salt affected soils. The TDR-315, TDR-315L and CS-655 can measure bulk electrical conductivity up to 8–10 dS m^{-1}. However, inferring a pure water electrical conductivity from the bulk EC to determine leaching fraction is still limited by an accurate measurement of permittivity or soil water content, which occurs only at lower bulk EC values as described above. Estimation of pore water EC based on the Hillhorst Model was found to be prone to large errors even with an accurate measurement of apparent permittivity.

The development of the profiling soil moisture probe with a TDR circuit similar to the TDR-315L was beset by design problems related to the fabrication of a body resistant to mechanical stresses of insertion and water entry. Although several prototypes were designed, nominally evaluated, and found to be satisfactory, the costs of manufacturing were excessive relative to the price point. A new sensor design will be evaluated in the near future.

Water content data from the CRNP was biased to larger values by the presence of a fully developed maize crop in 2013. In both study years, the CRNP appeared to respond positively to increase near-surface atmospheric humidity that occurred after precipitation events. The CRNP was less sensitive to increases in soil water content during and after subsurface irrigation at 0.30 m. In 2017, the CRNP was sensitive to soil water content mainly in the shallow (0.02 and 0.06 m) soil depths, and nearly insensitive to soil water content at depths of 0.20 m and greater. In 2013, however, the CRNP was sensitive to changes in soil water content at greater depths. These outwardly inconsistent outcomes may be caused by a greater average radial distance of EM sensors from the CRNP (because of the inclusion of the

TDR-315L probes) and greater mean soil water contents in 2017 thereby reducing the sensitivity with depth compared to 2015 [5, 6]. Because of the relatively shallow depth of sensitivity, CRNP data would have little relevance for irrigation management for the field crops commonly grown in the Southern Great Plains. Because of the strong correlations with soil water content near the surface (0.02 and 0.06 m depths) and with absolute humidity of the air at 2-m elevation, the CRNP could have applications in mesoscale weather forecasting.

Examination of the field performance of the TDR-315 in a clay loam soil in Albacete, Castilla La Mancha, Spain showed that arrays of sensors deployed at depths of 0.1, 0.2, 0.3, and 0.4 m at two locations were able to resolve daily changes in profile water content and water depletion patterns associated with ET. However, because sensor arrays varied with respect to the distance from the emitters, this likely biased soil water contents (level of depletion) and cumulative fluxes related to irrigation and daily ET compared with the area averaged values. Changes in stored soil water during the first day after irrigation may reflect lateral fluxes of water, thereby biasing estimates of ET. The placement of the sensors with depth and horizontally relative to the drip emitters will need to be optimized, possibly with a greater number of sensor arrays, to accurately determine ET from the soil water balance in this surface drip irrigated field.

ACKNOWLEDGEMENTS

The authors are grateful for the support from IAEA CRP Reimbursable Agreement (#18210) and USDA SBIR Phase II Contract 2012-02152, from Acclima Inc. for furnishing prototype soil water sensors, and from the USDA-ARS Ogallala Aquifer Program, a consortium between the USDA Agricultural Research Service, Kansas State University, Texas A&M AgriLife Research, Texas A&M AgriLife Extension Service, Texas Tech University, and West Texas A&M University, as well as the dedicated support of USDA-ARS Bushland staff Karen Copeland, Brice Ruthardt, Bridgette DeWitt, and Logan Hopper. This material is based in part upon work that is supported by the National Institute of Food and Agriculture, U.S. Department of Agriculture, under award number 2016-67021-24420.

REFERENCES

[1] MAZAHRIH, N.T., et al., Field calibration accuracy and utility of four down-hole water content sensors, Vadose Zone J. **7** (2008) 992–1000.

[2] EVETT, S.R., et al., Soil water sensing for water balance, ET and WUE, Agric. Water Manage. **104** (2012) 1–9.

[3] SCHWARTZ, R.C., et al., Soil permittivity response to bulk electrical conductivity for selected soil water sensors, Vadose Zone J. **12** (2013)

[4] EVETT, S.R., et al., No. 8,947,102 B1, Soil Water and Conductivity Sensing System, filed 24 February 2012 with claims priority to Provisional Serial No. 61/515,381 – Filed 5 August 2011. Patent allowed on 7 October 2014. Patent granted on 30 December 2014, issued 3 February 2015.

[5] DESILETS, D., et al., Nature's neutron probe: Land surface hydrology at an elusive scale with cosmic rays, Water Resour. Res. **46 (**2010) W11505.

[6] KÖHLI, M., et al., Footprint characteristics revised for field-scale soil moisture monitoring with cosmic-ray neutrons, Water Resour. Res. **51** (2015) 5772–5790.

[7] CASANOVA, J.J., et al., Design of access-tube TDR sensor for soil water content: Theory, IEEE Sensors J., **12** (2012) 1979–1986.

[8] CASANOVA, J.J., et al., Design of access-tube TDR sensor for soil water content: Testing, IEEE Sensors J., **12** (2012) 2064–2070.

[9] CASANOVA, J.J., et al., Design and field tests of an access-tube soil water sensor, Appl. Eng. Agric. **28** (2012) 603–610.

[10] CASANOVA, J.J., et al., Directly coupled vs. conventional time domain reflectometry in soils, Applied Engr. Agric. **29** (2013) 771–777.

[11] CASANOVA, J.J., et al., Design and field tests of a directly coupled waveguide-on-access-tube soil water sensor, Appl. Engr. Agric. **30** (2014) 105–112.

[12] SCHWARTZ, R.C., et al., Complex permittivity model for time domain reflectometry soil water content sensing. I. Theory, Soil Sci. Soc. Am. J. **73** (2009) 886–897.

[13] BIRCHAK, J.R., et al., High dielectric constant microwave probe for sensing soil moisture, Proc. IEEE **62** (1974) 93–98.

[14] GIESE, K., TIEMANN, R., Determination of the complex permittivity from thin-sample time domain reflectometry improved analysis of the step waveform, Adv. Mol. Relax. Process. **7** (1975) 45–59.

[15] LIN, C.-P., et al., Clarification and calibration of reflection coefficient for electrical conductivity measurement by time domain reflectometry, Soil Sci. Soc. Am. J. **72** (2008) 1033–1040.

[16] SCHWARTZ, R.C., et al., A reevaluation of TDR propagation time determination in soils, Vadose Zone J. **13** (2014)

[17] SCHWARTZ, R.C., et al., Evaluation of a direct-coupled TDR for determination of soil water content and bulk electrical conductivity, Vadose Zone J. **15** (2016)

[18] EVETT, S.R., et al., Overview of the Bushland Evapotranspiration and Agricultural Remote sensing Experiment 2008 (BEAREX08): A field experiment evaluating methods quantifying ET at multiple scales, Adv. Water Resour. **50** (2012) 4–19.

[19] EVETT, S.R., et al., Can weighing lysimeter ET represent surrounding field ET well enough to test flux station measurements of daily and sub-daily ET? Adv. Water Resour. **50** (2012) 79–90.

[20] CHÁVEZ, J.L. EVETT, S.R., Using soil water sensors to improve irrigation management, In Proc. 24th Annual Central Plains Irrigation Conf., Colby, Kansas (2012) 187–202.

[21] EVETT, S.R., et al., TDR laboratory calibration in travel time, bulk electrical conductivity, and effective frequency, Vadose Zone J. **4** (2005) 1020–1029.

[22] TOPP, G.C., REYNOLDS, W.D., Time domain reflectometry: A seminal technique for measuring mass and energy in soil, Soil Till. Res. **47** (1998) 125–132.

[23] DOMÍNGUEZ, A., et al., Real farm management depending on the available volume of irrigation water (part I): Financial analysis, Agric. Water Manage. **192** (2017) 71–84.

[24] LEITE K.N., et al., Distribution of limited irrigation water based on optimized regulated deficit irrigation and typical meteorological year concepts, Agric. Water Manage. **148** (2015) 164–176.

[25] LÉLLIS, B.C., Efecto del riego deficitario controlado optimizado por etapas, para volúmenes limitados de agua, en el rendimiento y la calidad del ajo morado de las Pedroñeras, Tesis Doctorado, Universidad de Castilla La Mancha, Albacete, España (2017).

[26] WANG, Z., et al., A comparison of second-order derivative based models for time domain reflectometry waveform analysis, Vadose Zone J. **16** (2017)

[27] ALLEN, R.G., et al., Crop evapotranspiration - Guidelines for computing crop wáter requirements. FAO Irrigation and drainage paper 56. Food and Agriculture Organization of the United Nations, Rome (1998).

[28] HILHORST, M.A., A pore water conductivity sensor, Soil Sci. Soc. Am. J. **64** (2000) 1922–1925.

[29] BALENDOCK, J., et al., Wet sensor pore water EC calibration for three horticultural soils, Acta Hort. (ISHS) **691** (2004) 789–796.

[30] SCHWARTZ, R.C., et al., Comments on “J. Singh et al., Performance assessment of factory and field calibrations for electromagnetic sensors in a loam soil” [Agric. Water Manage. **196** (2018) 87–98], Agric. Water Manage. **203** (2018) 236–239.

[31] EVETT, S.R., et al., Soil profile water content determination: Spatiotemporal variability of electromagnetic and neutron probe sensors in access tubes, Vadose Zone J. **8** (2009) 926–941.

9. IMPROVEMENT OF IRRIGATION PRACTICE TO MITIGATE ROOT ZONE SALINITY FOR ENHANCING RICE PRODUCTION IN A COASTAL AREA OF NORTH VIETNAM THROUGH ISOTOPIC AND RELATED TECHNIQUES

DANG DUC NHAN
Vietnam Atomic Energy Institute
Ha Noi, Vietnam

DUONG HAI SINH, KHUONG MINH CUONG
Institute for Water Resources Research
Ha Noi, VietNam

HA LAN ANH
Institute for Nuclear Sciences and Technology,
Ha Noi, Vietnam

L.K. HENG
International Atomic Energy Agency,
Vienna, Austria

Abstract

The purpose of this study was to search for an appropriate irrigation practice to replace the traditional practice to mitigate root zone salinity for improving the yield of the special "fragrance" rice varieties planted on Haplic Salic Fluvisols in a coastal area of the Hai Hau district, Nam Dinh province, North Vietnam. Isotopic combined with hydrogeological techniques were applied to investigate the sources of salinity in water within the root zone. The techniques included (i) determination of the relationship between deuterium and oxygen-18 signatures (δ^2H and $\delta^{18}O$) in the local precipitation, in the irrigation water, and in water within the root zone (ii) investigation into the relationship between concentrations of exchangeable Ca^{2+}, Mg^{2+} and Na^+ cations and concentration of chloride in soil-pore water (iii) investigation into the relationship of the $\delta^{18}O$ and chloride concentration in water within the root zone. Knowing the source of salinity in the root zone one should be able to suggest a new irrigation practice to mitigate the salinity in the cultivated soil.

The stable isotopic signatures in water within the root zone of rice revealed that it originated from the Ninh Co River that irrigated the field, whereas the coastal tide did not affect the groundwater table beyond the root zone. Seawater does not intrude into the shallow aquifer in the study region. Under the traditional farming practice, the pattern of the variation of $\delta^{18}O$ in soil pore-water during the meteoric year was similar to those in the local rain water, but in between the two rice seasons the $\delta^{18}O$ soil in pore-water became more enriched compared to this signature during the cropping period. At the same time, the chloride concentration in water within the root zone did not change much within a wide range of the $\delta^{18}O$ variation, indicating the intensive evaporation of irrigation water under the traditional cultivation practice. Sodium concentrations in water within the root zone increased during the cropping period, implying that the Ca^{2+} cation in irrigation water exchanged with the Na^+ cation adsorbed onto the soil surface, but not from the salt intrusion. It appeared that the traditional irrigation practice with

drainage of all surface water before rice harvesting followed by cutting and burning straw, facilitates evaporation of the irrigation water, but maintains salinity within the root zone. It is clear that the high salinity in water within the root zone mostly resulted from the dissolution of halides concentrated in the soil layer by the irrigation water, following the intensive evaporation of the saline water between the two cropping seasons. The Ca-Na cation exchange between Ca^{2+} in the irrigation water and Na^{+} adsorbed onto the soil surface also seems to contribute a part of the salinity in the soil water.

An alternative irrigation practice including keeping the irrigation water in the field without burning straw after rice harvesting was investigated. The salinity in water within the root zone could diffuse downwards throughout the year by gravity, thus reducing the concentration of salinity in water in the cultivated soil layer. The new farming practice resulted in an increase in rice yield in the experimental field by up to 5%. The improvement in rice yield was not pronounced because the rice variety was the traditional one. However, the local farmers would be happy as 5% increase in yield of the "fragrance rice" allows them to earn enough profit for compensation for their expense of fertilizer and the irrigation tax.

9.1. INTRODUCTION

During a long history of the geological development in the northern part of Viet Nam, the Red River has created a fertile plain known as the Red River delta (RRD). The RRD occupies an area of around 15,000 km^2 (1.5 million hectares) in which almost 20 million inhabitants are residing. It was estimated that more than 50% of the total RRD's area is situated lower than 2 m above the mean sea level [1]. Out of the total area of the delta, 1.2 million ha is currently used for farming [2]. The annual yield of cereal crops from the delta was estimated as high as 6.1 million tons [2]. To maintain the yield irrigation was a priority for the Vietnamese feudal dynasties as well as the local farmers. There a dense network of earthen dikes that have been constructed since the 13th century to protect the land against floods from the river system and typhoons from the sea. Recently, the sea dikes have been modernized by concrete as shown in Fig. 9.1.

FIG. 9.1. Dike along the sea coats of the RRD has been modernized by concrete for more effective protection against typhoons (Photo was taken from Giao Lac commune, Giao Thuy district, Nam Dinh province in 2015).

The main irrigation practice used in the RRD region is paddy rice watering with low water use efficiency and high electricity expense (around 300 kw ha^{-1}) [3]. Nowadays, in the RRD the farming practice has been much changed by mechanization. For easier operating the machines before harvesting rice, the local farmers drain out all water from their fields and straw is collected and burnt (Fig. 9.2a). In between the two rice seasons the fields are bare leading to cracking of the soil under the hot weather (Fig. 9.2b). The cracked soil facilitated evaporation leaving salt in the soil to persist in root zone of 1.0-1.2 m depth. High salinity in the cultivated soil was thought to be a reason for low crop yields along the marine coast of the RRD.

(a) (b)

FIG. 9.2. (a) Rice straw collected and burnt to get the ash-bed effect of additional potassium and (b) with surface salt accumulation under the hot weather.

The aim of this study was to develop an alternative irrigation practice to improve the yield of rice cultivated on Haplic Salic Fluvisols with relatively high salinity in the Hai Hau district, North Vietnam. The research was assisted with the use of isotopic techniques, namely the use of stable isotopic signatures of deuterium and oxygen-18 in different sources of water (precipitation, irrigation water, water within root zone) and its relation to the concentration of chloride as an indicator of sea salt. The isotopic techniques have not previously been applied for this purpose in Viet Nam.

9.2. MATERIALS AND METHODS

9.2.1. Study site

An area of 5 ha in the Hai Thinh commune, Hai Hau district, Nam Dinh province that is located in the southwest apex of the RRD was chosen for this study. Fig. 9.3 depicts A sketch of the study location and the field used for the research are shown in Fig. 9.3 and Fig. 9.4, respectively.

The Hai Hau district in the Nam Dinh province is known throughout the country, and some parts of the world for its traditional special “fragrant” rice variety, Tam, that was for a long time previously exported to France at a premium price. During the last decades the rice yields have been declining. Vietnamese agronomists determined the reason for the reduced rice yield in the region was due to be the increase of the salt content in the soil, although the irrigated water was not saline. The concentration of chloride in the soil water of the study region was found to be more than 2,500 mg l^{-1}. The pH of the soil both in water and KCl solution ranges from 5 in the surface soil to 7.8 at a depth of 140-160 cm [4]. The irrigation practice currently used by the local farmers is traditional paddy field like those in other coastal regions as mentioned above.

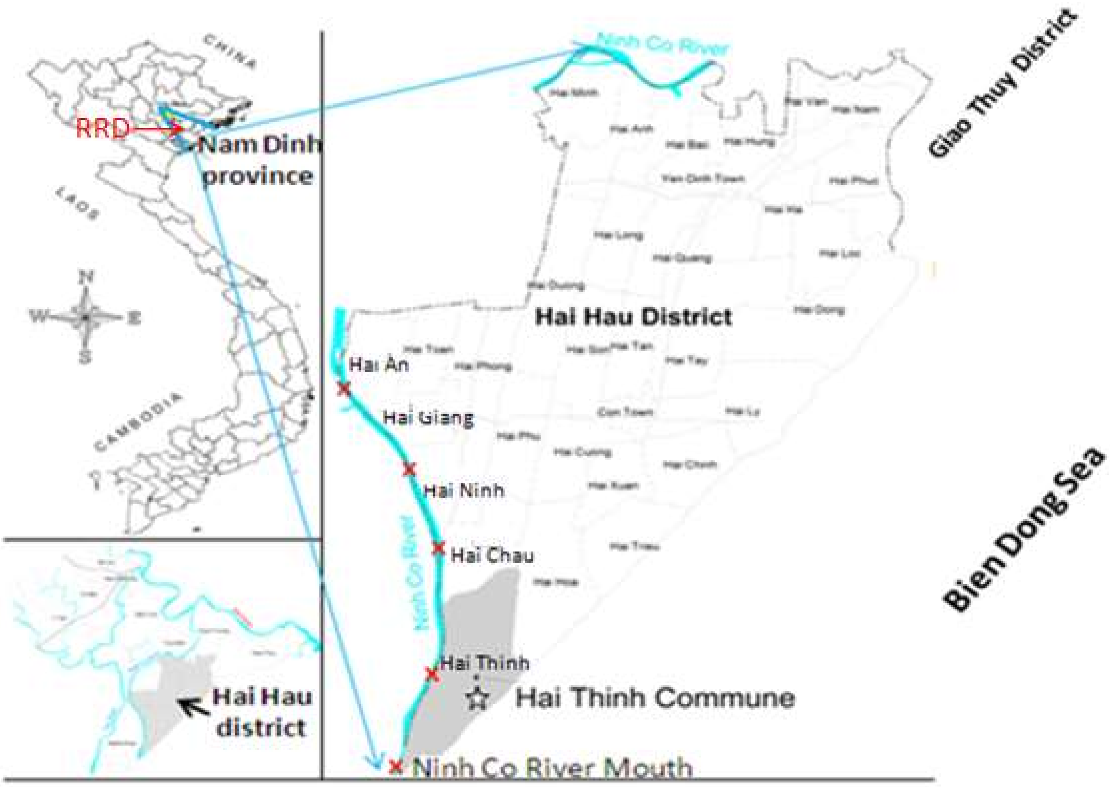

FIG. 9.3. A sketch showing the study area in the Hai Thinh commune, Hai Hau district, Nam Dinh province which is located in the Southwest apex of the Red River delta (RRD).

FIG. 9.4. A field of 5 ha was used for the research in the Hai Thinh Commune, Hai Hau district, Nam Dinh province.

The salt intrusion is currently being studied by Vietnamese as well as International hydro-geologists and the issue is still under debate. The question is whether the salinity in the shallow aquifer comes from the sea or it is from diffusion from the pores of the aquifer sediment.

9.2.2. Climate in the region

The monthly average air temperature (ºC) and precipitation (mm) and evaporation (mm) in the RRD that were collected from January 2000 to December 2013 (14 years) is shown in Fig. 9.5 and Fig. 9.6, respectively [5].

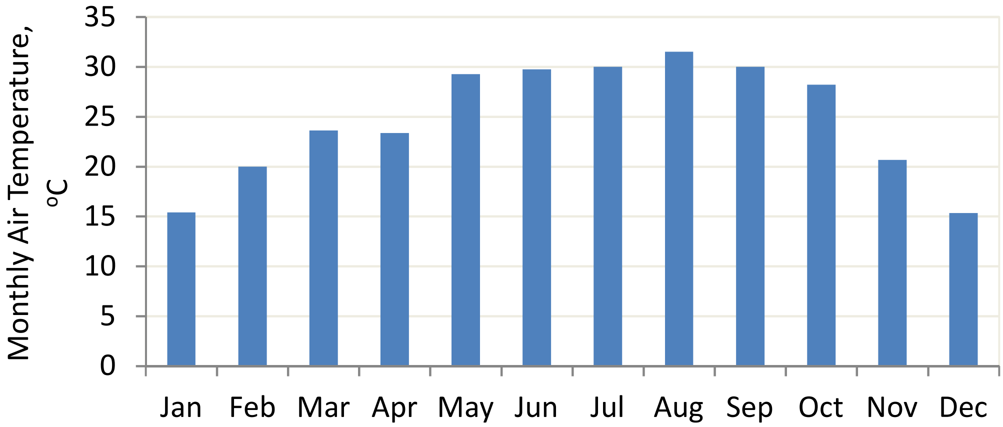

FIG. 9.5. Monthly average air temperature in the Red River delta region, North Vietnam.

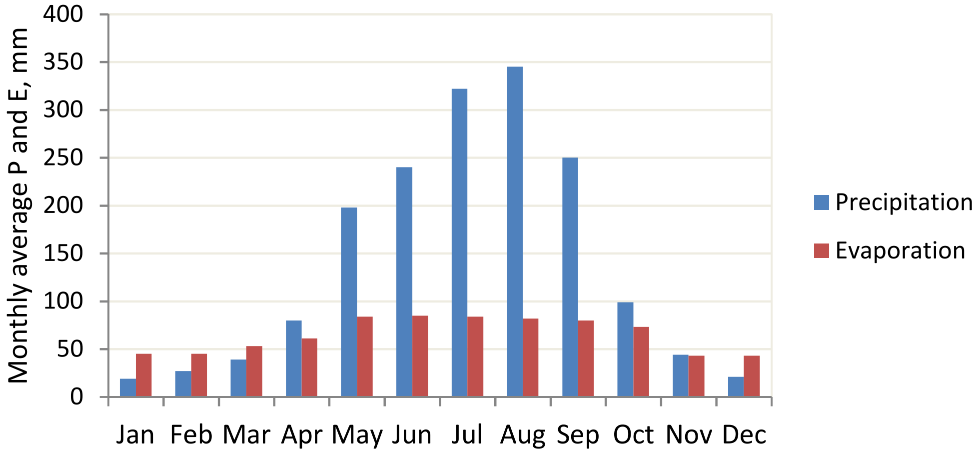

FIG. 9.6. Monthly average precipitation (P) and evaporation (E) in the Red River delta region, North Vietnam.

9.2.3. Irrigation and drainage system

Irrigation water in the Hai Hau district is taken by pumping from the Ninh Co River (Fig. 9.3), a tributary of the Red River. The water is distributed first into 218 km-long primary canals and then to the secondary canals 838 km long and finally to the fields through farmer-constructed cross-channels. Irrigation usually is scheduled during the farming season by the irrigation company of the district. The total number of pumping stations in the Hai Hau district is 68 with a capacity of around 60 000 m^3 h^{-1}. The pumping stations in the Hai An, Hai Giang and Hai Ninh communes in the North function as irrigation stations, but those in the Hai Chau and Hai Thinh communes in the South function as drainage stations (Fig. 9.3). The irrigation and drainage factors of the Hai Hau district were estimated as 1.16 and 4.8 l s^{-1} ha^{-1}, that were slightly lower than the target values of 1.25 and 5.5 l s^{-1} ha^{-1}, respectively [6].

9.2.4. Sampling procedure

Soil samples were taken from eight positions around the edges and one position in the center of the field. Out of the nine positions, three locations along a diagonal of the field were assigned to take soil profile samples from the surface down to 1.0 m depth, the rooting depth of rice. In the other six locations around the edges of the field, soil samples were collected from the cultivated soil layer only, i.e. from the surface 0-20 cm depth. The soil samples were taken using a corer (Eijkelkamp, Netherlands). The profile soil samples were separated into 20-cm sections and all the sub-samples and surface soil samples were stored in plastic jars with tight caps. The samples were transported to the laboratory in Ha Noi and were kept in a refrigerator at 4 °C until analysis.

The local precipitation was collected on a monthly basis using a device constructed following an IAEA recommendation [7]. The device was set up on the roof of the Center for Irrigation and Environment of the Marine Coast and Islands of North Vietnam, which is located in Thinh Phong township, about 2 km from the field. In the middle day of each month water in the container was thoroughly mixed, and then pipetted into a high-density polyethylene (HDPE) vial of 50-ml capacity and sent to the laboratory in Ha Noi for analysis of the stable isotopic composition. Irrigation water was sampled from five points from the mouth of the Ninh Co River to 20 km up-stream to the Hai An pumping station (cross points depicted in Fig. 9.3) in August and December each year, as the middle months of the rainy and dry seasons, respectively.

9.2.5. Influence of tide to the water table and chemistry of groundwater to infer the salt intrusion

To monitor the influence of the tide on the groundwater table in the root zone, two shallow wells of 1.5 m depth were made in two corners of the study field. Each well consisted of two casing tubes made from PVC resin. The outside-casing tube had an ID of 120 mm and length of 1800 mm so that 300 mm of the tube height was above the field surface to protect from the ingress of surface irrigation water, but nevertheless allowed infiltration of water from the saturated soil. The inside casing-tube had an ID of 60 mm and was the same length. The end of the inside tubes of 400 mm in length was perforated to let water in. The perforated part of the tube was covered by mesh of PVC material to protect the holes from being clogged by sand and soil. The space in between the casing tubes was filled with coarse and fine sand to prevent suspended matter and soil to enter inside. The hole was again packed with soil. The water table level in the wells was monitored using a piezometer (Solinst 101 P2, Canada). The tubes were tightly capped to protect from rainwater and to ensure that water inside was from the root zone only. The installation method is shown in Fig. 6.

The water table in the study area was high enough that water samples were easily taken from the wells by hand. Water samples of about 100 ml for chemical analyses were filtered through polycarbonate membranes of 0.45 μm mesh, and then split into two portions. One aliquot was acidified with 1-2 drops of HNO_3 (65%, PA grade, Merck, Germany) to pH 1-2 for analysis of cations (Na^+, K^+, Ca^{2+} and Mg^{2+}). Another portion that was not acidified was for the analysis of anions (Cl^-, PO_4^{3-}) and stable isotopic composition. All of the samples were kept in HDPE vials of 50-ml capacity and then transported to the laboratory in Ha Noi.

9.2.6. Sources of water within the rice root zone

The sources of water within the root zone of both sub-fields were determined for each season based on the natural abundance of the stable isotopes of oxygen and deuterium ($\delta^{18}O$, δ^2H) in the local precipitation, in water from the Ninh Co river and in water within the root zone collected from the two shallow wells [8].

9.2.7. Study the improvement of the modified irrigation practice to mitigate salinity in root zone

The field was split into two sub-fields by an earthen dike. In one sub-field the traditional irrigation practice was maintained (Fig. 9.7) and referred to as the reference field, but in the second sub-field the newly modified irrigation practice was applied. The newly modified practice was designed to maintain water around the year and was not drained during the harvesting period as well as between two rice seasons (Fig. 9.8). The rice planted in the fields was the variety “fragrant Tam” as known by the local name. The cultivation and fertilizer regime for rice in the two sub-fields were the same. The experiment was conducted in two seasons: summer-autumn (June-September) and winter-spring (January-May) in the 2015-2017 years. The productivity of the two sub-fields was compared through the yields of the rice grain after sun-drying (by the farmers’ experience) and separated from empty grains.

FIG. 9.7. Water was maintained, and straw was left on the field and then turned over by ploughing during the soil treatment for the next rice season as an alternative practice to reduce salinity in the root zone of rice in the Hai Hau district, Nam Dinh province.

FIG. 9.8. Installation of shallow wells to monitor the influence of tide on the groundwater table and chemistry of groundwater in the study field.

9.2.8. Saltwater intrusion and desalination of soil study

Salt water intrusion or desalination of soil was studied based on the relationship between the chloride concentration and concentrations of exchangeable sodium, calcium and magnesium, and based on the relationship between the $\delta^{18}O$ signature and the concentration of chloride in water within the rice root zone, as described by Clark and Fritz [9] and Appelo and Postma [10].

9.2.9. Analytical methods

Soil particle size distribution was analyzed using the pipette method [11] at the Institute of Soil and Agrochemicals, Academy of Agricultural Sciences, with some modifications [12]. Soil pH was measured on a suspension of 25 g of air-dried soil in 1M KCl solution (soil: solution = 1:5) using a glass electrode (TOA, Japan). The probe was calibrated using 4.75 and 8.20 standard pH solution. Exchangeable Na^+, K^+, Ca^{2+} and Mg^{2+} was measured on an extract of 25 g of air-dried soil in 1M ammonium acetate solution at pH 7 (soil: solution = 1:5), following shaking and filtration through polycarbonate filters of 0.45 μm pore size. Cations and anions (Cl^-, NO_3^- and PO_4^{3-}) were determined by ion-chromatography using DIONEX 600 (USA). Soil-pore water was separated from the soil samples by cryogenic distillation under vacuum [13] for the analysis of stable isotope composition, which was performed on a continuous flow Isotope Ratio Mass Spectrometer (Micro Mass, UK) equipped with a Euro-vector (Italy) Elemental Analyzer [12]. Before the analysis, water samples were filtered through polycarbonate membranes of 0.45 μm pore size to remove any suspended material. The stable isotope composition was expressed in the delta (δ) notation as follows.

$$\delta^2 H = \left(\frac{R_{^2H,sample}}{R_{^2H,std}} - 1\right) * 1000$$

$$\delta^{18} O = \left(\frac{R_{^{18}O,sample}}{R_{^{18}O,std}} - 1\right) * 1000$$

where $R_{^2H,sample}$, $R_{^2H,std}$, $R_{^{18}O,sample}$, and $R_{^{18}O,std}$ are the isotopic ratios of $^2H/^1H$, $^{18}O/^{16}O$ in samples and standard, respectively. The value of the delta is expressed in per mil (‰). The international standard used in the stable isotope analysis was Vienna Standard Mean Ocean Water (VSMOW) [14].

The precision of both δ^2H and $\delta^{18}O$ was better than ± 0.2 ‰. A quality assurance and quality control program were applied for the ionic content determination by analyzing standard solutions supplied by the IC supplier (DIONEX). The standard deviation of the analytical results was better than ± 3% from the certified value.

9.3. RESULTS AND DISCUSSION

9.3.1. Isotopic composition of the local precipitation, seawater and water from the Ninh Co River

The meteoric water line of the δ^2H *vs.* $\delta^{18}O$ relationship for the local precipitation collected on a monthly basis in the Thinh Long township, Hai Hau district during the 2013-1016 years is depicted in Fig. 9.9, which also shows the isotopic compositions of seawater and water from the Ninh Co River as the source of irrigation water. Seawater and water from the Ninh Co River were taken in the middle of August and December, representing the rainy and dry season, respectively.

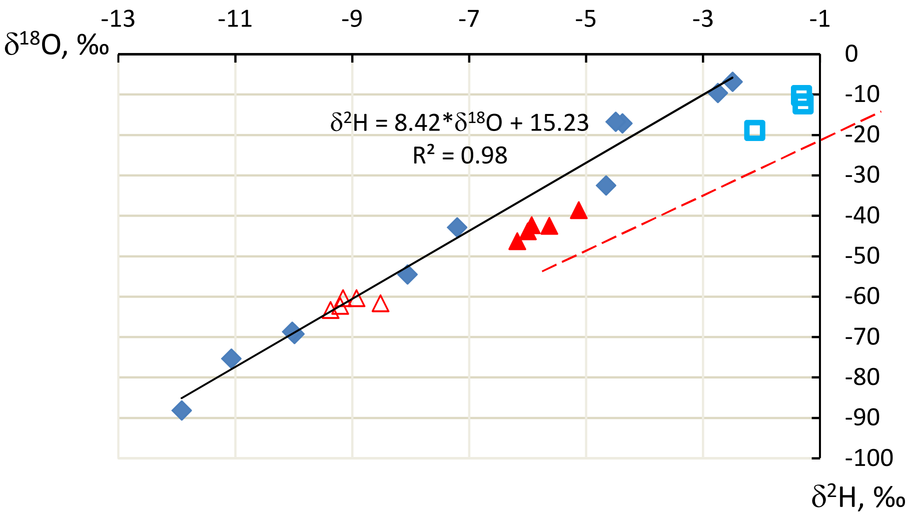

FIG. 9.9. The local meteoric water line (solid line) and isotopic compositions of seawater taken from the mouth of the Ninh Co river (open blue square) and that of water from the Hai Thinh pumping station at the Ninh Co river in rainy (red open triangles) and dry season (red solid triangles) representing the isotopic compositions of irrigation water in the region.

In the rainy season the isotopic compositions of water from the Ninh Co River are similar to that of the local precipitation, but in the dry season water from the River appears to be influenced by evaporation so its isotopic compositions became enriched (Fig. 9.9). Additionally, it seems that in the dry season seawater intruded into the River and mixed with freshwater from up-stream as shown by the dashed line in Fig 9.9. This is the reason why the Hai Thinh pumping station is functioning for drainage purposes only and not for irrigation around the year.

9.3.2. Isotopic composition of soil water

The δ^2H *vs.* $\delta^{18}O$ relationship for water in the cultivated soil layer (0–20 cm) in the rainy (August) and dry seasons (December) is shown in Fig. 9.10, which illustrates that water within the cultivated soil layer was from the Ninh Co River as the main source of irrigation water in the region.

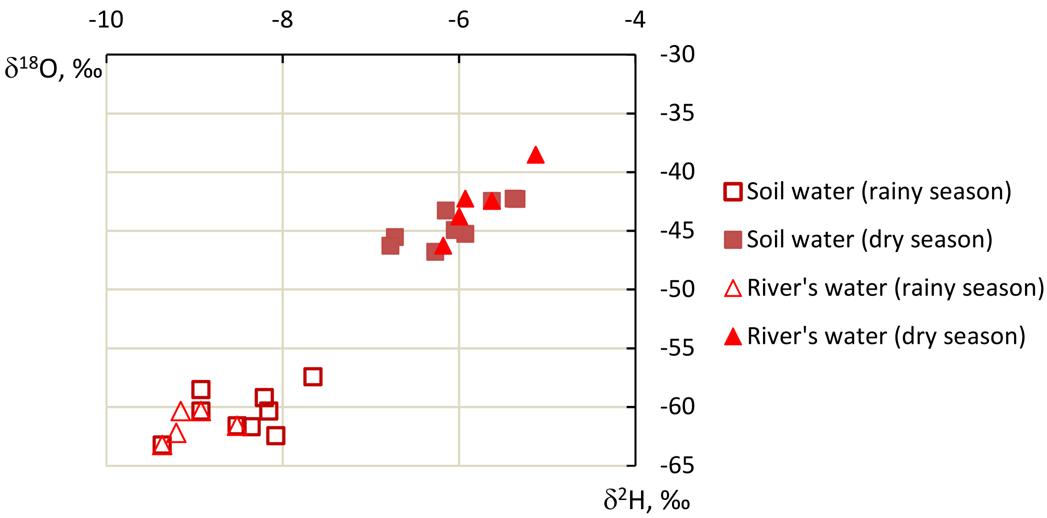

FIG. 9.10. Comparison of isotopic compositions of soil-pore water in the cultivated soil layer of the study field and those of the Ninh Co River during the rainy and dry seasons.

9.3.3. Soil properties

The properties of soils (0-20 cm) in the root zone are shown in Table 9.1. These data represent arithmetic average values from the nine sampling locations over the study field. However, for the deeper layers the data were average values for the three locations along the diagonal of the field. These analyses were carried out before the field was divided into two sub-fields to study the improved irrigation practice.

TABLE 9.1. PROPERTIES OF THE SOIL (0-20 CM) IN THE STUDY FIELD (AUGUST 2013)

Depth	Total content (g kg^{-1})				pH	Cation exchange (meq 100^{-1} g)					Particle size (g kg^{-1})		
(cm)	N	P	K	Cl^-	(KCl)	CEC	Na^+	K^+	Ca^{2+}	Mg^{2+}	Sand	Silt	Clay
0-20	2.4	1.6	5.2	0.7	5.4	5.34	0.41	0.10	1.89	1.96	28	853	119
20-40	1.2	1.5	3.6	1.1	5.8	5.04	0.56	0.05	1.80	1.98	26	843	131
40-60	0.8	0.7	3.2	1.5	6.5	4.96	0.67	0.04	1.84	2.04	61	804	135
60-80	0.5	0.5	3.0	2.1	6.0	5.12	0.77	0.03	1.78	1.92	34	883	83
80-100	0.6	0.5	3.2	2.0	6.8	4.07	0.71	0.05	1.80	1.96	32	863	105

CEC, cation exchange capacity

Results are in good agrement with those determined by Pham Anh Tuan et al. [4]. Surface soil is slightly acidic (pH_{KCl} = 5.4) and represents a silty-clay texture by the USDA's classification. In the rainy season salt in the surface soil migrates downwards so that in the soil 40-60 cm depth the chloride concentration was double compared to that in the surface soil (Table 9.1). It seems that in the root zone desalination is occurring during the rainy season because the chloride concentration in water increases with increasing exchangeable sodium content in soil, while the concentrations of exchangeable calcium and magnesium do not change much with the increase of chloride concentration (Table 9.1 and Fig. 9.11). It was thought that the fresh irrigation water from the river dissolves salt entrapped in soil pores and the saline water diffuses downwards making the water in deeper soil layers more saline compared with the surface layer (Table 9.1).

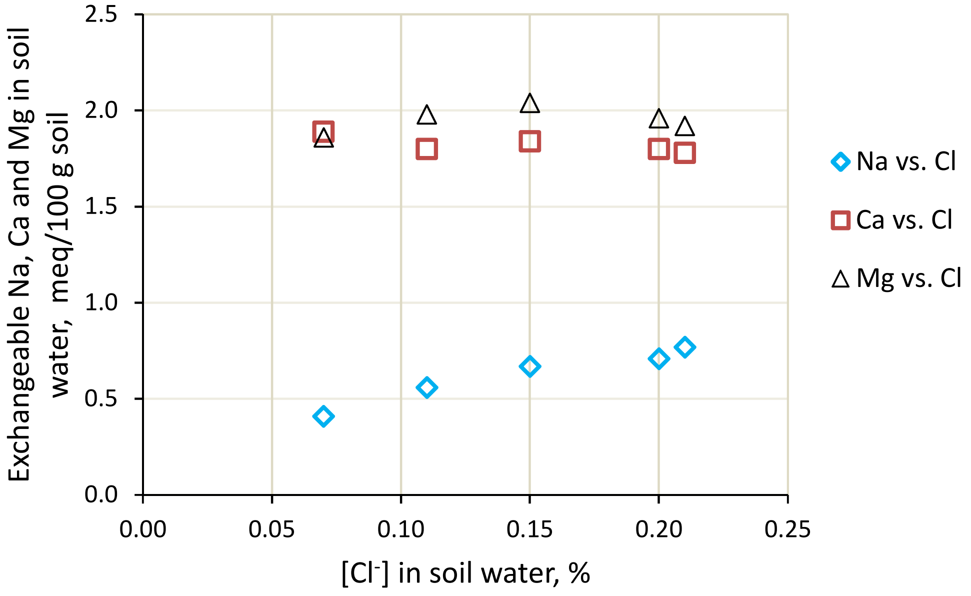

FIG. 9.11. Relationship between chloride concentration in water and exchangeable content of Na+, Ca2+ and Mg2+ in soil.

9.3.4. Influence of tide on the salinity in water within root zone in the study field

The variation of tide height and the level of the groundwater table in the study field in early September 2014 and March 2015 are shown in Fig. 9.12 and Fig. 9.13, respectively. The tide height was taken from the record of the Quang Phuc hydrological monitoring station located 50 km in the Northeast of the Red River's mouth [15]. The groundwater table in the root zone remained almost constant with the change of the tide height. A minor shift upwards of the groundwater table was seen for the both seasons, but it did not mean that seawater intruded into the field. The change in the groundwater table was thought to be due to rain that occurred hours before, as marked in the Figs.

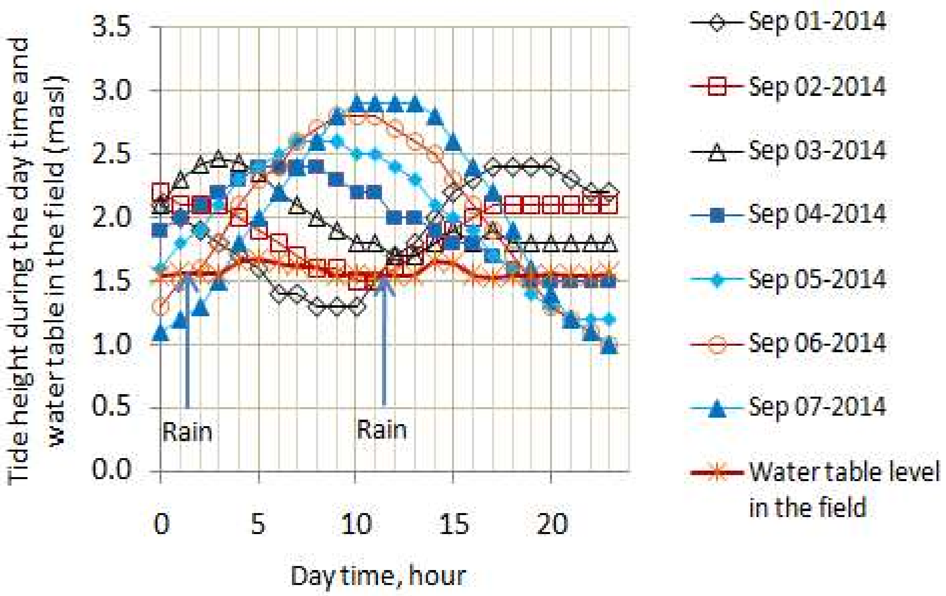

FIG. 9.12. The change of the tide height and groundwater table level (in m above sea level, masl) in the rainy season (Sept 2014).

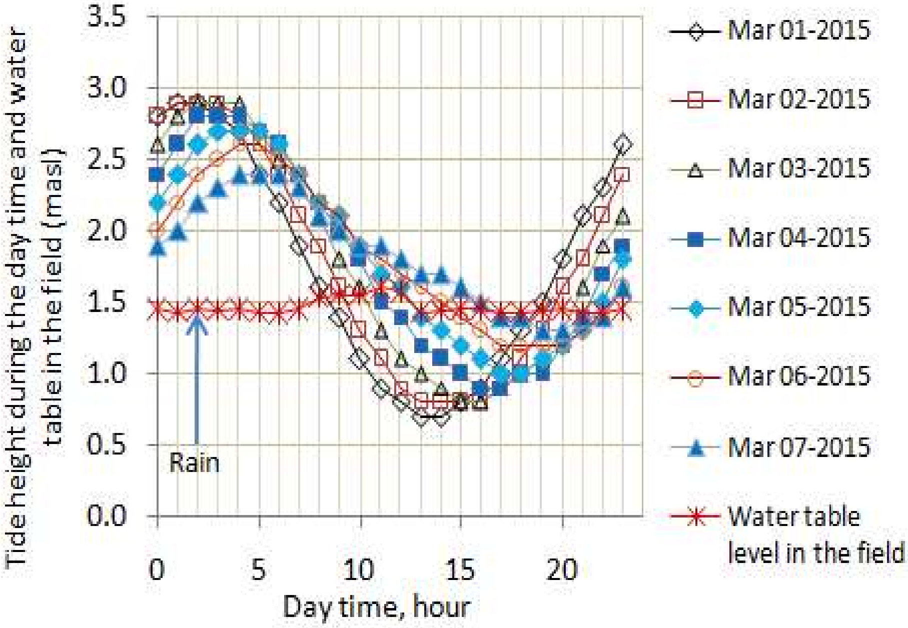

FIG. 9.13. The change of the tide height and groundwater table level (masl) in the dry season (March 2015).

In the dry season the groundwater table level was a slightly lower compared to the rainy season. The mean value of the water table in the dry season was 1.46 m (asl) but in the rainy season it was 1.54 m (asl). From Fig. 9.12 and Fig. 9.13 one may conclude that in the study area groundwater in the root zone is not affected by the sea. i.e. there is no seawater intrusion. The oxygen-18 signature in water within the root zone was similar to those of the rainwater and water from the Ninh Co River during both rainy and dry seasons, as shown in Fig. 9.14.

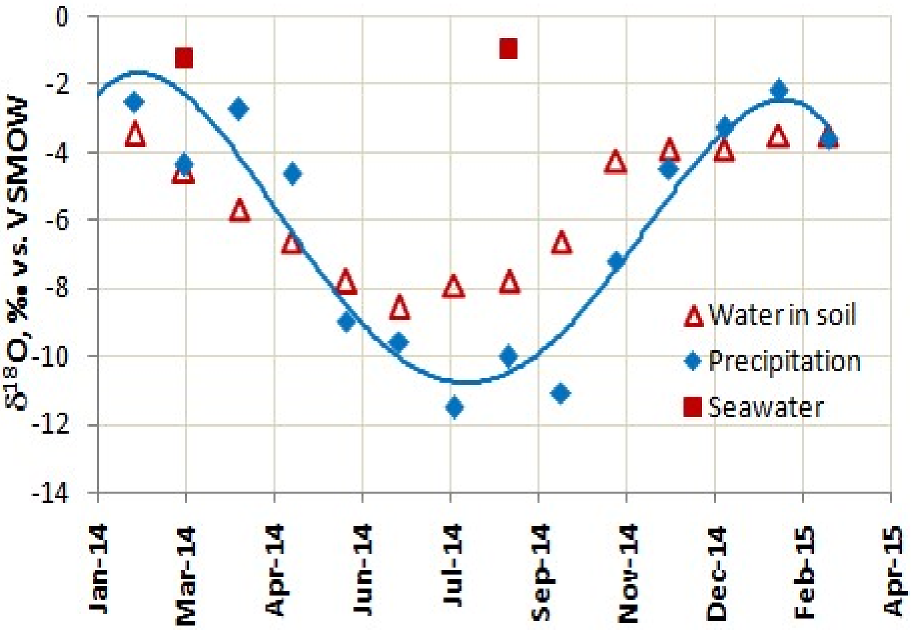

FIG. 9.14. The variation of the ^{18}O signature in water within the root zone, in seawater and in the precipitation over the study area for both rainy and dray seasons.

In between the two rice seasons, during the rainy season from June to September, the isotopic composition of ^{18}O in water within the root zone appeared to be more enriched compared to the precipitation (Fig. 9.14). This can be explained by the fact that about a month before harvesting the rice, the local farmers drained off surface water from their fields and after separating the grain from straw the stover was burned leaving the field bare and cracked under the hot weather. The cracked soil facilitates water loss within the root zone by evaporation that causes the isotopic composition of the heavy isotopes of water to be enriched.

The farming practice applied in the region could lead to the loss of water and could also disallow the salt dissolved in the irrigation water during the farming season to infiltrate downwards beyond the root zone (desalination). Then in between the two rice seasons (July-September) the salt migrates upwards under the influence of evaporation. The relationship of $\delta^{18}O$ *vs.* chloride concentration in water in the root zone is shown in Fig. 9.15. Clark and Fritz [9] and Gaye [16] have shown that variation in the enrichment of oxygen-18 in groundwater occurred with insignificant variation of chloride concentration due to the evaporation. Water evaporates leaving salt in the soil and in the new rice season when farmers irrigate with freshwater the salt again dissolves. However, the farmers do not wish to limit irrigation because of the tax on the water. With new rice varieties, the rice season usually prolongs for a short time, around 3 months. The limitation of freshwater and the short time period of the crop rotation reduces desalination. The end-result of is that the crop could be affected by the salt persisting in the root zone.

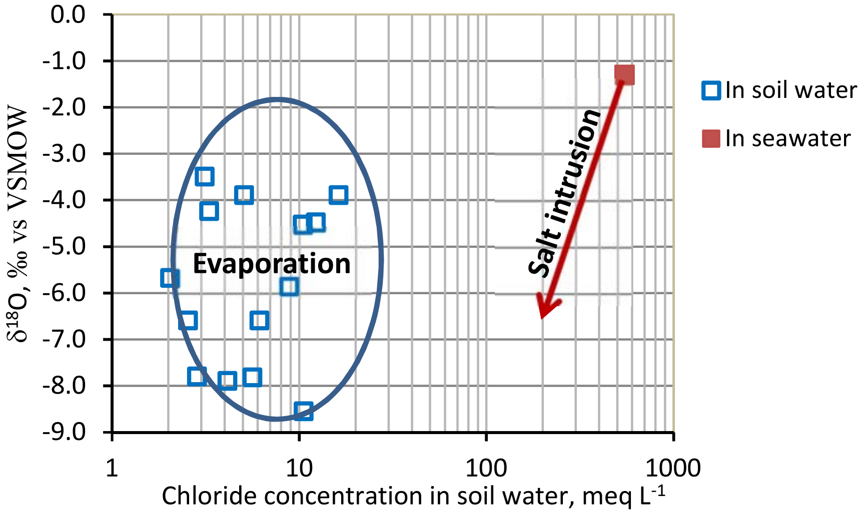

FIG. 9.15. Relationship of $\delta^{18}O$ vs. chloride concentration in the soil pore water.

The $\delta^{18}O$ signature in the soil water clearly showed that the traditional cultivation practice probably dissolves salt temporarily but then is re-adsorbed onto the soil surface when water evaporates under the hot dry weather. At the present time, salt intrusion does not occur in the study region. This conclusion provided a way to develop an alternative practice to facilitate the desalination in the root zone to eliminate the effect of salt on the yield of the crops.

9.3.5. Comparison of the chemistry and $\delta^{18}O$ signature in soil water within the root zone in the reference and alternative irrigation sub-fields

The alternative irrigation practice involved maintenance of water in the field year-round in order for the salt to continuously dissolve and infiltrate downwards beyond the root zone by gravity. The chemistry and $\delta^{18}O$ signature in water within the root zone of the reference field in the summer-autumn (S-A) and winter-spring (W-S) seasons is shown in Table 9.2. Similar data for the field where the alternative irrigation practice was applied is given in Table 9.3, together with data of the local precipitation (P) in the two seasons.

The pH of water in root zone of the reference field was 8.3 and it differed from the sub-field with alternative irrigation practice which was 6.7 (Tables 9.2 and 9.3). The increase in pH in water was the result of salt dissolution and Na^{+}-Ca^{2+} cation exchange. The concentration of sodium and chloride in water in the root zone of the reference sub-field was much higher compared to the field with the alternative irrigation practice.

TABLE 9.2. THE CHEMISTRY AND ISOTOPIC SIGNATURE OF OXYGEN-18 ($\delta^{18}O$) IN WATER WITHIN THE ROOT ZONE OF THE REFERENCE SUB-FIELD IN THE SUMMER-AUTUMN (AUG-2015-2016) AND WINTER-SPRING (MAR-2016-2017) SEASONS

Sample	Time	pH	Concentration (mg l^{-1})									$\delta^{18}O$
ID			Na^{+}	K^{+}	Ca^{2+}	Mg^{2+}	NH_4^{+}	Cl^{-}	NO_3^{-}	SO_4^{2-}	HCO_3^{-}	(‰)
SW	Aug 15/16		11	2.3	20	7.3	1.5	15	0.3	25	110	–8.2
	Mar 16/17	7.5	16	3.2	19	7.3	0.8	14	0.2	16	114	–5.6
RZW1	Aug 15/16		108	11	69	11	14	277	15	4.8	120	–7.3
	Mar 16/17	8.3	163	16	48	12	11	328	13	2.6	124	–4.2

SW, surface water from the Ninh Co River; RZW1, water within the root zone

TABLE 9.3. THE CHEMISTRY AND ISOTOPIC SIGNATURE OF OXYGEN-18 ($\delta^{18}O$) IN WATER WITHIN THE ROOT ZONE OF THE SUB-FIELD IN WHICH THE ALTERNATIVE IRRIGATION PRACTICE WAS APPLIED IN THE SUMMER-AUTUMN (AUG-2015) AND WINTER-SPRING (MAR-2016) SEASONS

Sample ID	Time	pH	Concentration (mg l^{-1})									$\delta^{18}O$ (‰)
			Na^{+}	K^{+}	Ca^{2+}	Mg^{2+}	NH_4^{+}	Cl^{-}	NO_3^{-}	SO_4^{2-}	HCO_3^{-}	
SW	Aug 15/16		11	2.3	20	7.3	1.5	15	0.3	25	110	–8.2
	Mar 16/17	7.5	16	3.2	19	7.3	0.8	14	0.2	16	114	–5.6
RZW2	Aug 15/16		5.8	7.7	24	7.2	14	31	13	5.2	140	–8.0
	Mar 16/17	6.7	6.1	7.1	27	6.3	12	47	13	4.3	138	–4.4
P	Aug 15/16		0.5	0.4	1.8	0.1	nd	2.6	0.2	nd	nd	–11.9
	Mar 16/17	6.2	0.5	0.4	2.6	0.2	nd	3.8	0.4	nd	nd	–5.4

SW, surface water from the Ninh Co River; RZW1, water within the root zone; P, precipitation; nd, not determined

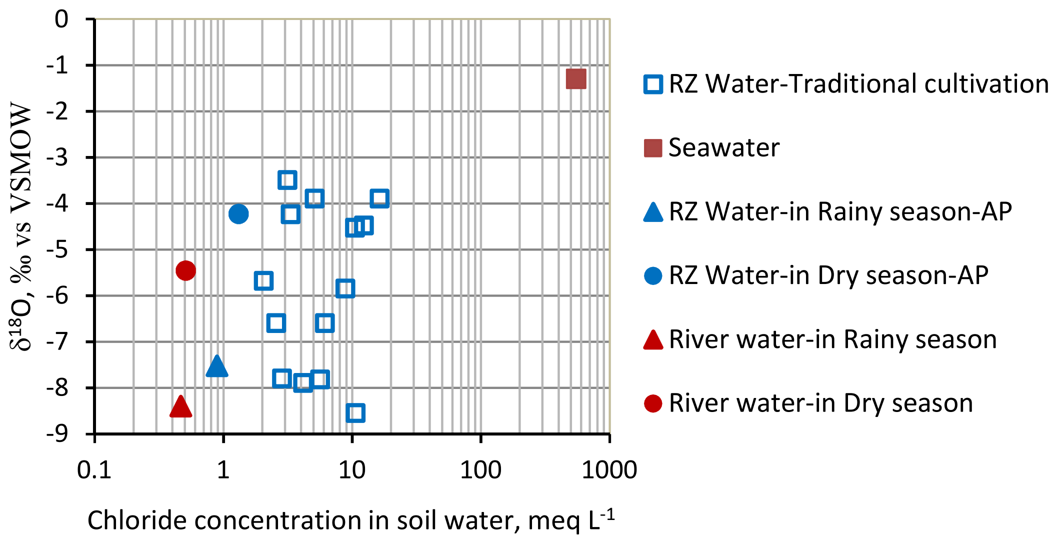

FIG. 9.16. The chloride concentration in water within the root zone (RW) of the sub-field with the new irrigation practice (NIP).

For the field with new irrigation practice it seems that after four rice seasons much salt in the surface soil was washed out by the irrigated water and most saline water infiltrated beyond the root zone leaving the water there as fresh as river water with salinity less than 100 mg l^{-1} (Table 9.3). Assuming that water in the root zone was a mixture of the local precipitation and river water and based on the pH of the two types of water (Table 9.3), one can compute the contribution of each type of water into the mixing water by a two-end member model. Therefore, in the W-S season (in March 2016) in the sub-field with the modified irrigation practice the water in the root zone comprised of around 40% of river's water and around 60% of the precipitation that probably remained from the previous S-A season. In both seasons and both sub-fields the heavy isotope of oxygen in soil water in the rooting zone was always more enriched compared to that in the river water (Tables 9.2 and 9.3) implying evaporation of water under the hot weather conditions. By maintaining irrigation water in the field during the whole year, salt in the root zone dissolves and migrates to deeper soil layers under rice cultivation (Fig. 9.16).

In the field with new irrigation practice the chloride concentration in water within the root zone was 31.1 and 46.5 mg l^{-1} (0.89 and 1.31 meq l^{-1}) for the S-A and W-S cultivation seasons, respectively. Meanwhile in the reference field the chloride concentration was as high as 277 mg l^{-1} (7.8 meq l^{-1}) and 328 mg l^{-1} (9 meq l^{-1}) in the S-A and W-S seasons, respectively (Tables 9.2 and 9.3, and Fig. 9.16). By maintaining fresh irrigation water in the field during the whole year favorable condition were created for desalination, with the salt dissolving and infiltrating downwards beyond the root zone. The productivity of the crop could thus be improved. The yield of rice grain produced from the two sub-fields is presented in Table 9.4.

TABLE 9.4. THE YIELD OF RICE GRAIN (T HA^{-1}) PRODUCED FROM THE REFERENCE SUB-FIELD AND THE SUB-FIELD IN WHICH THE NEW IRRIGATION PRACTICE WAS APPLIED FOR THE S-A AND W-S CULTIVATION SEASONS DURING 2015 THROUGH 2017

Field	Summer-Autumn season			Winter-Spring season		
	Empty grain	Full grain	Total	Empty grain	Full grain	Total
Reference	0.28 ± 0.11	5.63 ± 0.23	5.91 ± 0.17	0.37 ± 0.13	5.47 ± 0.16	5.84 ± 0.15
New practice	0.14 ± 0.12	5.77 ± 0.25	5.91 ± 0.18	0.15 ± 0.14	5.63 ± 0.14	5.78 ± 0.14

The yield of full grain in both fields in the S-A cultivation season was higher than that for the W-S season (Table 9.4). This might be due to the difference in the weather conditions between the two seasons. In 2015-2017 the air temperature during the winter on average was as low as 15-16 ºC and this was not preferable for rice to develop its root system, particularly in the early stage, from days 1 to 10 after transplanting. On the other hand, the yield of total grain produced from the two sub-fields in the two seasons was comparable to each other, ranging from 5.8 to 5.9 t ha^{-1} (Table 9.4). However, the amount of empty grain in the reference field varied from 280 to 370 kg ha^{-1} which was almost two times more than that from the field of the new irrigation practice. It seems that the new irrigation practice improved the mobility of nutrients for the crop to successfully produce full grain leading to the increase of the yield of the edible grain.

9.4. CONCLUSIONS

The salinity in soil-pore water within the root zone in rice paddies in the coastal region of the Hai Hau district, Nam Dinh province, North Vietnam is associated with the marine sediment which existed since the Red River delta was formed. Irrigation water makes the salinity in the sediment pores to migrate/diffuse into the water. However, the traditional farming practice including drainage of the irrigation water before rice harvesting followed by gathering and burning the straw does not allow the saline water to infiltrate downwards, and thus the salinity persists in the soil within the root zone. It is strongly recommended that the irrigation water should not be drained, and the field should not be cleaned in order to reduce evaporation that created a hydraulic pressure that caused saline water to infiltrate beyond the root zone by gravity.

ACKNOWLEDGEMENT

We thank the International Atomic Energy Agency (IAEA) for providing financial support under Research Contract No. 17915. The research team would like to express their gratitude to the family of Mr. Tuong, Thinh Long town, Hai Thinh commune, Hai Hau district, Nam Dinh province, for offering the rice field for this experiment.

REFERENCES

[1] PRUSZAK, Z., et al., Coastal Processes in the Red River Delta Area, Vietnam, Internal Report, Institute of Mechanics, National Center for Natural Science and Technology of Vietnam, Hanoi (2001).

[2] MARD, Ministry of Agriculture and Rural Development of Viet Nam, The current farming achievement in the Red River and Mekong Rivers deltas, A Report to the Government of the Ministry for the five-year Plan 2005–2010 (2010).

[3] FONTENELLE, J-P., Water management decentralization in the Red River delta, Vietnam: An uncompleted transition process toward local governance, Paper for the 8th Biennial IASCP Conference, Bloomington, May 31 to June 4 (2001).

[4] PHAM ANH TUAN, Properties of Soils in Hai Hau District, Namdinh Province, J. Sci. Dev. **11** (2013) 532–541.

[5] NCHMF, National Center for Hydro-Meteorological Forecastings of Vietnam (2014). http://www.nchmf.gov.vn Retreived on July 20, 2017.

[6] NDDARD, Nam Dinh Department of Agriculture and Rural Development: Irrigation and Drainage Planning for the Agricultural Sector of the Nam Dinh province-vision to 2030, Nam Dinh, Viet Nam (2011) 113 p.

[7] IAEA, International Atomic Energy Agency, Water and Environment Newsletter of Isotope Hydrology Section, Issue No. 16, Vienna, Austria (2002).

[8] DANG DUC NHAN, et al., The hydrochemical process to cause high salinity in soil water within root zone of a rice paddy in the Hai Hau district, Nam Dinh province (North Viet Nam), Progress Report to the IAEA for Research Contract No. 17915-R1 (2015) 6 p.

[9] CLARK, I.D., FRITZ, P., Environmental Isotopes in Hydrology, Lewis Publishers, Boca Raton (1997) 311 p.

[10] APPELO, C.A.J., POSTMA, D., Geochemistry, Groundwater and Pollution, 2nd Edn., Balkema Publisher, Amsterdam (2007) 649 p.

[11] OLMSTEAD, L.B., et al., A pipette method of mechanical analysis of soils based on improved dispersion procedure, Technical Bulletin No.170, USDA, Washington D.C. (1930) 23 p.

[12] ISA, Institute of Soil and Agrochemicals, Manual for Analyses of Soil, Water, Fertilizers, and Plants, Publishing House of Agriculture, Ha Noi (1998). In Vietnamese.

[13] NHAN, D.D., et al., Water use efficiency of coffee (*Robusta*) under mulch and drip irrigation on the Tay Nguyen Plateau, Viet Nam. In: Proc. FAO/IAEA Int. Symp. "Managing soils for food security and climate change adaptation and mitigation", FAO, Rome (2012) 303–308.

[14] COPLEN, T.B., Reporting of stable hydrogen, carbon, and oxygen isotopic abundances, Pure Appl. Chem. **66** (1994) 273–276.

[15] NCMH, National Center for Monitoring the Hydrology in the Marine Coast, The hydrological regime along the marine coast, North Vietnam in the 2014 and 2015 years, Annual Report to the General Directorate of Meteorology and Hydrology of Vietnam, Ha Noi (2015).

[16] GAYE, C.B., Isotope techniques for monitoring groundwater salination, Paper presented at the First International Conference on Saltwater Intrusion and Coastal Aquifers-Monitoring, Modeling, and Management, Essaouira, Morocco, April 23–25 (2001) 11 p.

10. SOIL SALINITY MANAGEMENT FOR RICE PRODUCTION IN THE MEKONG RIVER DELTA, VIET NAM

D.K NHAN, TRAN HUU PHUC, TRAN VAN DUNG
Can Tho University
Ha Noi, Vietnam

DANG DUC NHAN
Atomic Energy Institute
Ha Noi, Vietnam

L.K. HENG
International Atomic Energy Agency
Vienna, Austria

Abstract

Soil salinization from sea water intrusion is a big threat for sustainable rice production in the coastal Mekong Delta of Vietnam. An on-farm study quantified the effectiveness of flushing salinity from paddy soil and identified strategies for rice production under salinity intrusion, by applying oxygen isotopic technique combined with hydro-geological and bio-economical methods. The study consisted of two on-farm trials. The first trial investigated salinity source and the effectiveness of soil desalinization using isotopic oxygen-18 technique. The second trial tested for approriate soil nutrient management practices for rice production under salinity. Three fertilizer application treatments were: (1) farmer's fertilizer application practice, (2) applying 50% nitrogen (N) and 300% potassium of (1), and (3) applying 25% nitrogen (N) and 300% potassium of (1) plus 400 kg commercial organic fertilizer per hectare. Fifteen farm plots measuring 1000 m^2 each were used for the experimentation.

Soil desalinization using rainwater and evaporation strongly influenced salinity in the root zone of rice. Rainwater was the important source while irrigation canal water was not reliable for soil desalinization. Only about 40% of saltwater in the root zone was flushed out in the rainy season. Potassium and organic fertilizer application to rice highly facilitated flushing sodium from the root zone and improving rice yields. Organic fertilizer application, however, was not economically feasible. Rice yields did not significantly change with nitrogen application reduction by 50%. The combined application of the isotopic technique, hydro-geological and bio-economical methods is useful to explain the interactions among soil – water – crop for dealing with salinity intrusion in low land regions.

10.1. INTRODUCTION

Salinity is a serious abiotic stress of crop productivity world-wide. More than 800 million ha of land throughout the world are salt-affected [1], significantly reducing crop yield, especially for rice in coastal low-lying areas [2–6]. In Vietnam, about 2.3 million ha rice land, of which 74% is located in the Mekong Delta, is salinity-affected from seawater intrusion [6, 7]. Variations in the hydrological cycle and rising sea levels from a warmer climate will significantly increase soil salinity, resulting in the expansion of areas affected by this problem [4, 6].

Adaptive measures of agricultural production to salinity include "*hard*" measures (i.e. salinity-control structure) and/or "*soft*" measures (i.e. cropping practices) [8, 9]. The former needs costly investments while the latter is considered relative more cost-effective and flexible to socio-economic and environmental uncertainties, prior to infrastructure investments [9]. In the Vietnamese Mekong Delta with seawater intrusion since 1999, adaptative cropping practices such as rice-based farming systems, salinity-tolerant rice varieties, soil tillage and agro-chemical applications to facilitate flushing soil salinity using freshwater from precipitation and/or irrigation canals have been considered [10]. Salinity-tolerance capacity differs with varieties and growth stages [2, 11], and most varieties can tolerate up to a salinity concentration of 4% [6, 12]. Scientific evidence has clearly shown that the application of potassium fertilizer, gypsum or organic matter can facilitates both flushing soil salinity and rice plants well tolerant to high sodium levels [10, 13, 14]. The effectiveness of soil desalinization before rice establishment is critical to achieve potential grain yield. This, however, depends upon soil properties, freshwater sources, drainage and evaporation, which differ greatly from place to place. Thus, an understanding of interactions in the whole soil (salinity and nutrients) – water – crop system is necessary. Such knowledge is still limited for rice production with salinity intrusion in the Mekong Delta.

The oxygen isotopic composition in natural waters is a tool to investigate the source of various water types and possible interconnection between them. Many studies have used the variation in oxygen isotopes to understand the mechanism of seawater intrusion into groundwater [15–18]. The isotopic signatures vary with water sources. The application of oxygen isotopic analysis to understanding seawater intrusion in surface water has been little used in the Mekong Delta. On-farm trials conducted under a range conditions were aimed to answer three major questions: (1) where does the salt in the root zone come from? (2) which is the major water source for flushing salinity, rain water or canal water? and (3) what are major adaptive strategies for rice production under salinity intrusion, technologically? Oxygen isotopic and hydro-geological techniques were applied. This work was part of a larger study aimed at optimizing on-farm management practices for rice production to adapt to salinity in the Mekong Delta, Vietnam.

10.2. MATERIALS AND METHODS

10.3. STUDY SITES

Three study sites were selected in the coastal zone: (1) My Xuyen district, Soc Trang province, (2) Thoi Binh district and (3) U Minh district, Ca Mau province (Fig. 10.1). Site 1 is strongly affected by the tidal effect from the estuary, while sites 2 and 3 are relatively low-lying and annually inundated in October and November. For all three sites, soils are affected by salt from January to July, when farmers grow shrimp in the paddy fields, using saltwater from the sea (Table 10.1). Rice is grown in the wet season, relying on rainwater. After harvesting shrimp, farmers use rainwater to flush salinity in the topsoil to a level low enough to establish the rice crop afterwards. The year 2015 was abnormally dry with a total rainfall of 1378 mm, compared to 1826 mm in the previous year (Fig. 10.2). Rice production in rotation with shrimp is considered as an adaptive measure to projected salinity intrusion in the Mekong Delta [10]. Soil desalinization before crop establishment, however, is very important to ensure rice production.

10.3.1. Experimental design

10.3.1.1. The effectiveness of soil desalinization

There were two trials. The first trial aimed to determine the source of salinity in soil and to test the effectiveness of soil desalinization in the paddy field. A plot of about 5 ha was used at sites 1 and 2 each. Devices were installed for sampling water from the root zone for analysing oxygen-18 ($\delta^{18}O$) and chloride in water. The relative abundance of oxygen-18 is expressed as the deviation (δ) between the ratio of the sample and the same ratio in an internationally accepted standard. In the case of stable isotopes of oxygen in water samples, the reference material is a standard ocean water sample called Vienna–Standard Mean Oceanic Water (VSMOW). Therefore, a negative (δ) value (lower than the standard) represents an isotopically depleted sample through dilution with freshwater from rainfall or canals; whereas a positive value represents an isotopically enriched sample through evaporation. In cases where the contribution of freshwater from rainfall or rivers into the sea is dominant, then the isotopic composition of seawater will be less than the mean seawater composition [19, 20].

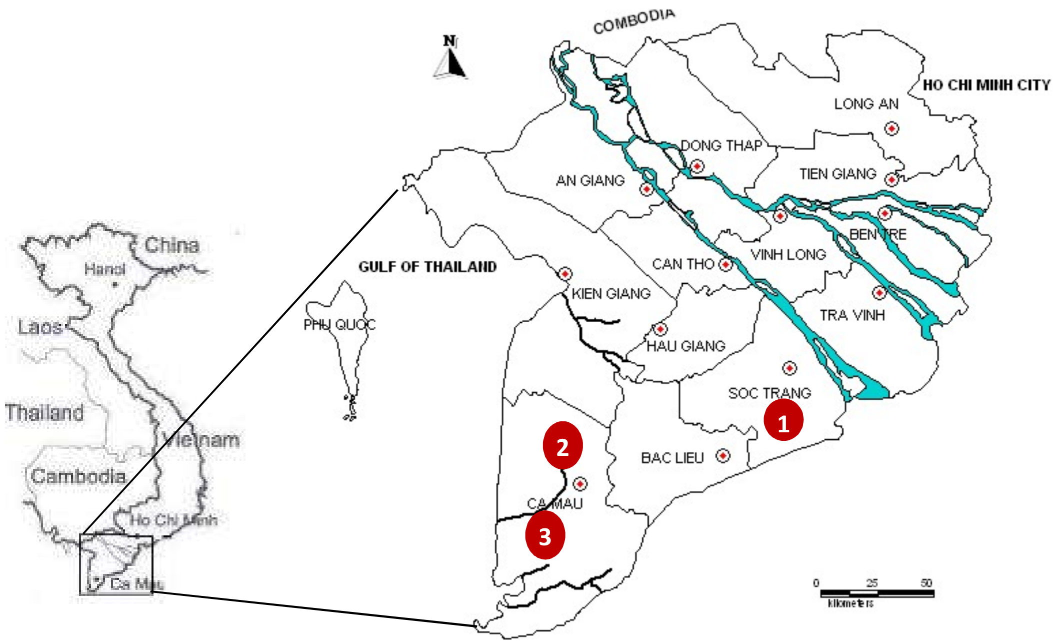

FIG. 10.1. Map of the Mekong Delta showing three study sites: (1) My Xuyen district (Soc Trang province), (2) Thoi Binh district and (3) U Minh district (Ca Mau province).

TABLE 10.1: MAJOR SOIL CHARACTERISTICS OF THE STUDY SITES

Sites	Soil types	Major characteristics	Major farming systems
Site 1	Typic tropaquepts, salic [21] or Salic Gleysols (Eutric) [22]	Well-developed and salinity-affected soil, oxidized soil horizon with jarosite mottles in 15 – 90 cm deep, reduced horizon starting below 140 cm and marine alluvial materials occurring from 120 cm deep	Rotational rice and shrimp
Site 2	Typic sulfaquepts, salic [21] or Salic Fluvisols (Epi Orthi Thionic) [22]	Less developed and salinity-affected soil, sulfuric horizon with jarosite mottles in 20 – 65 cm deep and pyrite materials from 100 cm deep.	Rotational rice and shrimp
Site 3	Sulfuric tropaquepts, salic [21] or Salic Gleysol [22]	Well developed, intermediately acidic and salinity-affected soil, oxidized soil horizon with jarosite mottles in 25 – 70 cm deep and pyrite materials from 90 cm deep.	Rotational rice and shrimp

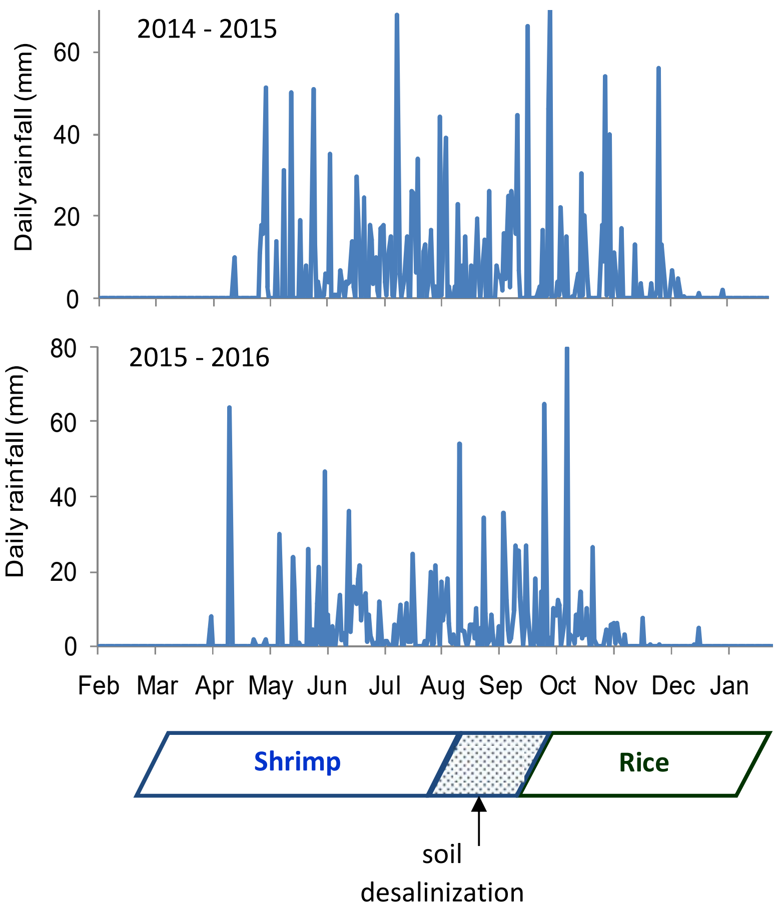

FIG. 10.2. Daily rainfall (mm) in Soc Trang province from February 2014 to February 2016, soil desalinization and cropping calendar of shrimp and rice (source: rainfall data from Soc Trang province weather station).

10.3.1.2. Soil nutrient management

The second trial aimed to determine an adaptive strategy of rice to production to salinity by appropriate fertilizer application. A total of 15 farmers participated in the trials on a voluntary basis. Seven farmers were located at site 1 and four farmers at sites 2 and 3 each. Each farmer offered one farm plot, which was split into three sub-plots, measuring about 0.1 ha each, with different fertilizer application techniques (treatments) as follows:

(1) farmer's fertilizer application rate (T1);
(2) applying 50% nitrogen (N) and 300% potassium (K) of T1 (T2);
(3) applying 25% nitrogen (N) and 300% potassium of T1 plus 400 kg commercial organic fertilizer per hectare (T3).

Urea, diammonium phosphate (DAP) and complete N-P-K (20-20-15) fertilizers were used. For T2 & T3, urea and potassium sulphate (K_2SO_4) were applied to adjust N and K application rates according to the pre-determined treatments, respectively. The commercial organic fertilizer contained organic matters (25%), total N (2%), total P (1%), K (2%), humic acid (0,5%) and other mineral elements. Practical fertilizer application rates varied with farmers. For T1, farmers applied an average of 86 kg N, 56 kg P and 30 kg K per ha and they did not use organic fertilizers at all. Fertilizer application rates of T2 and T3 varied among farms. The fields were harrowed and desalinized with rain water by alternate flooding and draining for about 30 days before seeding the rice.

10.3.2. Soil, water and rice sampling

To investigate soil salinity source and the effectiveness of soil desalinization, water samples from soil extract at 5-30 cm deep, field drainage, canals and rainfall were taken for $\delta^{18}O$ and chloride analyses in a monthly interval from November to January. A composite water sample from five sub-samples at five diferent locations each site per sampling time was used for the analysis. Sampling and analysing methods are the same as those applied in Nhan et al. (this TECDOC). Isotopic results were expressed as ‰ deviation (δ notation) relative to VSMOW with the analytical precision of ±0.2‰.

Besides $\delta^{18}O$, soil salinity dynamics were investiated through pH, EC, Na^+, Mg^{2+} and Cl^- analyses. Soil extract, field drainage and irrigation canal water were sampled at 15-day intervals from 30 days after seeding to 15 days before rice harvest. Soil extract was taken at the depth of 5-15 cm and 20-30 cm using a PVC tube (1.7 cm in diameter) and syringes installed in the field. Samples were taken from three representative plots at each site. Rice yields (14% moisture content) from the trial plots were sampled. In addition, rice yields from 10 farms of different farmers at each site were recorded as the reference.

10.4. RESULTS AND DISCUSSION

10.4.1. The salinity source and the effectiveness of soil desalinization

Saline water in the root zone of paddy fields was a mixture of sea water (from shrimp culture in the dry season), water from irrigation canals and rainwater. Sea water carried over in the irrigation canals. Each source is characterized by its $\delta^{18}O$ signature as presented in Fig. 3. The $\delta^{18}O$ in water from irrigation canals was around –4‰, and that in the local rainwater and sea water were –7.5‰ and –1‰ (*vs*. VSMOW), respectively. Building on data presented in Fig. 10.3, one can compute the contribution of each water source in the water budget within the root zone with the use of three end-members conservative mixing model. Let the contribution of the rainwater be x, and that from irrigation canals and the sea be y and z, respectively, then:

$$x + y + z = 1 \quad (1)$$

$$x*\delta^{18}O_r + y*\delta^{18}O_{ir} + z*\delta^{18}O_{sea} = \delta^{18}O_{sample} \quad (2)$$

$$x*[Cl^-]_r + y*[Cl^-]_{ir} + z*[Cl^-]_{sea} = [Cl^-]_{sample} \quad (3)$$

where "r", "ir" and "sea" stand for the local rainwater, irrigation and sea water, respectively; $[Cl^-]$ is the chloride concentration in the respective samples.

By using the equations 1-3, one can find that the contribution of the sea water during shrimp culture in the dry season was up to 60% of the total amount of water in the root zone of rice at site 1. At site 2, which is relatively more low-lying, the drainage was poor or sometimes absent. The saline water in the root zone, therefore, mostly remained and was diluted with captured rainwater. This implies that soil desalinization in practice was not effective enough to ensure normal rice production, due to unreliable rainfall and/or poor drainage. The question, therefore, is whether canal water can replace rainwater to flush salinity from the soil.

The effectiveness of using water from rainfall or irrigation canals to flush salinity from the soil was investigated. $\delta^{18}O$ values and chloride concentrations showed that canal water could not be used to desalinize the soil for rice crop establishment, particularly in a dry year with low rainfall like 2016. Chloride concentrations in canal water did not significantly differ from that in the drainage, and increased at the 3rd sampling (January), due to salinity intrusion from the estuary, especially at site 1 (Fig. 10.4). At both sites, soil water chloride decreased at the 2nd sampling (December), due to salinity dilution from rainwater and salinity flushing, and increased at the 3rd sampling, because of low rainfall and consequently limited salinity flushing, salt accumulation and saltwater intrusion from canals. The values of $\delta^{18}O$ in the drainage were higher than those in canal water, probably because of evaporation and low rainfall. The values of $\delta^{18}O$ in the drainage were higher than that in rainwater at most of sampling times.

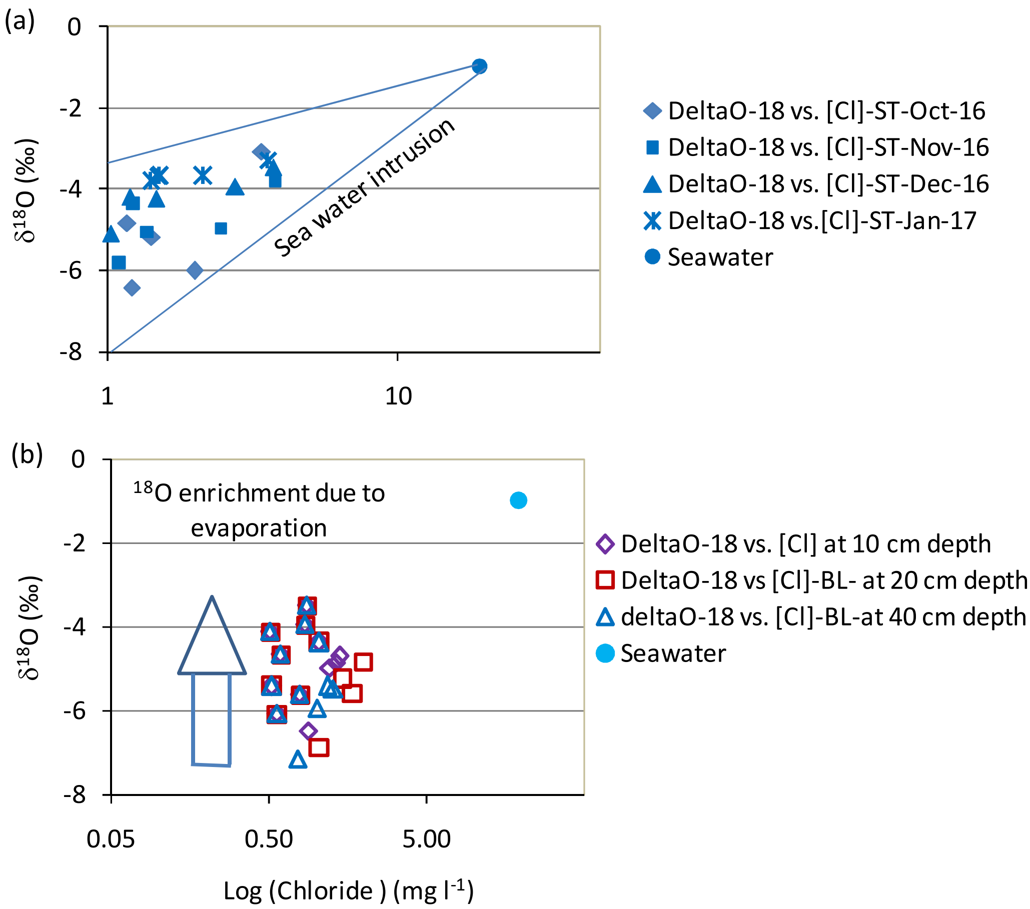

FIG. 10.3. Relationship between oxygen-18 signatures ($\delta^{18}O$) and chloride concentrations in water within the root zone of paddy rice at sites 1 (a) and 2 (b).

This is the first study located in monsoon tropical climate where the isotopic oxygen composition was applied to investigate paddy soil salinity in the Mekong Delta of Vietnam. The values of $\delta^{18}O$ in rain water were greater than the range from –6.6 to –9.0‰ as reported in previous publications [18, 23, 24]. The values of $\delta^{18}O$ in soil extracts are in the range of those in rain water and sea water, reflecting the mixture of sea water intruding the paddy fields in the dry season and of rain water in the wet season. Results suggest that soil desalinization for good establishment of the rice crop using rain water and/or local irrigation canals would be unpredictable or hardly feasible. The soil desalinization period should be longer and/or drainage should be done more frequently. This would make the rice production more risky from a longer rice cropping season together with salinity intrusion at the end of the rice crop. In addition, frequent drainage requires costly water pumping. Thus, multple solutions of soil desalinization are needed, with appropriate application of fertilizers to enable further flushing of soil salinity and better performance of rice.

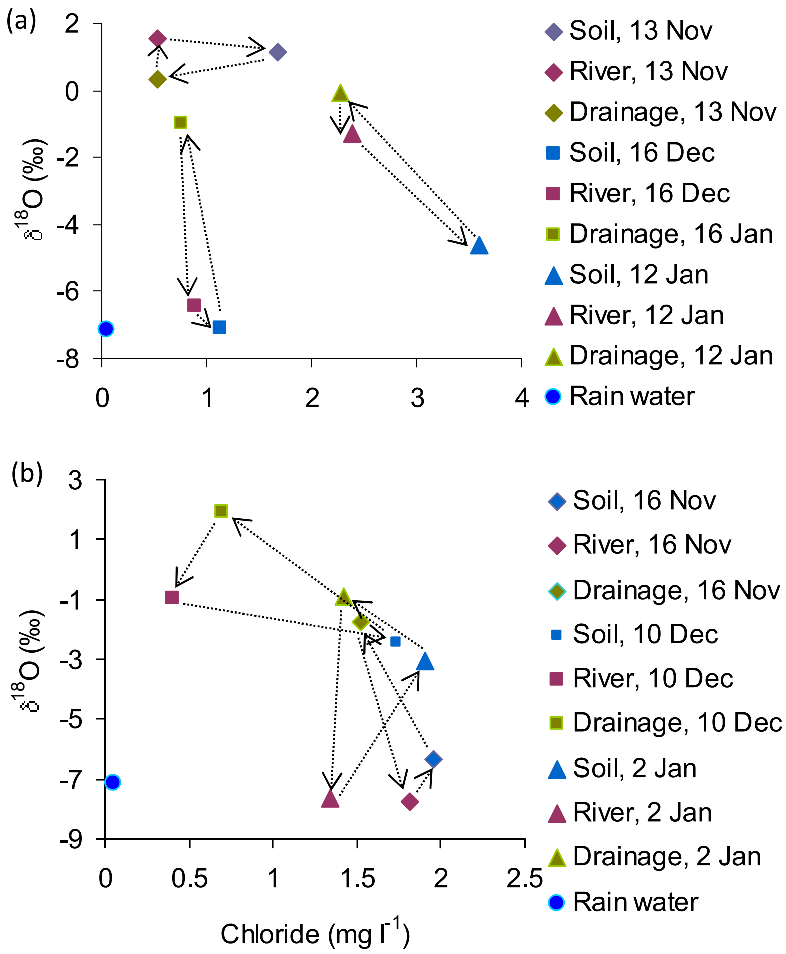

FIG. 10.4. Relationships between water $\delta^{18}O$ values and chloride concentrations by water source (i.e. soil extract, river and drainage water) and sampling time (i.e. date and month) at site 1 (a) and site 2 (b). Arrows show the relationships among soil – drainage – canal water per sampling time.

10.4.2. Effects of fertilizer application on soil salinity

The application of potassium (K) and organic fertilizers facilitated flushing sodium in the topsoil of the paddy fields. For site 1, sodium (Na^+), magnesium (Mg^{2+}) and chloride (Cl^-) in soil extracts had the same trend (Fig. 10.5a - h). The concentrations of Na^+, Mg^{2+} and Cl^- were higher with treatments (T) 2 and 3 than with T1 at 30, 60 and 75 days after seeding (DAS). More soluble Na^+, Mg^{2+} and Cl^- were available in the deep soil than topsoil at 45 and 75 DAS, due to a relatively higher density of saline water (Fig. 10.5a, c & e). This reflects the positive effect of potassium or organic fertilizer application and the effective flush of salinity for the topsoil.

Different fertilizer application treatments did not affect electrical conductivity (EC) in soil extracts till 60 DAS but the higher K and organic fertilizer application rates caused an increase in electric conductivity (EC) at 75 and 92 DAS in both surface and deep soil (Fig. 10.5g). The EC values increased with the growth of the rice crop to 60 DAS. Given EC values in the topsoil from 60 DAS onwards, the soil would be too salty (i.e. a salinity level of 5-6 g l^{-1}) for normal rice growth and yields [10, 25]. Deep soil extract EC was higher than topsoil extract EC at 45 DAS onwards, due to accumulation of salts during the rice crop. At the end of the rice crop, salinity flushing was limited by very little rain and high salinity contents in adjacent irrigation canals. Concentrations of Na^+, Mg^{2+} and Cl^- in the drainage of the fields (effluent) were the same as those in the irrigation canals at 30 and 45 DAS. More Na^+ and Mg^{2+} were present in the canals than in the drainage at 60 and 75 DAS. This confirms the aforementioned results that irrigation canal water could not be used to desalinize the soil before and during the rice crop.

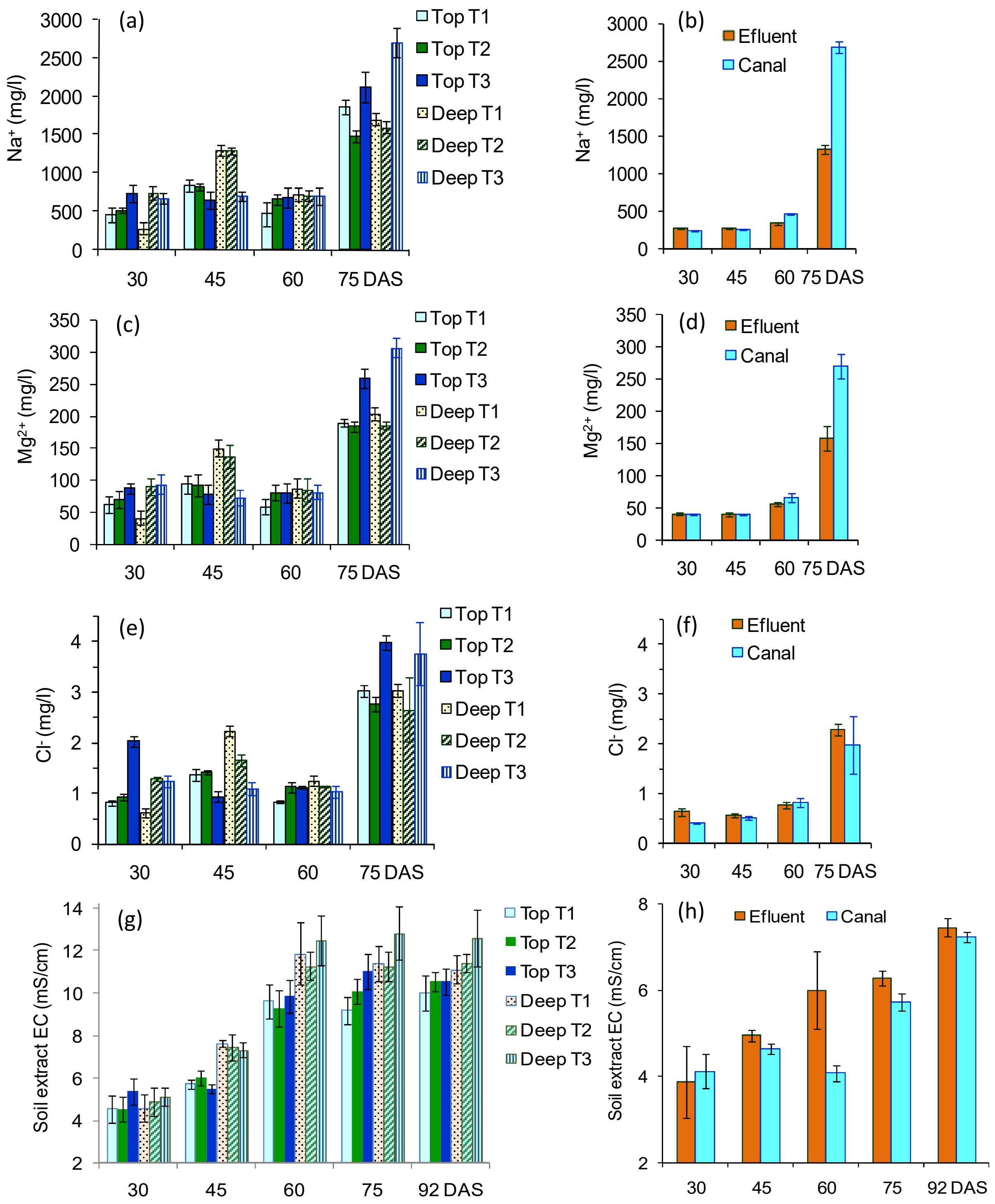

FIG. 10.5. Physico-chemical parameters in the extract of the topsoil (5-15 cm) and the deep soil (20-30 cm) by treatment (T) and sampling time (DAS = days after seeding) at site 1: T1 (farmer's fertilizer application), T2 (50% of N and 300% of K), and T3 (25% of N and 300% of K plus 400 kg organic fertilizer). The data are means with standard errors.

Unlike site 1, the effect of fertilizer application on soil salinity dynamics was less clear-cut at site 2. The effectiveness of potassium and/or organic fertilizer application on salinity flushing took place in the deep soil only (Fig. 10.6a, c & e). This is probably because the topsoil is less developed at site 2 than site 1.

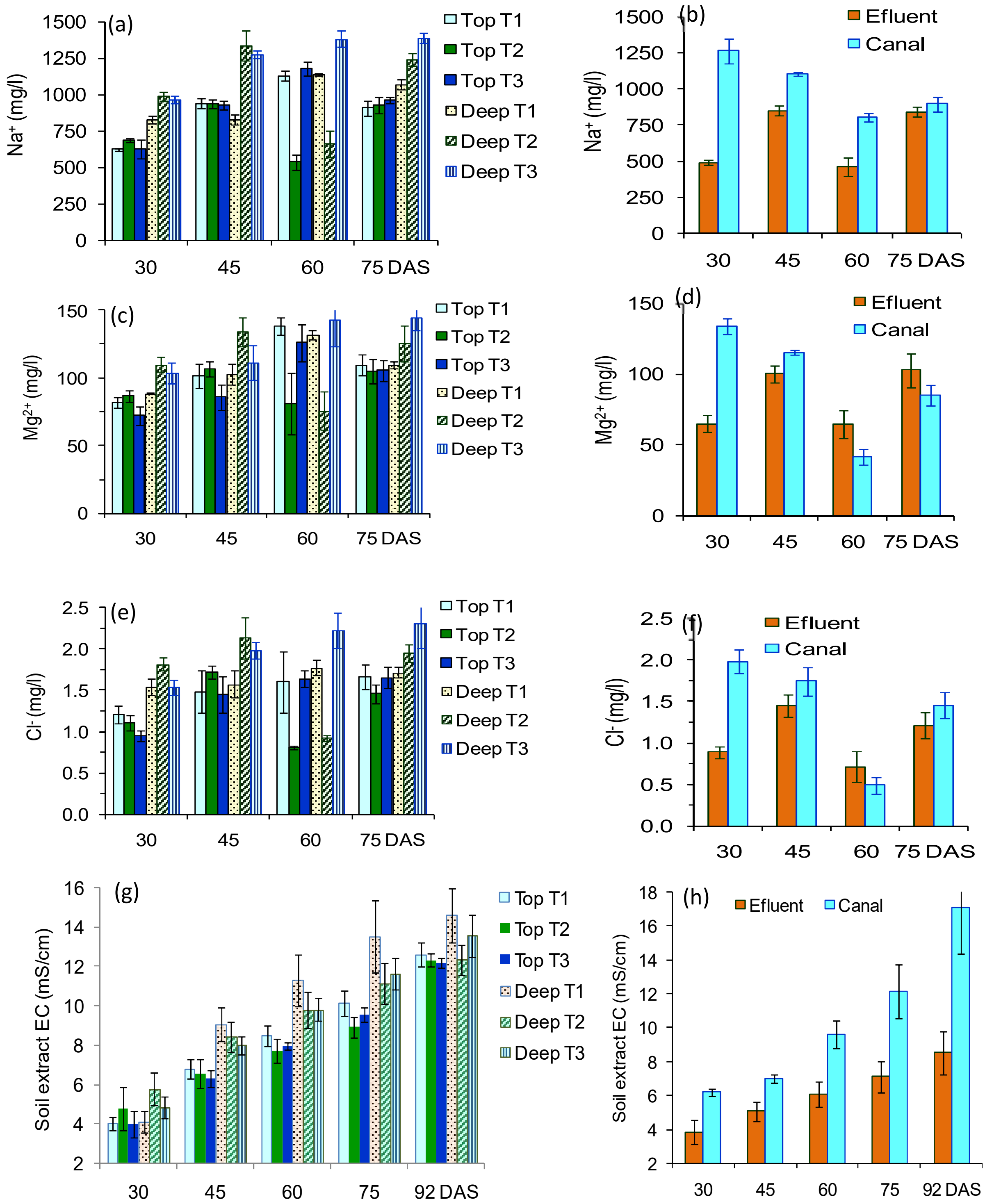

FIG 10.6. Concentrations of chemical parameters in the extract of the surface and deep soil by treatments (T) at the sampling time (DAS = days after seeding) at site 2 in Ca Mau province.

Different fertilizer application treatments did not significantly affect EC in soil extracts (Fig. 10.6g). The EC values steadily increased towards the end of the crop. Deep soil extract EC was higher than that in the topsoil at 45 DAS onwards. Like site 1, concentrations of Na^+, Mg^{2+} and Cl^- as well as EC in the drainage were lower than those in irrigation canals during the rice crop, implying that canal water could not be used for flushing soil salinity at this site as well (Fig. 10.6b, d, f & h). Regression analysis for combined data from sites 1 and 2 showed the positive effect of organic matter on flushing soil Na^+ (Fig. 10.7). Soil soluble Na^+ concentrations at 30 DAS were positively correlated with soil organic matter content. These results confirm the need of organic fertilizer application to amend soil physical properties [13, 26], and hence facilitate soil desalinization for rice production with soils of low organic matter contents.

Saline intrusion is a naturally occurring phenomenon in the coastal Mekong Delta, even in the absence of shrimp farming. In the wet season, farmers flush salts from the topsoil mostly relying on rainwater and discharge effluent to adjacent canals or rivers by gravity or pumping. The current study revealed that salinity accumulation in deep soil is a major constraint for rice production in a dry year under climate change, or in the case of gradual intensification of shrimp farming in the dry season.

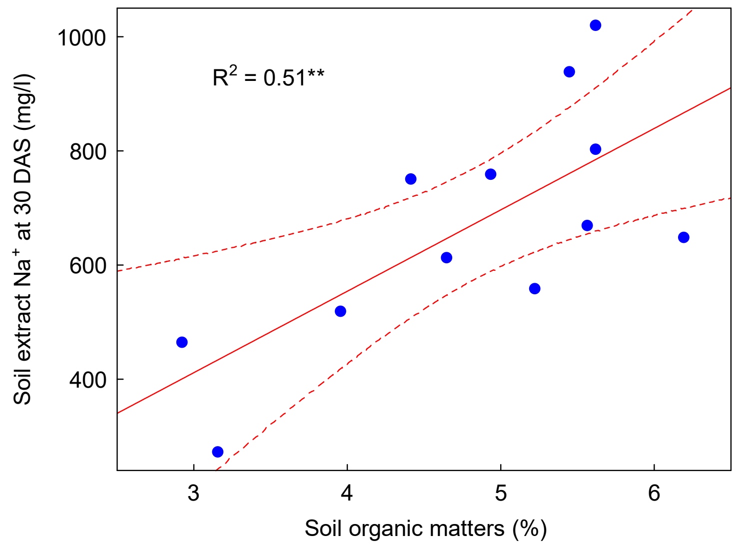

FIG. 10.7. The relationship between organic matter contents and sodium extract in soil. The regression line with 95% confidence limits with significance level at 1%.

10.4.3. Rice yield and profit

The application of potassium and organic fertilizers improved rice yields under salinity. Rice yielded higher with the higher application level of potassium (T2) and/or organic fertilizers (T3) (Fig. 10.8a). Rice yields did not significantly decrease by reducing nitrogen application rate up to 75% of farmer's practice. This indicates that farmers applied a surplus rate of nitrogen to the rice crop and/or that available nitrogen in the soil was abundant for the current rice practice. The average rice yield in the community of the study site was lower than those of the trial fields at sites 2 and 3, probably because of poor desalinization of soil and/or salinity intrusion at the end of the rice crop. These findings confirm previous studies that the application of potassium fertilizer enables both flushing Na^+ from the soil and promotes tolerance of rice to salinity [10]. Rice yielding higher with organic fertilizer application is probably due to its effect on improving soil physical properties and hence flushing more salts from the soil [13, 26], as well as possibly providing micro-elements for better plant growth.

Compared with farmer's fertilizer practice (T1), the high rate of potassium application was economically viable (Fig. 10.8b). The economic feasibility of commercial organic fertilizer application was low, even by reducing 75% of nitrogen input cost, due to the high input cost of commercial organic fertilizer. Organic fertilizer application was not economically viable in the area with organic-matter-rich soils like site 3. Farmers lost production without appropriate salinity management in the dry year 2016. Optimal nitrogen application for rice production is necessary, both economically and environmentally [27–29].

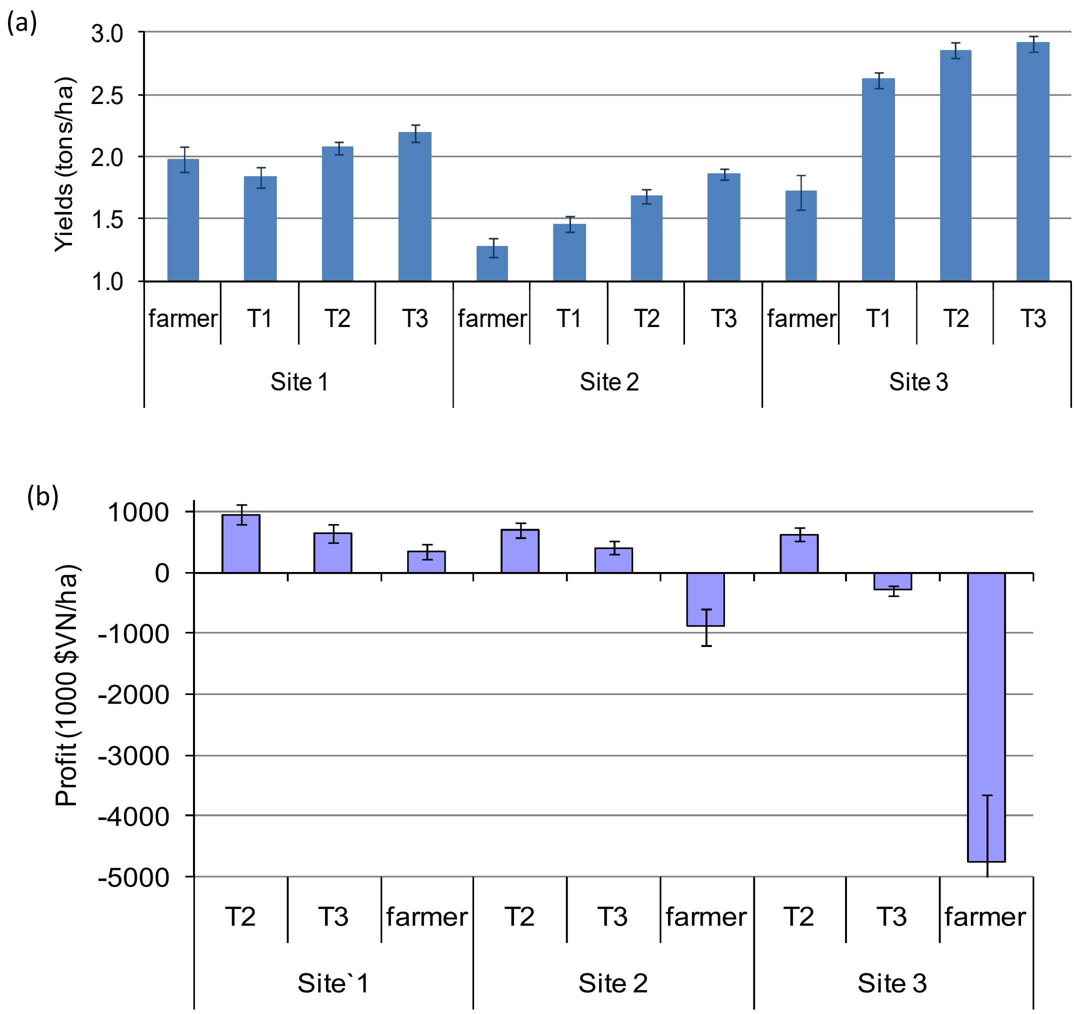

FIG. 10.8. Paddy yields (a) and economic profitability (b) by fertilizer application treatments. For economic feasibility assessment, T1 is used as the reference. Treatment "farmer" means the average of 10 surrounding fields under local farmers' practice. Data are means with standard errors. One Euro = 26,700 $VN.

10.5. CONCLUSIONS

This is the first study quantifying the effectiveness of flushing salinity from paddy soil and identifying adaptive strategies for rice production under salinity intrusion by applying the oxygen isotope technique in combination with physico-chemical soil and water analyses, and bio-economical methods in the Mekong Delta. The saltwater within the root zone of rice comes from sea water intruding in the dry season. Rainwater, but not irrigation canal water, is the important source for soil desalinization. Soil salinity flushing, however, was ineffective because of low rainfall within a short period and high evaporation rates under the dry climate. Canal or river water was too salty to be used for desalinizing the soil. Soil nutrient management, therefore, is a supporting solution for improving the resilience of rice production to projected climate change and sea level rise in the future.

Optimal application of nitrogen, potassium and organic fertilizer application to rice is of great importance to both soil desalinization and rice production and profitability. Potassium and organic fertilizer application facilitated flushing sodium out of the root zone of rice through physical and chemical mechanisms. Rice yielded higher with potassium and organic fertilizer application. Organic fertilizer application, however, was not economically feasible, due to its high input cost. The use of low-cost organic fertilizers is of great importance in flushing salinity and improving soil fertility. In addition, optimal nitrogen application for rice production is necessary, both economically and environmentally. The current study shows that the combined application of isotopic techniques, hydro-geological and bio-economical methods is a useful approach for understanding the interactions among soil, water and crop response for dealing with salinity intrusion in lowland regions.

ACKNOWLEDGEMENTS

The present work is as part of the project "*Landscape Salinity and Water Management for Improving Agricultural Productivity*" (D1.20.13), funded and coordinated by the Soil and Water Management & Crop Nutrition Section of the International Atomic Energy Agency (IAEA). The Mekong Delta Development Research Institute and the Department of Soil Sciences (Can Tho University) contributed staff and laboratory facilities to the implementation of the study. Local farmers and extension staff wholeheartedly participated in the study.

REFERENCES

[1] FAO (Food and Agriculture Organization of the United Nations), Land and Plant Nutrition Management Service (2008). Retrieved from http://www.fao.org/ag b/agl /agll/spush/

[2] ZENG, L., et al., Timing of salinity stress effects rice growth and yield components, Agric. Water Manage. **48** (2001) 191–206.

[3] MAHAJAN, S., TUTEJAN, N., Cold, salinity and drought stresses: An overview, Arch. Biochem. Biophys. **444** (2005) 139–158.

[4] HINKEL, J., et al., Coastal flood damage and adaptation costs under 21st century sea-level rise, Proc. Nat. Acad. Sci. USA **111** (2014) 3292–3297.

[5] CLARKE, D., et al., Projections of on-farm salinity in coastal Bangladesh, Environ. Sci. Processes Impacts **17** (2015) 1127–1136.

[6] SMAJGL, A., et al., Responding to rising sea levels in the Mekong Delta, Nature Climate Change **5** (2015) 167–174.

[7] NGUYEN, T.B.Y., et al., Salinity intrusion and rice production in Red River Delta under changing climate conditions, Paddy Water Environ. **15** (2017) 37–48.

[8] PELLING, M. Adaptation to Climate Change: From Resilience to Transformation, Routledge, Abingdon, Oxon. UK (2011).

[9] RICKARDS, L., HOWDEN, S.M., Transformational adaptation: agriculture and climate change, Crop Pasture Sci. **63** (2012) 240–250.

[10] NHAN, D.K., et al., Rice production response and technological measures to adapt to salinity intrusion in the coastal Mekong delta. A project technical report (2011).

[11] RAD, H.E., et al., Response of rice to different salinity levels during different growth stages, Res. J. Appl. Sci. Eng. Technol. **4** (2012) 3040–3047.

[12] SALEQUE, M.A., et al., Mineral nutrition and yield of four rice genotypes in the farmers' fields of salt-affected soils, J. Plant Nutr. **28** (2008) 865–875.

[13] WANG, L., et al., Application of organic amendments to a coastal saline soil in north China: Effects on soil physical and chemical properties and tree growth, PLoS ONE **9** (2014) 1–9.

[14] DONG, N.M., et al., Effects of salinity flushing measures on soil and water properties and rice yields in rotational rice-shrimp farming systems in Phuoc Long district, Bac Lieu province, Vietnam, Can Tho Univ. Sci. J. **15** (2016) 25–31. (in Vietnamese with English abstract).

[15] FAYE, S., et al., Groundwater salinization in the Saloum (Senegal) delta aquifer: Minor elements and isotopic indicators, Sci. Total Environ. **343** (2005) 243–259.

[16] GHOSH, P., et al., Short- and long-term temporal variations in salinity and the oxygen, carbon and hydrogen isotopic compositions of the Hooghly Estuary water, India, Chem. Geol. **335** (2013) 118–127.

[17] NAIR, I.S., et al., Geochemical and isotopic signatures for the identification of seawater intrusion in an alluvial aquifer, J. Earth Syst. Sci. **124** (2015) 1281–1291.

[18] GEMITZI, A., et al., Seawater intrusion into groundwater aquifer through a coastal lake - complex interaction characterised by water isotopes H and O, Isot. Environ. Health Stud. **50** (2017) 74–87.

[19] VENGOSH, A., et al., Geochemical and boron, strontium, and oxygen isotopic constraints on the origin of the salinity in groundwater from the Mediterranean coast of Israel, Water Resource Res. **35** (1999) 1877–1894.

[20] ROHLING, E.J., Oxygen isotope composition of seawater, In: Encyclopedia of Quaternary Science, Vol. **2** (2013) 915–922.

[21] USDA, Soil taxonomy: A basic system of soil classification for making and interpreting soil surveys. 2nd edition. Natural Resources Conservation Service, U.S. Department of Agriculture Handbook 436 (1999).
[22] FAO (Food and Agriculture Organization of the United Nations), World Reference Base for Soil Resources, Rome (1998).
[23] CELLE, H., et al., Oxygen-18 variations of rainwater during precipitation: application of the Rayleigh model to selected rainfalls in Southern France, J. Hydrol. **289** (2004) 165–177.
[24] MONGELLI, R., et al., Tracing groundwater salinization processes in coastal aquifers: a hydrogeochemical and isotopic approach in the Na-Cl brackish waters of northwestern Sardinia, Italy, Hydrol. Earth Syst. Sci. **17** (2013) 2917–2928.
[25] PHONG, N.D., et al., Salinity dynamics and its implications for cropping patterns and rice performance in rice-shrimp farming systems in My Xuyen and Gia Rai, In: PRESTON N., CLAYTON, H. (Eds), Rice-shrimp Farming in the Mekong Delta: Biophysical and Socioeconomic Issues, Australian Centre for International Agricultural Research, Canberra (2003) 70–88.
[26] DEB, S., et al., Soil organic carbon: Towards better soil health, productivity and climate change mitigation, Climate Change Environ. Sustain. **3** (2015) 26–34.
[27] BANGER, K., et al., Do nitrogen fertilizers stimulate or inhibit methane emissions from rice fields? Global Change Biol. **18** (2012) 3259–3267.
[28] KUMAR, A., et al., Greenhouse gas emission from direct seeded paddy fields under different soil water potentials in Eastern India, Agric. Ecosyst. Environ. **228** (2016) 111–123.
[29] MOHANTY, S., et al., Crop establishment and nitrogen management affect greenhouse gas emission and biological activity in tropical rice production, Ecol. Eng. **104** (2017) 80–98.

CONTRIBUTORS TO DRAFTING AND REVIEW

Ali, M.H., Bangladesh Institute of Nuclear Agriculture, Bangladesh

Atif Riaz, M., Nuclear Institute for Agriculture and Biology, Pakistan

Chen, Y., China Agricultural University, P.R. China

Dang, D. N., Vietnam Atomic Energy Institute, Vietnam

Dominguez, A., Regional Center for Water Research (CREA, Spain

Duong, H. S, Institute for Water Resources Research, Vietnam

Evett, S.R., USDA Agricultural Research Service, USA

Gong, D.Z., Chinese Academy of Agricultural Sciences, P.R. China

Ha, L. A., Institute for Nuclear Sciences and Technology, Vietnam

Ishaque, W., Nuclear Institute for Agriculture and Biology, Pakistan

Jahanbazi, L., University of Tehran, Iran

Jiao, H., China Agricultural University, P.R. China

Khamzina, A., Korea University, South Korea

Khuong, M. C, Institute for Water Resources Research, VietNam

Lellis, B.C., Regional Center for Water Research (CREA, Spain

Li, B., China Agricultural University, P.R. China

Li, H.R. Chinese Academy of Agricultural Sciences, P.R. China

Mei, X.R., State Engineering Laboratory of Efficient Water Use of Crops and Disaster Loss Mitigation, P.R. China

Mirkhani, R., Nuclear Science and Technology Research Institute, Iran

Mirzaei, M., University of Tehran, Iran

Mondal, M.S., Bangladesh Institute of Nuclear Agriculture, Bangladesh

Nhan, D.K, Institute for Nuclear Sciences and Technology, Vietnam

Pardo, J.J., Regional Center for Water Research (CREA), Spain

Perveen, S., Bangladesh Agricultural University, Bangladesh

Romy, K.R.E., Chinese Academy of Agricultural Sciences, P.R. China

Saha, D., Bangladesh University of Engineering and Technology, Bangladesh

Schwartz, R.C., USDA Agricultural Research Service, USA

Sheng, Y., Xinjiang Institute of Ecology and Geography, P.R. China

Shi, J., China Agricultural University, P.R. China

Tran, H. P., Institute for Nuclear Sciences and Technology, Vietnam

Tran, V. D., Institute for Nuclear Sciences and Technology, Vietnam

Ul Haque, M.E., Bangladesh Institute of Nuclear Agriculture, Bangladesh

Wang, G., China Agricultural University, P.R. China

Zhang, W.Y., Hebei Academy of Agriculture and Forest Science, P.R. China

Zhao, C., Xinjiang Institute of Ecology and Geography, P.R. China

IAEA
International Atomic Energy Agency

No. 26

ORDERING LOCALLY

IAEA priced publications may be purchased from the sources listed below or from major local booksellers.

Orders for unpriced publications should be made directly to the IAEA. The contact details are given at the end of this list.

NORTH AMERICA

Bernan / Rowman & Littlefield

15250 NBN Way, Blue Ridge Summit, PA 17214, USA
Telephone: +1 800 462 6420 • Fax: +1 800 338 4550

Email: orders@rowman.com • Web site: www.rowman.com/bernan

REST OF WORLD

Please contact your preferred local supplier, or our lead distributor:

Eurospan Group

Gray's Inn House
127 Clerkenwell Road
London EC1R 5DB
United Kingdom

Trade orders and enquiries:

Telephone: +44 (0)176 760 4972 • Fax: +44 (0)176 760 1640
Email: eurospan@turpin-distribution.com

Individual orders:

www.eurospanbookstore.com/iaea

For further information:

Telephone: +44 (0)207 240 0856 • Fax: +44 (0)207 379 0609
Email: info@eurospangroup.com • Web site: www.eurospangroup.com

Orders for both priced and unpriced publications may be addressed directly to:

Marketing and Sales Unit
International Atomic Energy Agency
Vienna International Centre, PO Box 100, 1400 Vienna, Austria
Telephone: +43 1 2600 22529 or 22530 • Fax: +43 1 26007 22529
Email: sales.publications@iaea.org • Web site: www.iaea.org/publications

International Atomic Energy Agency
Vienna
ISSN 1011–4289